Glued-in Rods for Timber Structures

Effect of distance between rods and between rods and timber edge on the axial strength

by

Hans Joachim Blaß und Bernd Laskewitz

Versuchsanstalt für Stahl, Holz und Steine
Abteilung Ingenieurholzbau
Universität Fridericiana Karlsruhe
Univ.-Professor Dr.-Ing. H.J. Blaß

2001

This research project was financially supported by the European Commission through the Standards, Measurements and Testing (SMT) programme

Table of Contents

1 Preface

The objective of GIROD (Glued-in Rods in Timber Structures) is to provide the information required to prepare standards that will allow an increased, more advanced and more reliable use of glued-in rods in timber structures. The steps involved in achieving this objective are:

1.Perform theoretical and experimental work leading to a calculation model for axially loaded glued-in rods based on the adhesive bond properties as well as the wood and rod material properties. This must take into account the effect of varying climatic and loading conditions as well as fatigue. This step will provide information required by CEN.TC250/SC5 in the preparation of Eurocode 5 - Design of Timber Structures.

2.Develop test methods for the evaluation of adhesives for glued-in rods with respect to strength, durability, creep and creep rupture behaviour under different climatic conditions. This will support the work of CEN.TC193/SC1 (Wood adhesives).

3.Derive test methods for the production control of structural glued-in rod connections. This will support the work of CEN.TC124/WG6 (Glued-in rods in timber structures).

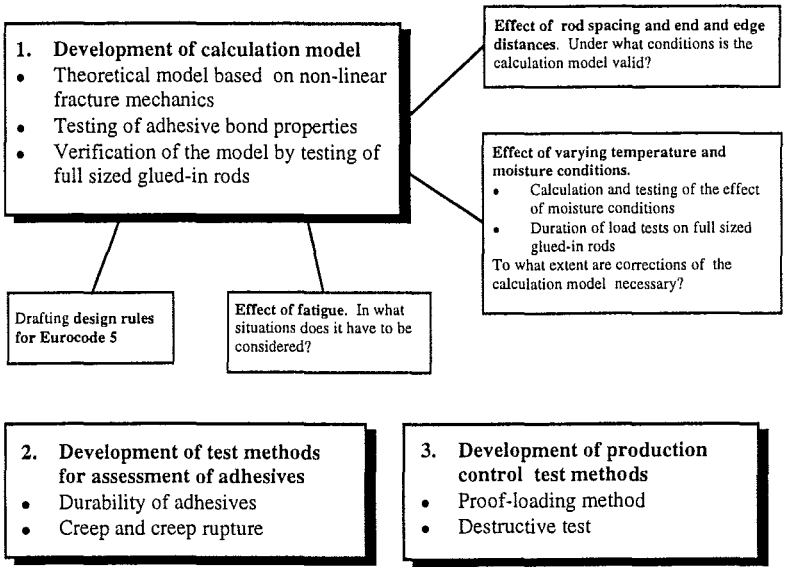

The objective of the third working package of GIROD is to study and to quantify the effect of the spacing between rods and the distance to the timber edges on the axial and lateral load-carrying capacity. Hence University of Karlsruhe performed tests with glued-in rods parallel and perpendicular to the grain loaded axially as well as laterally. Furthermore some theoretical investigations were carried out to describe the behaviour of glued-in rods depending on spacings and distances of rods.

2 Determination of the Minimum Distances

2.1 Preliminary Tests

First of all the testing equipment for the tests with rods glued-in parallel to the grain and loaded axially was defined and the test set-up was designed and produced. In order to try out the test set-up, preliminary tests with one rod and three rods per specimen glued-in parallel to the grain and loaded axially were performed.

The rods with a diameter of 16 mm and the strength class 8.8 were bonded in a glued laminated timber member. The rods were zinc-coated (galvanised) and were not degreased before bonding. There was hardly any grease on the surface of a rod, and this small amount of grease obviously had no effect on the load-carrying capacity of the glued-in rods.

The adhesive was a Kleiberit PUR Plastic Mastic 573.8, the drilled hole had a diameter of 17 mm and the glued-in length was 320 mm. The specimen and the testing and loading arrangement are shown in figure 1.

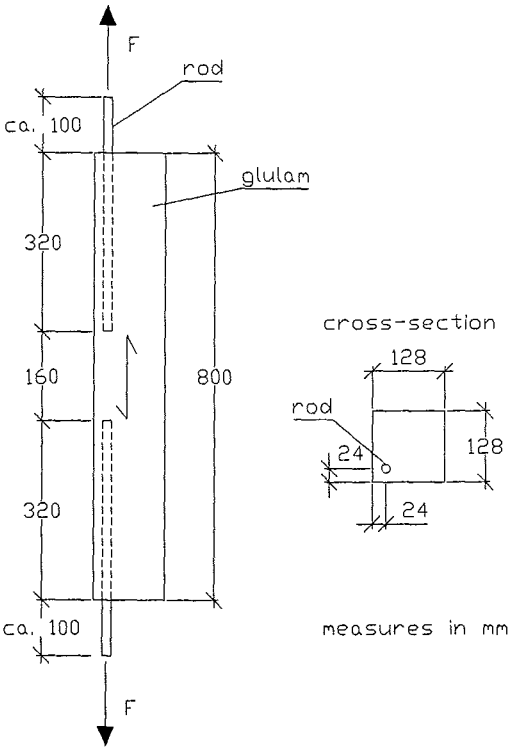

Figure 1: Dimensions and design of the specimens for preliminary tests with one rod

The aim of these tests was to verify the testing equipment and test set-up. Furthermore it was studied whether the eccentric load would cause a deflection in horizontal direction of the glued laminated timber member. Therefore the rod was glued-in with an edge distance of 24 mm to the rod axis. This corresponds to 1.5 times the rod's diameter. To measure the horizontal displacement a mechanical measuring gauge was mounted in the middle of the member. Furthermore the force F and the slip v of the rods in vertical direction were measured.

The results of the three tests and a representative load-slip-diagram are shown in table 1 and figure 2. The tests showed that the deflection of the member due to the bending moment was in the average less than half a millimetre.

Table 1: Results of the pre-testing of one rod glued-in

Denotation of Test	F_{max} [kN]	v_{max} [mm]	Density [kg/m³]	Moisture Content [%]
T-1-1	84.1	1.42	339	10.9
T-1-2	68.7	0.55	422	10.9
T-1-3	77.6	1.33	474	11.2
Mean	76.8	1.10	411	11.0

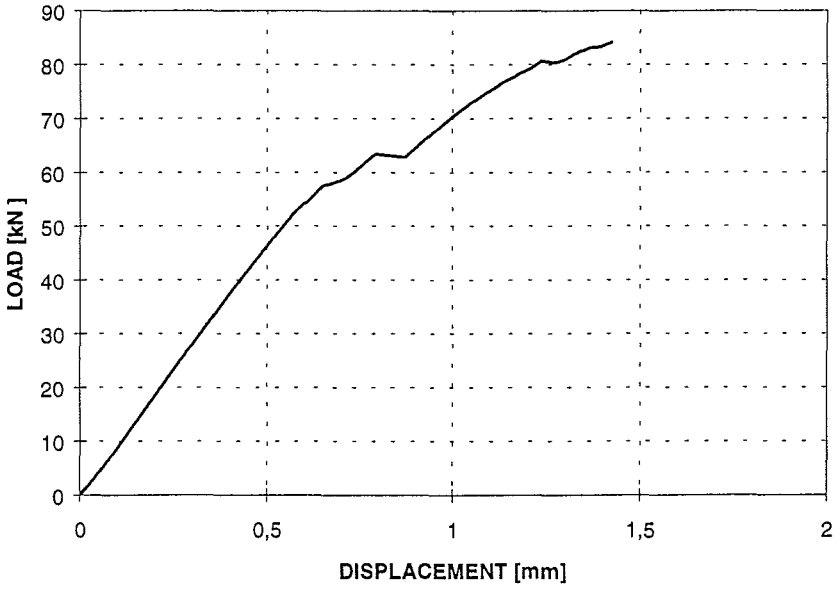

Figure 2: Typical load-displacement diagram for shear block failure

Furthermore the expected failure mechanism, shear block failure, i.e. breaking away of the edge of the timber, occurred. Test T-1-2 was the only one whose failure was caused by pulling out of the rod.

The results confirmed the suitability of the testing equipment and arrangement. Nevertheless it was decided to use another testing arrangement in the main series.

The aim of the development of the test equipment for the tests with three rods glued-in parallel to the grain and loaded axially was the avoidance of an unequal loading of the three rods. For that reason a test set-up was built which has a very high bending stiffness. The preliminary tests exhibited the suitability of the test set-up because of the maximum transmitted load as represented in table 2. If the load of the rods is divided into three equal parts (each for every rod), it can be seen that the load-

carrying capacity of one rod has been reached. The specimen and the testing and loading arrangement are shown in figure 3. The spacing between two rods a_1 was 104 mm, the edge distance a_2 was 32 mm. The definitions of spacings and distances are given in enclosure 1.

Table 2: Results of the pre-testing of three rods glued-in

Denotation of Test	F_{max} (three rods) [kN]	F_{max} (one rod) [kN]	Density [kg/m³]	Moisture Content
T-2-1	233	77.7	396	9.5
T-2-2	209	69.7	428	9.7

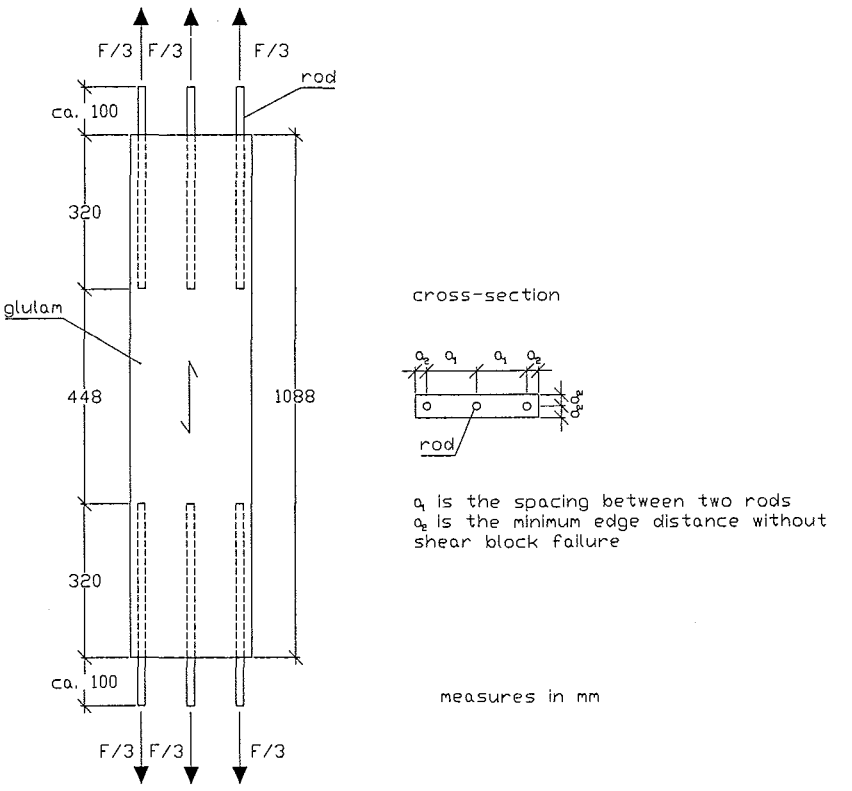

Figure 3: Dimensions, design and loading arrangement of specimens for axial loading (three rods glued-in parallel to the grain)

2.2 Tests to Determine the Minimum Edge Distance

The equipment and the test set-up of the main tests with one or three rods glued-in parallel to the grain and loaded axially is similar to the preliminary tests. A distinctive feature of the main tests to determine the minimum rod-to-edge distance is the use of two rods instead of only one rod because of the possible influence of the eccentricity.

Comparative tests were performed with one rod in the middle of the cross section. Figure 4 shows the test set-up and figure 5 the arrangement of the transducers to determine the minimum rod-to-edge distance. The rods had pinned supports except for the tests with an edge distance of 48 mm because the distance of the rods was too small to provide the necessary space for the hinges. The set-up and the equipment for the tests to determine the minimum spacing between rods is similar.

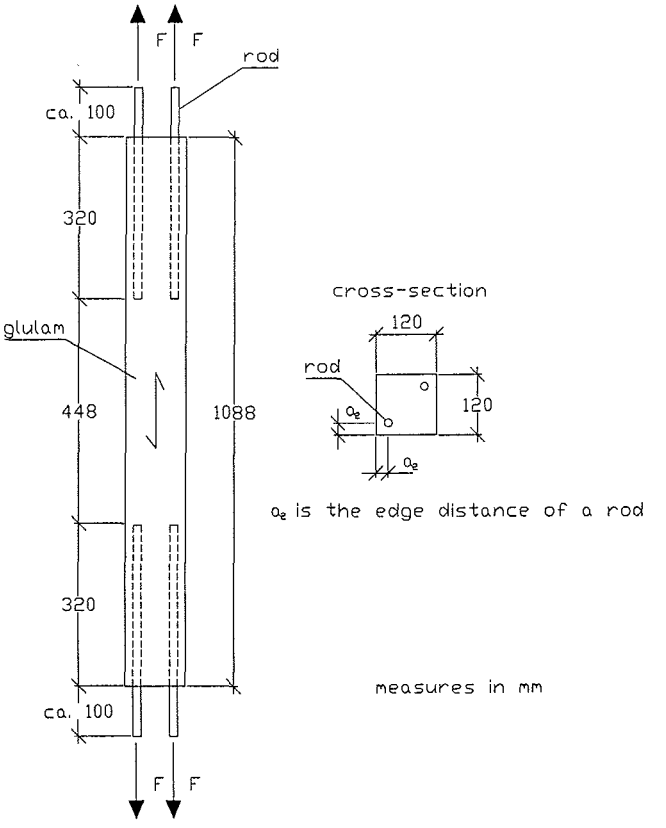

Figure 4: Dimensions, design and loading arrangement of specimens for axial loading (two rods glued-in parallel to the grain)

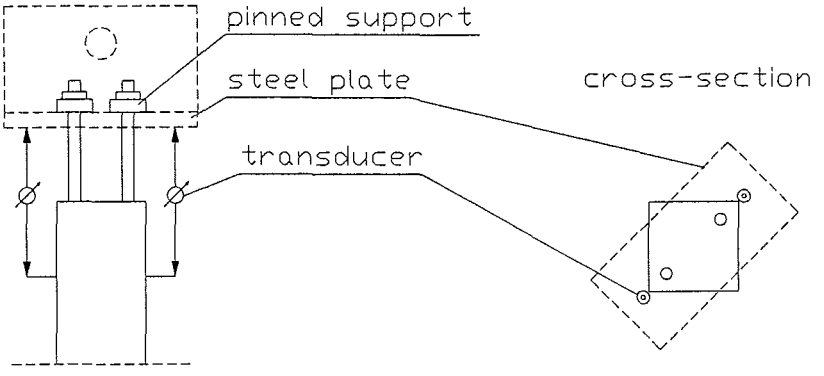

Figure 5: Arrangement of transducers

2.2.1 Materials and Dimensions

In order to make the results comparable with those of other working packages it was agreed to use glued laminated timber made of lamellas of strength class C35. The moisture content of the timber should be 12 %. The threaded rods should correspond to strength class 8.8 and be zinc-coated (galvanised) and not degreased. The diameter of the rods should be 16 mm. They were to be glued-in in oversized holes of 17 mm diameter drilled parallel to the grain. The adhesive should be a Casco PRF. Additionally, some tests were performed to investigate the influence of two different adhesives, Kleiberit Plastic-Mastic 573.8, a PUR, and WEVO Spezialharz, an Epoxy. Also, some tests with different rod diameters were carried out.

The dimensions and the design of the test specimens with two (one) rod(s) per side are shown in figure 4. The end-to-end distance of two rods was determined as 1.4 times the glued-in length. FMPA [1] has performed a FEM-calculation to determine the distance and ascertain that if both ends of the two rods have a distance of 1.4 times the glued-in length, there is only a negligible influence of the distance of the rod ends on the shear stresses of the bond line. Furthermore it was agreed to use a lamella thickness of 42 mm and a cross-section of 120 x 120 mm² for the tests with one or two glued-in rods.

2.2.2 Test Program

After agreeing the size of the test specimens and other properties as strength and moisture content of the timber, the specimens for the tests with one or two rods glued-in parallel to the grain and loaded axially were prepared. The rods had different distances from the edge of the timber to determine the minimum edge distance without causing shear block failure. That means if the distance of the rod to the edge is too small, a part of the timber including the rod breaks away.

Table 3 shows the test program. The definitions of spacings and distances are given in enclosure 1.

Table 3: Test program for rods glued-in parallel to the grain and loaded axially

Test series	Type of glue	Length of specimen/ Diameter of rod [mm]	Glued-in length [mm]	Spacing a_1 [mm]	Edge distance a_2 [mm]	Number of rods per test and side	Number of tests
Gi-1	PRF	1088/16	320	101.8	24	2	5
Gi-2	PRF	1088/16	320	79.2	32	2	5
Gi-3	PRF	1088/16	320	56.6	40	2	5
Gi-4	PRF	1088/16	320	33.9	48	2	5
Gi-5	PRF	1088/16	320	-	60	1	5
Gi-6	PUR	1088/16	320	-	60	1	3
Gi-7	Epoxy	1088/16	320	-	60	1	3
Gi-8	PRF	1360/20	400	-	60	1	5
Gi-9	PRF	816/12	240	-	60	1	5

The aim of these tests was to determine the minimum rod-to-edge distance without any influence on the load-carrying capacity. Therefore, University of Karlsruhe performed tests with different distances of the rod to the edge. To compare these tests, tests with one rod in the middle of the cross-section, glued with PRF, PUR and Epoxy, were carried out. Additionally some tests with different rod diameters (12 mm and 20 mm) were performed. The drilled hole for the tests with a rod diameter of 20 mm was 2 mm larger than the nominal rod diameter instead of only 1 mm.

2.2.3 Test Results

This chapter describes the results of the test series Gi-1 to Gi-9.

Table 4a and 4b show the results of the tests (F_{max} is the load-carrying capacity of one rod, τ is the mean value of the bond strength, according to the rod's diameter), figure 7 contains typical load-displacement curves of the tests with a rod-to-edge distance of 24 to 48 mm. Figure 8 shows load-displacement curves of the tests with one rod in the middle of the cross-section glued with PRF, PUR and Epoxy. Figure 9 presents all test results expect for those with different diameters of the used rod in

one diagram. The load-displacement curves of all tests are shown in figures 3 to 43 (enclosure 2 to 26). Figure 6 shows a failed specimen.

The measured displacement is the mean value of both transducers per side (top side or bottom side).

The failure that occurred in most tests with a rod-to-edge distance of 24 to 48 mm was splitting of the wood. However, some test specimens failed because of pulling-out of the rod. The tests with one rod in the middle always failed due to rod pulling-out.

The shear strength shown is defined as the failure load divided by the surface of a cylinder with a height equal to the glued-in length and a diameter equal to the outer diameter of the rod.

According to figure 9 the load-carrying capacity increases with an increasing edge distance. However, even the tests with the smallest distance from the edge (24 mm) showed a remarkable bond line shear strength. The most common failure mode was splitting of the wood. Only the tests with one rod in the middle of the cross-section failed by pulling out the rod because of reaching the shear strength of the timber and the glue line. The test results with an edge distance of 48 mm do not follow the general trend. An explanation of this behaviour could be that the rod spacing is getting an increasing influence and the influence of the timber edge distance is becoming smaller.

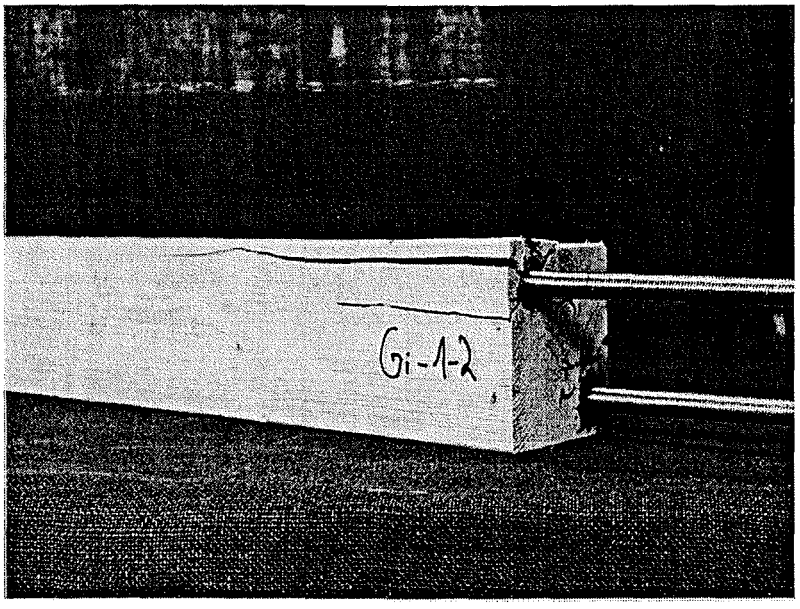

Figure 6: Failed specimen with an edge distance of 1.5 times of the rod diameter

In table 4 no coefficient of variation of the density and the moisture content is given because these are just mean values of the properties of the lamellas of the glued laminated timber members.

Table 4a: Results of the tests to determine the minimum rod-to-edge distance

Denotation of Test	F_{max} [kN]	τ [N/mm²]	Edge Distance [mm]	Type of Glue	Density [kg/m³]	Moisture Content [%]
Gi-1-1	73.7	4.58	24	PRF	457	11.8
Gi-1-2	75.0	4.66	24	PRF	507	12.1
Gi-1-3	71.6	4.45	24	PRF	434	11.8
Gi-1-4	77.6	4.82	24	PRF	486	12.0
Gi-1-5	76.7	4.77	24	PRF	445	11.6
Mean	74.9	4.66	-	-	466	11.9
Coefficient of Variation [%]	3.2	3.2	-	-	-	-
Gi-2-1	80.4	5.00	32	PRF	480	11.8
Gi-2-2	69.2	4.30	32	PRF	485	11.8
Gi-2-3	85.7	5.33	32	PRF	455	11.9
Gi-2-4	77.7	4.83	32	PRF	481	11.8
Gi-2-5	82.7	5.14	32	PRF	451	11.6
Mean	79.1	4.92	-	-	470	11.8
Coefficient of Variation [%]	8.0	8.0	-	-	-	-
Gi-3-1	84.6	5.26	40	PRF	491	11.2
Gi-3-2	78.6	4.89	40	PRF	463	11.4
Gi-3-3	83.8	5.21	40	PRF	485	11.4
Gi-3-4	83.6	5.20	40	PRF	461	11.4
Gi-3-5	82.1	5.10	40	PRF	509	11.0
Mean	82.5	5.13	-	-	482	11.3
Coefficient of Variation [%]	2.9	2.9	-	-	-	-
Gi-4-1	82.2	5.11	48	PRF	488	10.9
Gi-4-2	71.6	4.45	48	PRF	475	10.6
Gi-4-3	84.2	5.23	48	PRF	523	11.5
Gi-4-4	74.8	4.65	48	PRF	485	10.8
Gi-4-5	72.6	4.51	48	PRF	536	11.6
Mean	77.1	4.79	-	-	501	11.1
Coefficient of Variation [%]	7.5	7.5	-	-	-	-

Table 4b: Results of the tests to determine the minimum rod-to-edge distance

Denotation of Test	F_{max} [kN]	τ [N/mm²]	Edge Distance [mm]	Type of Glue	Density [kg/m³]	Moisture Content [%]
Coefficient of Variation [%]	7.5	7.5	-	-	-	-
Gi-5-1	81.2	5.05	60	PRF	512	12.7
Gi-5-2	94.5	5.88	60	PRF	525	11.7
Gi-5-3	93.3	5.80	60	PRF	457	11.4
Gi-5-4	84.9	5.28	60	PRF	506	11.7
Gi-5-5	85.4	5.31	60	PRF	538	12.4
Mean	87.9	5.46	-	-	508	12.0
Coefficient of Variation [%]	6.6	6.6	-	-	-	-
Gi-6-1	65.2	4.05	60	PUR	450	11.3
Gi-6-2	61.8	3.84	60	PUR	412	11.2
Gi-6-3	70.6	4.39	60	PUR	495	11.7
Mean	65.9	4.09	-	-	452	11.4
Gi-7-1	71.2	4.43	60	Epoxy	438	10.3
Gi-7-2	78.7	4.89	60	Epoxy	490	10.5
Gi-7-3	71.7	4.46	60	Epoxy	489	10.3
Mean	73.9	4.59	-	-	472	10.4
Gi-8-1	51.4	2.04	60	PRF	472	12.5
Gi-8-2	111.6	4.44	60	PRF	492	12.5
Gi-8-3	81.7	3.25	60	PRF	410	11.8
Gi-8-4	96.3	3.83	60	PRF	403	11.7
Gi-8-5	103.3	4.11	60	PRF	407	11.7
Mean	88.9	3.54	-	-	437	12.0
Coefficient of Variation [%]	26.6	26.6	-		-	-
Gi-9-1	46.4	5.13	60	PRF	443	11.7
Gi-9-2	47.4	5.23	60	PRF	421	11.4
Gi-9-3	48.1	5.31	60	PRF	460	11.7
Gi-9-4	48.2	5.33	60	PRF	443	11.6
Gi-9-5	47.6	5.26	60	PRF	444	11.7
Mean	47.5	5.26	-	-	442	11.6
Coefficient of Variation [%]	1.5	1.5	-	-	-	-

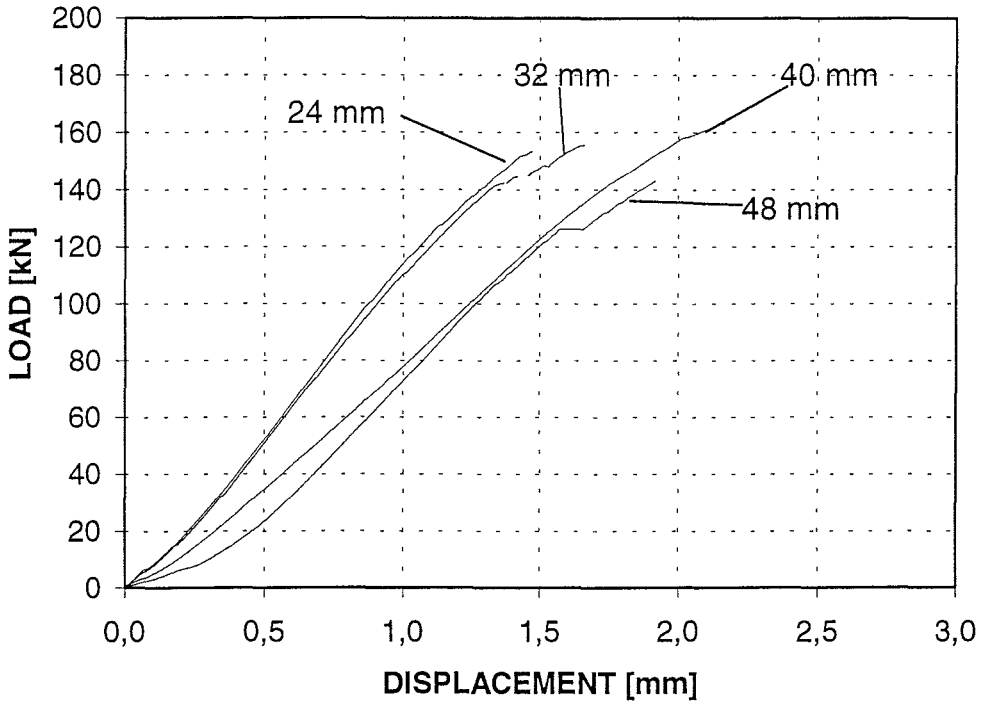

Figure 7: Representative load-displacement curves of tests to determine the minimum rod-to-edge distance

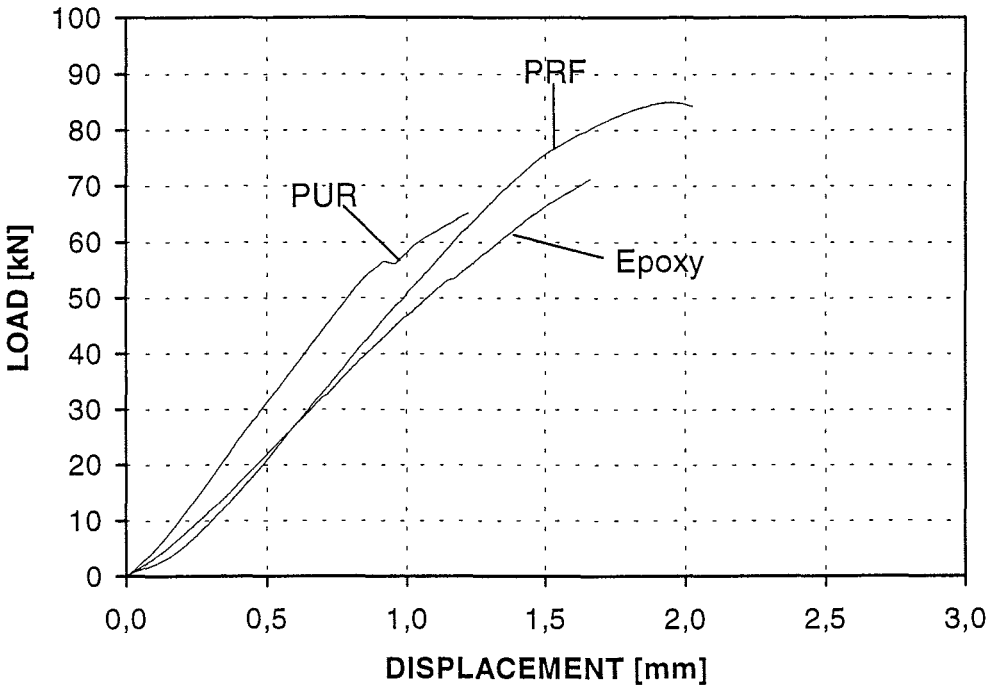

Figure 8: Load-displacement curves of tests with different glues

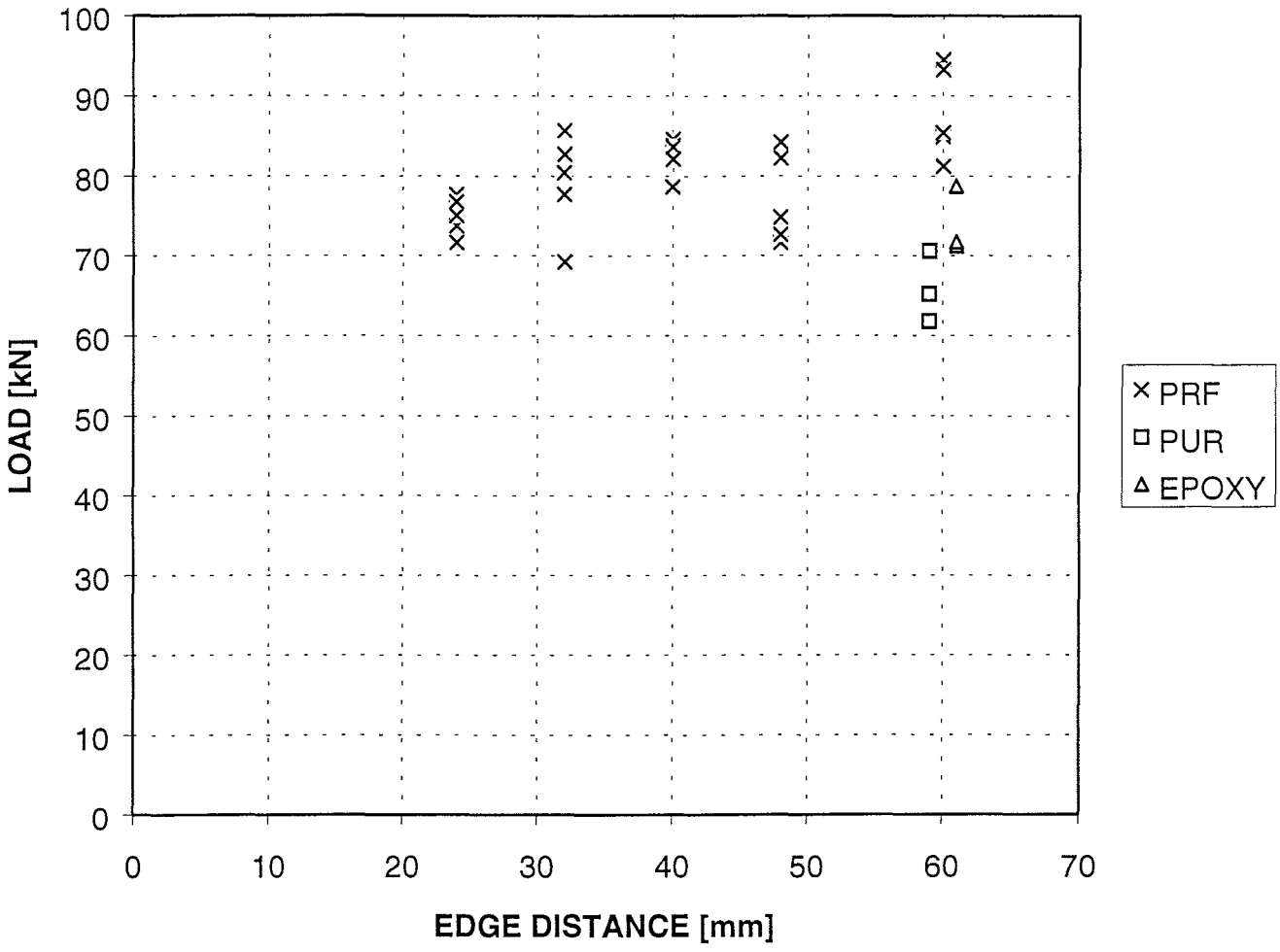

Figure 9: Failure load depending on edge distance and type of adhesive

As a conclusion it can be stated that an edge distance of 32 mm corresponding to two times the rod diameter will lead to the same load-carrying capacity compared with the tests with one rod in the middle of the cross-section.

Figure 10 shows the influence of different adhesives and different rod diameters.

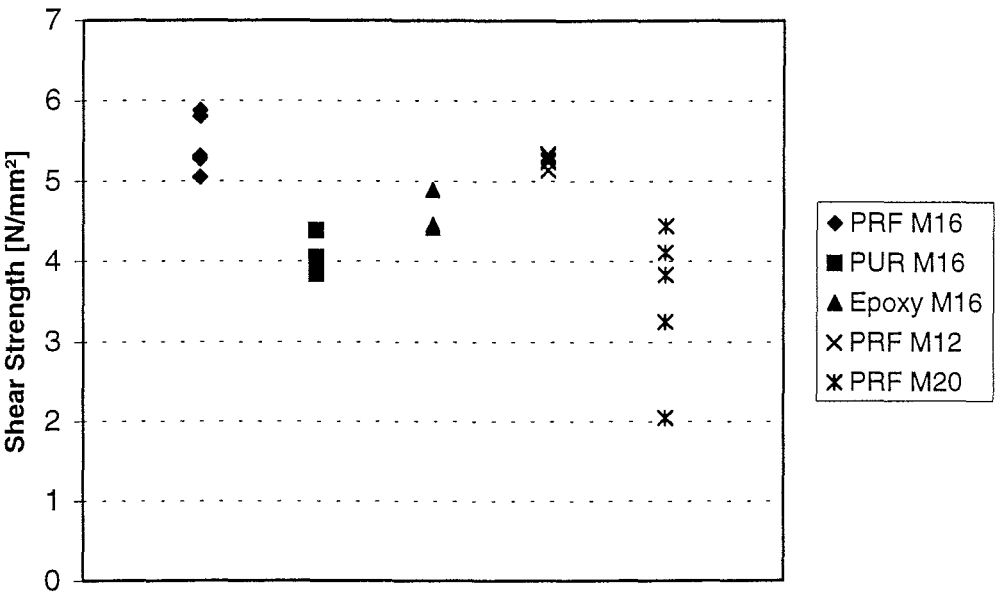

Figure 10: Mean shear strength for different adhesives and different rod diameters

The influence of the type of adhesive on the mean shear strength is significant. The specimens with PUR showed the lowest load-carrying capacity. The load-carrying capacities of the Epoxy bonded rods were slightly higher while the tests with PRF (an prototype glue) resulted in the largest strength values.

The comparative tests with different rod diameters using PRF showed a decrease of the mean shear strength and a larger variation for rods with a diameter of 20 mm although the glued-in length was always 20 times the rod diameter. The reason for this decrease is the different bond line thickness. The tests with a rod diameter of 12 mm had almost the same bond strength as the tests with a rod diameter of 16 mm. The tests with a rod diamter of 20 mm had a bigger COV and a lower average bond strength. The test specimens for the rod diameter of 20 mm were drilled with a diameter of 22 mm, while the specimens for the rod diameters of 12 mm and 16 mm had hole diameters of 13 and 17 mm, respectively. Therefore, the glue line for the 20 mm rods was thicker and caused the decrease of the load-carrying capacity.

These results could be validated by tests performed by SP within the GIROD project. It seems that the PRF adhesive is more sensitive for larger glue line thicknesses.

2.3 Tests to Determine the Minimum Spacing

2.3.1 Test program

The final dimensions and the design of the test specimens with three glued-in rods depended on the test results with one rod because of the minimum edge-to-rod distance without shear block failure. This distance was used for the other tests to avoid the influence of the edge distance, and only the influence of the rod spacing was investigated.

The dimensions and the design of the test specimens with three rods are shown in figure 3.

The materials, dimensions and other agreements are given in chapter 2.2.1. More details of these tests can be found in table 5.

Table 5: Test program to determine the minimum spacing

Test series	Type of glue	Glued-in length [mm]	Diameter of rod [mm]	Spacing a_1 [mm]	Number of rods per test and side	Number of tests
Gi3-1	PRF	320	16	32	3	5
Gi3-2	PRF	320	16	40	3	5
Gi3-3	PRF	320	16	48	3	5
Gi3-4	PRF	320	16	60	3	3

2.3.2 Test Results

Table 6 and figure 11 show the results of the tests to determine the minimum rod-to-rod distance without any significant influence on the load-carrying capacity.

Table 6: Results of the tests to determine the minimum rod-to-rod distance

Denotation of Test	F_{max} [kN]	τ [N/mm²]	Spacing [mm]	Type of Glue	Density [kg/m³]	Moisture Content [%]
Gi31-1	199.7	4.14	32	PRF	437	13.2
Gi31-2	189.6	3.93	32	PRF	449	13.2
Gi31-3	249.7	5.17	32	PRF	441	13.1
Gi31-4	210.5	4.36	32	PRF	440	13.2
Gi31-5	170.8	3.54	32	PRF	425	13.2
Mean	204.0	4.22	-	-	438	13.2
Coefficient of Variation [%]	14.4	14.4	-	-	-	-
Gi32-1	195.9	4.06	40	PRF	446	13.3
Gi32-2	214.0	4.43	40	PRF	434	13.3
Gi32-3	209.1	4.33	40	PRF	444	13.3
Gi32-4	188.7	3.91	40	PRF	465	13.1
Gi32-5	223.0	4.62	40	PRF	444	13.5
Mean	206.1	4.27	-	-	447	13.3
Coefficient of Variation [%]	6.7	6.7	-	-	-	-
Gi33-1	246.8	5.11	48	PRF	468	12.0
Gi33-2	232.1	4.81	48	PRF	490	11.9
Gi33-3	244.7	5.07	48	PRF	479	11.9
Gi33-4	230.2	4.77	48	PRF	470	11.9
Gi33-5	219.8	4.56	48	PRF	472	11.8
Mean	234.7	4.86	-	-	475	12.2
Coefficient of Variation [%]	4.7	4.7	-	-	-	-
Gi34-1	239.1	4.96	60	PRF	486	13.4
Gi34-2	246.9	5.11	60	PRF	471	13.3
Gi34-3	266.0	5.39	60	PRF	467	12.0
Mean	248.7	5.16	-	-	475	12.9

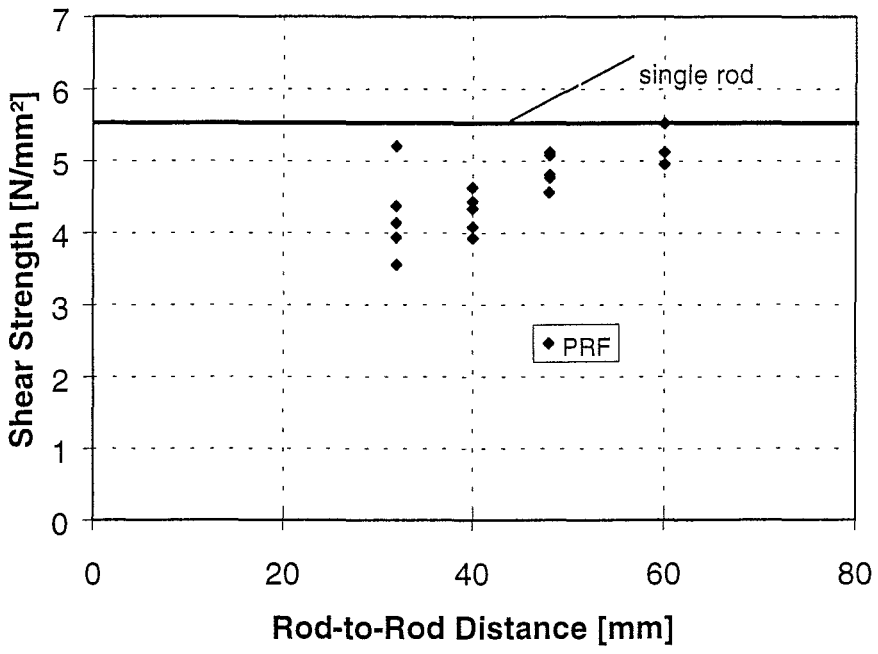

Figure 11: Shear strength versus rod-to-rod distance

The edge distance of the rods was 40 mm, respectively 2.5 times of the rod's diameter. Because of the very stiff loading arrangement equal loading of the three rods is assumed. Regarding the results it can be seen that like the previous tests the load-carrying capacity is increasing with the rod spacing. As a comparative item the values of the tests with one rod in the middle of the cross-section were added to the diagram. The expected failure, namely splitting off the wood, occurred.

Figure 12 shows a failed specimen. The load-displacement curves of all tests are shown in figures 44 to 63 (enclosure 27 to 38). The arrangement of the transducers was similar to the set-up of the tests to determine the minimum edge distance (figure 5).

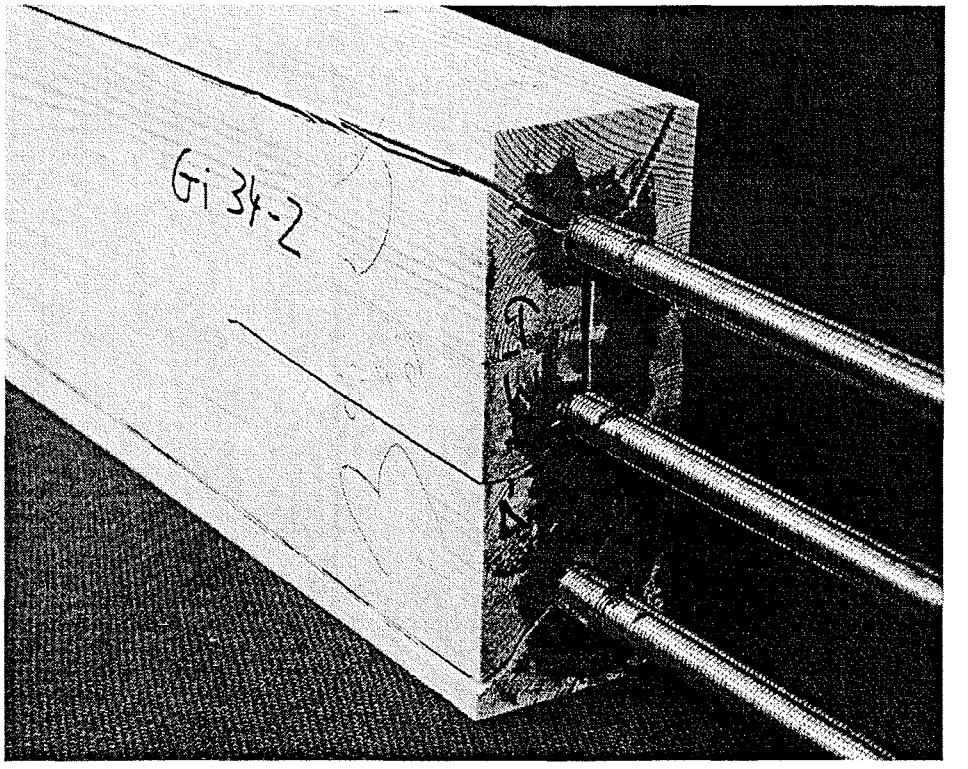

Figure 12: Failed specimen with a spacing of 3.75 times the rod diameter

2.4 Theoretical investigations

Combining all tests (Blaß, Laskewitz [2]) where PRF was used, those to determine the minimum edge distance as well as those to establish the minimum rod spacing, leads to the diagram presented in figure 14. The distance *a* on the abscissa is defined as follows: for the tests to determine the minimum edge distance, the distance *a* is the minimum of either half of the spacing or the edge distance. For the tests to establish the minimum rod spacing the distance *a* is defined as half of the rod spacing. A linear regression analysis leads to the following relation between mean shear strength and distance *a* [mm] to rod diameter *d* [mm] for a rod diameter of 16 mm:

$$\tau = 0.7 \cdot \frac{a}{d} + 3.7 \quad [\mathrm{N/mm^2}]. \qquad (1)$$

with $R^2 = 0.3003$

$$1 \le \frac{a}{d} \le 2.5$$

$$a = \min\begin{cases}\text{edge distance}\\ 1/2\ \text{spacing}\end{cases}$$

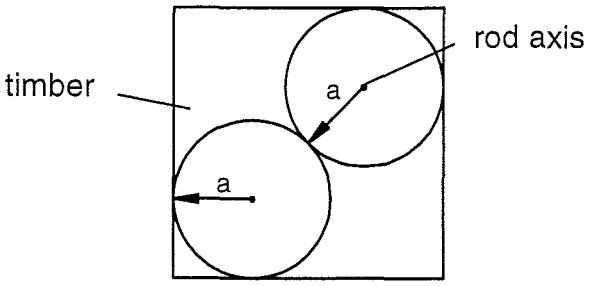

Figure 13: Definition of distance *a*

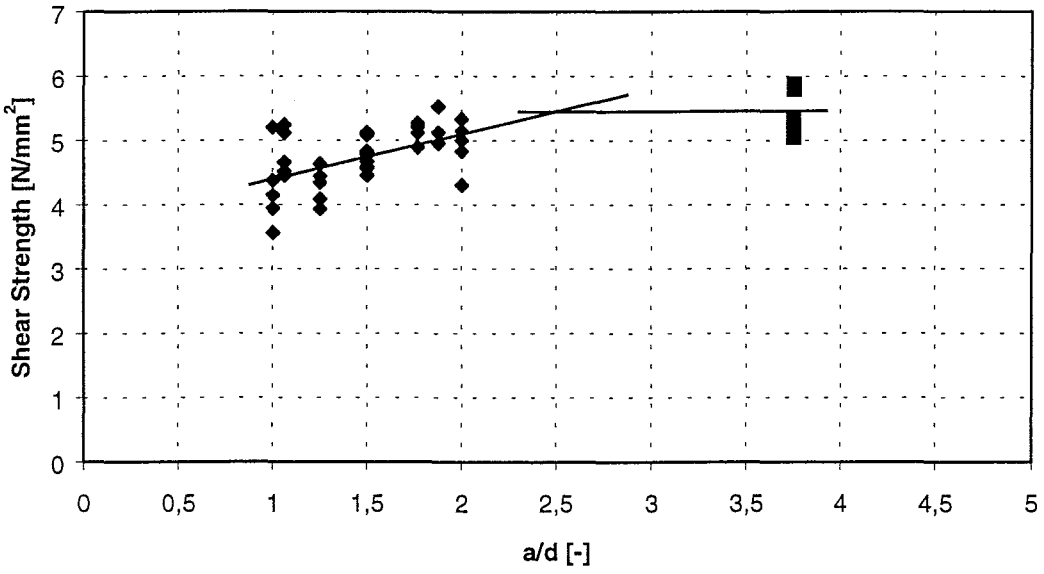

Figure 14: Mean shear strength versus distance *a* to rod diameter *d*

The horizontal straight line represents the mean value of the comparative tests with one rod in the centre of the cross-section. The point of intersection is situated close to a distance of 40 mm, or 2.5 times of the rod diameter. Consequently, a spacing of 80 mm or an edge distance of 40 mm does not cause a decrease of the load-carrying capacity compared to single rods with a diameter of 16 mm.

Additionally, a multiple linear regression was performed taking the density of the timber into account. The influence of the density was found to be not significant. However, only timber made of laminations of strength class C35 with a characteristic density of 400 kg/m³ was used in the tests. In order to verify the weak influence of the

density, more strength classes with different characteristic densities should be included in the study. Nevertheless a rod-to-edge distance of 2.5 times of the rod diameter and a spacing of 5 times of the rod diameter is suggested. Otherwise if the distance should be smaller, equation 1 should be used to calculate the bond stresses.

3 Rods Glued-in Perpendicular to the Grain and Loaded Axially

3.1 Preliminary Tests

The materials were the same as mentioned in chapter 2.2.1 except for the glulam. It corresponded to strength class GI 28. The dimensions and the test set-up are shown in figure 15. An overview of the test program is given in table 7. The rods were glued-in perpendicular to the grain in oversized holes with a diameter of 17 mm and were loaded axially. The rods had pinned supports to avoid moments at the support. The test series Giqp-1 and Giqp-2 were performed to investigate the influence of number of rods glued-in in the same cross-section. Test series Giqp-4 was performed to investigate the influence of the edge distance. The two tests of this series were performed with two different adhesives (Epoxy and PRF).

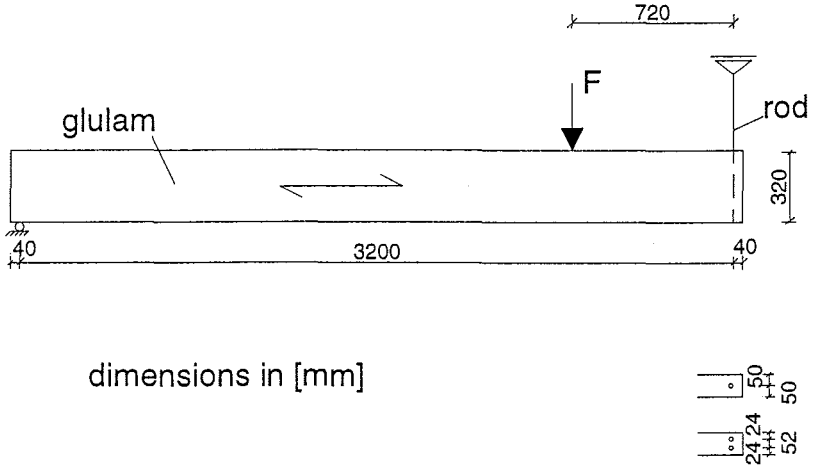

Figure 15: Test Set-Up

Table 7: Test program

Test series	Type of glue	Glued-in length [mm]	Diameter of rod [mm]	Edge distance a_5 [mm]	Edge distance a_4 [mm]	Spacing a_1 [mm]	Number of rods per test	Number of tests
Giqp-1	PRF	320	16	50	40	-	1	5
Giqp-2	PRF	320	16	24	40	52	2	3
Giqp-4	PRF/ Epoxy	320	16	50	60	-	1	2

The definitions of spacings, end and edge distances are given in enclosure 1.

Table 8 shows the results of the preliminary tests. Because of the test results it was decided to choose a single rod and a constant edge distance of 60 mm. The length between the supports was defined to be ten times the height of the cross-section of the specimens. The failure in most cases was pulling-out the rod combined with splitting of the wood.

In test series Giqp-4 there was no significant influence of the different adhesives.

Table 8: Test results

Test series	Mean shear strength in bond line [N/mm²]	Coefficient of variation [%]
Glqp-1	5.60	5.5
Glqp-2	3.24	-
Glqp-4	5.50	-

3.2 Main Test Series

The materials were the same as mentioned in chapter 2.2.1. The dimensions and the test set-up are shown in figure 16. An overview of the test program is given in table 9. The rods with a diameter of 16 mm were glued-in in oversized holes with a diameter of 17 mm. The depths and the lengths of the beams were varied. The glued-in length was either 160 mm or 320 mm. The distance to the edge of the rod was chosen to be 60 mm to avoid any influence of the edge on the load-carrying capacity. The length

between the supports was defined to be ten times the depth of the cross-section of the specimens.

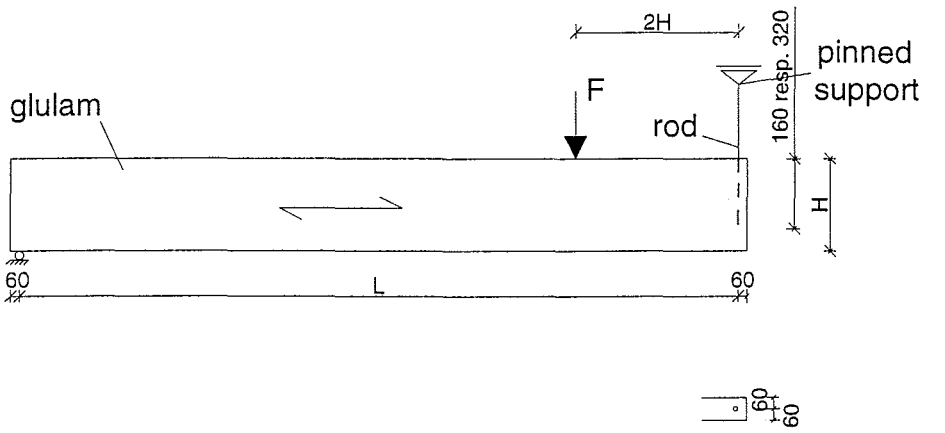

dimensions in [mm]

Figure 16: Test set-up for the main test series

Table 9: Test program

	H [mm]	B [mm]	L [mm]	glued-in length [mm]
Giq-1	320	120	3200	320
Giq-2	400	120	4000	320
Giq-3	480	120	4800	320
Giq-4	560	120	5600	320
Giq-5	240	120	2400	160
Giq-6	280	120	2800	160
Giq-7	320	120	3200	160
Giq-8	500	120	5000	160

3.2.1 Test Results

Table 10 shows the individual test results. The failure mode was pulling-out the rod combined with wood splitting for the test series with a glued-in length that was the same as the height of the beam. With increasing beam depth, the observed failure mode changed from pulling out the rod towards tensile perpendicular to the grain failure of the beam. The corresponding crack occurs always at the end of the rod. The pull-out strength of the rods which are glued-in perpendicular to the grain and glued-in the same as the height of the beam are similar to those results achieved by the tests with rods glued-in parallel to the grain. Figure 17 shows a failed specimen. The failure was reaching the tensile strength perpendicular to the grain. The load-displacement curves of all tests are shown in figures 64 to 103 (enclosure 39 to 62). The arrangement of the transducers was similar to the set-up of the tests to determine the minmum edge distance (figure 5).

Figure 17: Tensile failure perpendicular to the grain

Table 10a: Results of the tests with rods glued-in perpendicular to the grain and loaded axially (l_0=320 mm)

Denotation of Test	F_{max} [kN]	τ [N/mm²]	α (l_0/H)	Type of Glue	Density [kg/m³]	Moisture Content [%]
Giq-1-1	78.6	4.89	1.00	PRF	459	11.6
Giq-1-2	85.2	5.30	1.00	PRF	432	11.2
Giq-1-3	89.2	5.55	1.00	PRF	475	11.3
Giq-1-4	80.4	5.00	1.00	PRF	413	11.1
Giq-1-5	86.3	5.37	1.00	PRF	448	11.3
Mean	84.0	5.22	-	-	445	11.3
Coefficient of Variation [%]	5.2	5.2	-	-	-	-
Giq-2-1	82.6	5.14	0.80	PRF	436	11.2
Giq-2-2	74.3	4.62	0.80	PRF	471	10.8
Giq-2-3	84.5	5.25	0.80	PRF	412	10.9
Giq-2-4	78.5	4.88	0.80	PRF	398	10.7
Giq-2-5	83.8	5.21	0.80	PRF	431	11.0
Mean	80.7	5.02	-	-	430	10.9
Coefficient of Variation [%]	5.3	5.3	-	-	-	-
Giq-3-1	67.9	4.22	0.67	PRF	413	10.7
Giq-3-2	65.6	4.08	0.67	PRF	460	10.9
Giq-3-3	77.1	4.79	0.67	PRF	415	10.7
Giq-3-4	59.4	3.69	0.67	PRF	415	10.8
Giq-3-5	81.8	5.08	0.67	PRF	437	11.0
Mean	70.4	4.37	-	-	428	10.8
Coefficient of Variation [%]	12.8	12.8	-	-	-	-
Giq-4-1	66.6	4.14	0.57	PRF	430	10.4
Giq-4-2	54.7	3.40	0.57	PRF	433	11.2
Giq-4-3	71.4	4.44	0.57	PRF	431	10.3
Giq-4-4	76.0	4.72	0.57	PRF	437	11.5
Giq-4-5	61.4	3.81	0.57	PRF	435	11.2
Mean	66.0	4.10	-	-	433	10.9
Coefficient of Variation [%]	12.6	12.6	-	-	-	-

Table 10b: Results of the tests with rods glued-in perpendicular to the grain and loaded axially (l_0=160 mm)

Denotation of Test	F_{max} [kN]	τ [N/mm²]	α (l_0/H)	Type of Glue	Density [kg/m³]	Moisture Content [%]
Giq-5-1	35.2	4.38	0.67	PRF	440	11.6
Giq-5-2	44.9	5.58	0.67	PRF	441	11.5
Giq-5-3	41.9	5.21	0.67	PRF	447	11.5
Giq-5-4	50.1	6.23	0.67	PRF	440	11.5
Giq-5-5	40.0	4.97	0.67	PRF	448	11.4
Mean	42.4	5.27	-	-	443	11.5
Coefficient of Variation [%]	13.1	13.1	-	-	-	-
Giq-6-1	32.2	4.00	0.57	PRF	474	11.4
Giq-6-2	35.4	4.40	0.57	PRF	448	11.5
Giq-6-3	42.8	5.32	0.57	PRF	436	11.4
Giq-6-4	35.0	4.35	0.57	PRF	481	11.6
Giq-6-5	37.2	4.63	0.57	PRF	463	11.7
Mean	36.5	4.54	-	-	461	11.5
Coefficient of Variation [%]	10.8	10.8	-	-	-	-
Giq-7-1	43.8	5.45	0.50	PRF	451	11.1
Giq-7-2	37.4	4.65	0.50	PRF	433	10.9
Giq-7-3	34.2	4.25	0.50	PRF	462	11.5
Giq-7-4	35.7	4.44	0.50	PRF	447	10.9
Giq-7-5	37.4	4.65	0.50	PRF	421	11.5
Mean	37.7	4.69	-	-	443	11.2
Coefficient of Variation [%]	9.7	9.7	-	-	-	-
Giq-8-1	27.6	3.43	0.32	PRF	441	11.8
Giq-8-2	34.9	4.34	0.32	PRF	433	11.1
Giq-8-3	29.5	3.67	0.32	PRF	434	11.5
Giq-8-4	30.1	3.74	0.32	PRF	449	11.4
Giq-8-5	26.6	3.31	0.32	PRF	419	11.0
Mean	29.7	3.70	-	-	435	11.4
Coefficient of Variation [%]	10.8	10.8	-	-	-	-

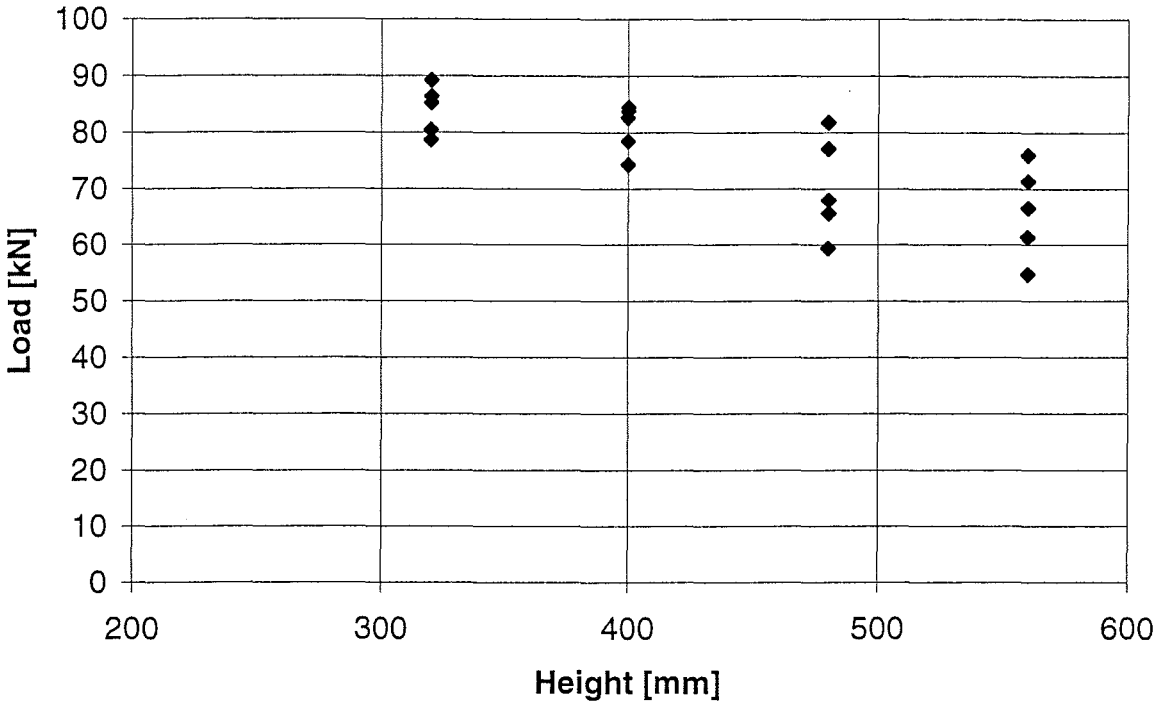

Figure 18: Test results for a glued-in length of 320 mm

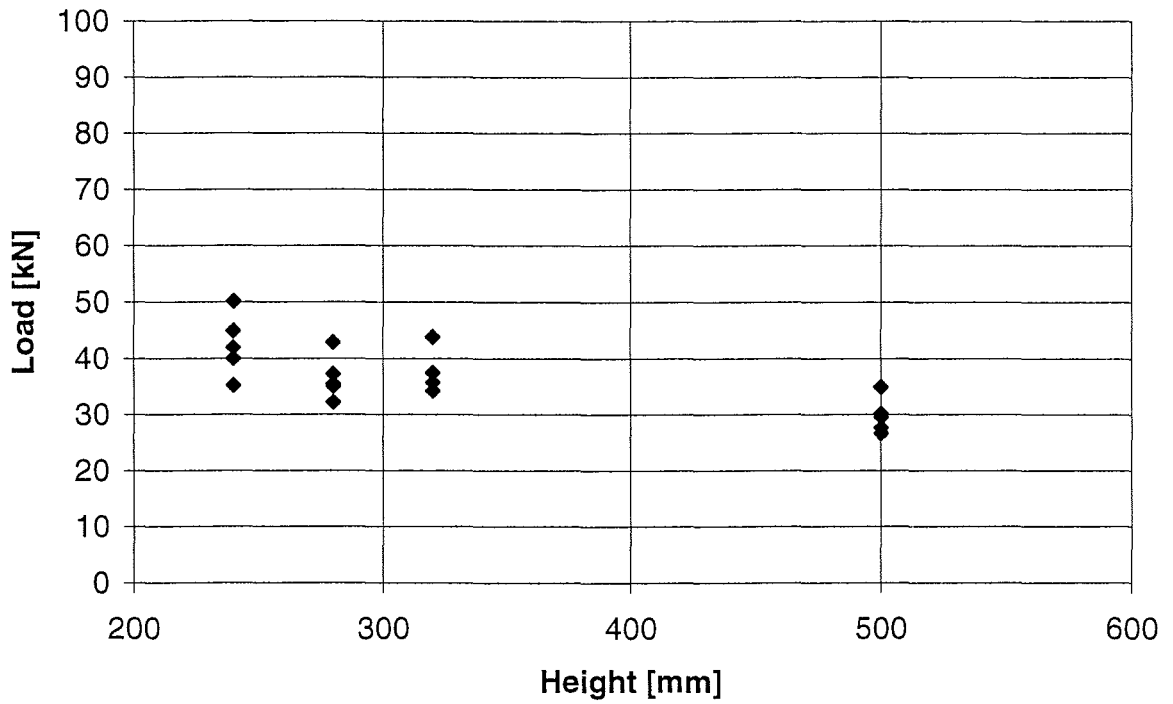

Figure 19: Test results for a glued-in length of 160 mm

Figures 18 and 19 show the test results for the glued-in lengths of 320 mm and 160 mm. It is obvious that the load-carrying capacity decreases with increasing height of the beam or a descending ratio of the glued-in length l_0 to the height of the beam H.

3.2.2 Theoretical Investigations

The test results with tensile failure perpendicular to the grain were evaluated both on the basis of the work of Görlacher [3] and using a fracture mechanics approach [4]. The failure is similar to that of notched beams and therefore the fracture mechanics approach seems to be an adequate solution. In Eurocode 5 the design rules for notched beams are also based on fracture mechanics. Nevertheless it is also possible to describe the load-carrying capacity of the tested specimens by using the design rules for connections loaded perpendicular to the grain. The load-carrying capacity of the specimens which failed due to pulling out the rod can be described by using the design rules for glued-in rods given in the draft of the German Timber Design Code DIN 1052 [5]. First the design rules for connections loaded perpendicular to the grain are regarded. The ultimate load for a rod glued-in perpendicular to the grain may be calculated as

$$F_{90} = \frac{13 A_{ef}^{0.8} f_{t,90}}{\eta k_r} \qquad (2)$$

where $$\eta = 1 - 3\left(\frac{l_0}{H}\right)^2 + 2\left(\frac{l_0}{H}\right)^3$$

l_0: glued-in length

H: Height of the beam

$$k_r = \frac{1}{n}\sum_{i=1}^{n}\left(\frac{h_1}{h_i}\right)^2 = \frac{H - l_0}{H}$$

$$A_{ef} = l_{r,ef} \cdot t_{ef}$$

$$l_{r,ef} = \sqrt{l_r^2 + (cH)^2}$$

$$l_r = d$$

$$c = \frac{4}{3}\sqrt{\frac{l_0}{H}\left(1 - \frac{l_0}{H}\right)^3}$$

$$t_{ef} = \min\begin{cases} b \\ 6 \cdot d \end{cases} \text{ (draft DIN 1052)}$$

b: Width of the beam

d: Outer diameter of the rod

Figure 21 shows a comparison between the failure loads reached in the tests and the calculated failure loads. The horizontal lines describe the pull-out capacity of both glued-in lengths used in the tests according to the proposal of DIN 1052:

$$R_{ax} = l_0 \pi d f_{k1} \qquad (3)$$

with f_{k1} bond strength.

Görlacher's model assumes a tensile stress distribution perpendicular to the grain at both sides of the connection reaching a maximum at the end of the glued-in rod and decreasing with increasing distance from the rod (see figure 20). Since an undisturbed distribution is only possible in one direction, the calculated load carrying capacities are divided by 2, although a certain amount of stresses is also transferred between rod and end grain surface. These stresses are disregarded in the following.

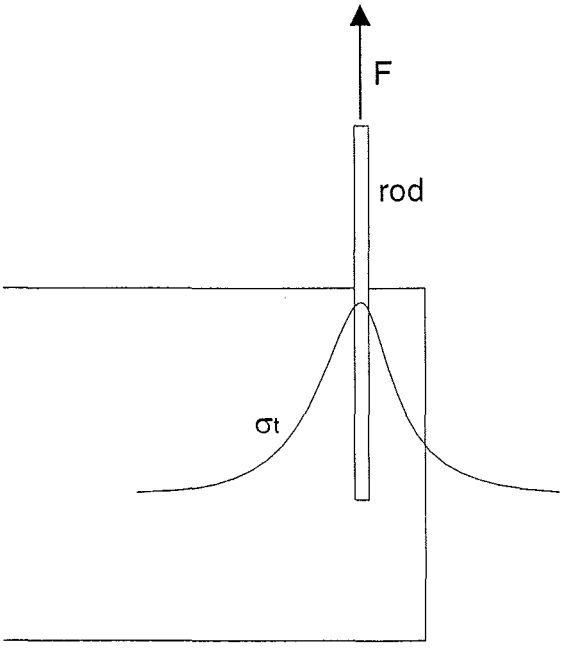

Figure 20: Tensile stress distribution

Characteristic values of the material properties according to the draft DIN 1052 were used when evaluating the load-carrying capacities. The tensile strength perpendicular to the grain is 0.5 N/mm² and the shear strength is 3.8 N/mm² for GI 32h.

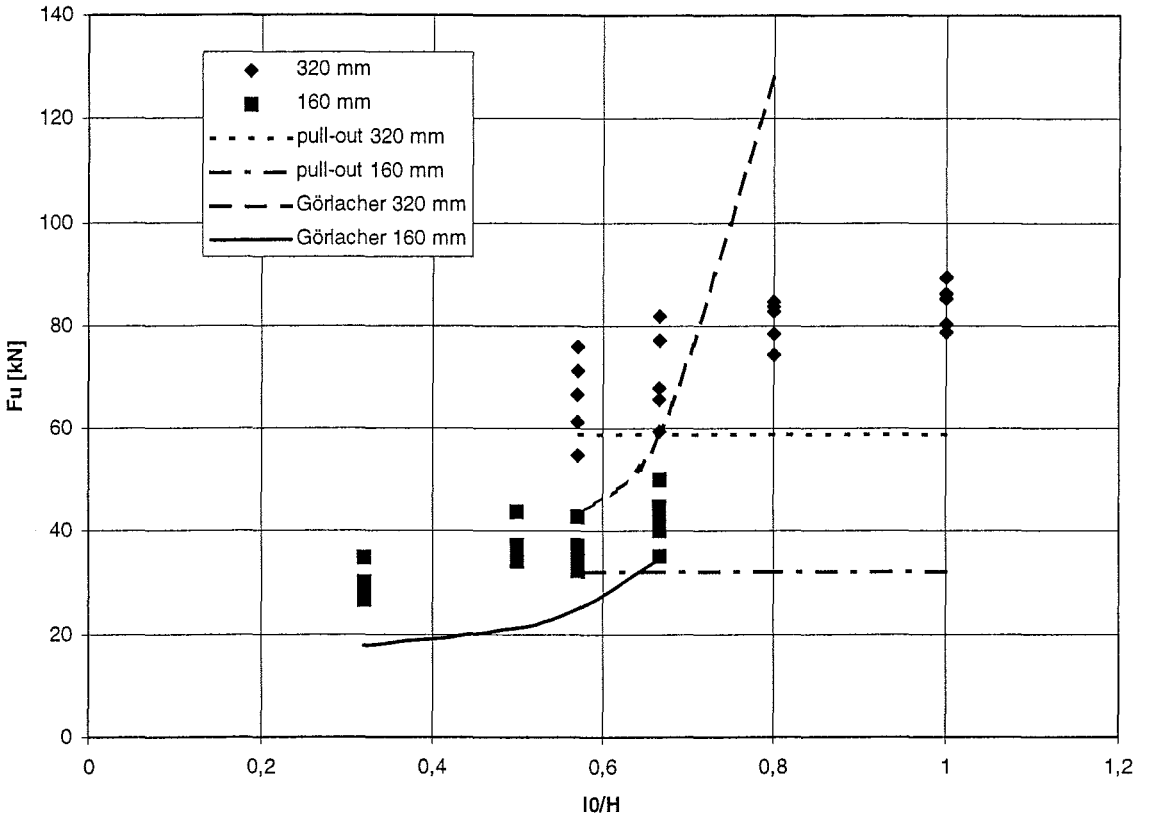

Figure 21: Test results compared to equations according to Görlacher [3]

For $\alpha = \frac{l_0}{H}$ approaching 1 the calculated load-carrying capacity reaches infinite values. In this case α is the ratio of the glued-in length to the height of the beam. In the case of a notched beam α = 1 would represent a beam without a notch. Therefore it is obvious that the model used gives infinite values. In reality the ultimate load is limited by rod pulling-out. The horizontal lines describe the pull-out strengths of rods glued-in perpendicular to the grain according to the draft of the German national standard DIN 1052. Considering the fact that the calculated results are based on characteristic material properties, Görlacher's equations describe the behaviour quite well.

The second calculation model evaluated here is the design rule for notched beams according to Eurocode 5 which is based on a fracture mechanics approach. The equation to describe the load-carrying capacity is

$$V = \frac{2}{3} \cdot k_v f_v b l_0 \qquad (4)$$

where $$k_v = \min\left\{ \frac{1}{\sqrt{H \cdot \alpha(1-\alpha)}} \right.$$

$$k_n = 6.5 \text{ (for glulam)}$$

$$\alpha = \frac{l_0}{H}.$$

k_v as a factor to describe the geometry of the notch is simplified according to the tested geometry. An advantage of this calculation model is that the width of the beam is taken into account more precisely.

Figure 22 shows a comparison between the failure loads from the tests and the calculated failure loads. The horizontal lines describe the pull-out strength for both glued-in lengths according to equation 3 as described before.

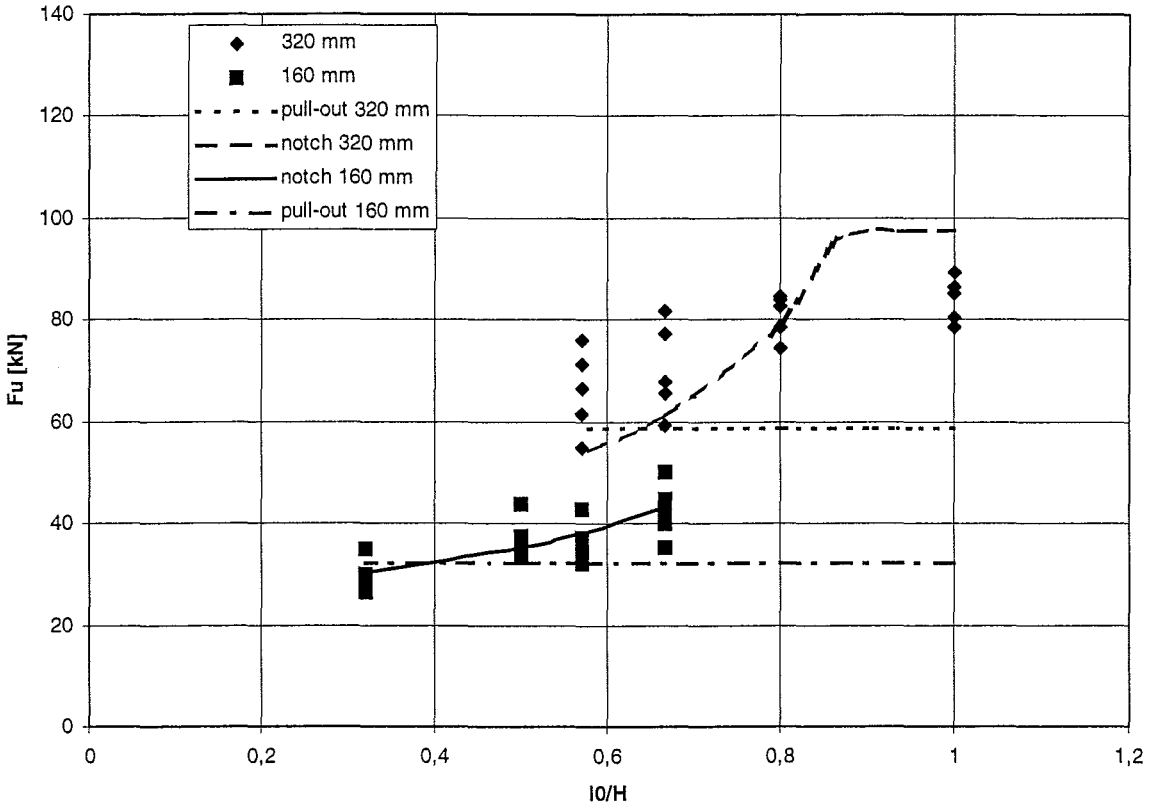

Figure 22: Test results compared to equations according to Eurocode 5 [4]

Although characteristic values were used to calculate the ultimate loads, especially for small ratios l_0/H the calculation model for notched beams overestimates the ultimate loads from the tests. The derivation of the ultimate loads according to the fracture mechanics approach is based on the deformation of a cantilever beam. If the

cantilever beam length approaches zero, the calculation model is not valid anymore. Therefore the calculation model of Görlacher is suggested to describe the load-carrying capacity of rods glued-in perpendicular to the grain.

In the draft DIN 1052 [5] simplified equations based on the theory of Görlacher [3] are given. Figure 23 shows the comparison of the test results with the design rules of DIN 1052. The difference between the original and the simplified equations in DIN 1052 is not significant. Further information on these design rules are given in the next paragraph.

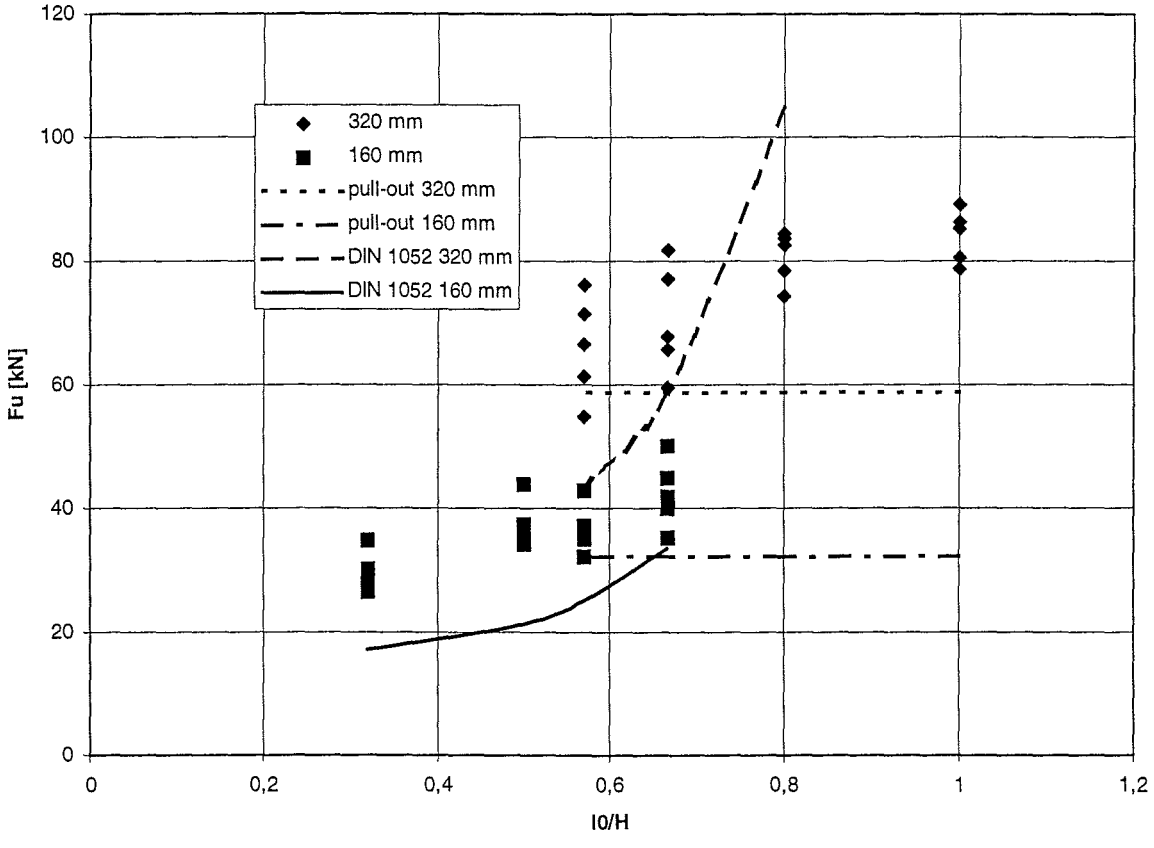

Figure 23: Test results compared to equations according to DIN 1052 [5]

4 Rods Glued-in Parallel to the Grain and Loaded Laterally

4.1 Test program

The materials were the same as mentioned in chapter 2.2.1. Only two test series were performed with GI 24h instead of GI 32h. The dimensions and the test set-up are shown in figures 24 and 25. An overview of the test program is given in table 11. The rods with a diameter of 16 mm were glued-in in oversized holes with a diameter of 17 mm. The edge distances of the rods were varied. The glued-in length was 320 mm. The adhesive used for all tests was PRF. The test specimens had either one or two glued-in rods. Additionally some tests with rods corresponding to strength class 4.6 were performed to investigate the influence of the steel quality on the load-carrying capacity. One test series was performed with a larger beam width. The transducers measured the displacement of the middle of the cross-section nearby the end grain of the beam.

If the supporting steel plate provided a pinned support for the glued-in rods, the rods rotated in the steel plates and the failure mode was characterised by reaching the embedding strength of the timber and one plastic hinge in the rod. Timber splitting was not observed. If, on the other hand, the rods were clamped in the supporting steel plates, higher ultimate loads were reached and two plastic hinges occured in each rod. At higher load levels, also tensile failures perpendicular to the grain in the timber were observed. Further information on this is given in chapter 4.2.

Table 11: Test program

Test series	Glulam	Strength class of the rod	H [mm]	B [mm]	L [mm]	Edge distance a_2 [mm]	Edge distance a_3 [mm]	Spacing a_1 [mm]	Number of rods	Number of tests
Gil4.6	Gl24h	4.6	220	100	2380	110	110	-	1	5
Gil8.8-1	Gl24h	8.8	220	100	2380	110	110	-	1	5
Gil8.8-2	Gl32h	8.8	300	100	3500	50	250	-	1	5
Gil8.8-3	Gl32h	8.8	300	100	3500	100	200	-	1	5
Gil8.8-4	Gl32h	8.8	300	100	3500	150	150	-	1	5
Gil8.8-5	Gl32h	8.8	300	100	3500	200	100	-	1	5
Gil8.8-6	Gl32h	8.8	300	150	3500	50	250	-	1	5
GilII-1	Gl32h	8.8	400	100	4500	50	270	80	2	5
GilII-2	Gl32h	8.8	400	100	4500	100	220	80	2	5
GilII-3	Gl32h	8.8	400	100	4500	150	170	80	2	5
GilII-4	Gl32h	8.8	400	100	4500	200	120	80	2	5

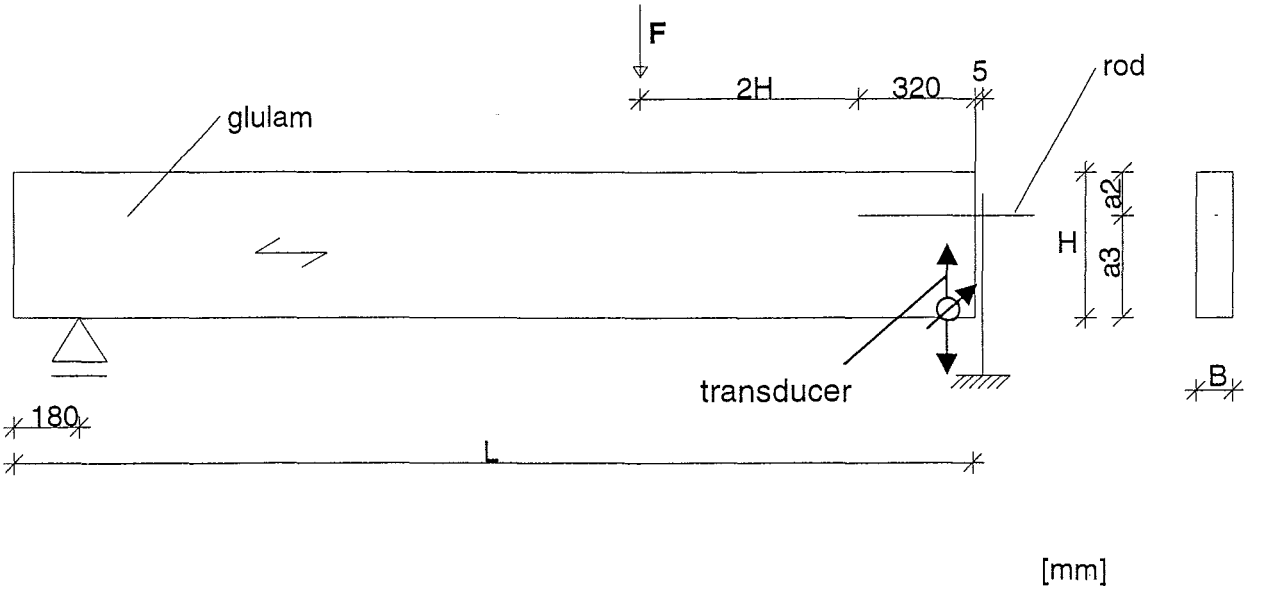

Figure 24: Set-up of the tests with one glued-in rod

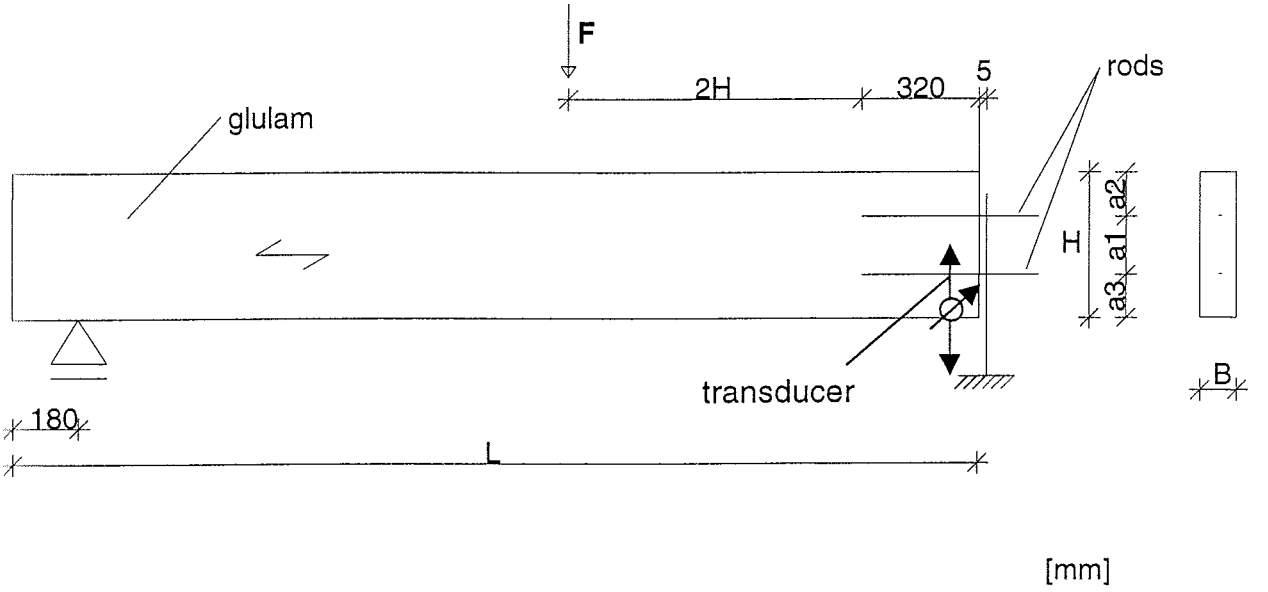

Figure 25: Set-up of the tests with two glued-in rods

4.2 Test Results

The load-displacement curves of all tests are shown in figures 104 to 157 (enclosures 63 to 94). The failure was in most cases first a simultaneous embedding failure of the timber and bending failure of the rod and subsequently almost all specimens failed due to tensile failure pependicular to the grain. Especially in the rods of strength class 4.6 two plastic hinges were formed, one in the timber and the other at the supporting steel plate. With decreasing edge distance a_3 larger embedding displacements were observed. Nevertheless also these specimens failed at last due to tensile failure perpendicular to the grain. Figures 26 and 27 show failed specimens and figure 28 shows an opened specimen after the test.

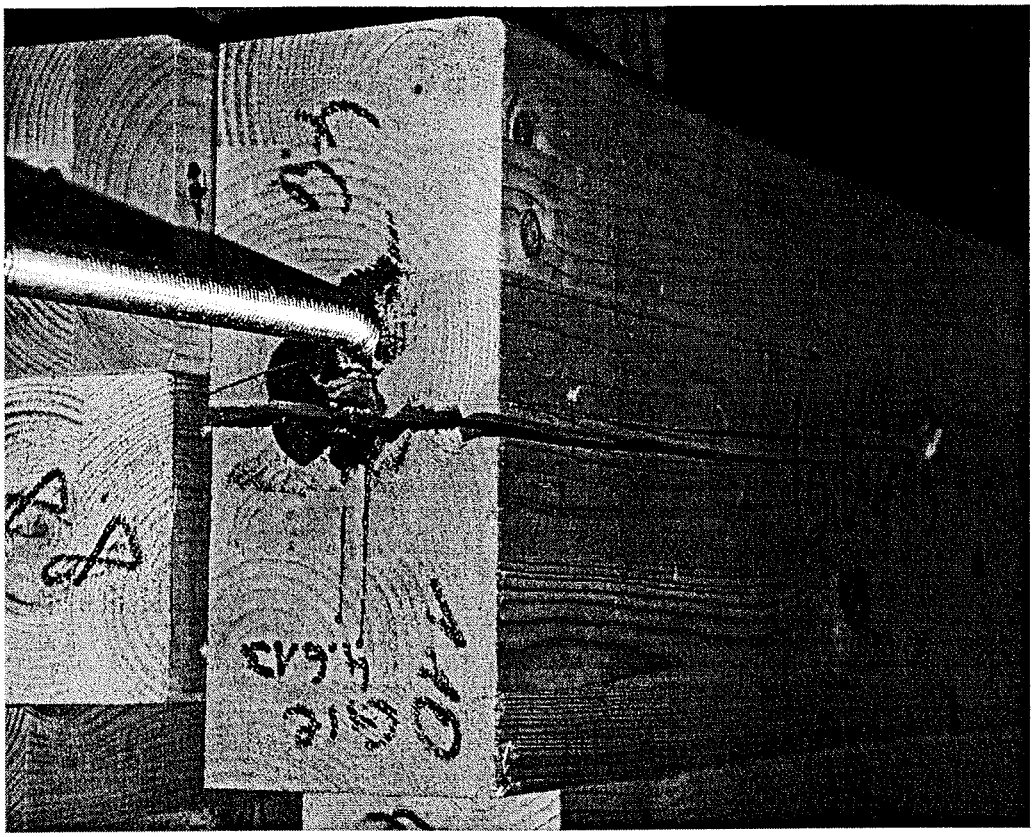

Figure 26: Failed specimen

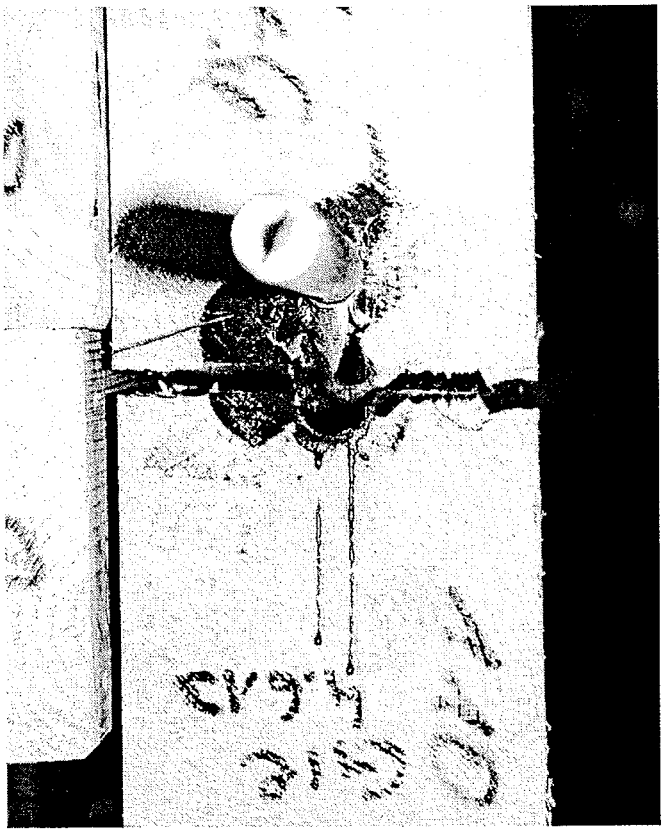

Figure 27: Failed specimen

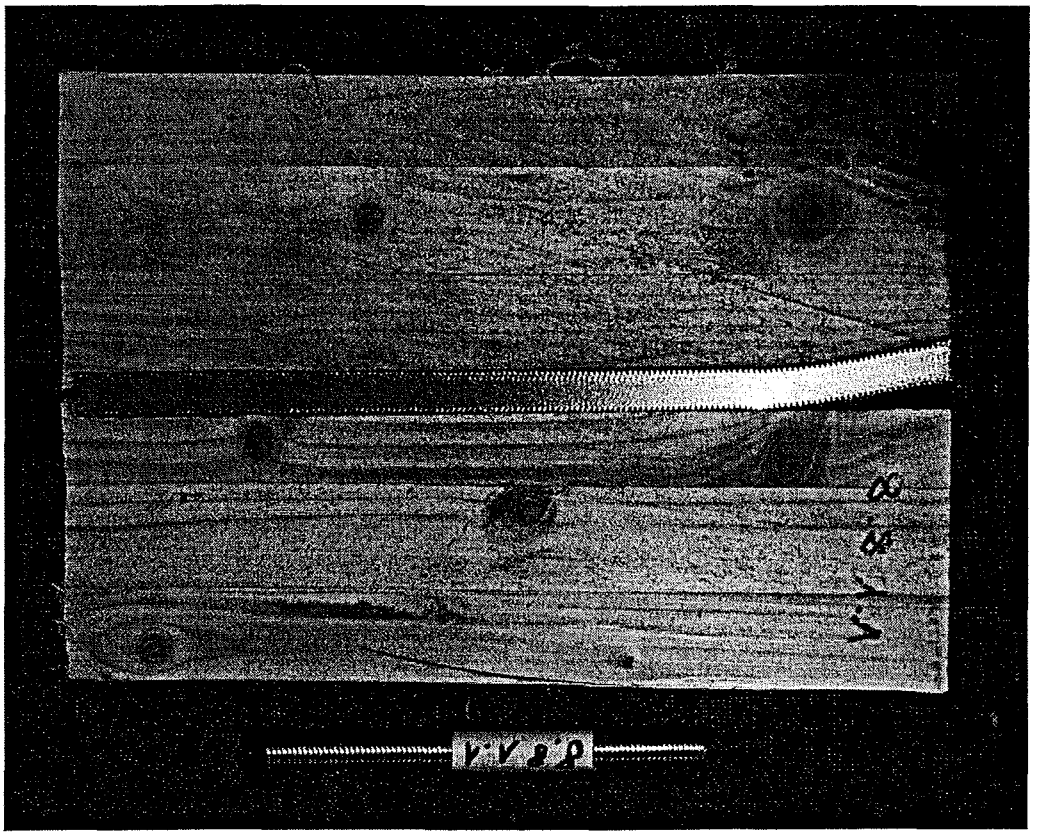

Figure 28: Opened specimen

In table 12 all test results are summarised. The maximum load is the force at the support of the threaded rods. In the tests with two glued in rods the maximum load is the force on both rods. The type of adhesive for all tests was PRF. Additionally the load corresponding to a displacement of 13 mm is given in the table. The displacements are the mean values of two transducers which measure the displacements from the middle of the cross-section to the ground at the end of the beam where the rods are glued-in.

Table 12a: Results of the tests with rods glued-in parallel to the grain and loaded laterally (one rod)

Denotation of Test	F_{max} [kN]	F 13 mm [kN]	α	Height of beam [mm]	Width of beam [mm]	Density [kg/m³]	Moisture Content [%]
Gil4.6-1-1	13.65	-	0.50	220	100	457	11.0
Gil4.6-1-2	19.71	15.53	0.50	220	100	463	11.2
Gil4.6-1-3	20.12	14.13	0.50	220	100	394	11.6
Gil4.6-1-4	25.70	13.92	0.50	220	100	401	11.0
Gil4.6-1-5	13.16	-	0.50	220	100	413	11.0
Mean	18.47	-	-	-	-	426	11.2
Coefficient of Variation [%]	28.1	-	-	-	-	-	-
Gil8.8-1-1	18.38	-	0.50	220	100	462	11.4
Gil8.8-1-2	20.68	-	0.50	220	100	415	11.3
Gil8.8-1-3	25.38	18.42	0.50	220	100	454	11.4
Gil8.8-1-4	20.68	-	0.50	220	100	432	11.1
Mean	21.28	-	-	-	-	441	11.3
Coefficient of Variation [%]	13.8	-	-	-	-	-	-
Gil8.8-6-1	11.20	-	0.17	300	150	435	12.9
Gil8.8-6-2	8.99	-	0.17	300	150	434	12.4
Gil8.8-6-3	10.06	-	0.17	300	150	420	12.4
Gil8.8-6-4	13.29	-	0.17	300	150	422	12.9
Gil8.8-6-5	11.31	-	0.17	300	150	452	13.4
Mean	10.97	-	-	-	-	433	12.8
Coefficient of Variation [%]	14.6	-	-	-	-	-	-

Table 12b: Results of the tests with rods glued-in parallel to the grain and loaded laterally (one rod)

Denotation of Test	F_{max} [kN]	F 13 mm [kN]	α	Height of beam [mm]	Width of beam [mm]	Density [kg/m³]	Moisture Content [%]
Gil8.8-2-1	5.15	-	0.17	300	100	431	12.2
Gil8.8-2-2	6.60	-	0.17	300	100	466	13.7
Gil8.8-2-3	6.35	-	0.17	300	100	468	12.8
Gil8.8-2-4	6.81	-	0.17	300	100	455	12.4
Gil8.8-2-5	5.99	-	0.17	300	100	459	11.9
Mean	6.18	-	-	-	-	456	12.6
Coefficient of Variation [%]	10.6	-	-	-	-	-	-
Gil8.8-3-1	9.47	-	0.33	300	100	463	13.3
Gil8.8-3-2	14.91	-	0.33	300	100	446	14.1
Gil8.8-3-3	13.96	-	0.33	300	100	454	13.9
Gil8.8-3-4	14.18	-	0.33	300	100	470	13.7
Gil8.8-3-5	12.22	11.23	0.33	300	100	440	12.4
Mean	12.95	-	-	-	-	455	13.5
Coefficient of Variation [%]	16.8	-	-	-	-	-	-
Gil8.8-4-1	21.80	12.34	0.50	300	100	422	11.1
Gil8.8-4-2	20.63	14.63	0.50	300	100	464	12.2
Gil8.8-4-3	26.46	17.68	0.50	300	100	428	10.7
Gil8.8-4-4	17.21	-	0.50	300	100	452	12.2
Gil8.8-4-5	17.00	14.21	0.50	300	100	447	10.9
Mean	20.62	-	-	-	-	443	11.4
Coefficient of Variation [%]	18.8	-	-	-	-	-	-
Gil8.8-5-1	27.96	17.54	0.67	300	100	436	12.1
Gil8.8-5-2	26.65	13.14	0.67	300	100	427	12.6
Gil8.8-5-3	24.32	15.39	0.67	300	100	439	12.7
Gil8.8-5-4	20.93	13.51	0.67	300	100	423	12.4
Gil8.8-5-5	22.54	14.36	0.67	300	100	435	12.7
Mean	24.48	-	-	-	-	432	12.5
Coefficient of Variation [%]	11.8	-	-	-	-	-	-

Table 12c: Results of the tests with rods glued-in parallel to the grain and loaded laterally (two rods)

Denotation of Test	F_{max} [kN]	F 13 mm [kN]	A	Height of beam [mm]	Width of beam [mm]	Density [kg/m³]	Moisture Content [%]
GilII-1-1	18.32	-	0.33	400	100	438	11.2
GilII-1-2	17.60	-	0.33	400	100	465	11.3
GilII-1-3	19.40	-	0.33	400	100	451	11.6
GilII-1-4	16.90	-	0.33	400	100	440	11.7
GilII-1-5	14.53	-	0.33	400	100	427	11.5
Mean	17.35	-	-	-	-	444	11.4
Coefficient of Variation [%]	10.5	-	-	-	-	-	-
GilII-2-1	24.50	-	0.45	400	100	448	11.3
GilII-2-2	28.90	-	0.45	400	100	430	11.3
GilII-2-3	31.54	28.65	0.45	400	100	461	11.7
GilII-2-4	29.86	-	0.45	400	100	436	11.2
GilII-2-5	25.24	-	0.45	400	100	465	11.4
Mean	28.01	-	-	-	-	448	11.4
Coefficient of Variation [%]	10.8	-	-	-	-	-	-
GilII-3-1	29.57	28.34	0.58	400	100	454	11.2
GilII-3-2	24.55	-	0.58	400	100	429	11.0
GilII-3-3	38.60	27.12	0.58	400	100	446	11.3
GilII-3-4	28.82	26.78	0.58	400	100	444	11.5
GilII-3-5	14.77	-	0.58	400	100	445	11.8
Mean	27.26	-	-	-	-	444	11.3
Coefficient of Variation [%]	31.8	-	-	-	-	-	-
GilII-4-1	33.61	28.12	0.70	400	100	450	11.4
GilII-4-2	34.26	27.68	0.70	400	100	433	11.4
GilII-4-3	33.55	29.15	0.70	400	100	470	11.6
GilII-4-4	48.29	28.84	0.70	400	100	423	11.3
GilII-4-5	47.76	30.54	0.70	400	100	461	11.5
Mean	39.49	-	-	-	-	447	11.4
Coefficient of Variation [%]	19.8	-	-	-	-	-	-

Table E1 in enclosures 95 and 96 contains values of the plastic moments of the rods. Parallel tests were performed to study the influence of the rod steel grade on the load-carrying capacity. Threaded rods of strength class 4.6 and 8.8 were used. Figures 29 and 30 show the test results with one or two rods, respectively. With

decreasing edge distance a_3 the load-carrying capacity rises and the failure mode is increasingly determined by the embedding strength of the timber and the bending capacity of the rod. Nevertheless at the end of the test almost all specimens failed due to tensile failure perpendicular to the grain. For larger edge distances a_3 the tensile strength perpendicular to the grain was reached earlier and with smaller embedding deformations.

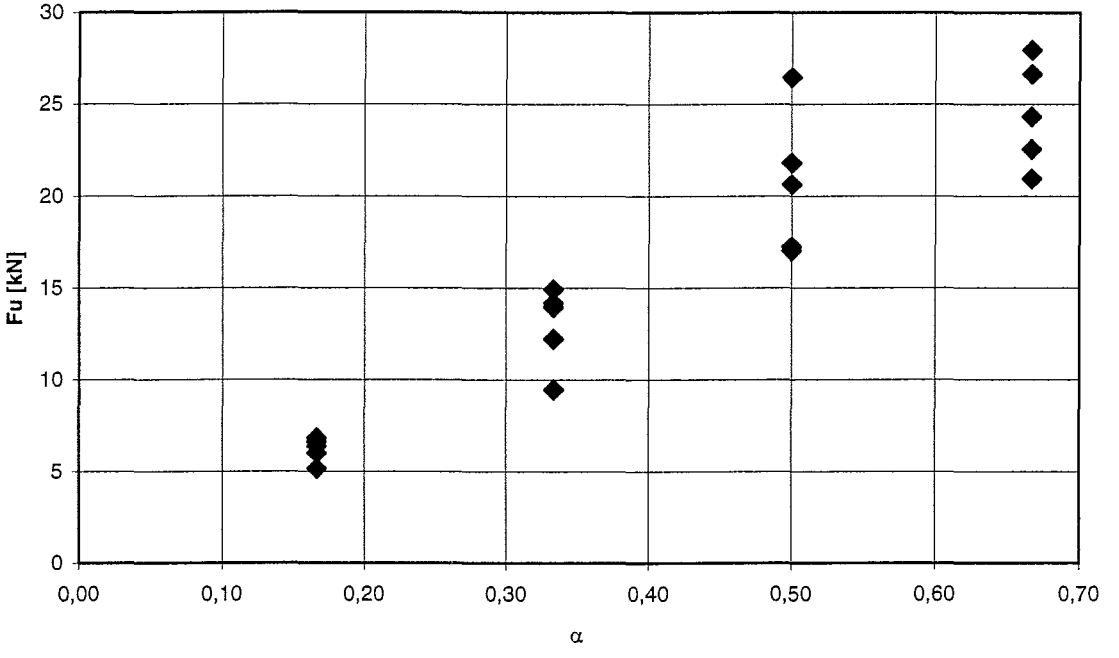

Figure 29: Test results (one rod) versus ratio α

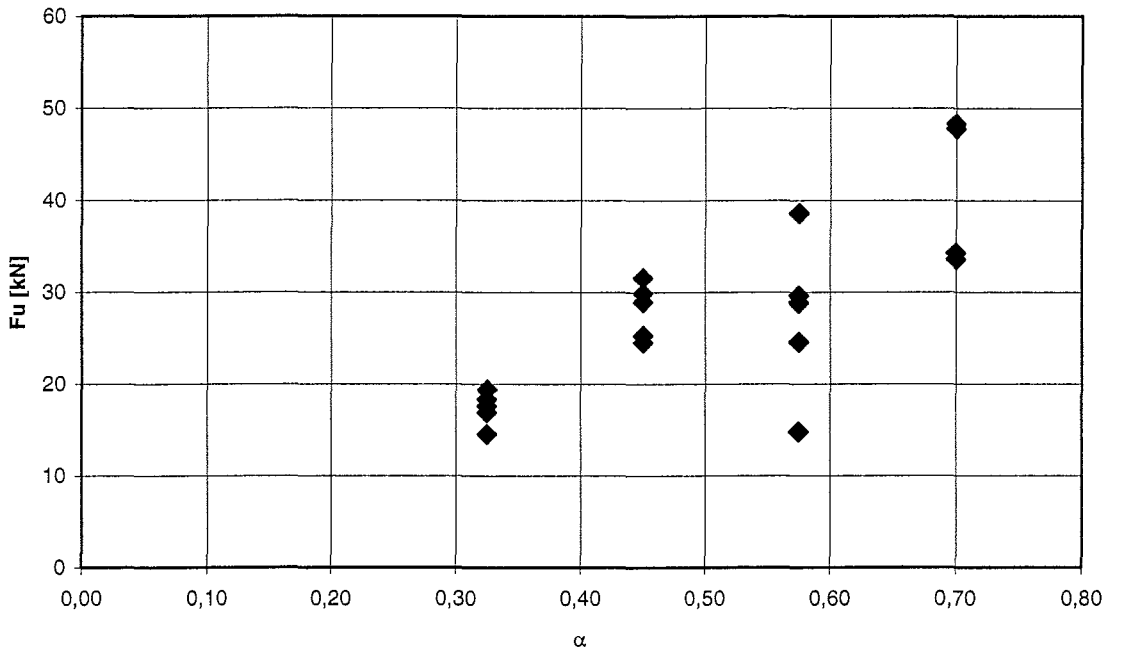

Figure 30: Test results (two rods) versus ratio α

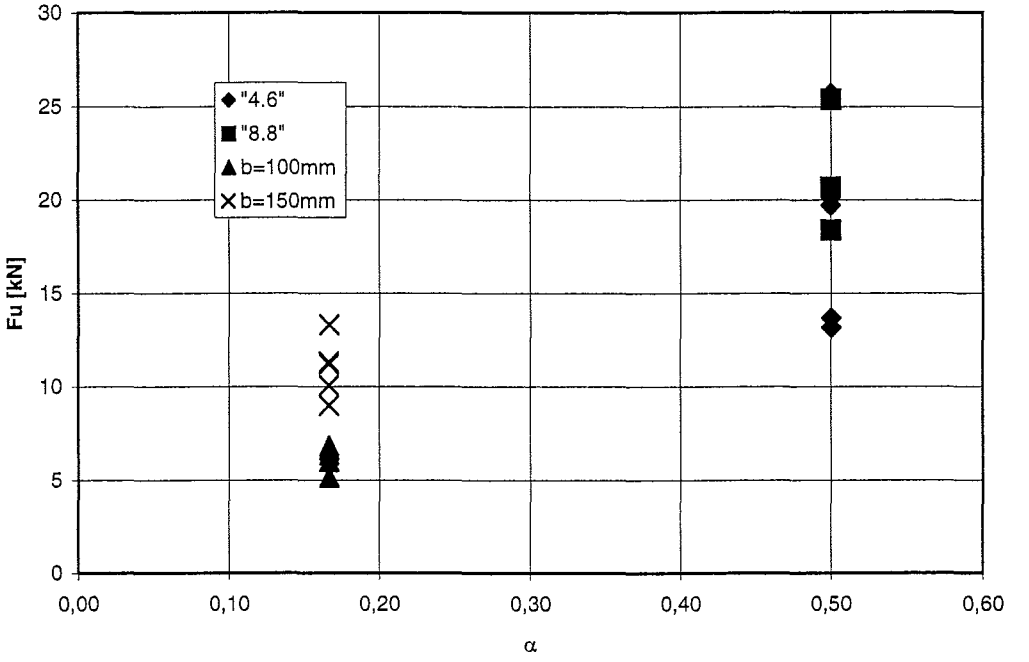

Figure 31: Comparison of different test results

Figure 31 presents a comparison of different test results with one glued-in rod. For a small ratio α the beam width was varied. The load-carrying capacities of the wider

specimens are higher. A reason for this is that the fracture area of these specimens is larger. Therefore more fracture energy is necessary to split the timber and larger ultimate loads result.

The comparison of different steel qualities does not show significantly different failure loads for strength classes 4.6 and 8.8. The mean value of the tests with rods 4.6 were slightly lower than those with a steel grade 8.8. An explanation could be that the most frequent failure mechanism was reaching the tensile strength perpendicular to the grain. Consequently, the embedding strength of the timber was not the governing parameter. Hence, the steel quality has hardly any influence for the described failure mechanism. However, for smaller values a_3 the rod steel grade will increasingly influence the load-carrying capacity, since embedding strength and bending capacity then mainly determine the failure mode.

4.3 Theoretical Investigations

Similar to the preceding paragraph concerning the rods glued-in perpendicular to the grain the equations based on the work of Görlacher [3] were used to calculate the load-carrying capacity for failures caused by splitting of the timber. The simplified equations from the draft DIN 1052 [5] were used. To describe the behaviour of the threaded rods in the case of smaller edge distances a_3 the Johansen theory [7] was used.

First the design rules given in the draft DIN 1052 are presented. The load-carrying capacity is reduced by 50%, because similiar to the tests with rods glued-in perpendicular to the grain no tensile stresses are carried outside of the timber. The parameter a_r giving the width of the connection is assumed as the distance of the plastic hinge from the end grain surface.

The load-carrying capacity of a rod glued-in parallel to the grain is given as

$$R_{90} = 0.5 \cdot k_s \cdot k_r \cdot \left(6.5 + \frac{18a^2}{H^2}\right)(t_{ef} H)^{0.8} \qquad (5)$$

where $$k_s = \max\left\{0.7 + \frac{1}{1.4a_r}\right.$$

$$k_r = \frac{n}{\sum_{i=1}^{n}\left(\frac{h_1}{h_i}\right)^2}$$

a: $a = H - a_3$ in mm

a_r: Distance from the end grain to the plastic hinge of the rod according to the theory of Johansen

H: Height of the beam

$$t_{ef} = \min\begin{cases} B \\ 6d \end{cases}$$

B: Width of the beam

d: Outer diameter of the rod

n: Number of rods

h_i: Distance of the rod i from the lower edge.

Based on the theory of Johansen [7] equations were derived where a gap between the end grain and the support was taken into account. Only the failure mechanism with two plastic hinges was regarded because of the failure mode observed in the tests, caused by the clamped support of the rods. The distance of the plastic hinge to the end grain is

$$b_1 = -t + \sqrt{t^2 + 4\frac{M_y}{f_{h,1}d}} \qquad (6)$$

The load-carrying capacity results as

$$R = f_{h,1} d b_1 \qquad (7)$$

where $M_y = 0.26 \cdot f_u \cdot d_m^{2.7}$ (according to the draft DIN 1052)

f_u: Tensile strength of the steel

d_m: Mean of the outer diameter and the core diameter of the rod

$f_{h,1}$: Timber embedding strength according to the draft DIN 1052

t: Distance from the end grain to the support.

With characteristic values for the embedding strength and the fastener yield moment, respectively, b_1 according to equation (6) results as b_1 = 137 mm. Here, the embedding strength for rods arranged parallel and loaded perpendicular to the grain is assumed as 10 % of the embedding strength of rods arranged perpendicular and loaded parallel to the grain. Because of the adhesive between rod and surrounding timber and the subsequent friction between fastener and wood, the embedding strength is then increased by 25%. The corresponding load-carrying capacity was

multiplied by two because of the tensile forces in the inclined part of the fastener, not taken into account in the Johansen theory. DIN 1052 suggests this increase in load-carrying capacity to be 25% of the axial load-carrying capacity for screws but not more than 100 % of the load-carrying capacity according to Johansen. For glued-in rods the limit of the 100 % increase always applies.

Figure 32 and 33 show the test results with one or two rods, respectively, compared with the calculations based on characteristic values. The suggested equations fit the test results quite well. Only for very small ratios α the calculated results are not conservative. However, Görlacher's model is limited to ratios $\alpha > 0{,}2$. Considering this limit, only one test result yields a value below the calculated curve. Therefore the minimum of the results according to equations 5 and 7 is proposed as the characteristic load-carrying capacity of rods glued-in parallel to the grain and loaded laterally, but limited to $\alpha > 0{,}2$.

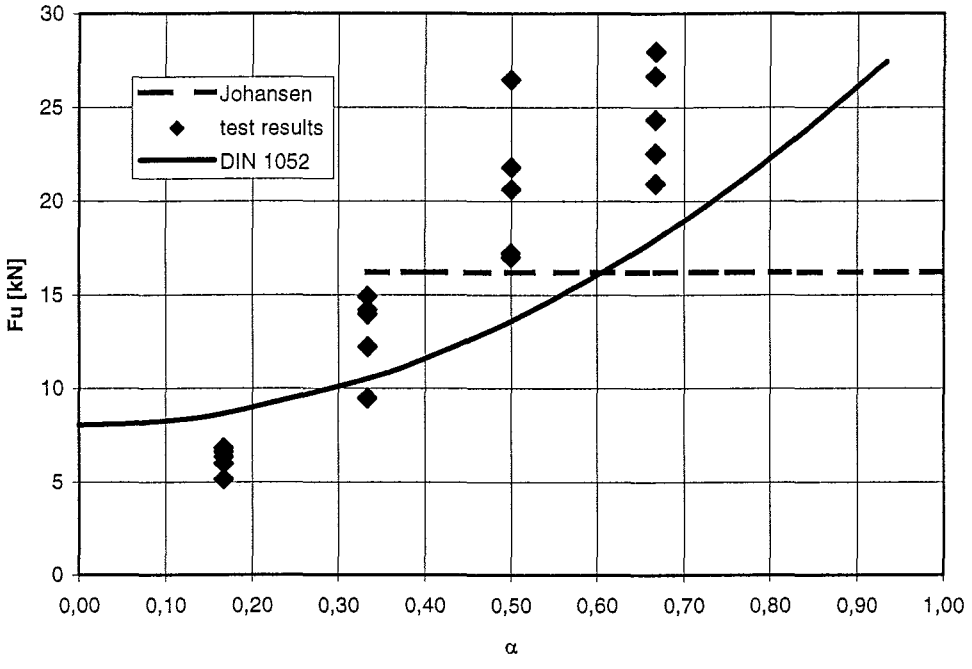

Figure 32: Test results with one rod compared with calculation models

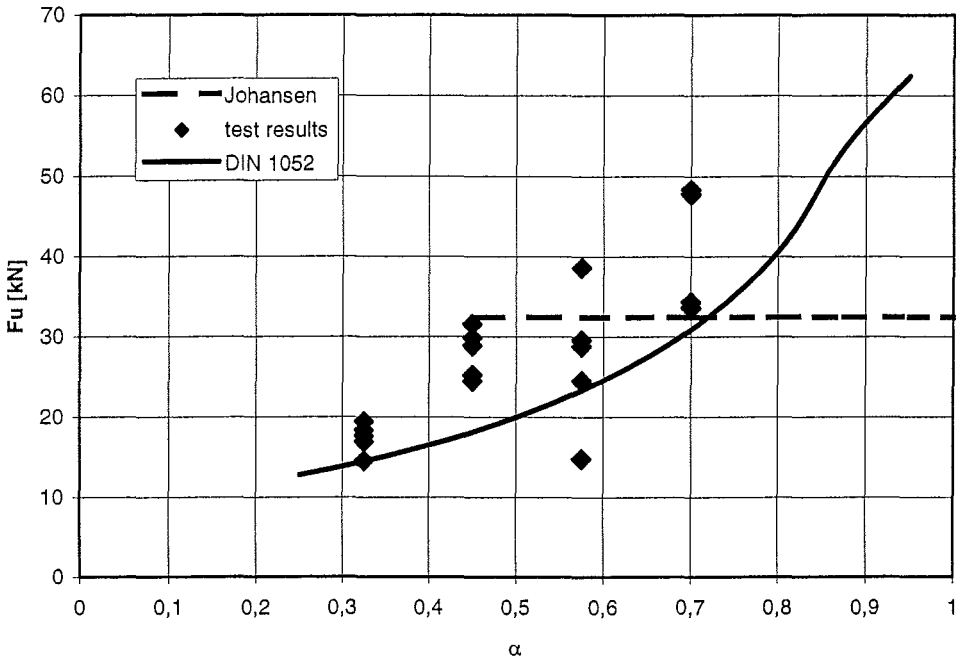

Figure 33: Test results with two rods compared with calculation models

5 Conclusion

The objective of the third working package of GIROD was to study and to quantify the effect of the spacing between rods and the distance to the timber edges on the axial and lateral load-carrying capacity. Hence University of Karlsruhe performed tests with glued-in rods parallel and perpendicular to the grain loaded axially as well as laterally. Furthermore theoretical investigations were carried out to describe the behaviour of glued-in rods depending on spacings and distances of rods.

In addition to this it was possible to propose design equations for rods glued-in parallel and perpendicular to the grain and loaded laterally and axially. Minimum distances to the timber edge and spacings for rods are also suggested.

References

[1] Aicher, S., Höfflin, L., Wolf, M. *Influence of Specimen Geometry on Stress Distributions in Pull-Out Tests of Glued-In Steel Rods in Wood.* Otto Graf Journal, Vol. 9 1998, Forschungs- und Materialprüfungsanstalt Baden-Württemberg FMPA

[2] Blaß, H.J., Laskewitz, B. *Effect of Spacing and Edge Distance on the Axial Strength of Glued-In Rods.* CIB-W18A, proceedings, Graz, Austria 1999

[3] Ehlbeck, J., Görlacher, R., Werner, H. *Determination of perpendicular-to-grain tensile stresses in joints with dowel-type fasteners; a draft proposal for design rules.*CIB-W18A, proceedings, Berlin, GDR 1989

[4] Eurocode 5: Design of Timber Structures

[5] Draft of DIN 1052, May, 2000

[6] Blaß, H.J., Ehlbeck, J.; Görlacher, R. *Zur Berechnung von Balkenschuhen nach Eurocode 5.* Bauen mit Holz 102 Vol. 6 p. 33-35, Vol. 7 p. 36-39, 2000

[7] Johansen, K.W. *Theory of Timber Connections* International Association for Bridge and Structural Engineering, Vol. 9, p.249-262

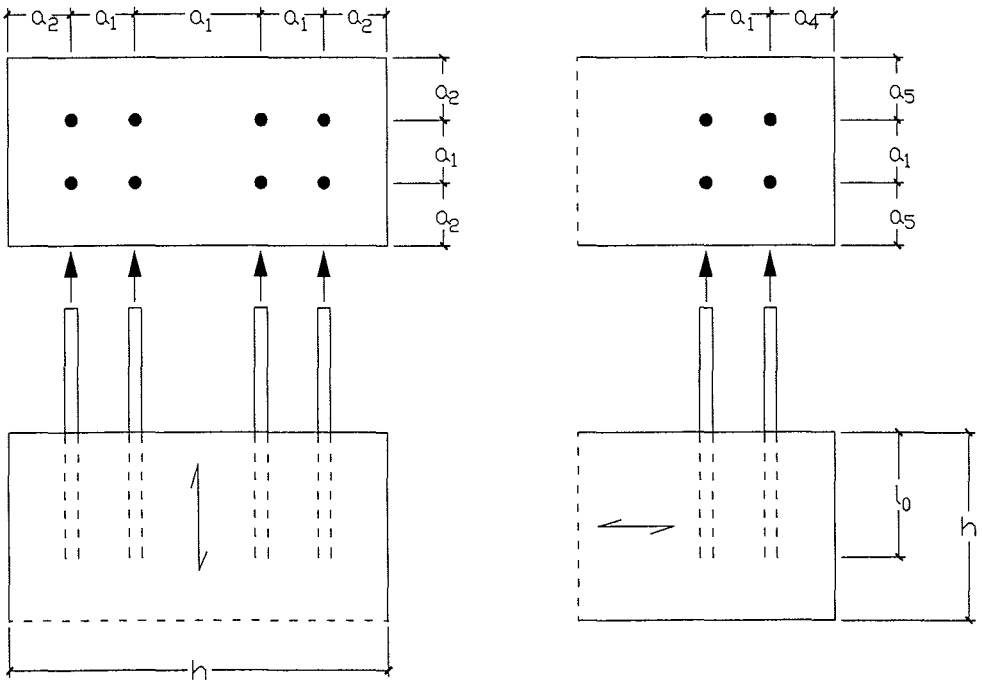

Figure 1: Definitions of spacings and distances

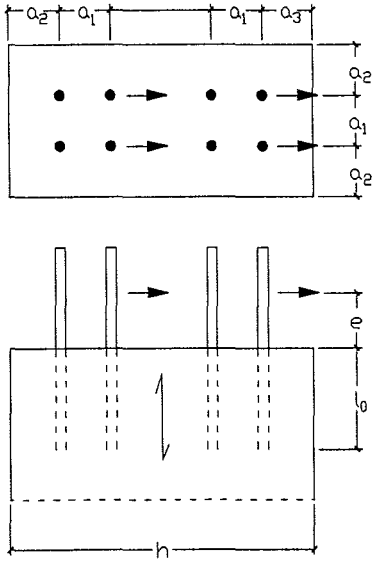

Figure 2: Definitions of spacings and distances

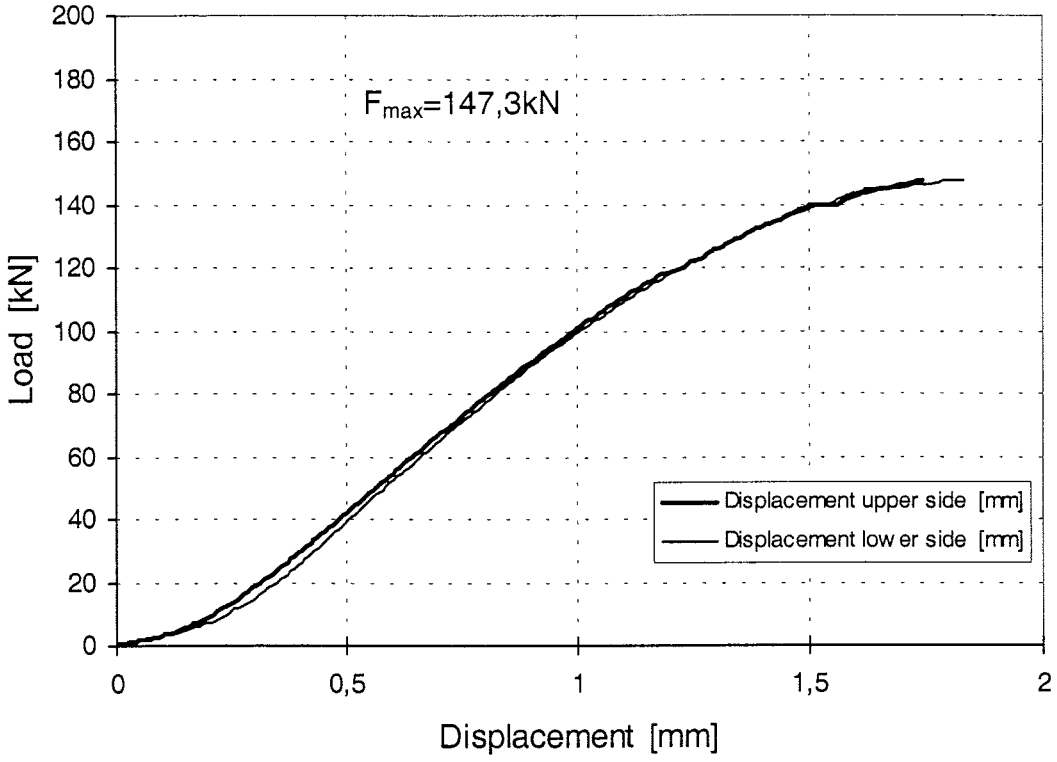

Figure 3: Load-displacement-curve of test Gi1-1

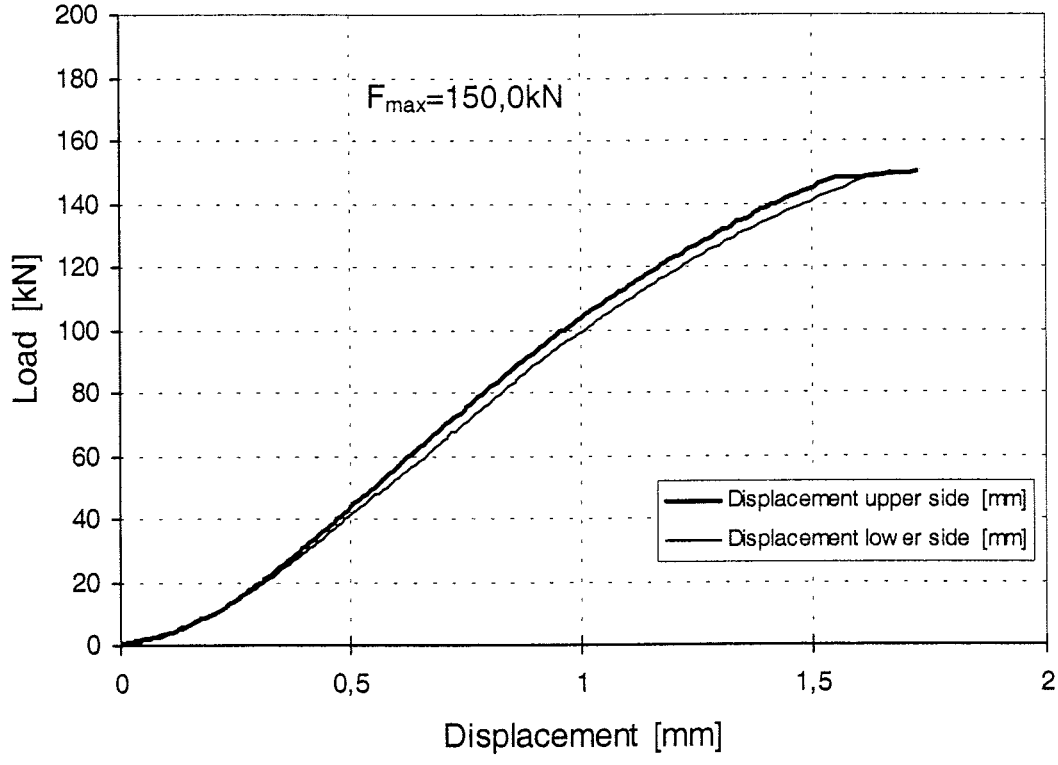

Figure 4: Load-displacement-curve of test Gi1-2

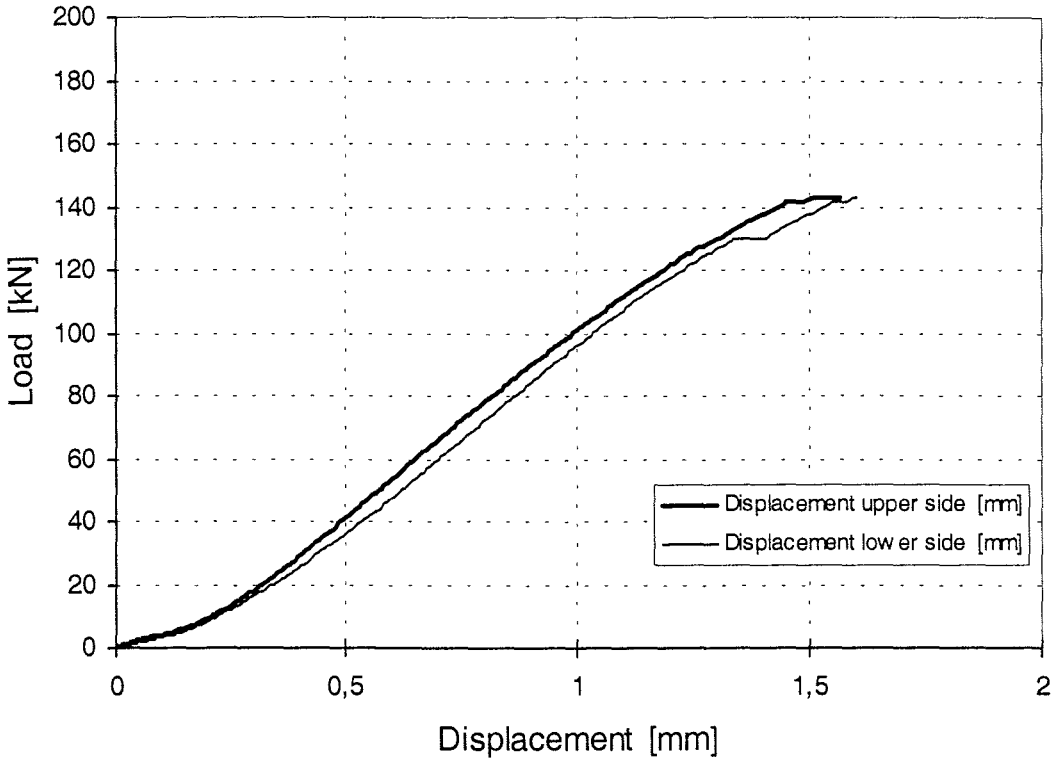

Figure 5: Load-displacement-curve of test Gi1-3

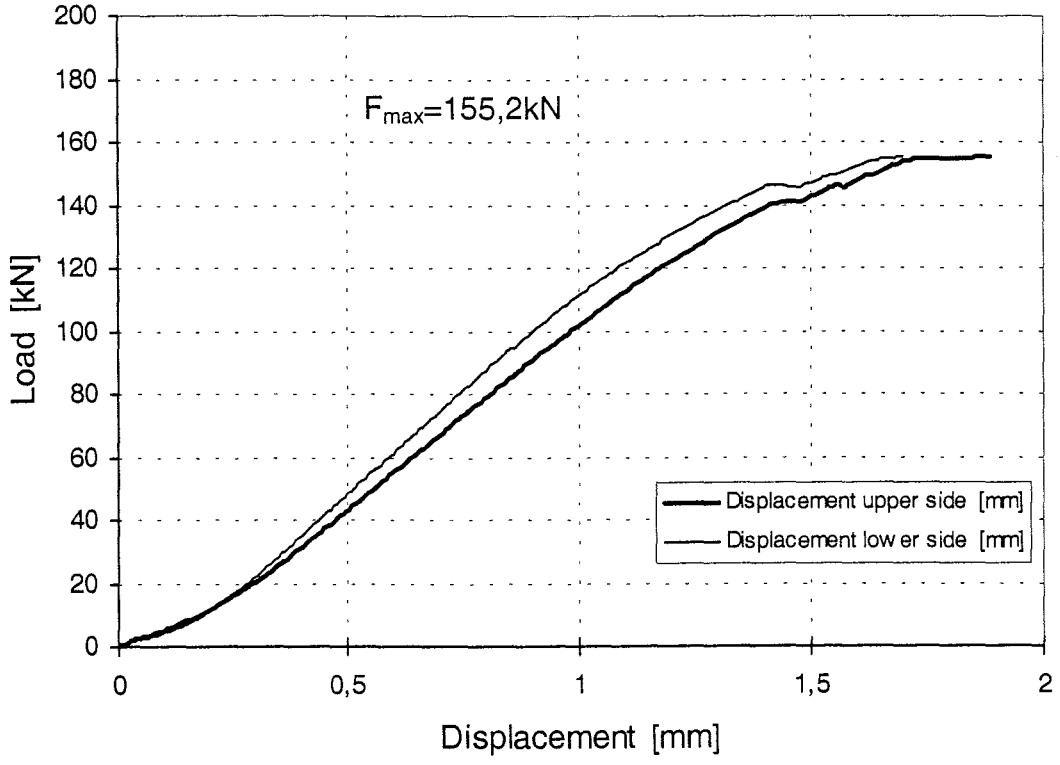

Figure 6: Load-displacement-curve of test Gi1-4

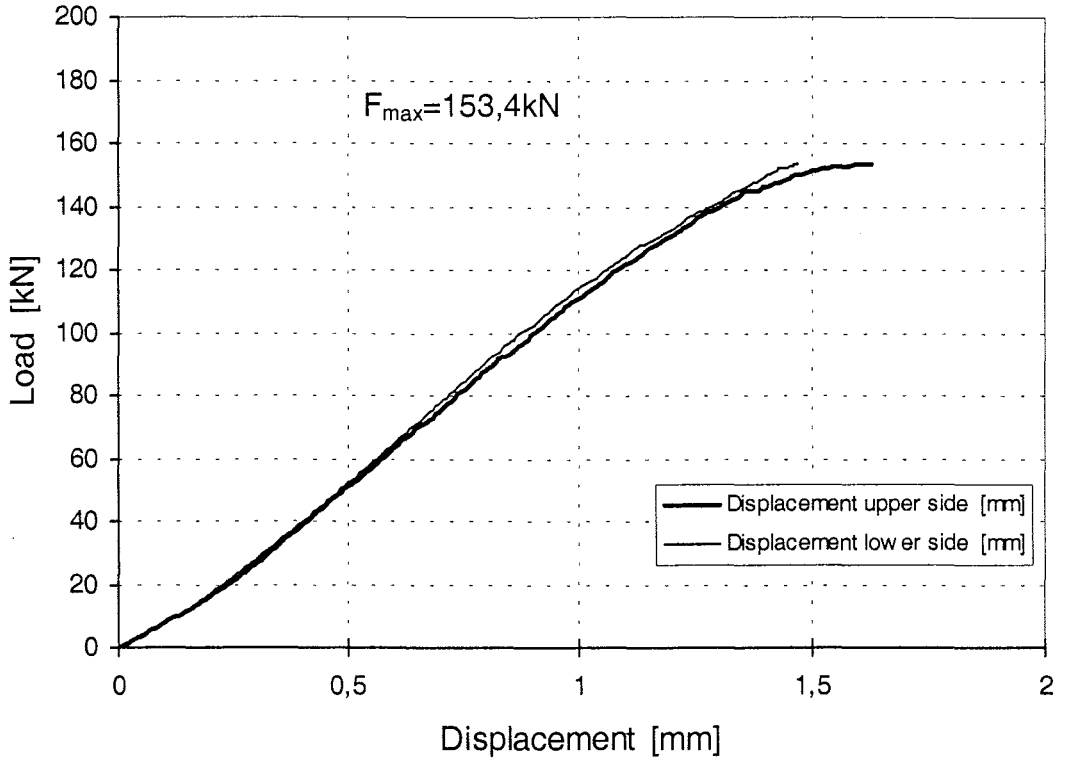

Figure 7: Load-displacement-curve of test Gi1-5

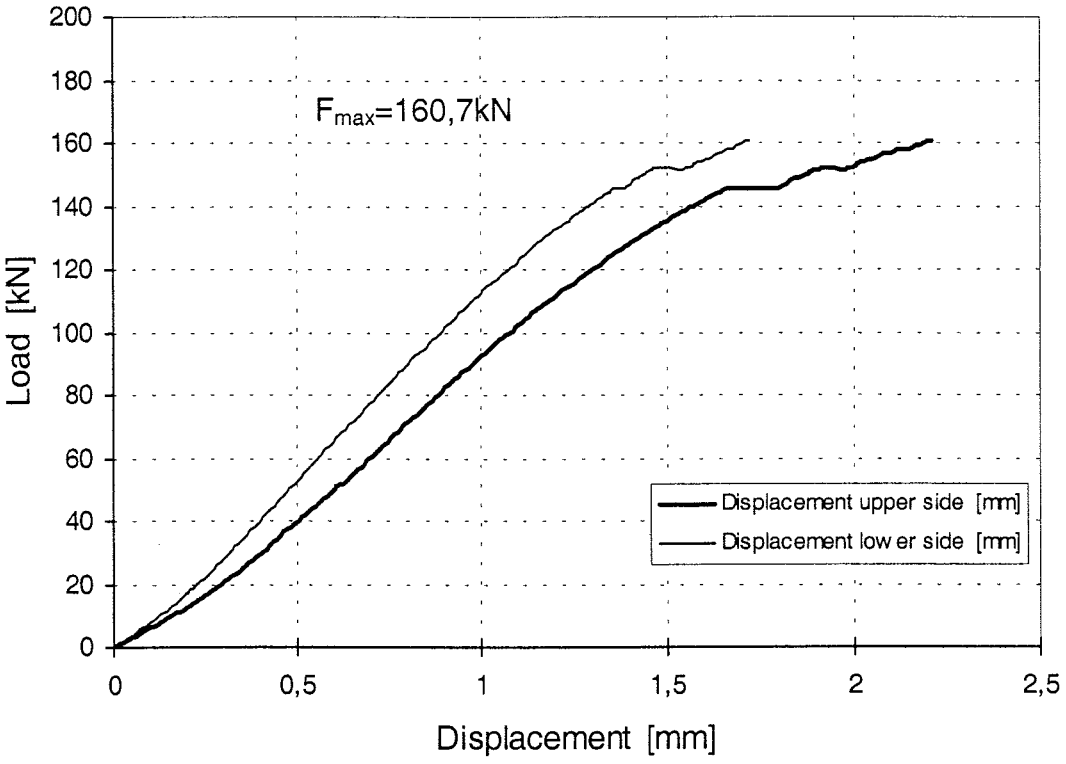

Figure 8: Load-displacement-curve of test Gi2-1

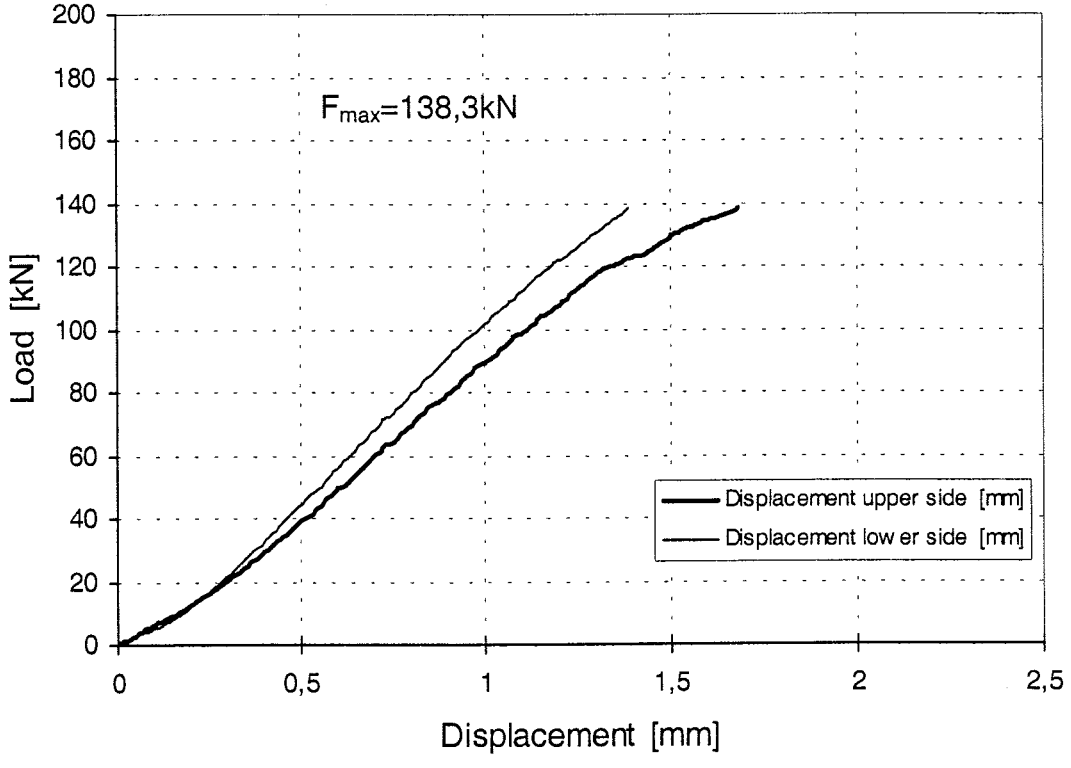

Figure 9: Load-displacement-curve of test Gi2-2

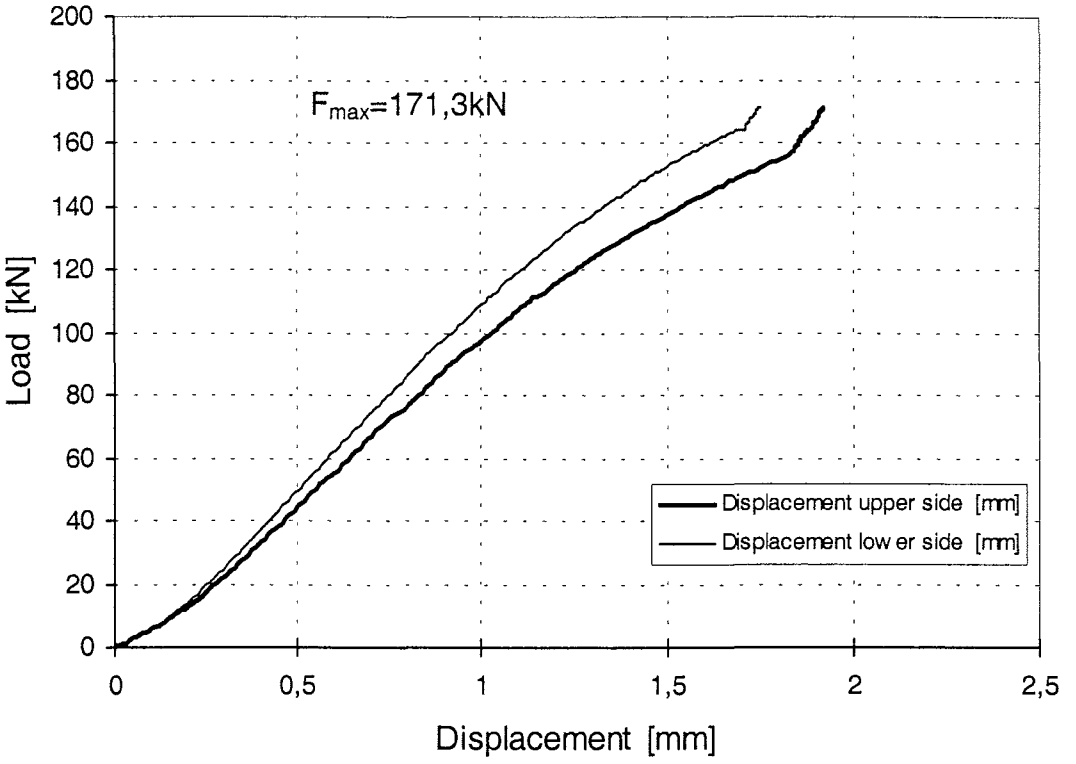

Figure 10: Load-displacement-curve of test Gi2-3

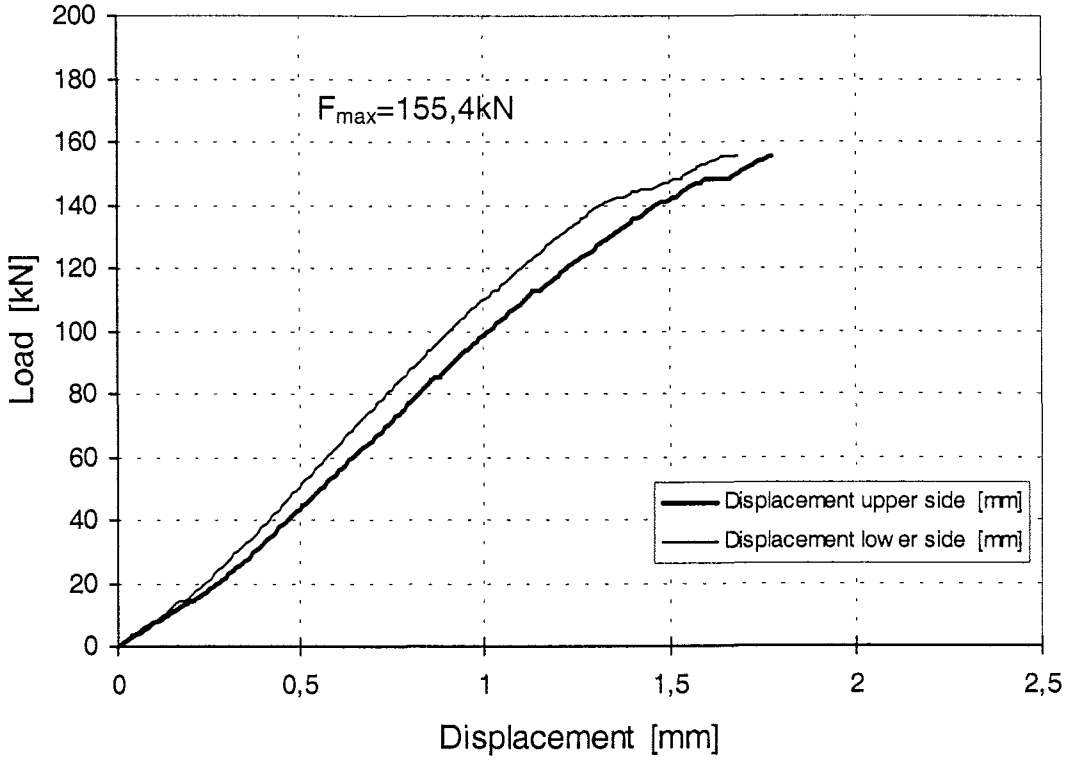

Figure 11: Load-displacement-curve of test Gi2-4

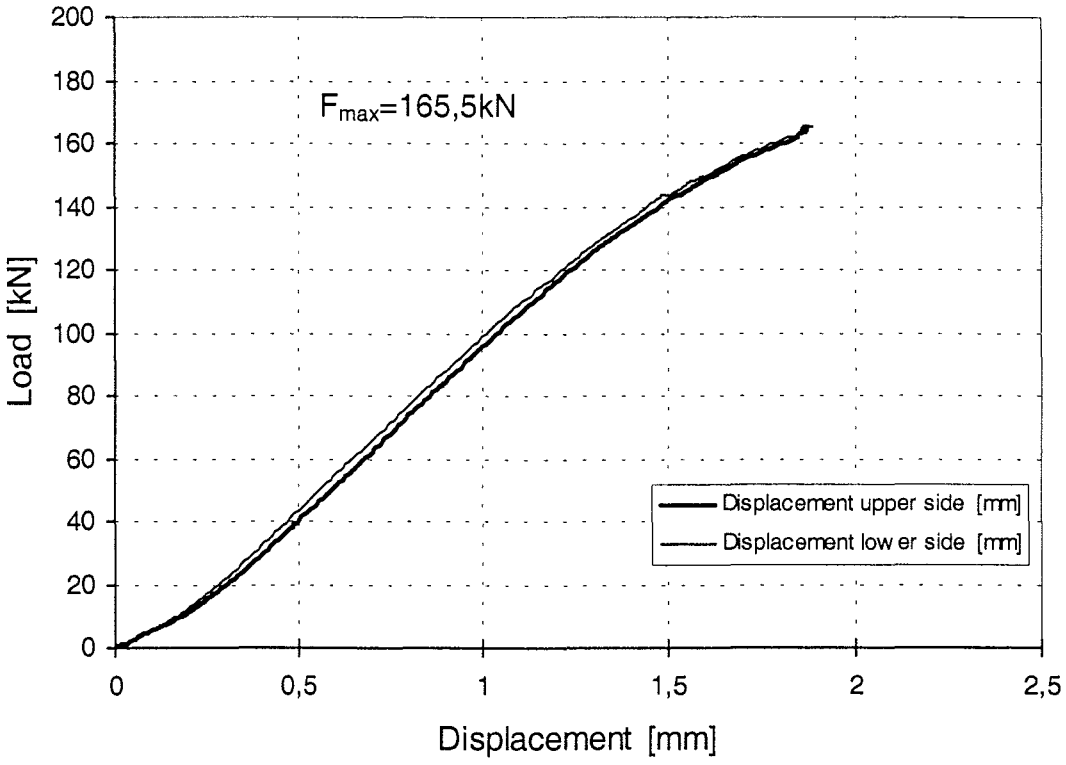

Figure 12: Load-displacement-curve of test Gi2-5

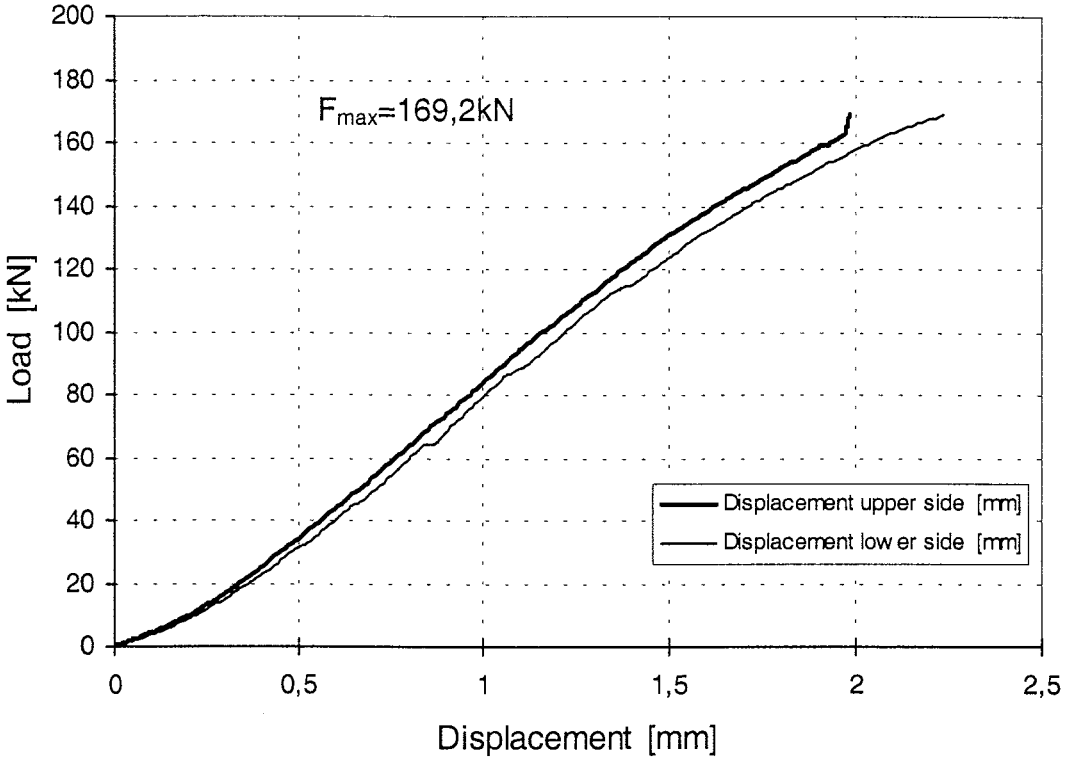

Figure 13: Load-displacement-curve of test Gi3-1

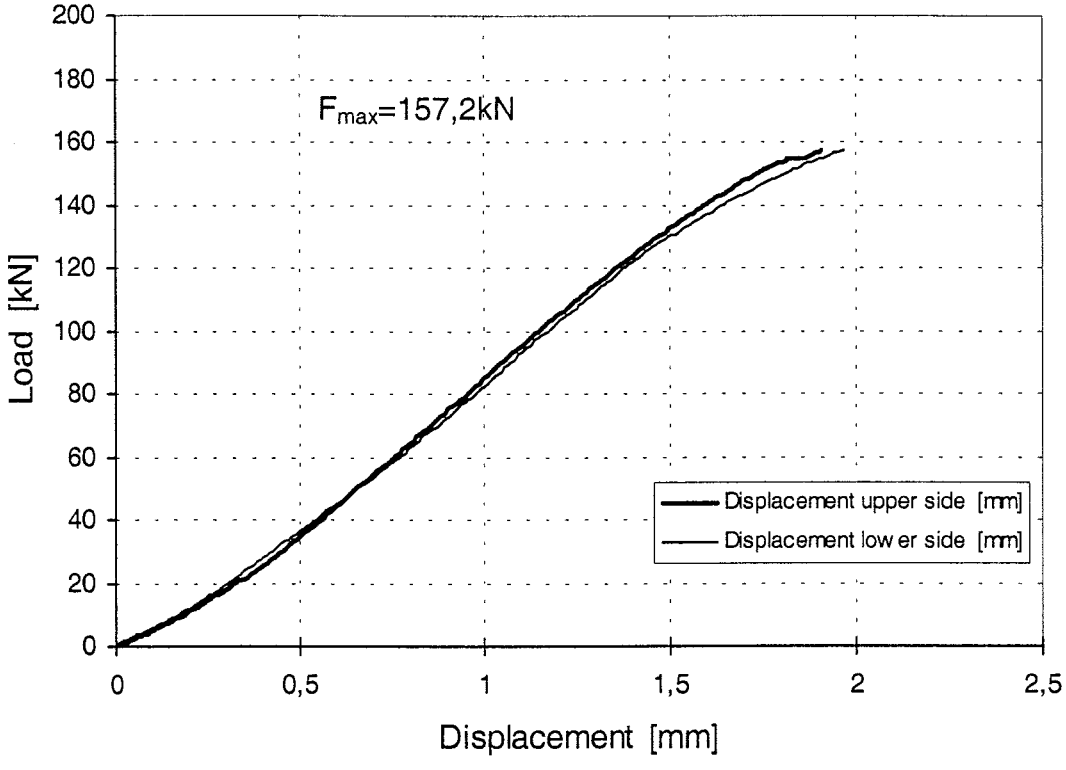

Figure 14: Load-displacement-curve of test Gi3-2

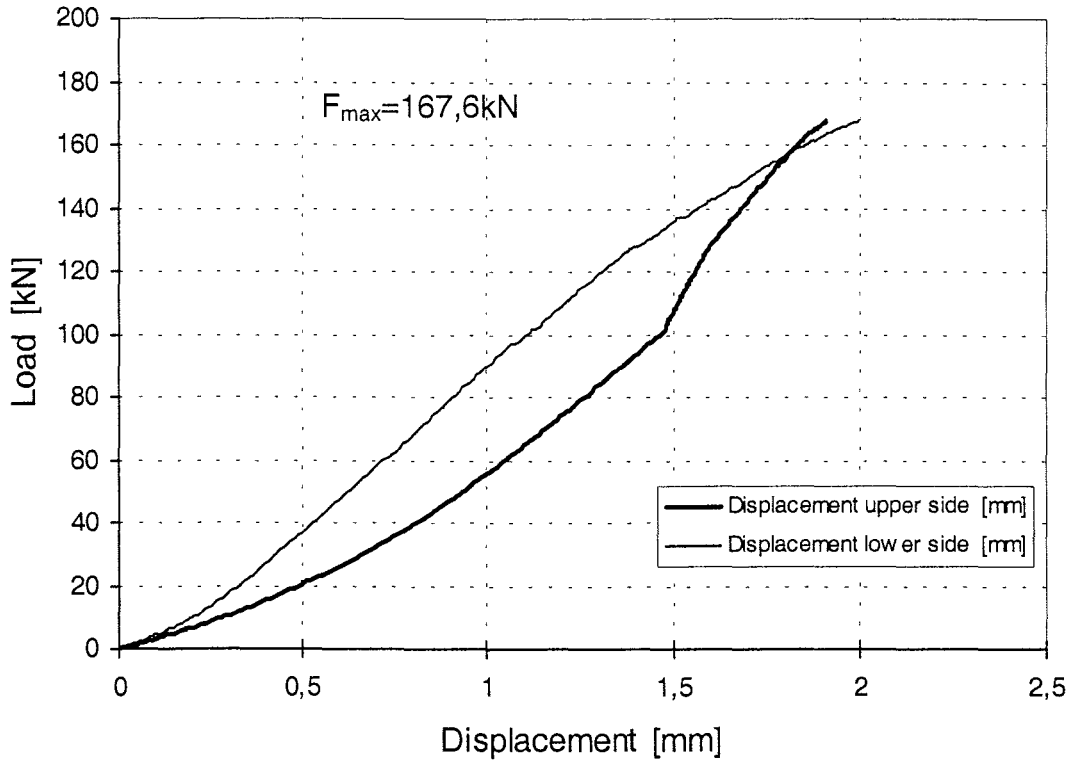

Figure 15: Load-displacement-curve of test Gi3-3

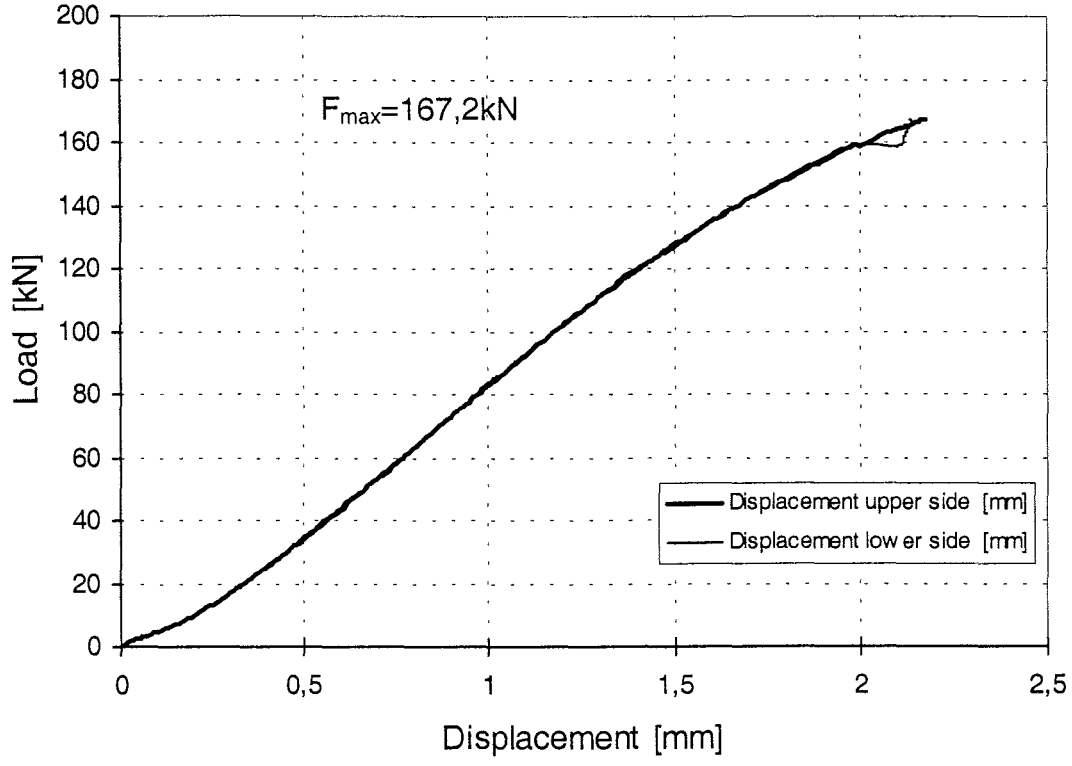

Figure 16: Load-displacement-curve of test Gi3-4

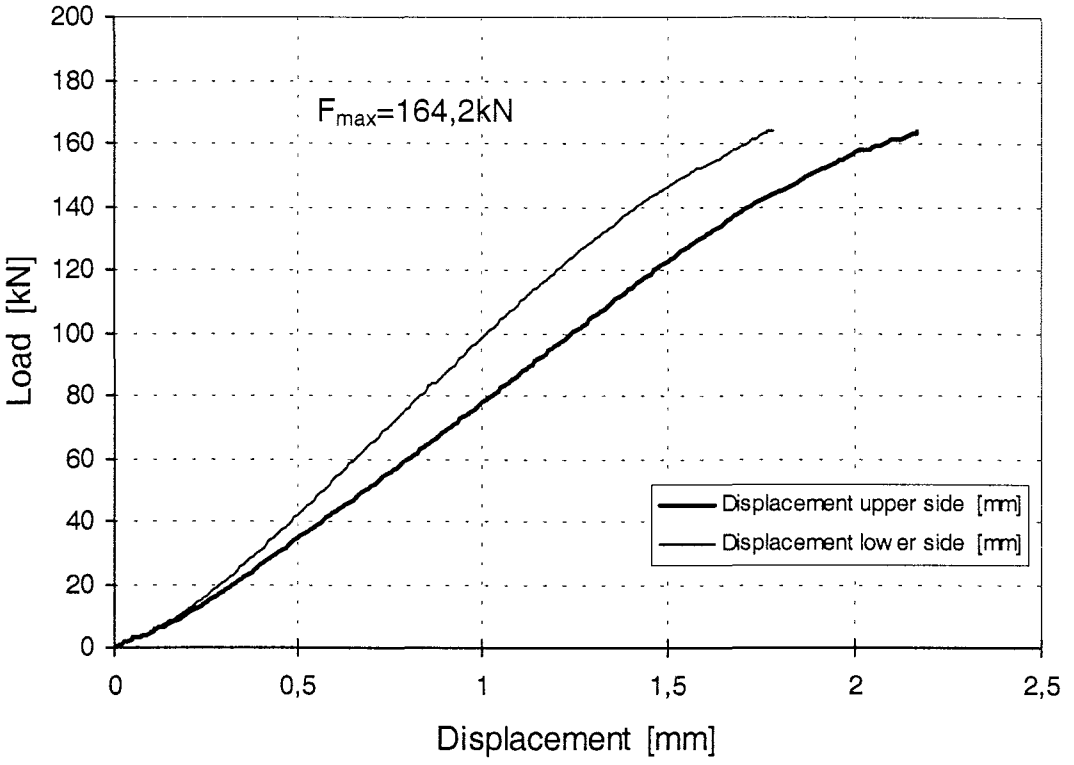

Figure 17: Load-displacement-curve of test Gi3-5

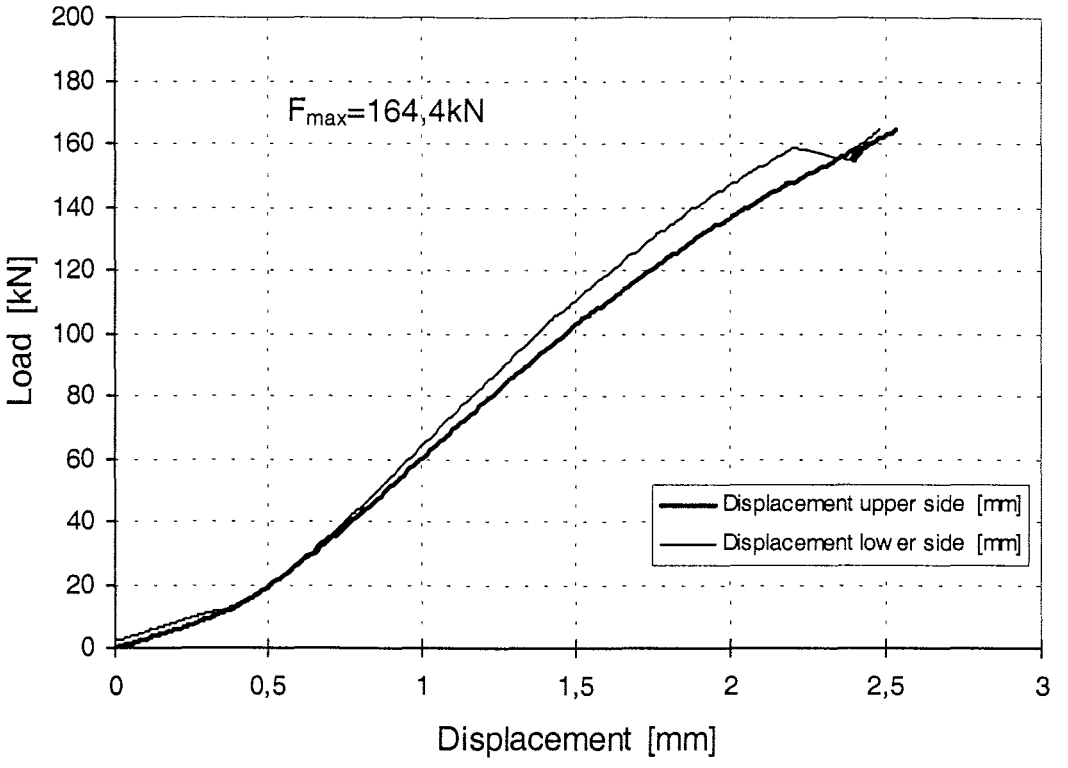

Figure 18: Load-displacement-curve of test Gi4-1

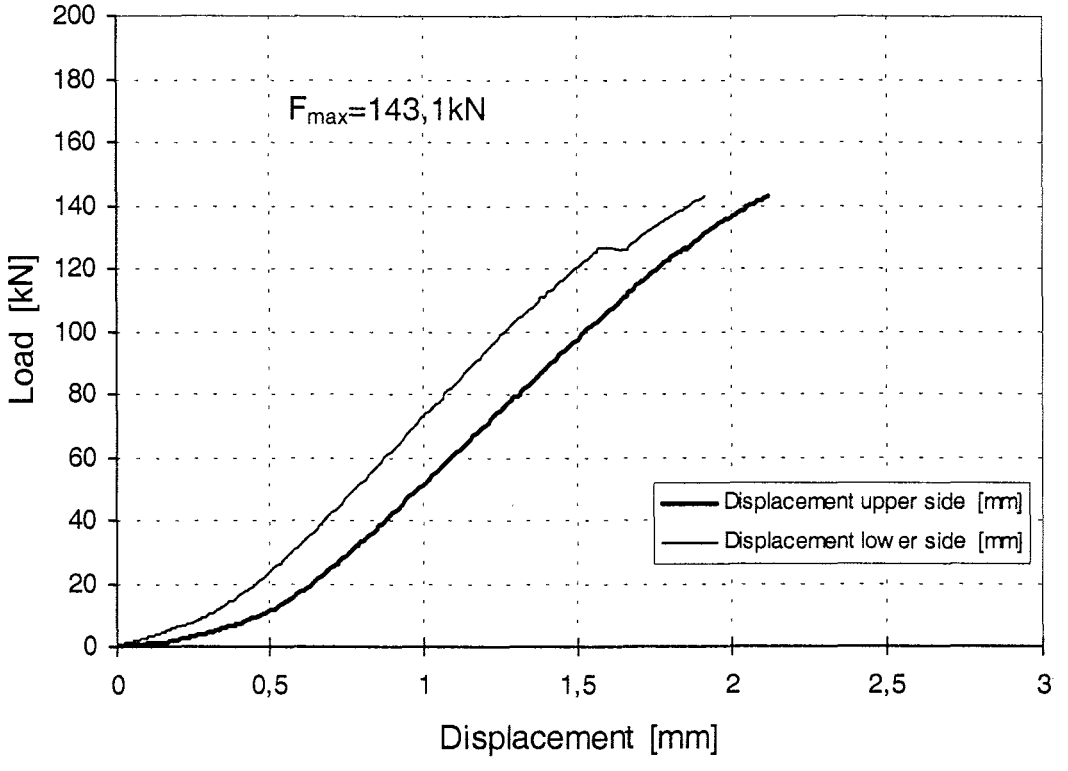

Figure 19: Load-displacement-curve of test Gi4-2

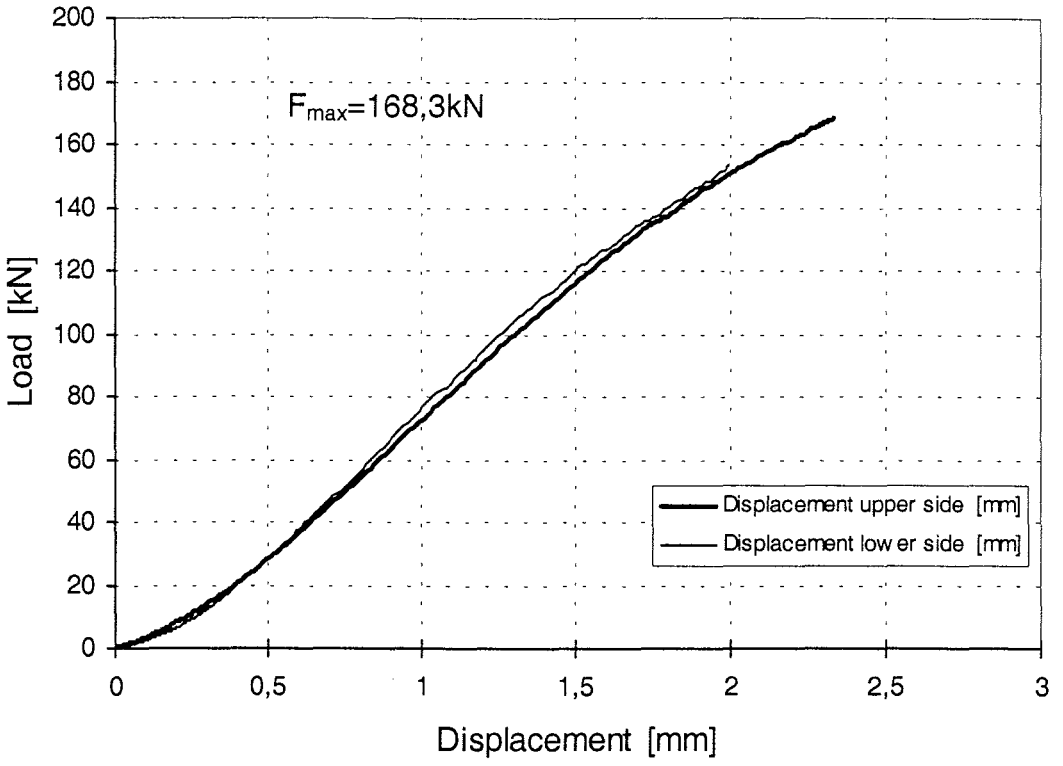

Figure 20: Load-displacement-curve of test Gi4-3

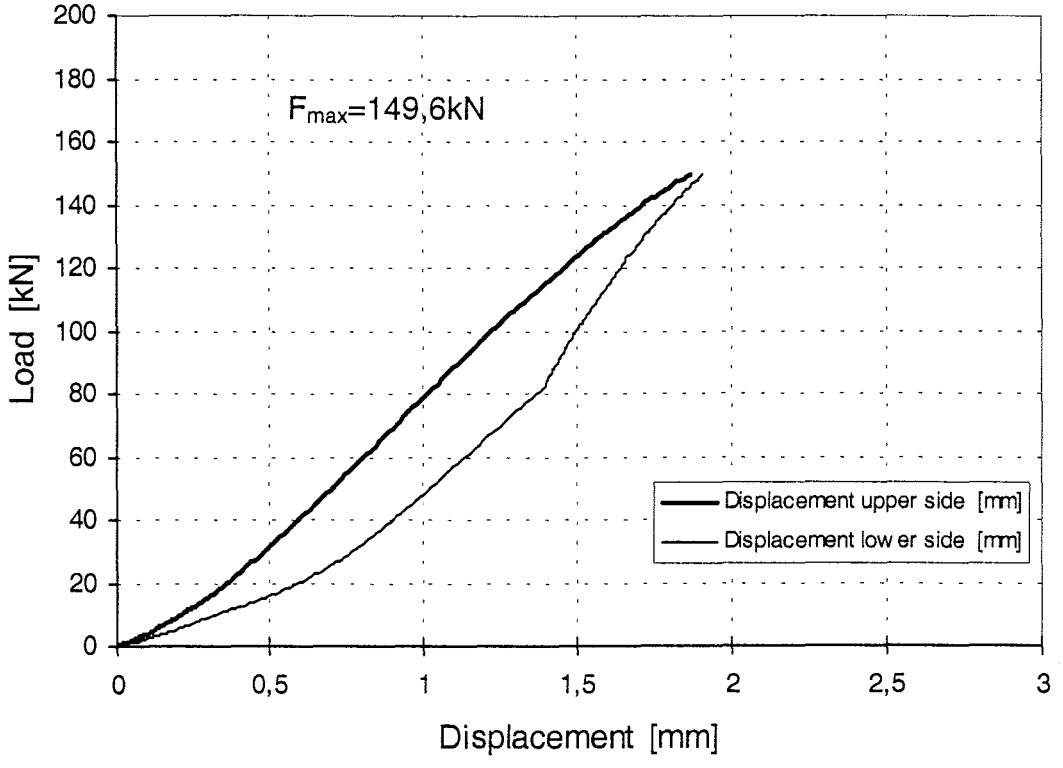

Figure 21: Load-displacement-curve of test Gi4-4

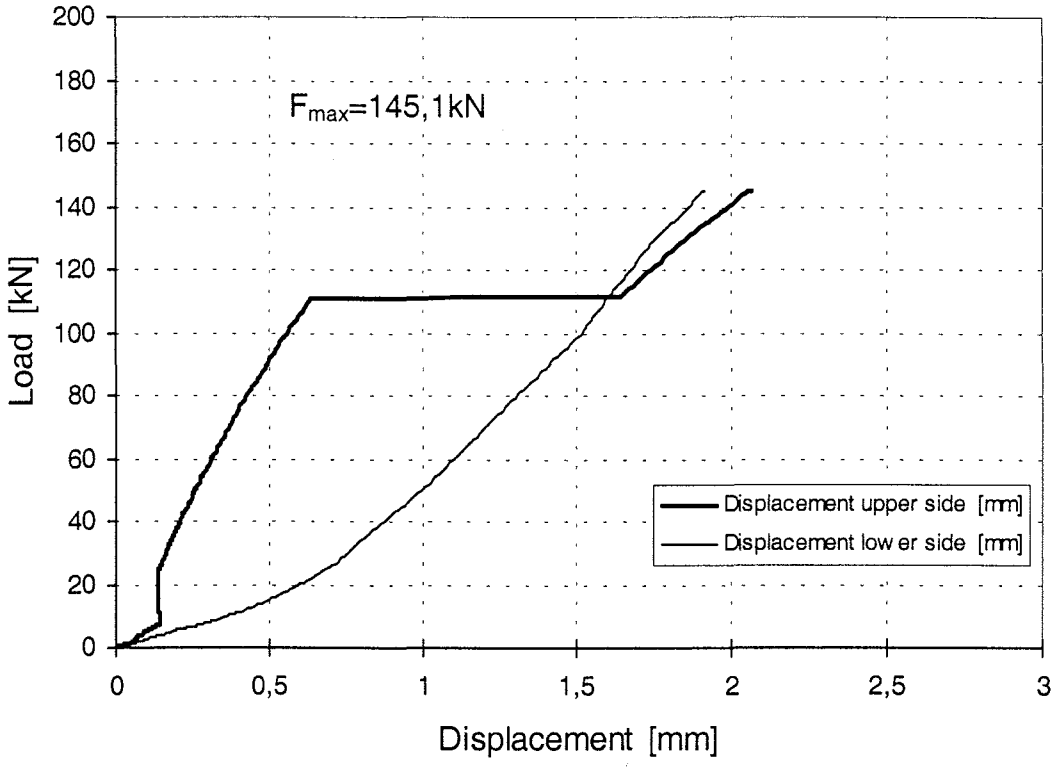

Figure 22: Load-displacement-curve of test Gi4-5

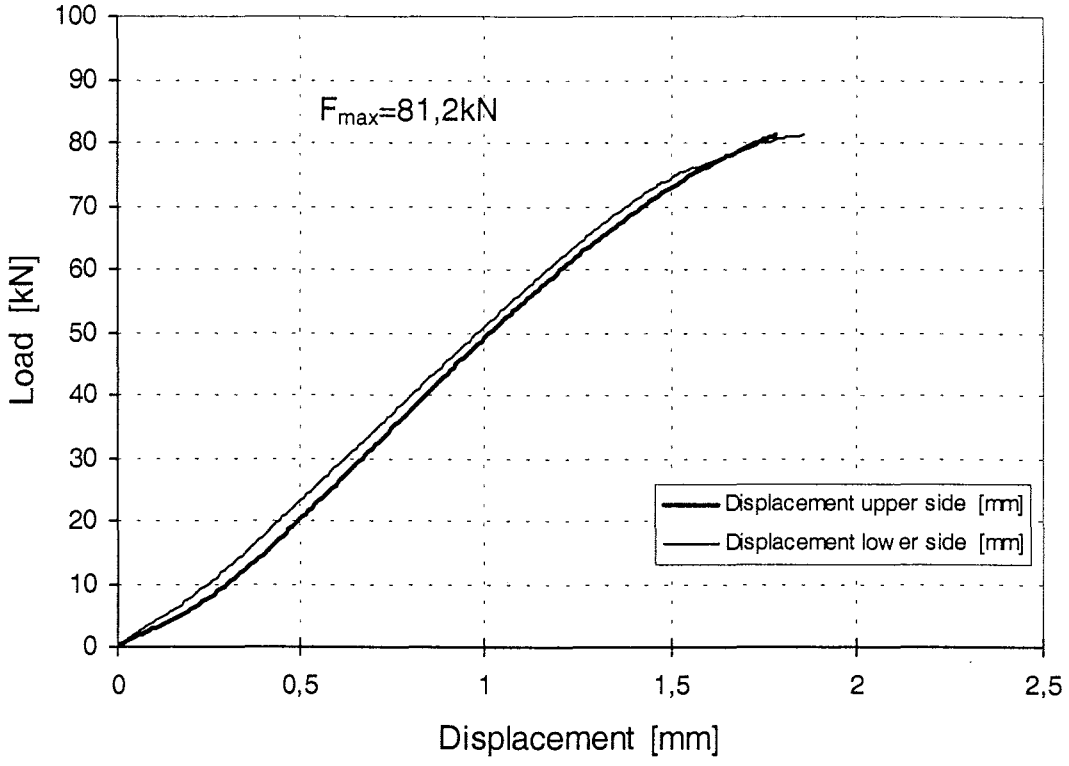

Figure 23: Load-displacement-curve of test Gi5-1

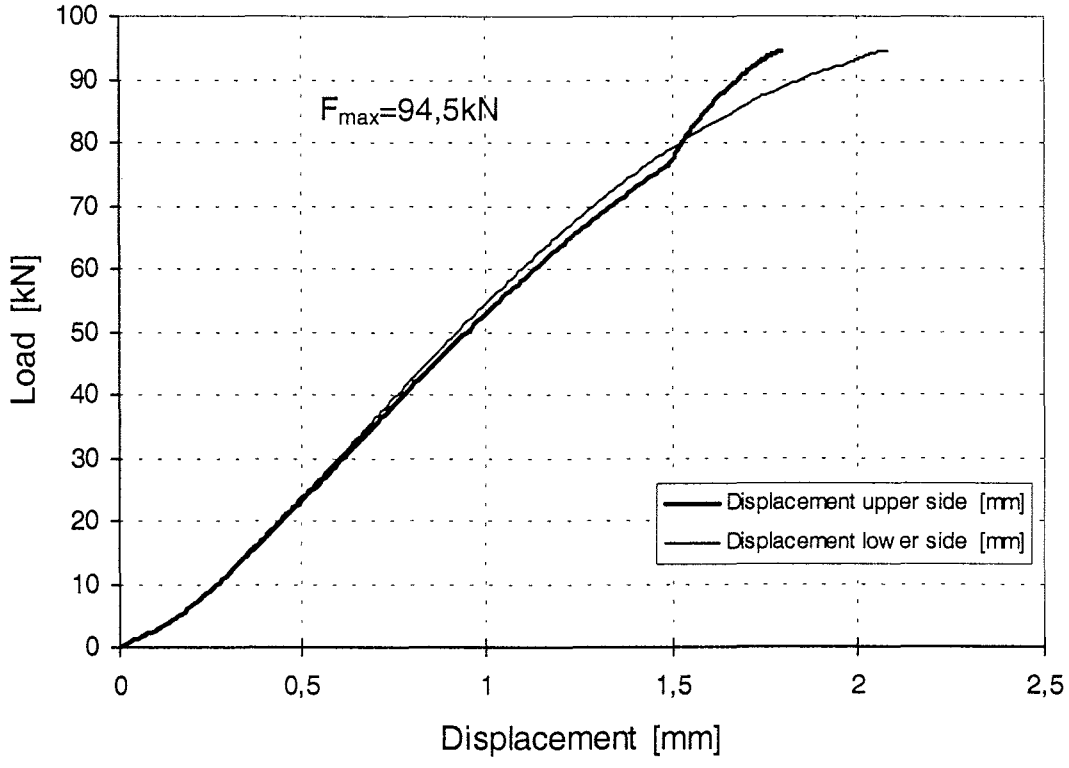

Figure 24: Load-displacement-curve of test Gi5-2

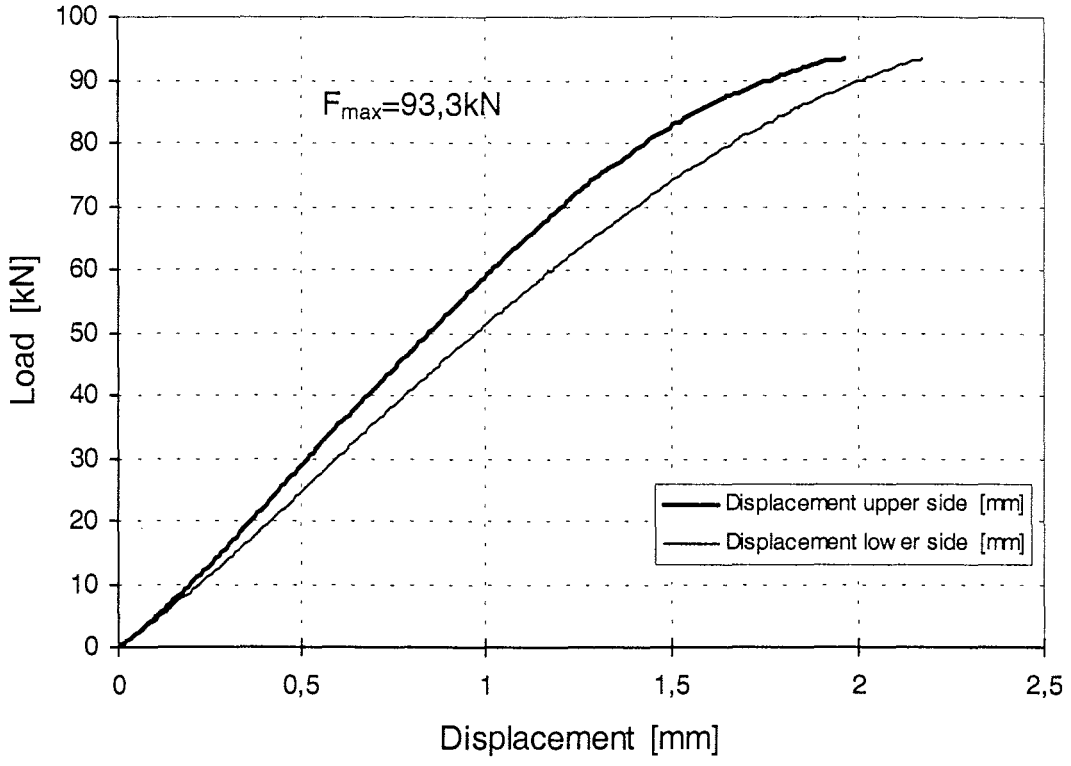

Figure 25: Load-displacement-curve of test Gi5-3

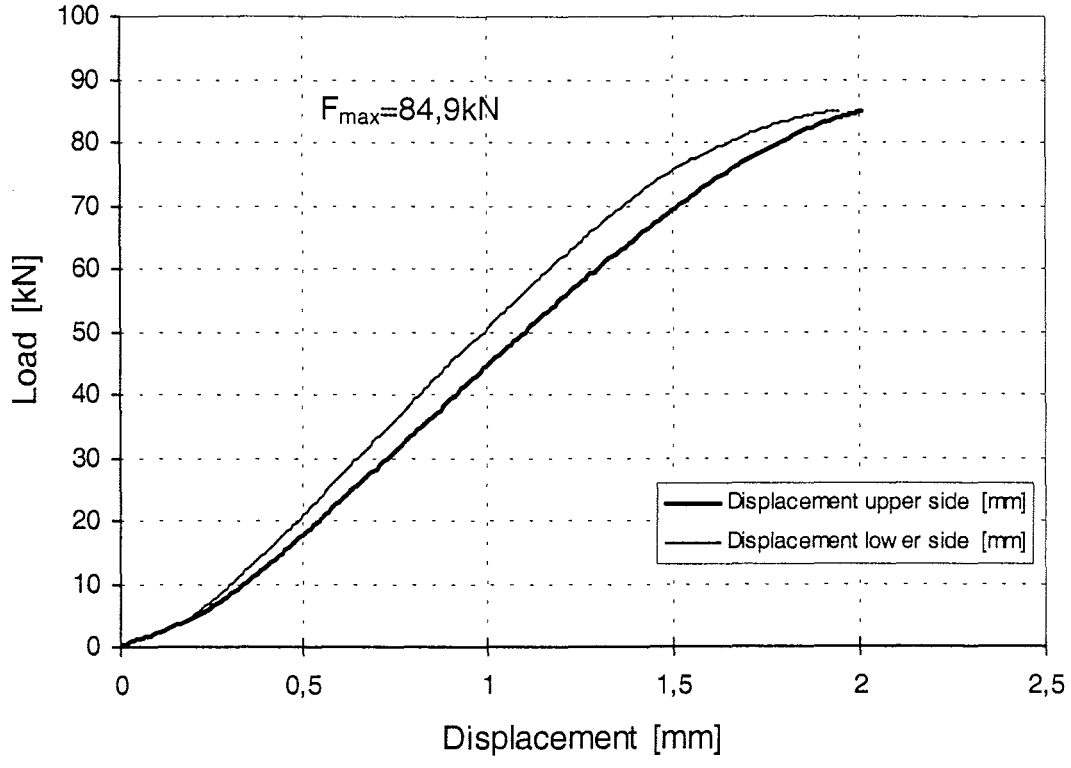

Figure 26: Load-displacement-curve of test Gi5-4

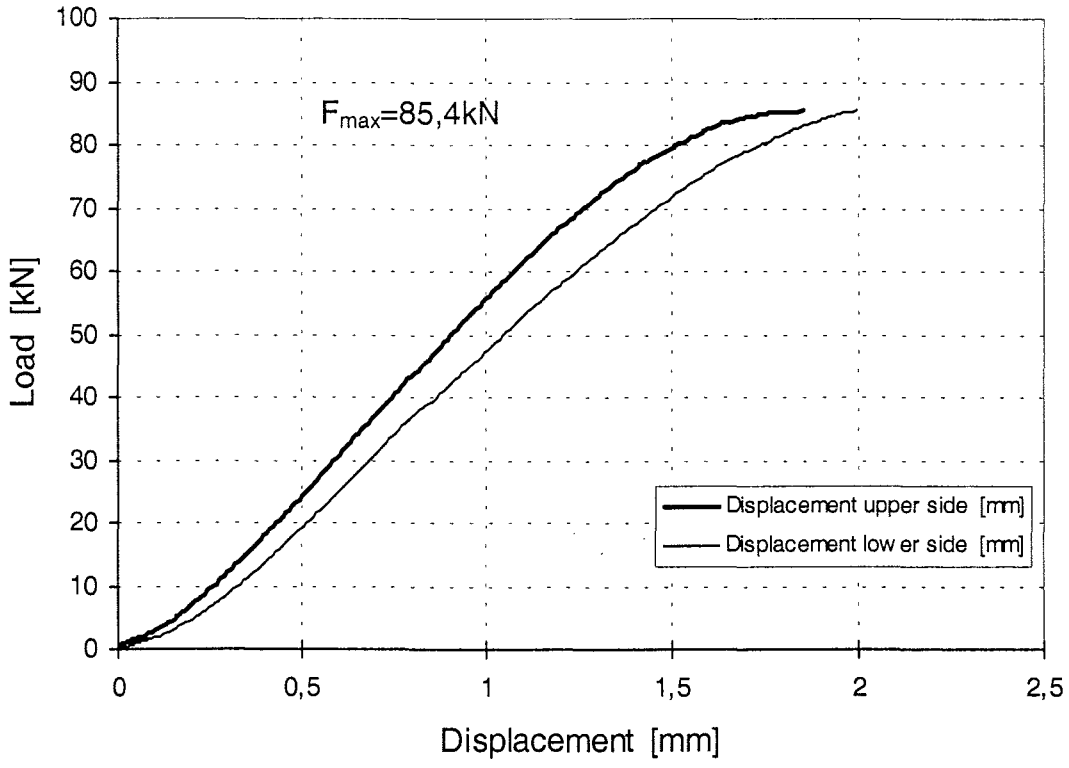

Figure 27: Load-displacement-curve of test Gi5-5

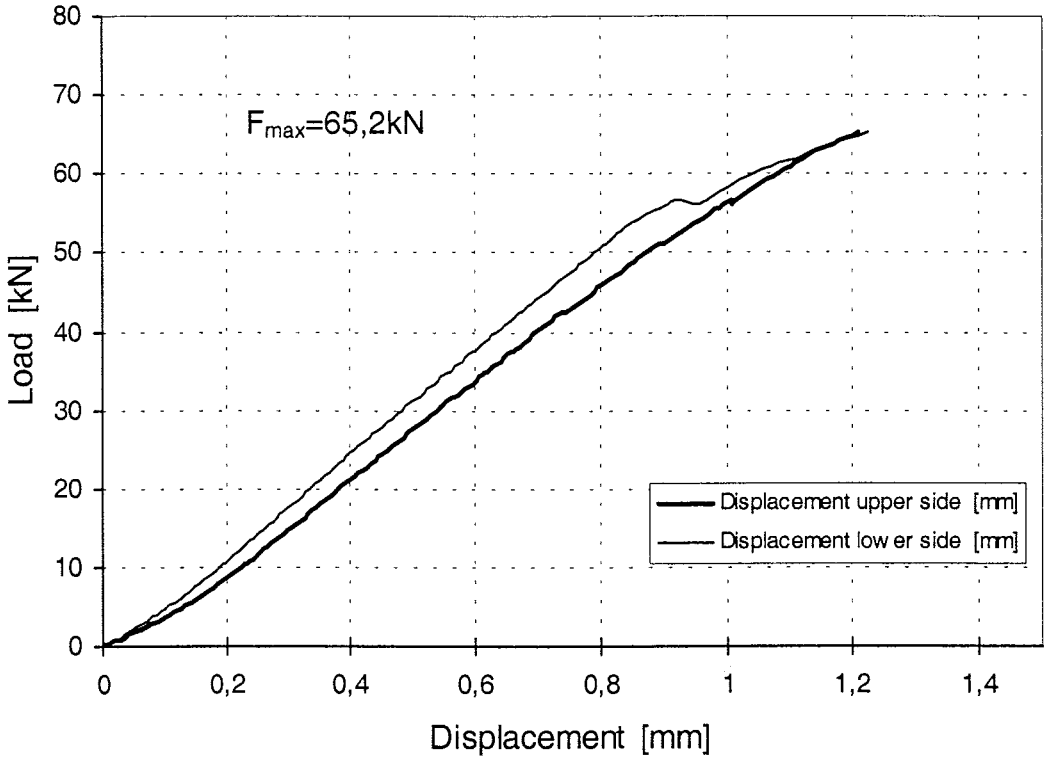

Figure 28: Load-displacement-curve of test Gi6-1

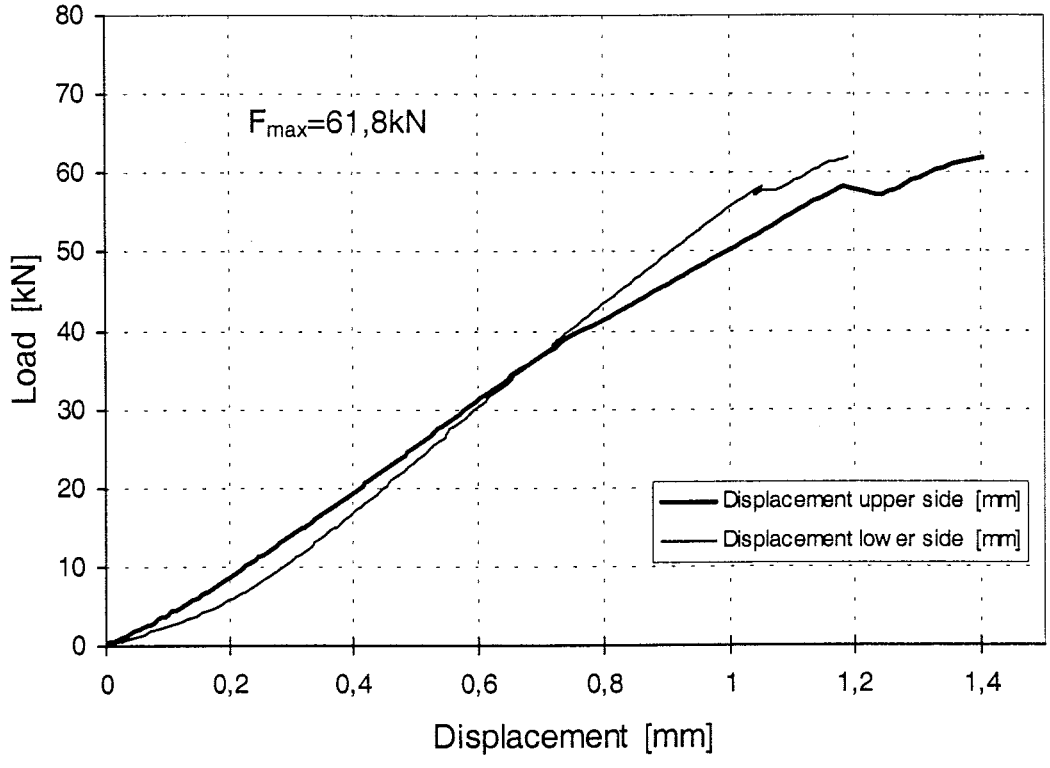

Figure 29: Load-displacement-curve of test Gi6-2

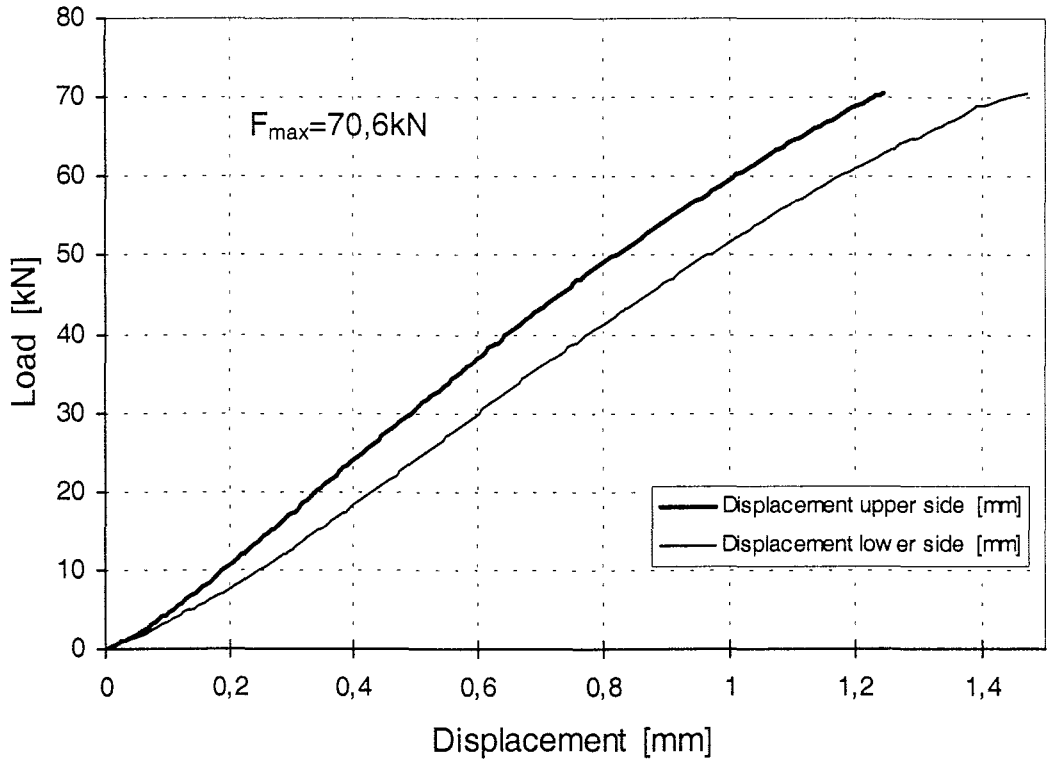

Figure 30: Load-displacement-curve of test Gi6-3

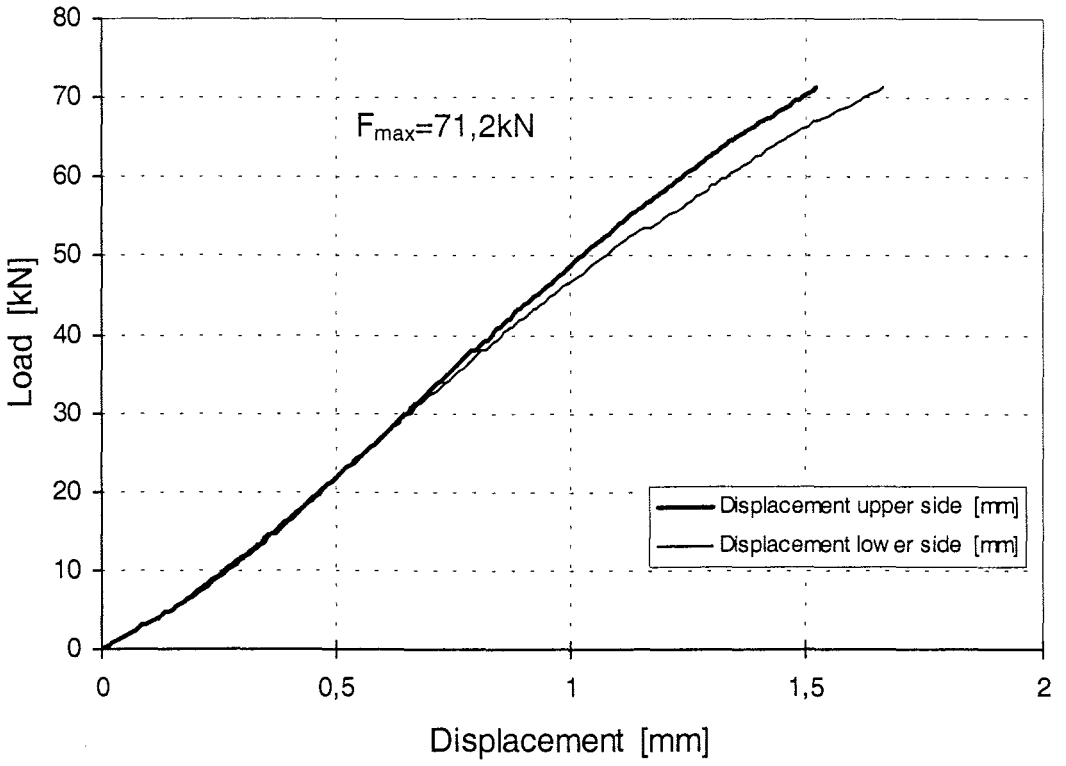

Figure 31: Load-displacement-curve of test Gi7-1

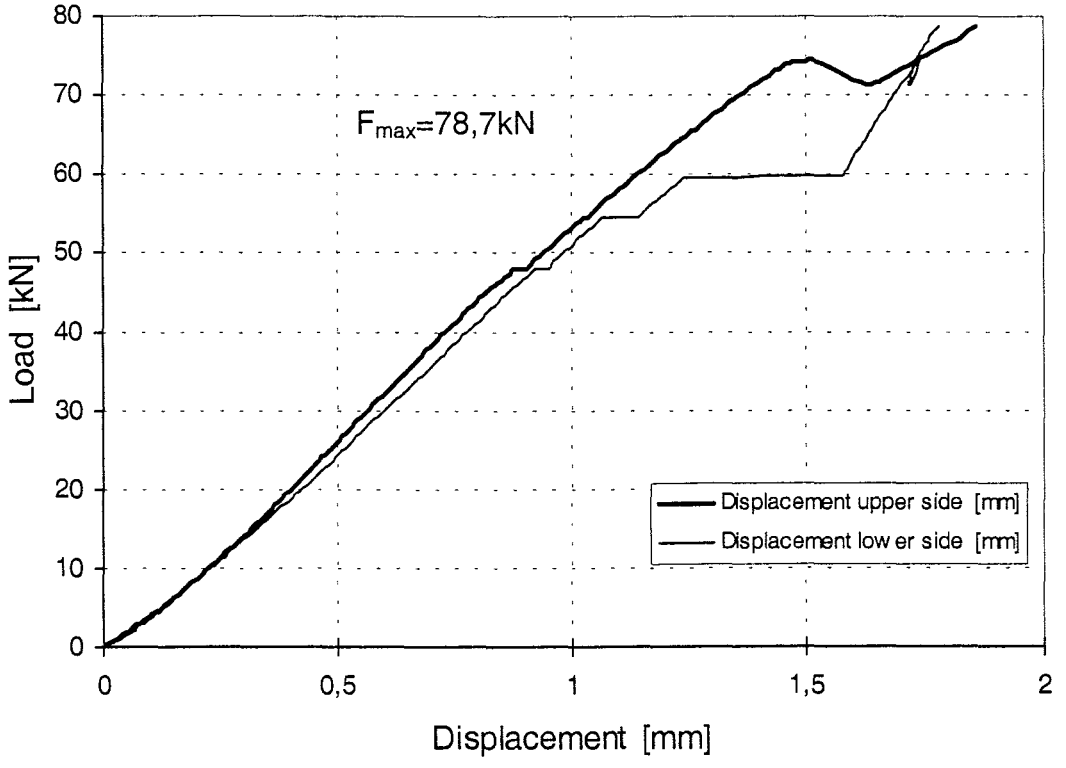

Figure 32: Load-displacement-curve of test Gi7-2

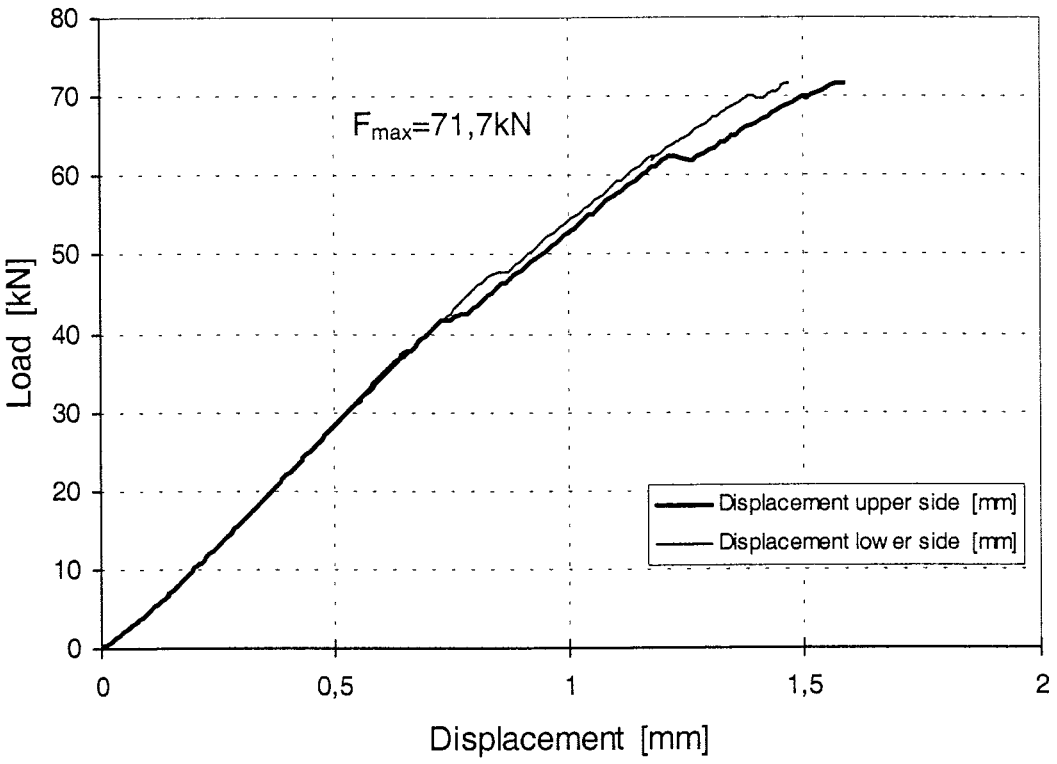

Figure 33: Load-displacement-curve of test Gi7-3

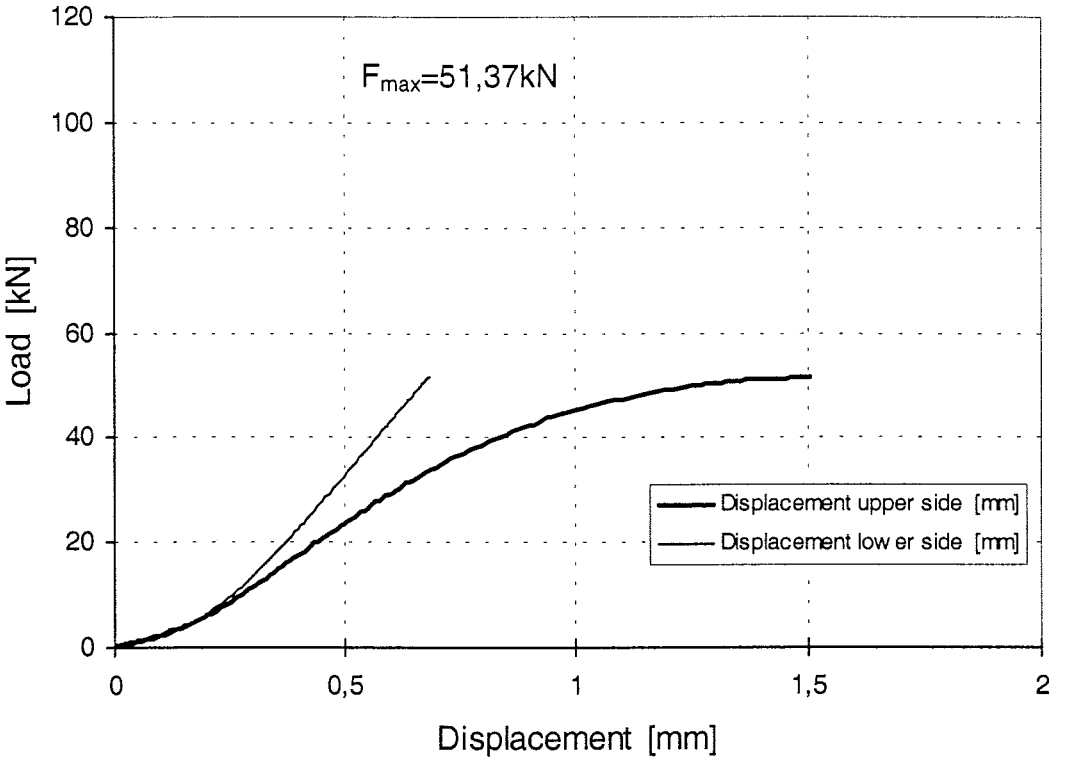

Figure 34: Load-displacement-curve of test Gi8-1

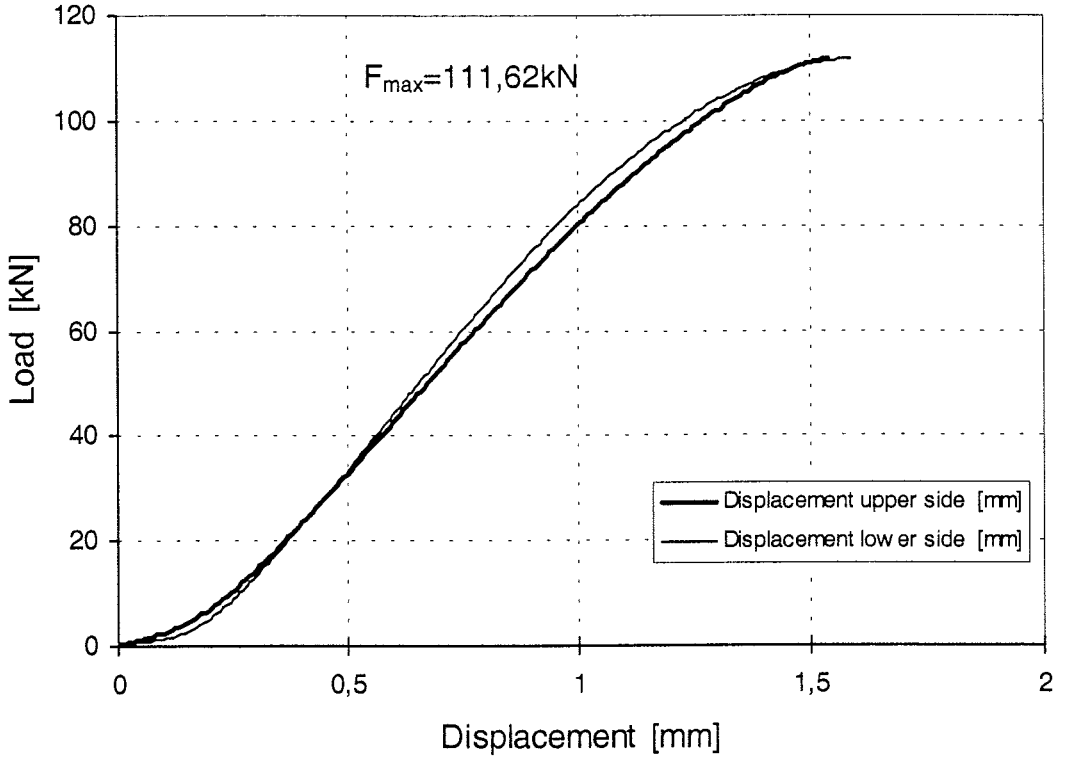

Figure 35: Load-displacement-curve of test Gi8-2

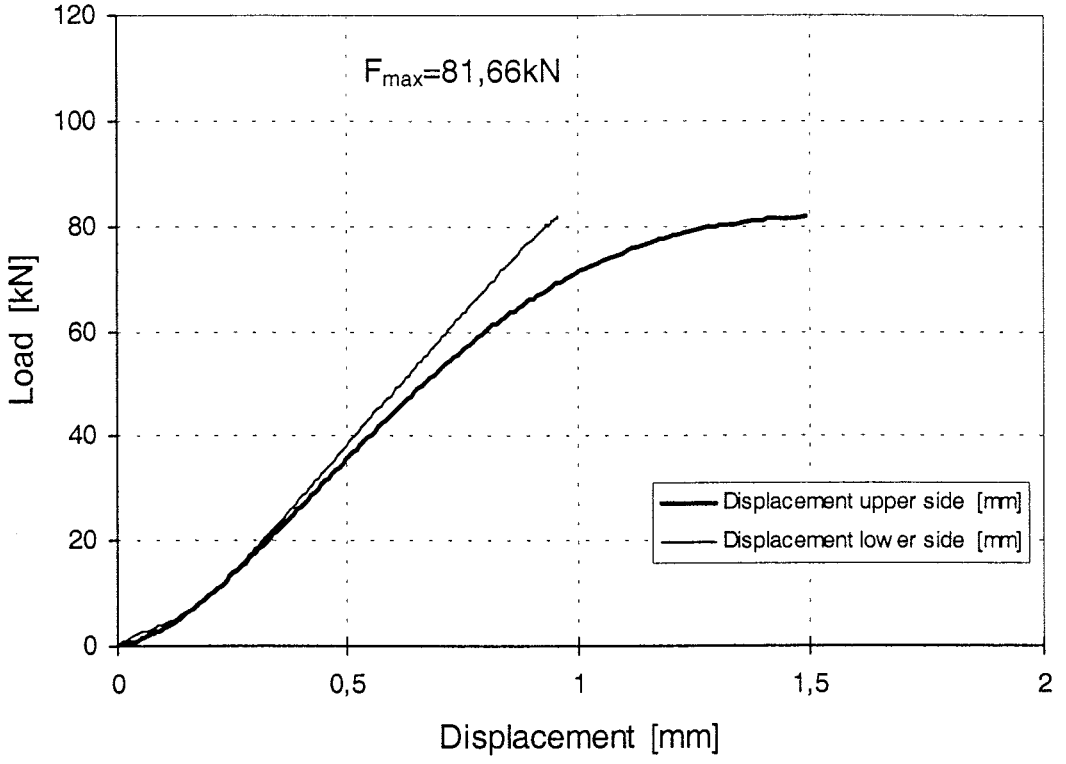

Figure 36: Load-displacement-curve of test Gi8-3

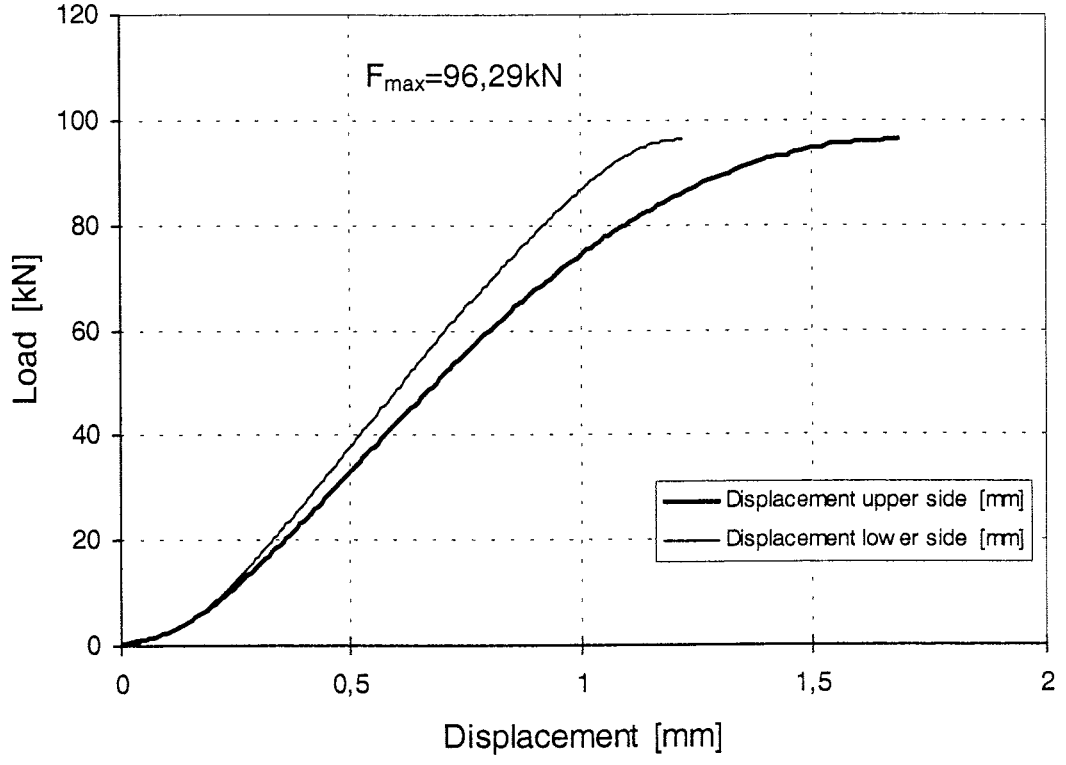

Figure 37: Load-displacement-curve of test Gi8-4

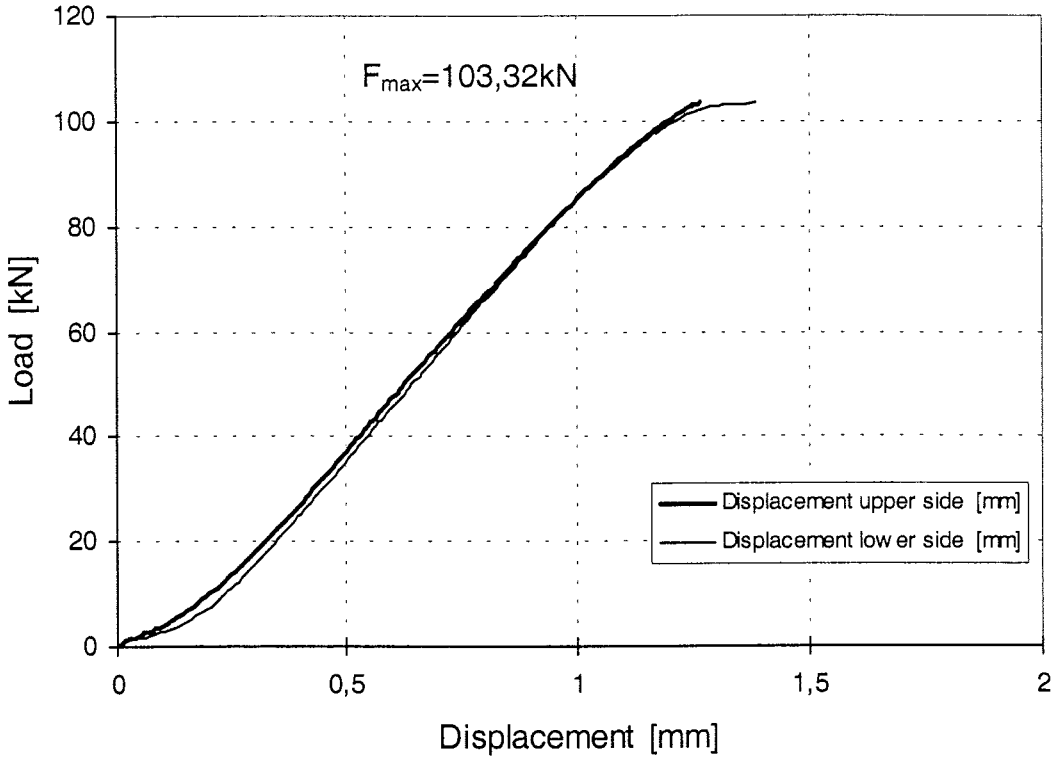

Figure 38: Load-displacement-curve of test Gi8-5

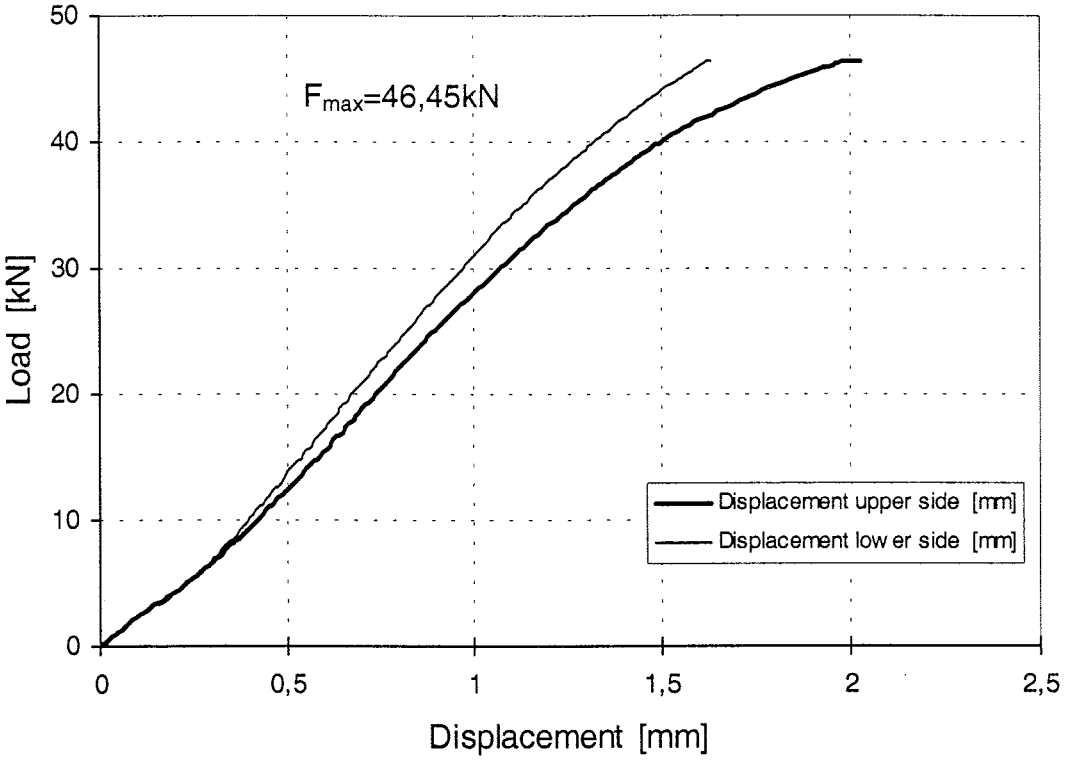

Figure 39: Load-displacement-curve of test Gi9-1

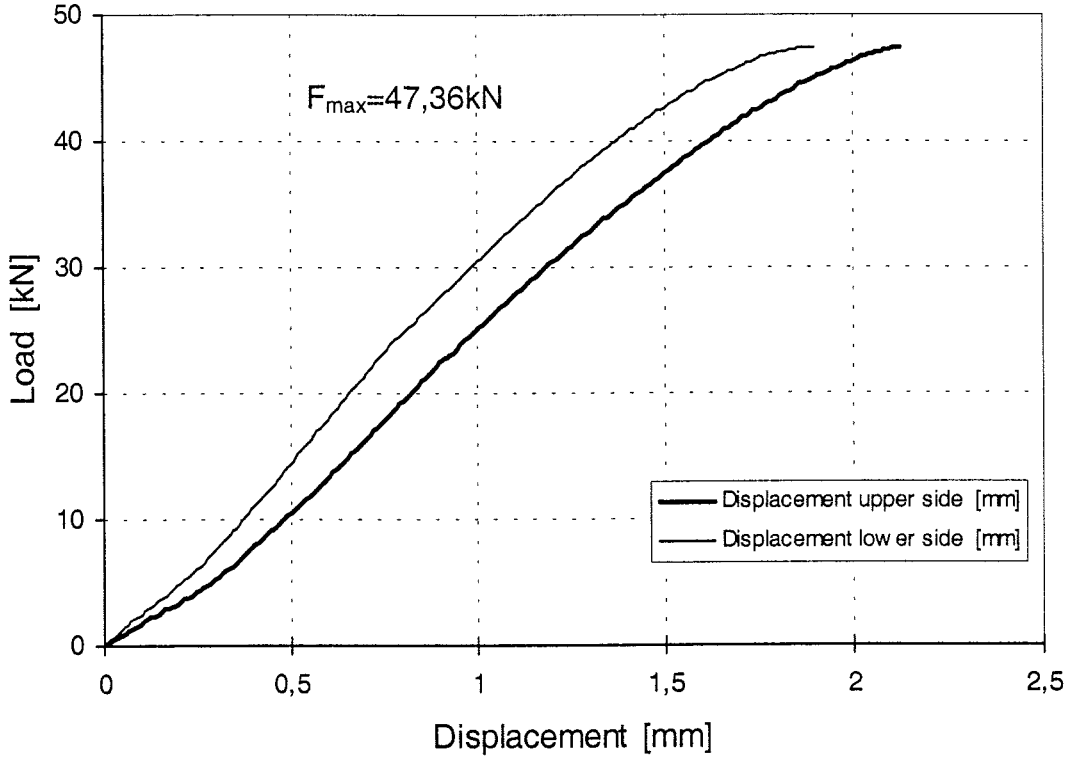

Figure 40: Load-displacement-curve of test Gi9-2

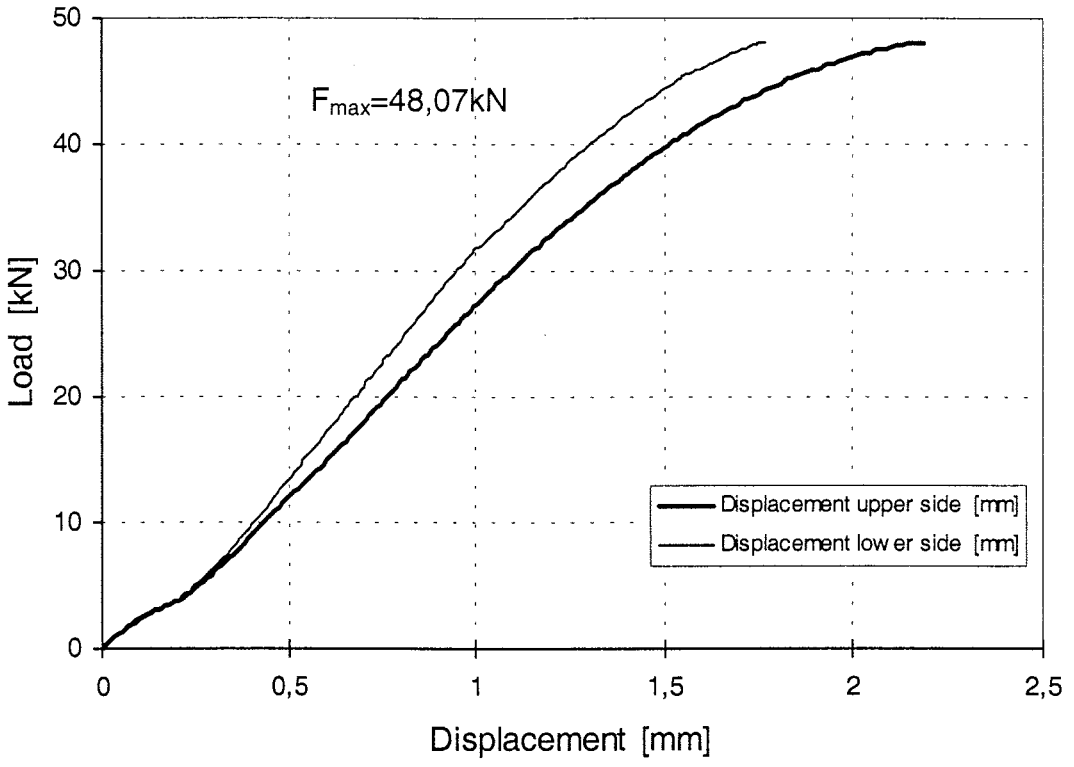

Figure 41: Load-displacement-curve of test Gi9-3

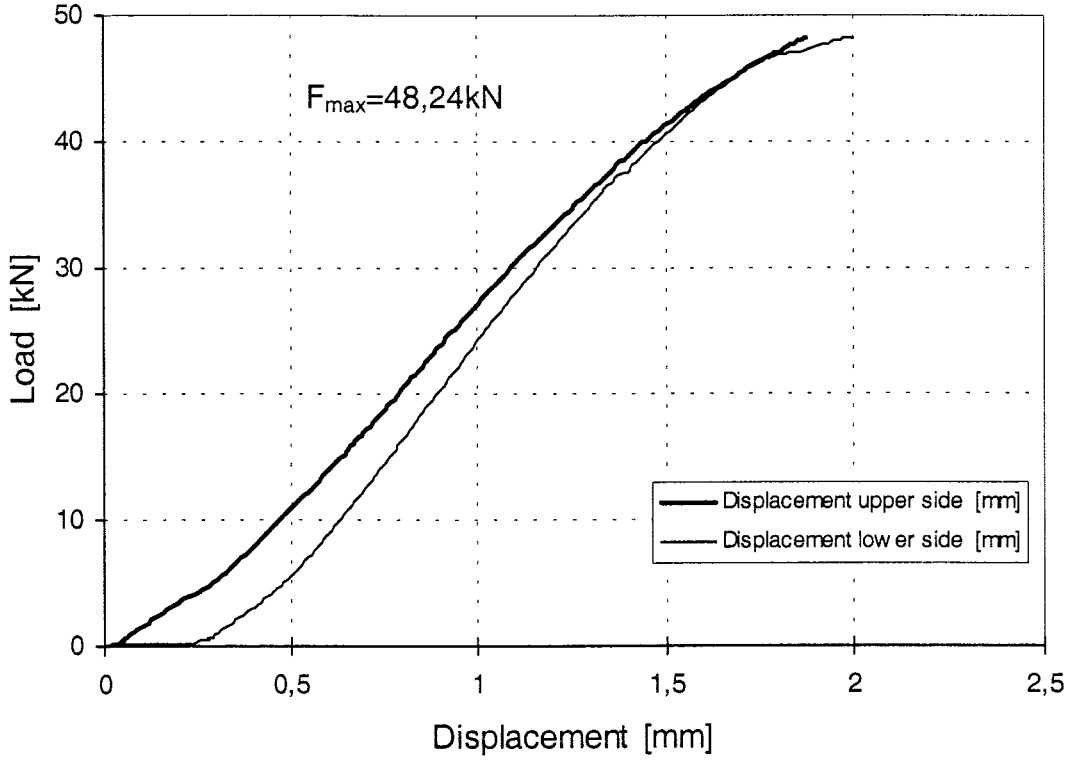

Figure 42: Load-displacement-curve of test Gi9-4

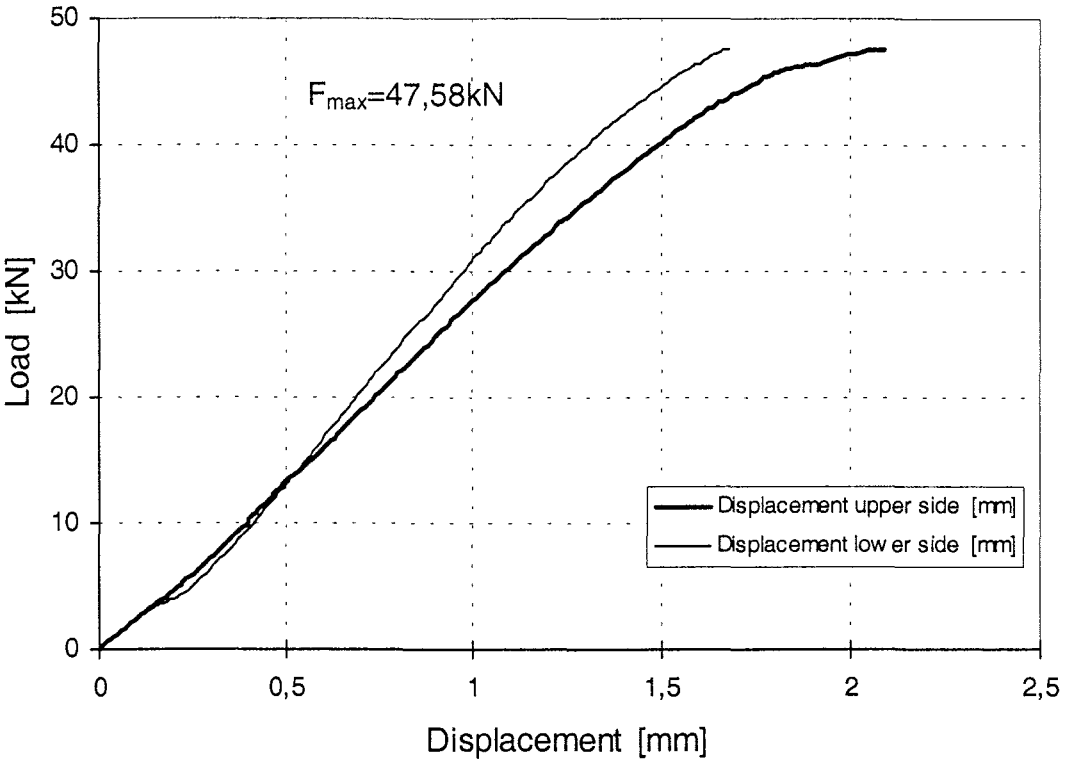

Figure 43: Load-displacement-curve of test Gi9-5

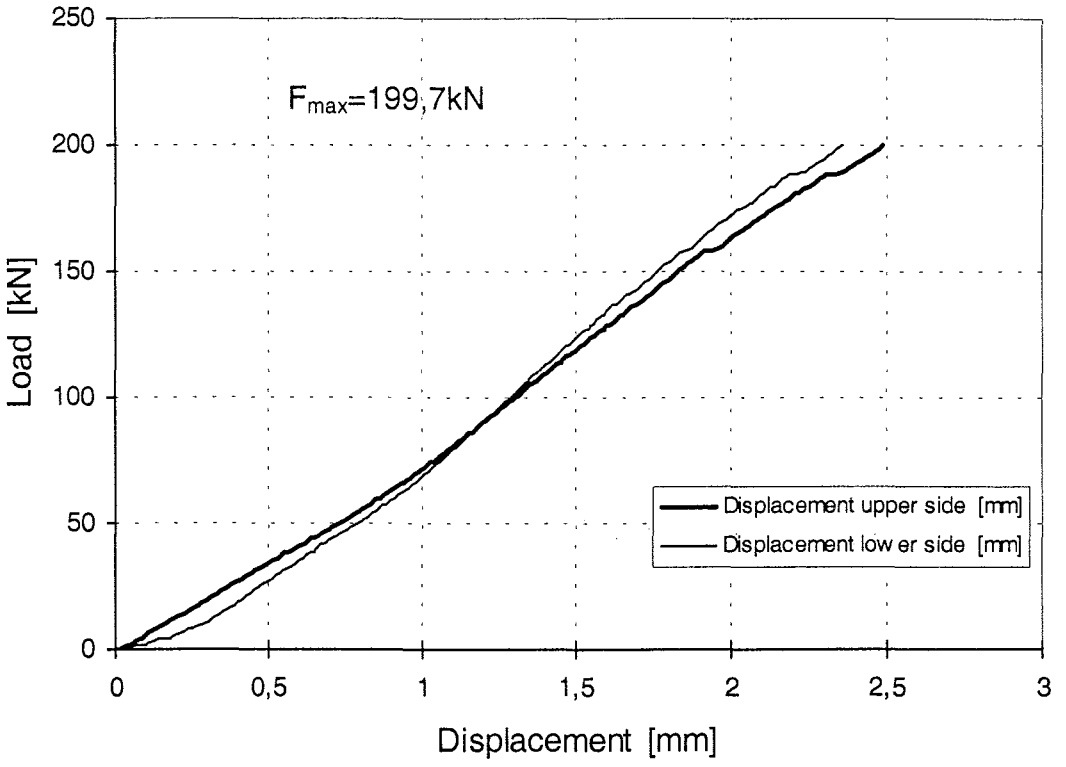

Figure 44: Load-displacement-curve of test Gi31-1

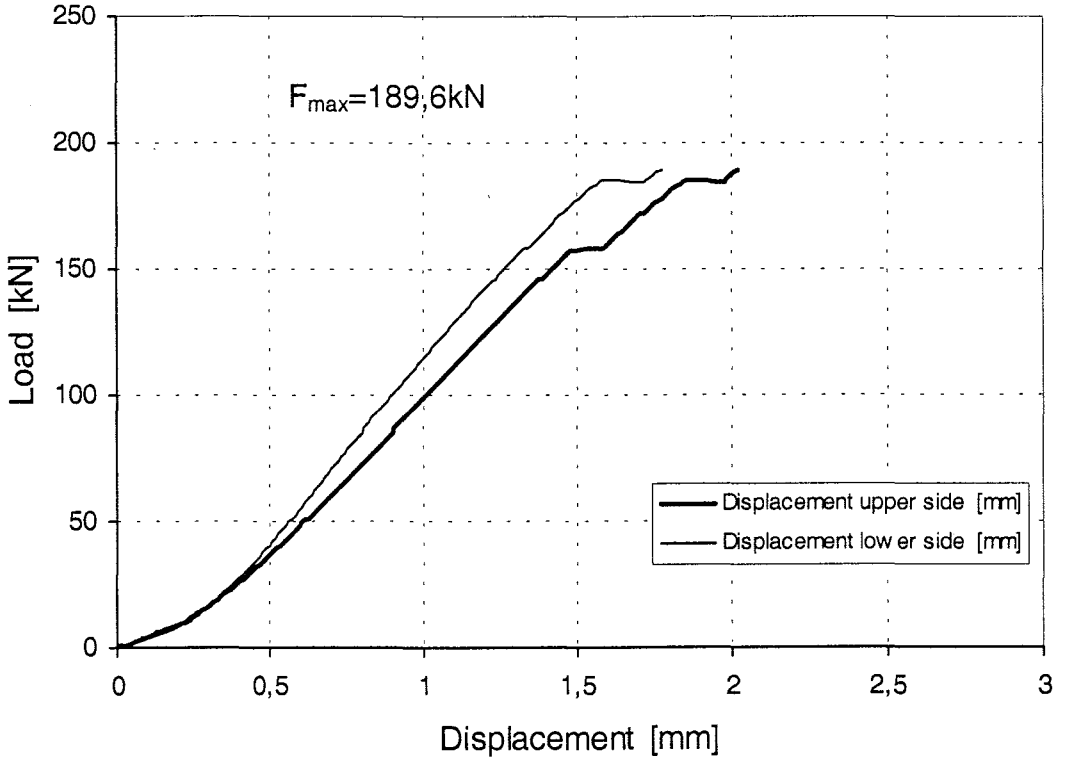

Figure 45: Load-displacement-curve of test Gi31-2

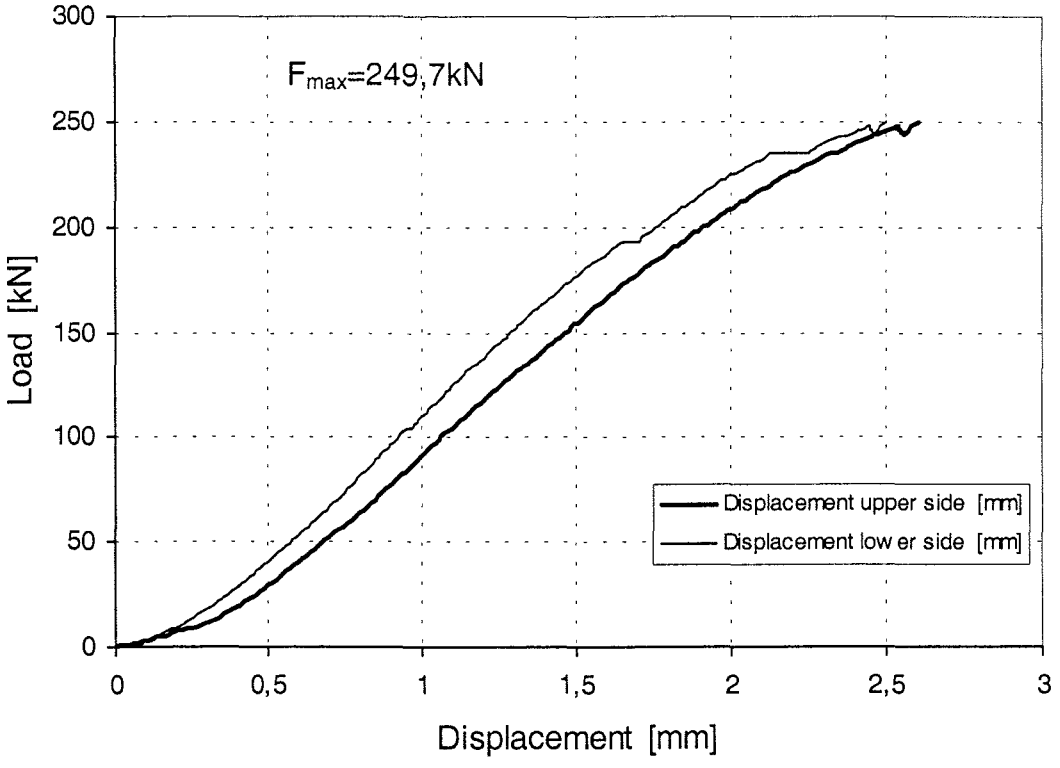

Figure 46: Load-displacement-curve of test Gi31-3

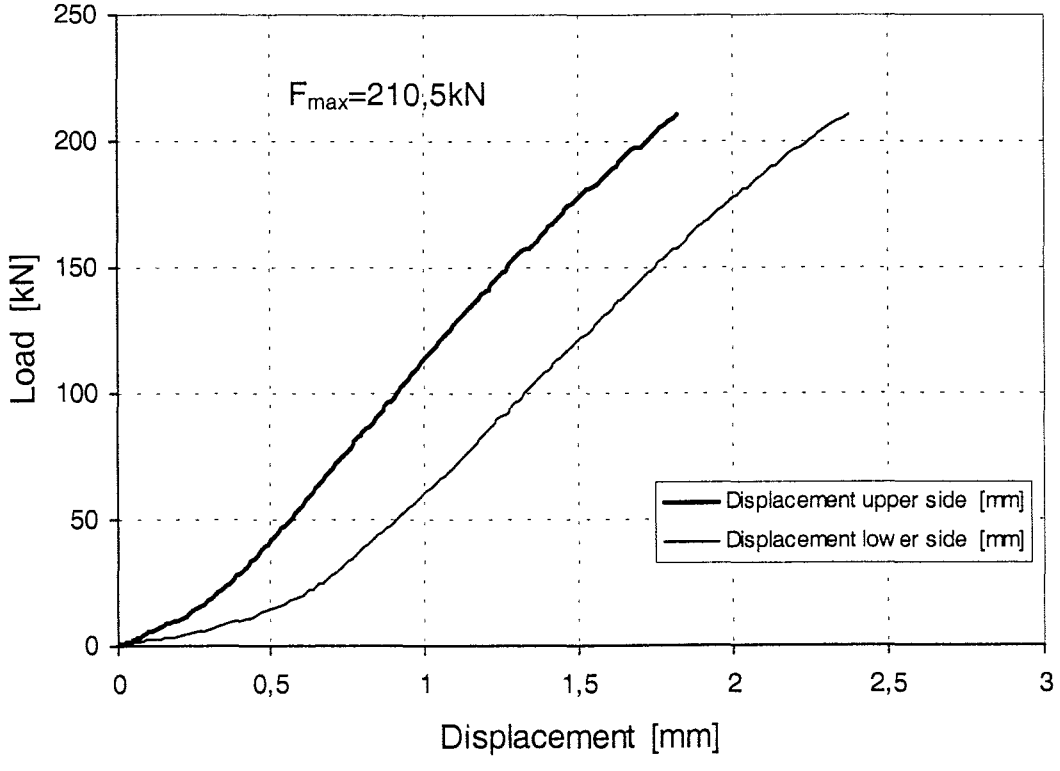

Figure 47: Load-displacement-curve of test Gi31-4

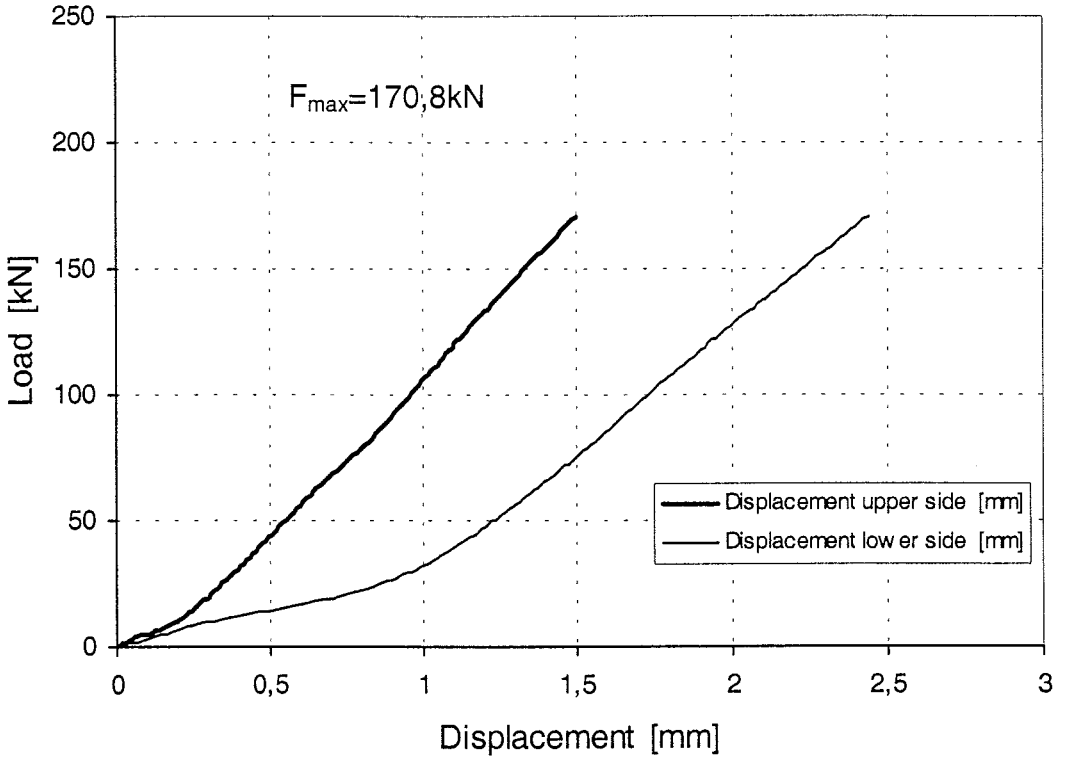

Figure 48: Load-displacement-curve of test Gi31-5

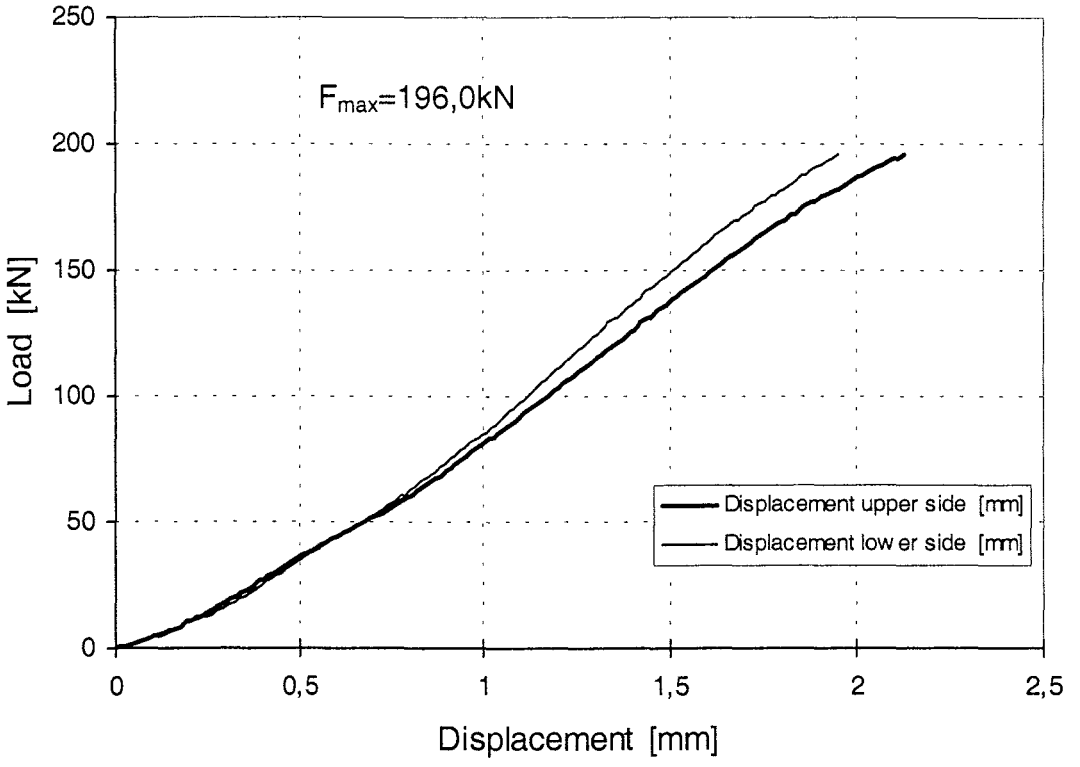

Figure 49: Load-displacement-curve of test Gi32-1

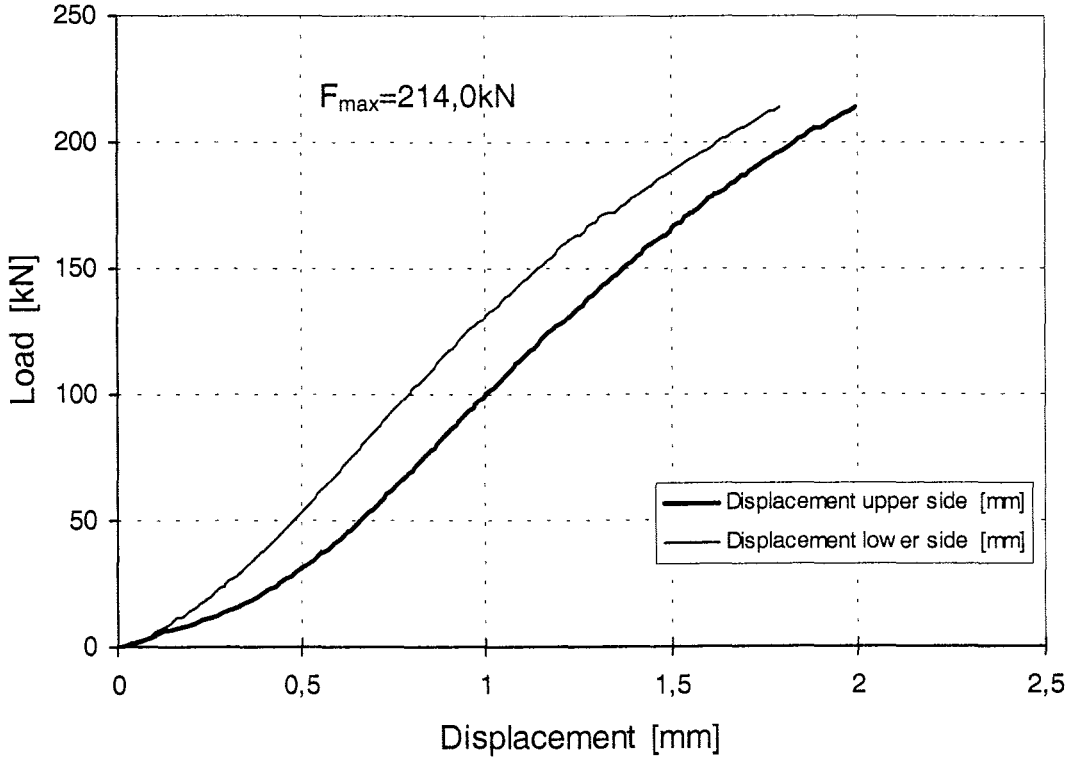

Figure 50: Load-displacement-curve of test Gi32-2

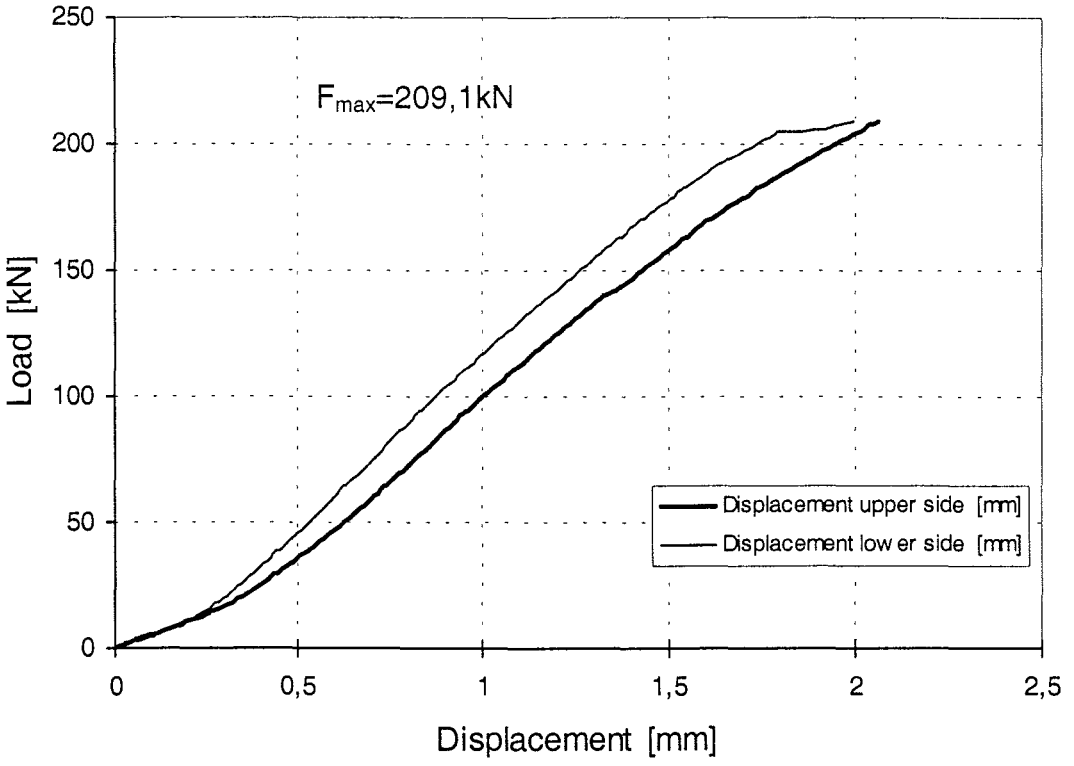

Figure 51: Load-displacement-curve of test Gi32-3

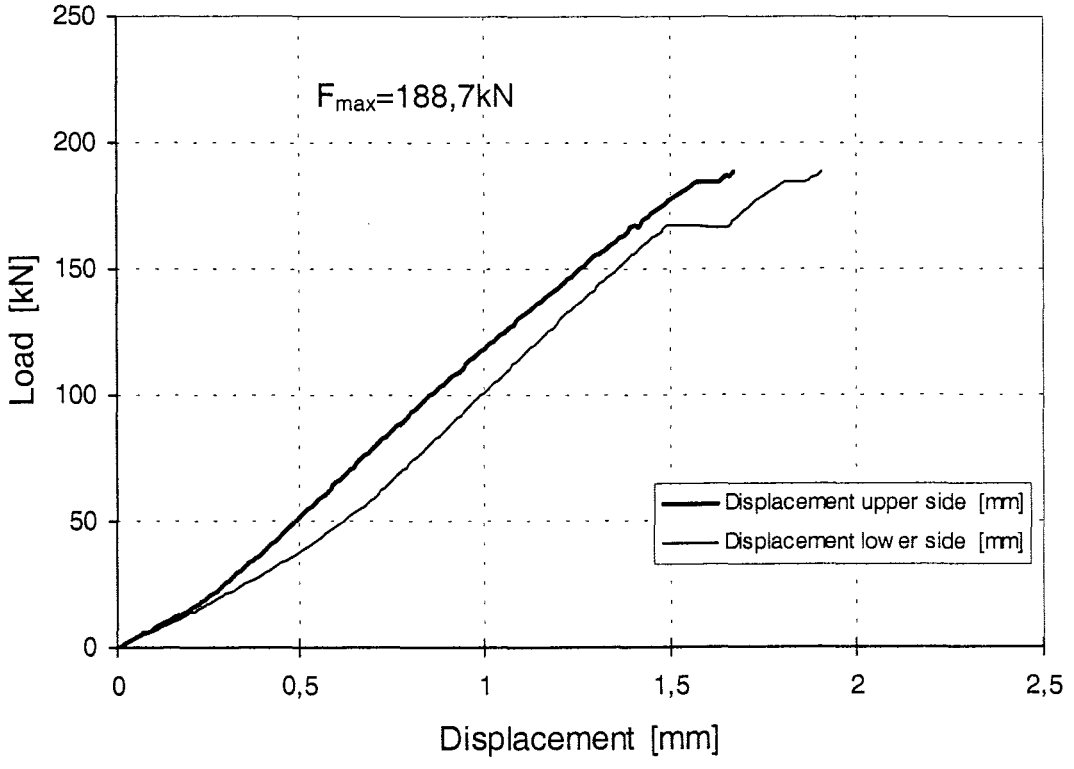

Figure 52: Load-displacement-curve of test Gi32-4

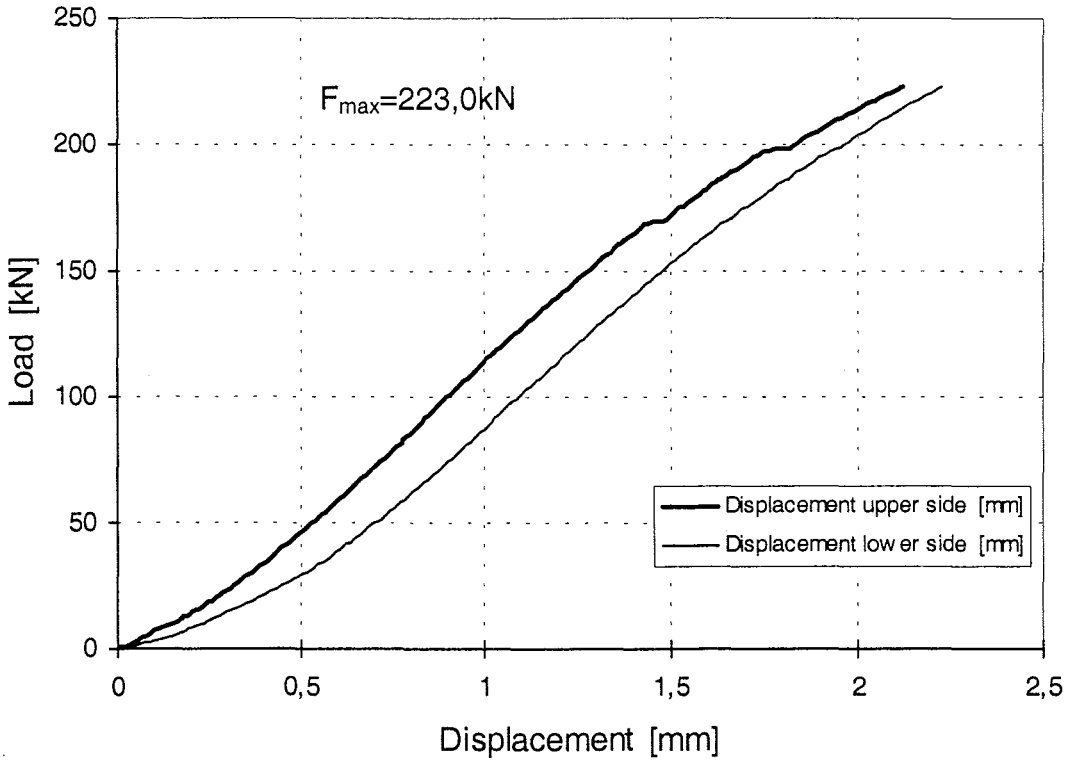

Figure 53: Load-displacement-curve of test Gi32-5

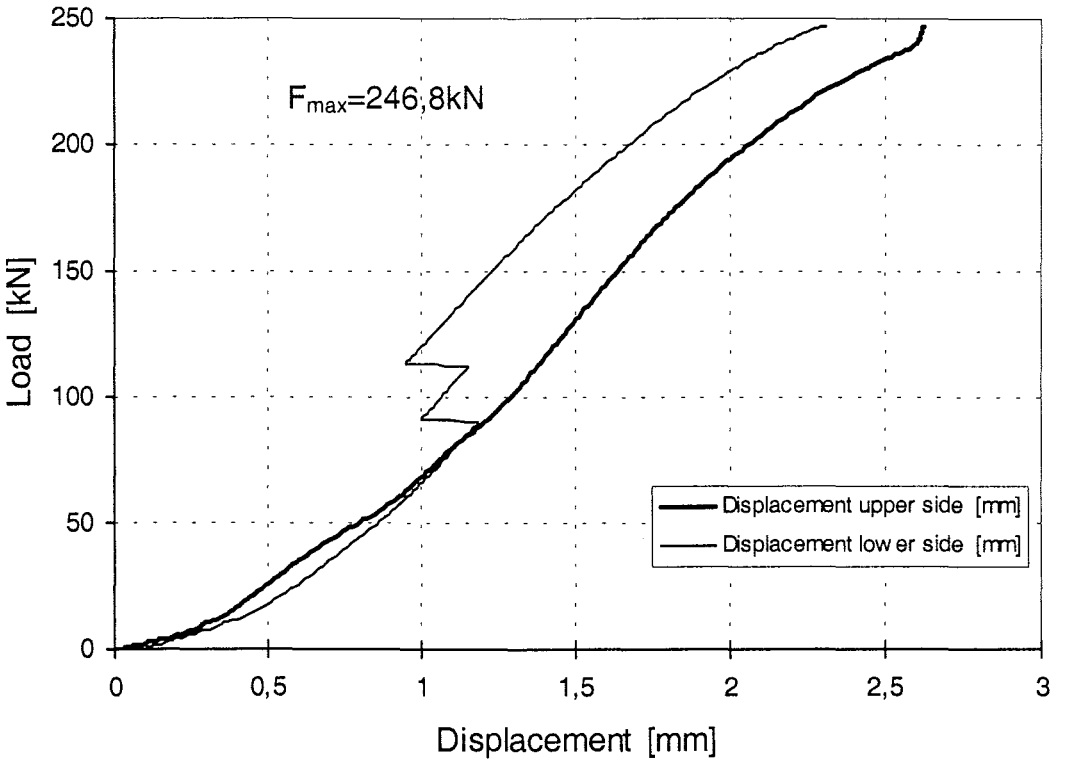

Figure 54: Load-displacement-curve of test Gi33-1

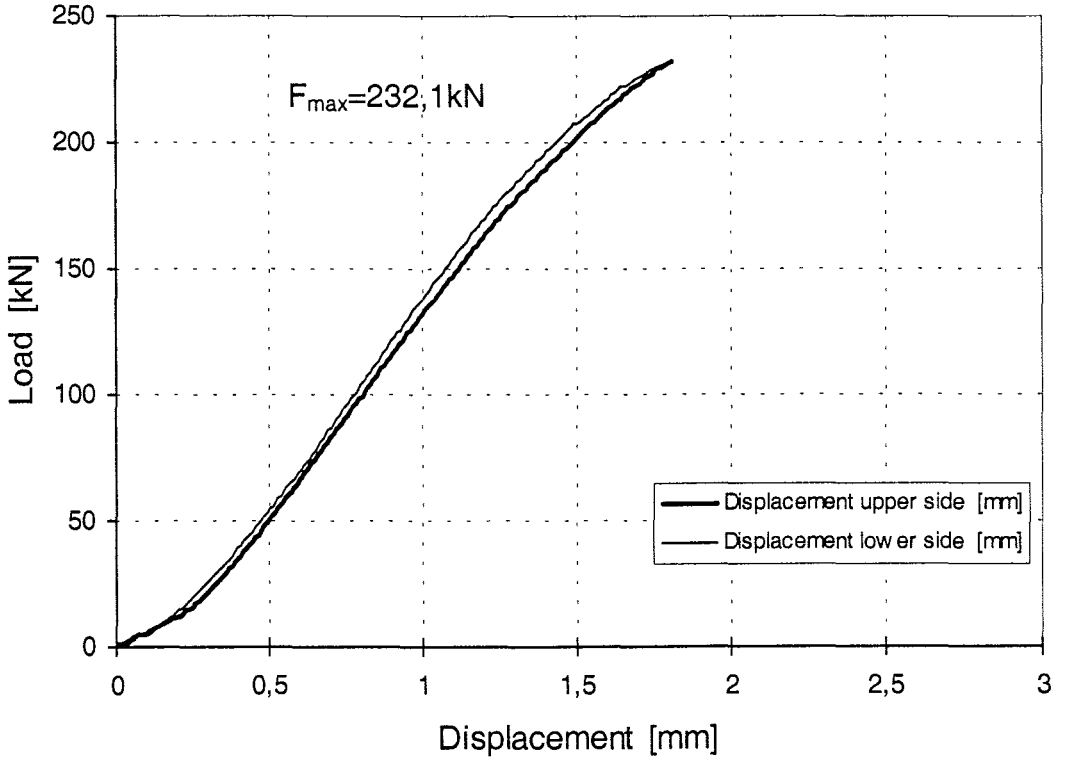

Figure 55: Load-displacement-curve of test Gi33-2

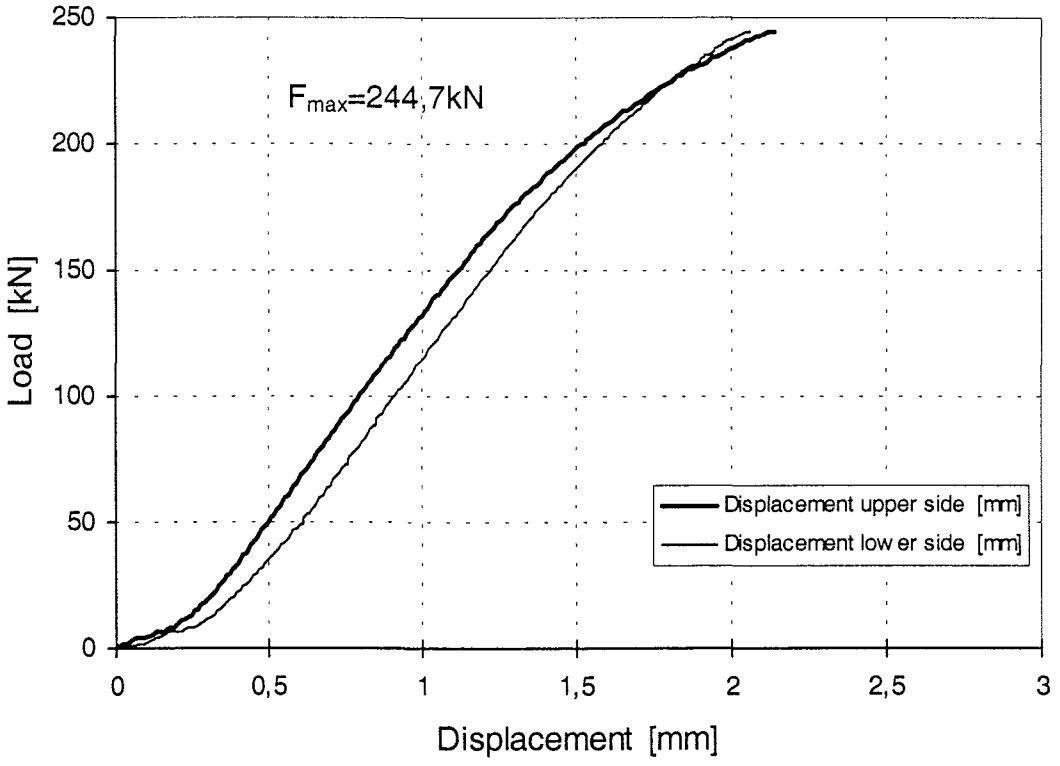

Figure 56: Load-displacement-curve of test Gi33-3

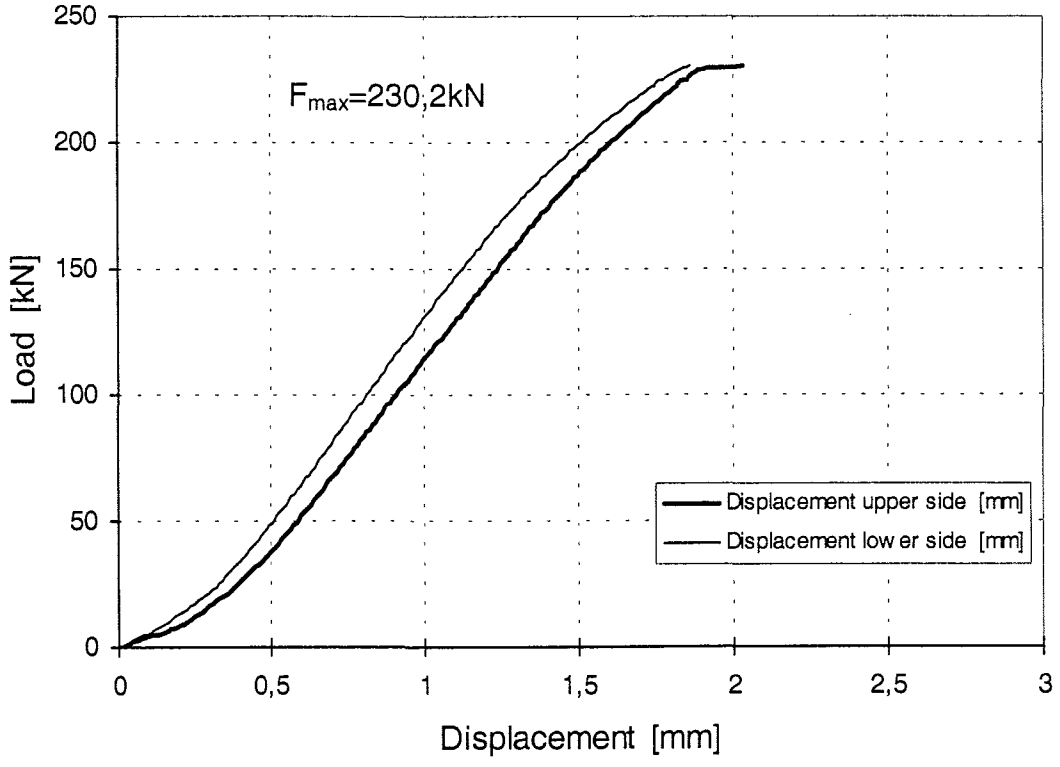

Figure 57: Load-displacement-curve of test Gi33-4

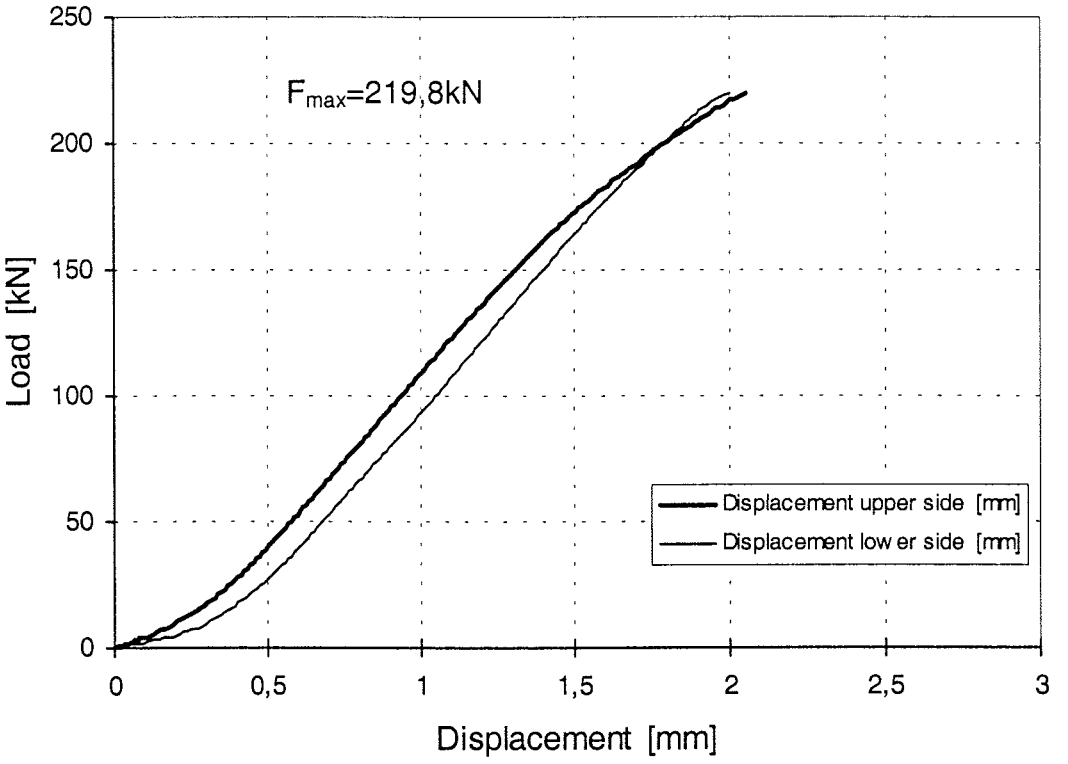

Figure 58: Load-displacement-curve of test Gi33-5

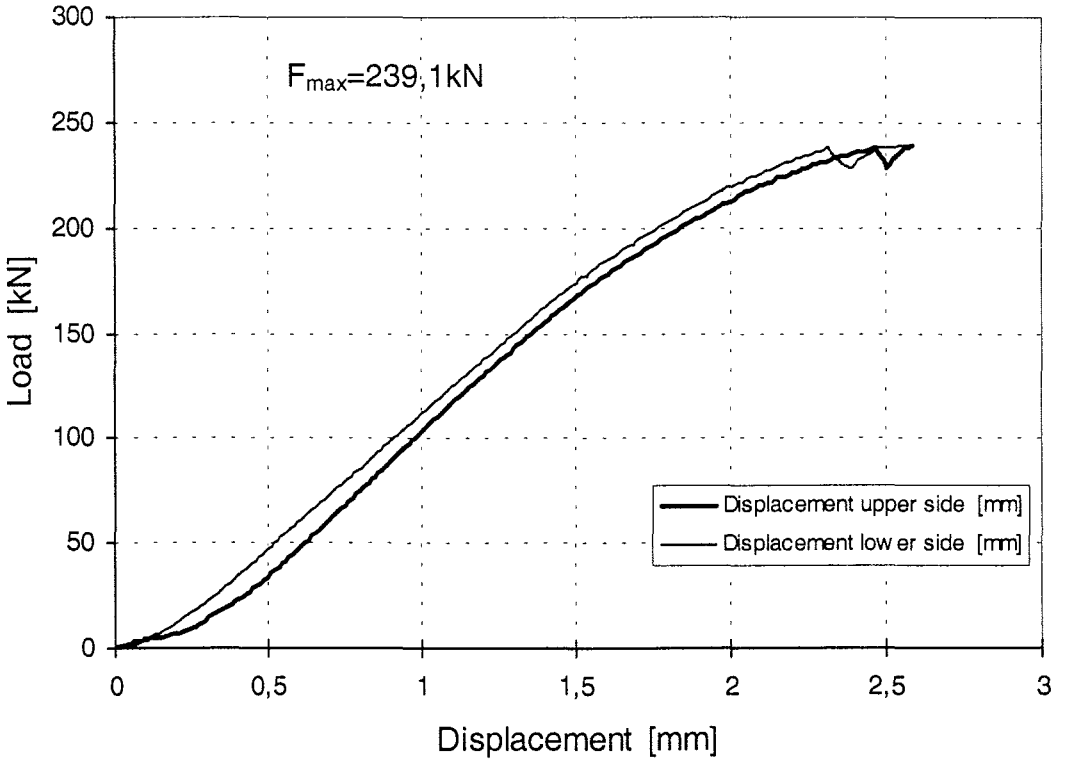

Figure 59: Load-displacement-curve of test Gi34-1

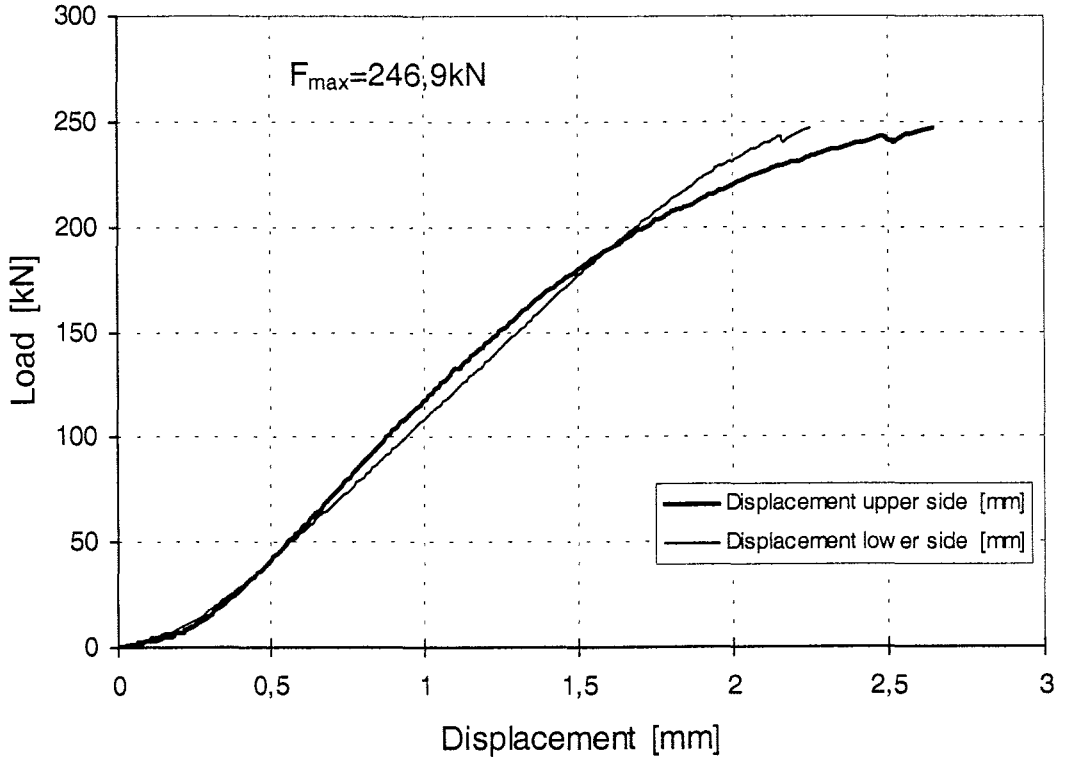

Figure 60: Load-displacement-curve of test Gi34-2

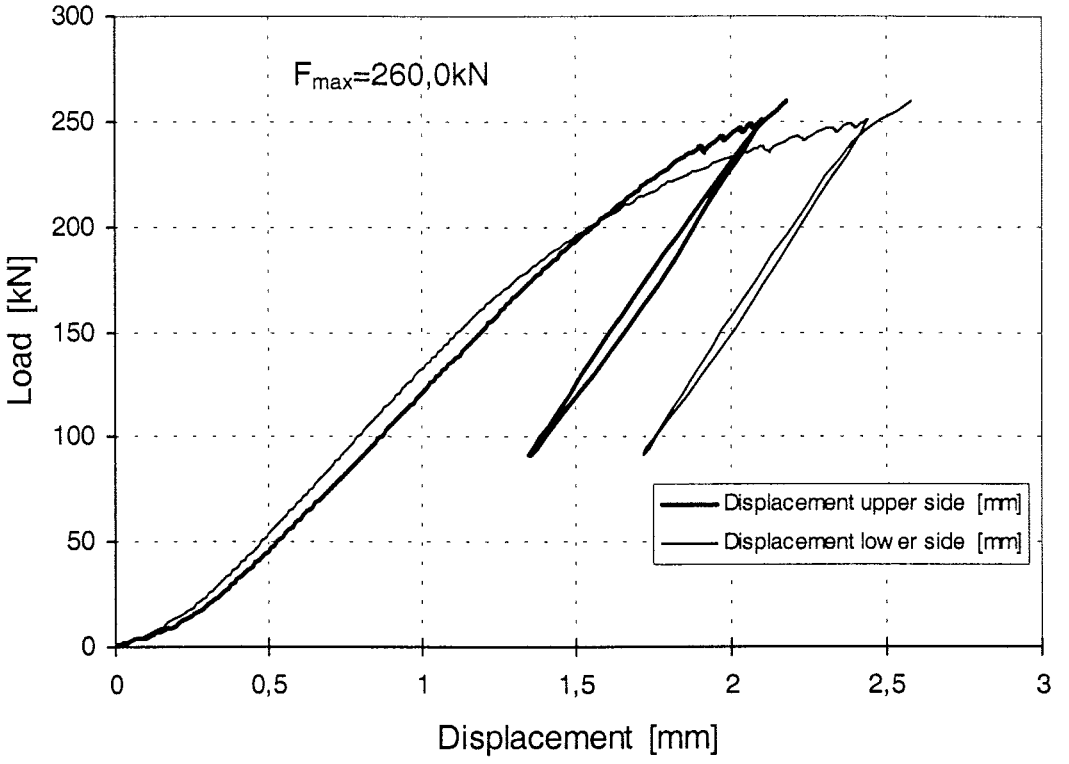

Figure 61: Load-displacement-curve of test Gi34-3

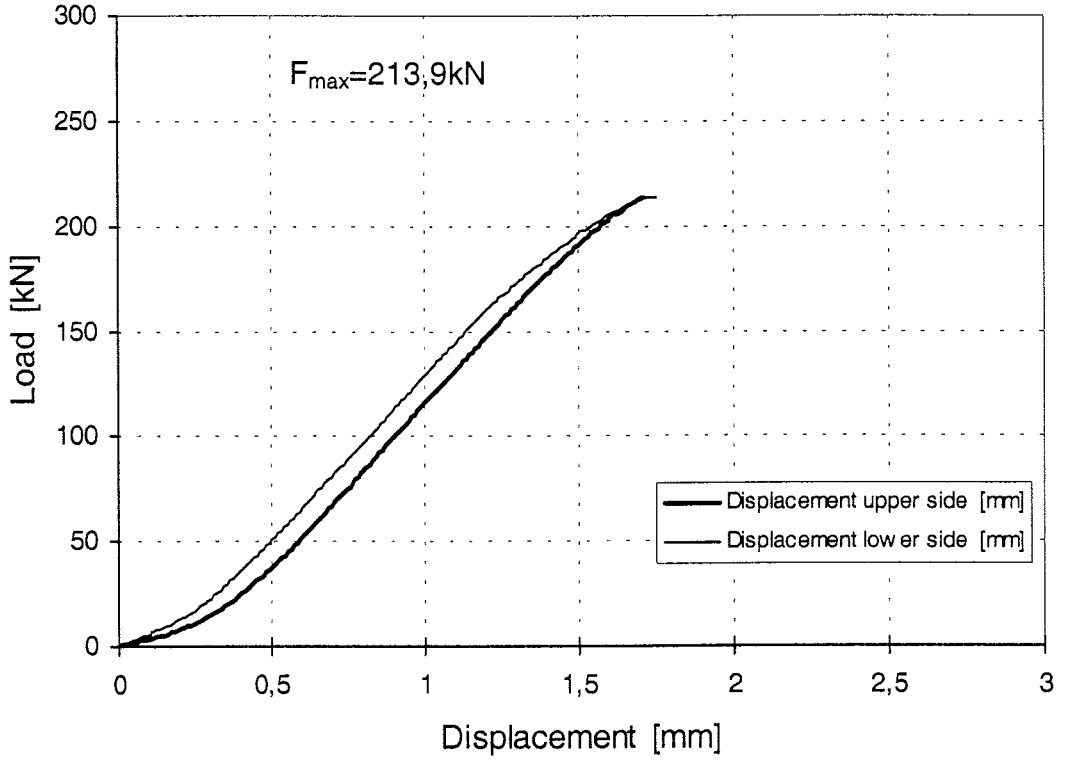

Figure 62: Load-displacement-curve of test Gi34-4

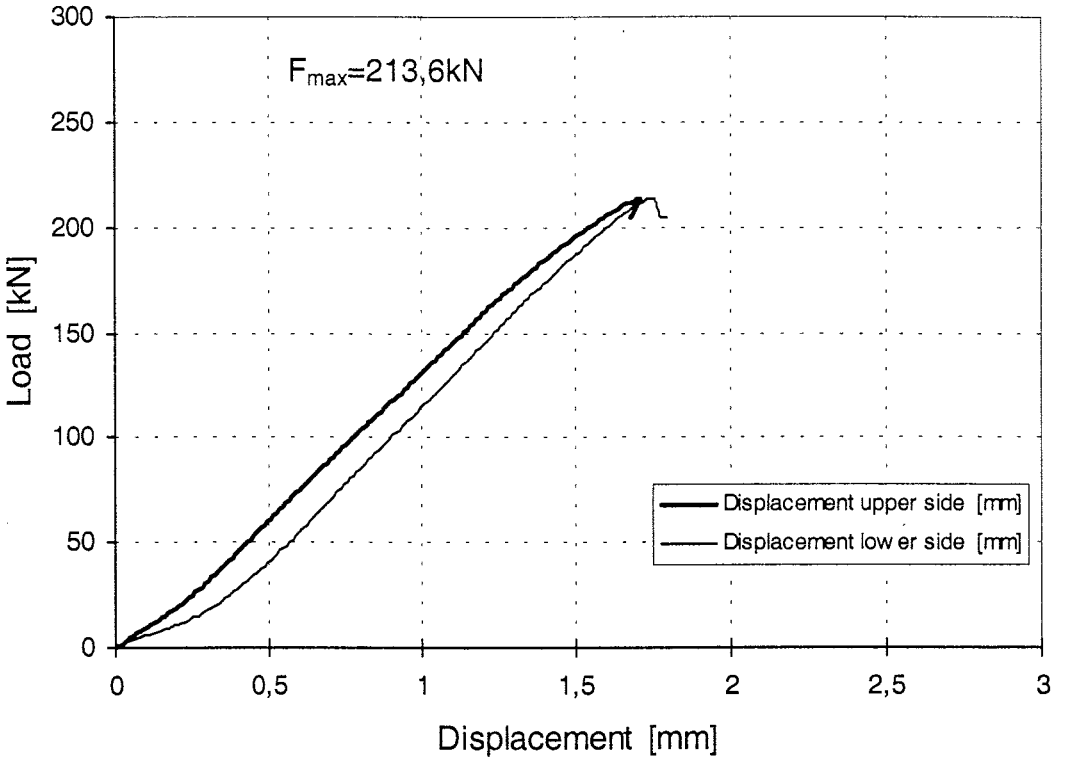

Figure 63: Load-displacement-curve of test Gi34-5

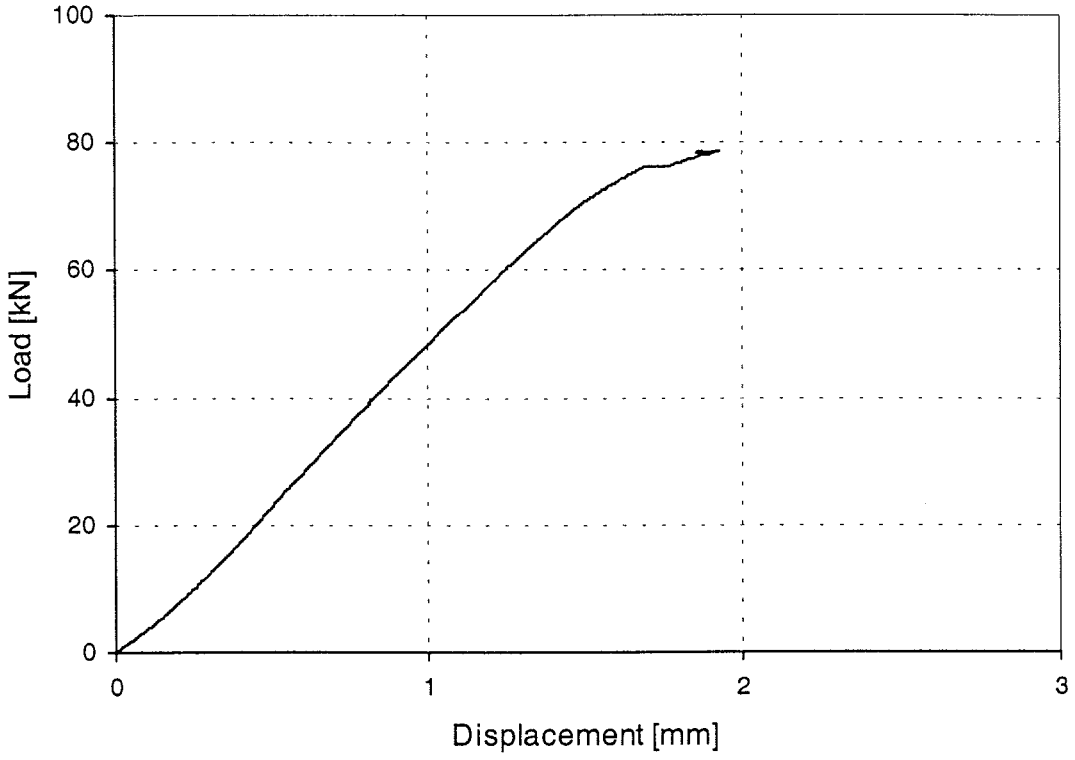

Figure 64: Load-displacement-curve of test Giq1-1

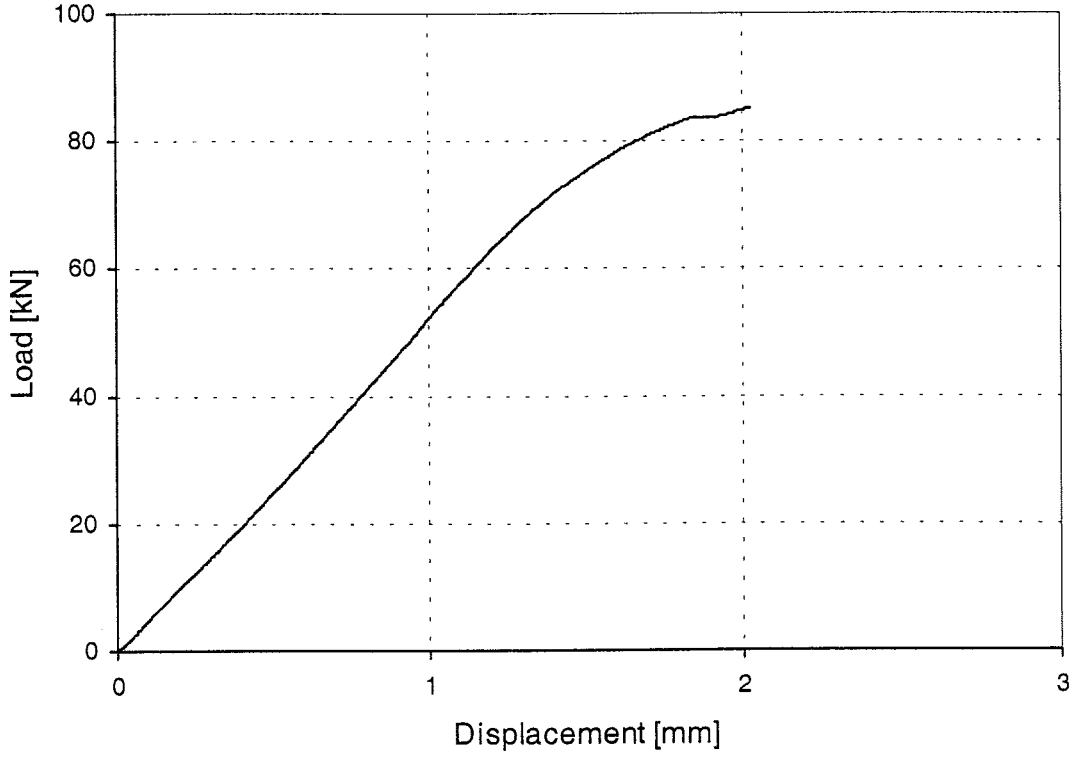

Figure 65: Load-displacement-curve of test Giq1-2

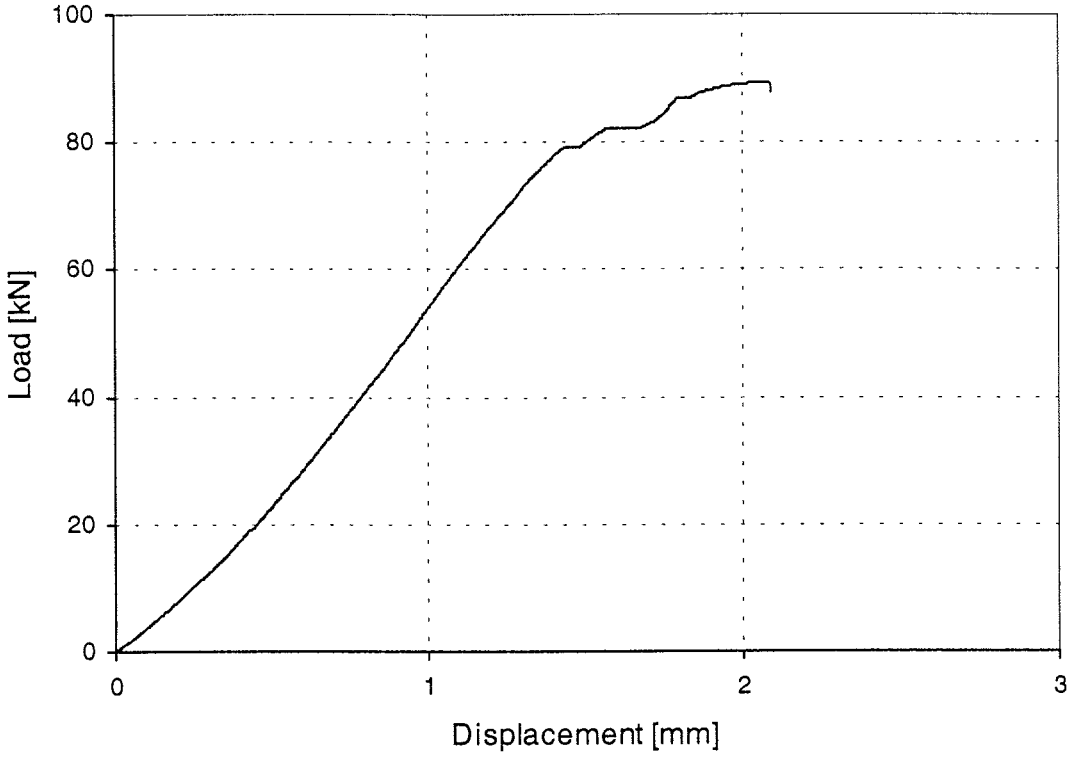

Figure 66: Load-displacement-curve of test Giq1-3

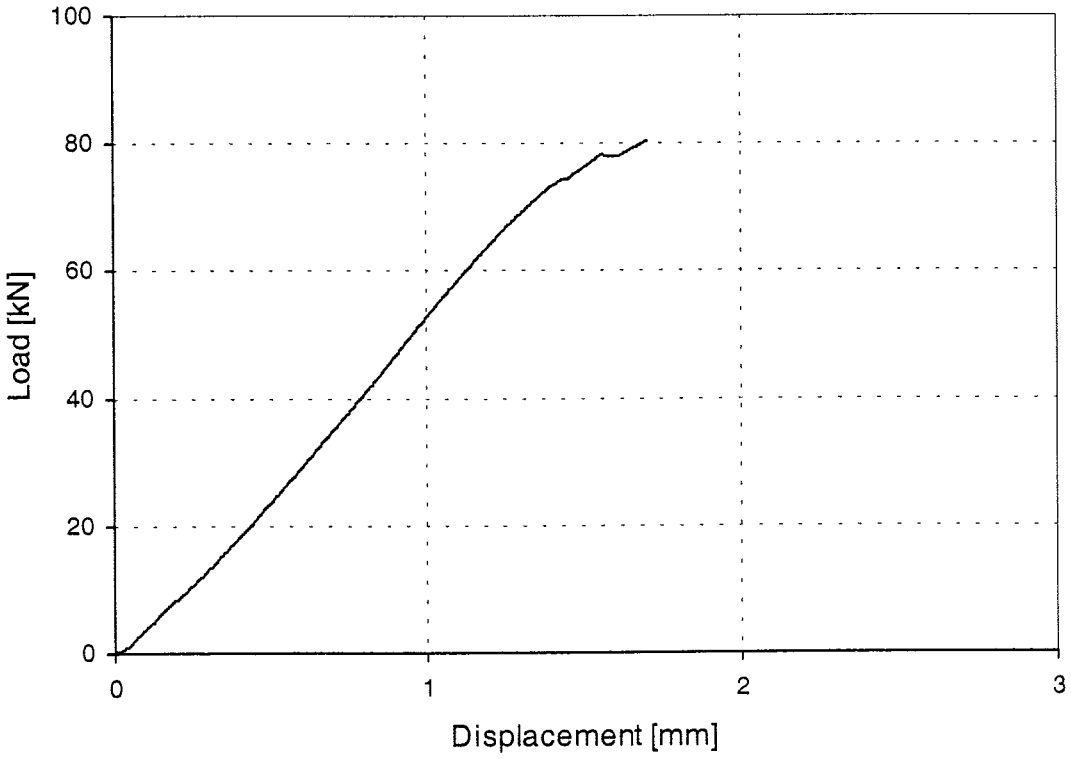

Figure 67: Load-displacement-curve of test Giq1-4

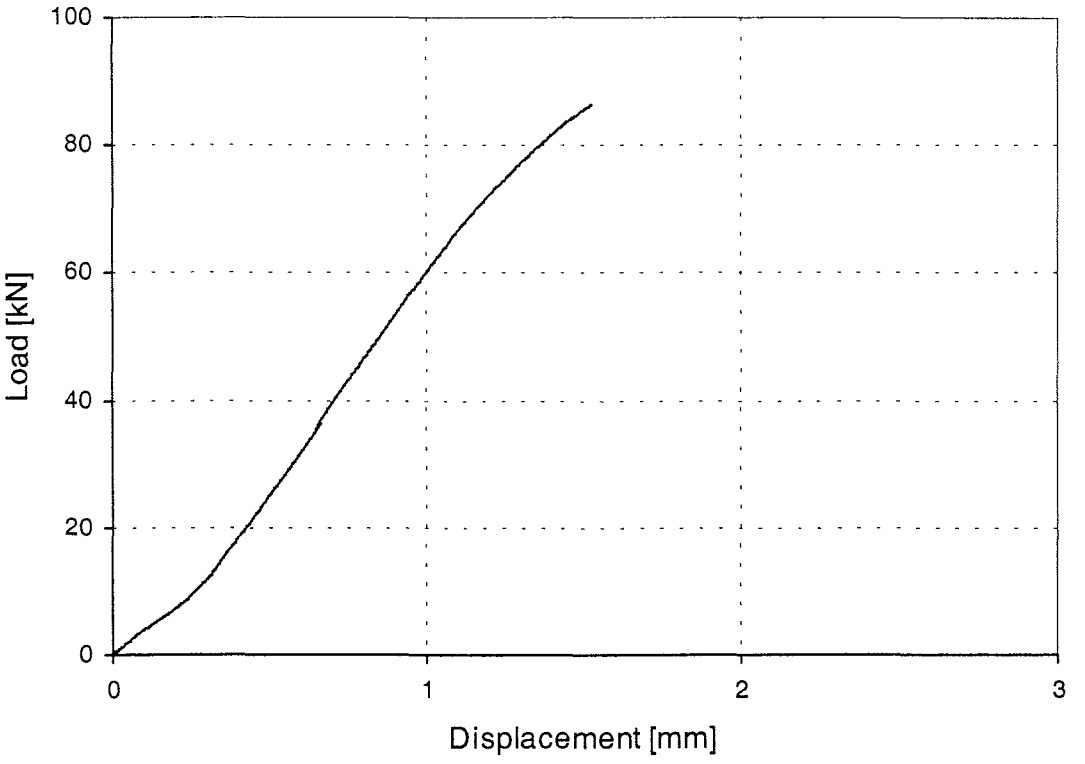

Figure 68: Load-displacement-curve of test Giq1-5

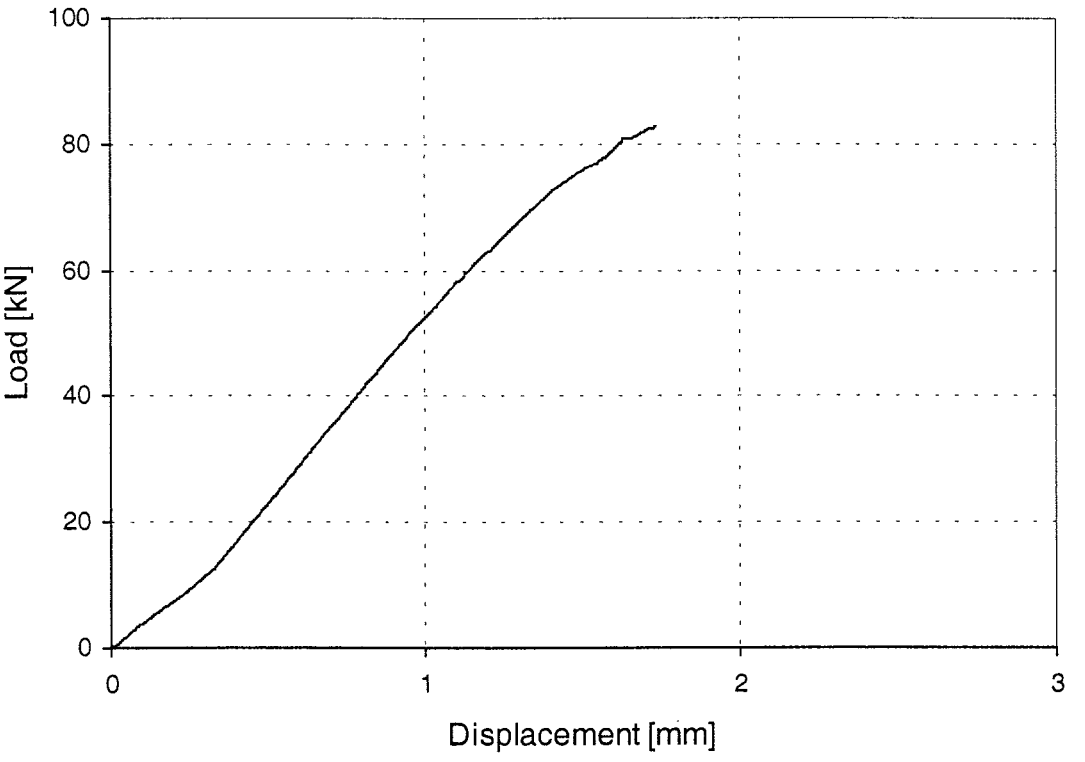

Figure 69: Load-displacement-curve of test Giq2-1

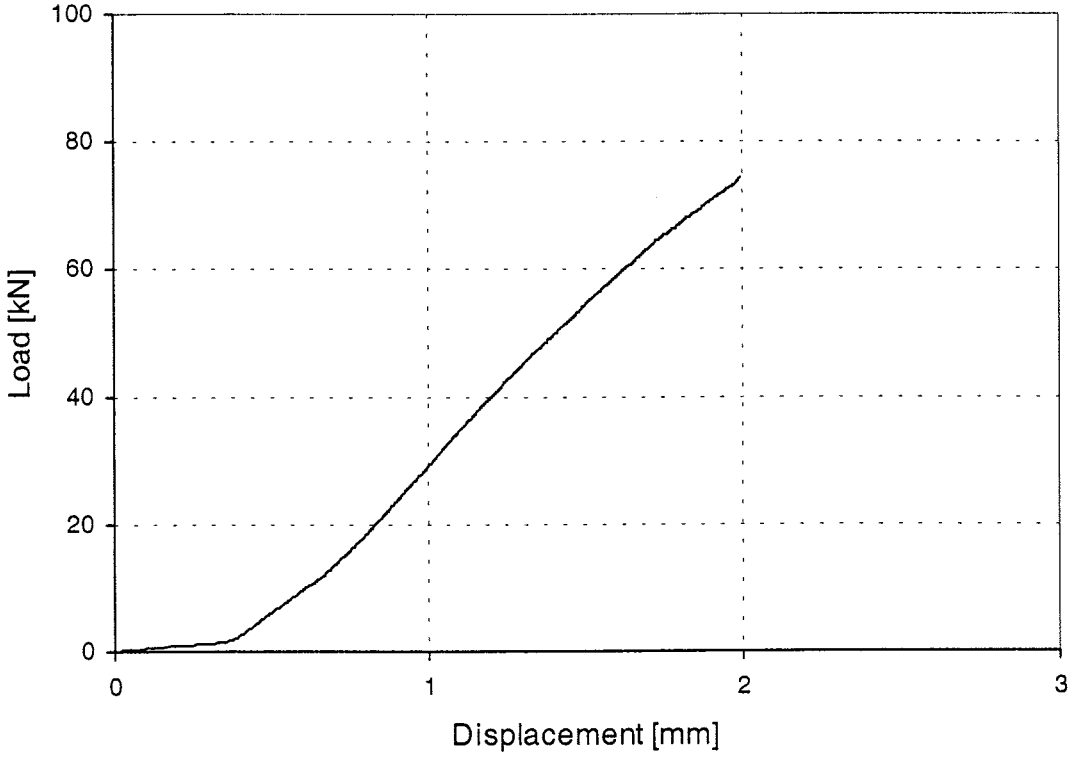

Figure 70: Load-displacement-curve of test Giq2-2

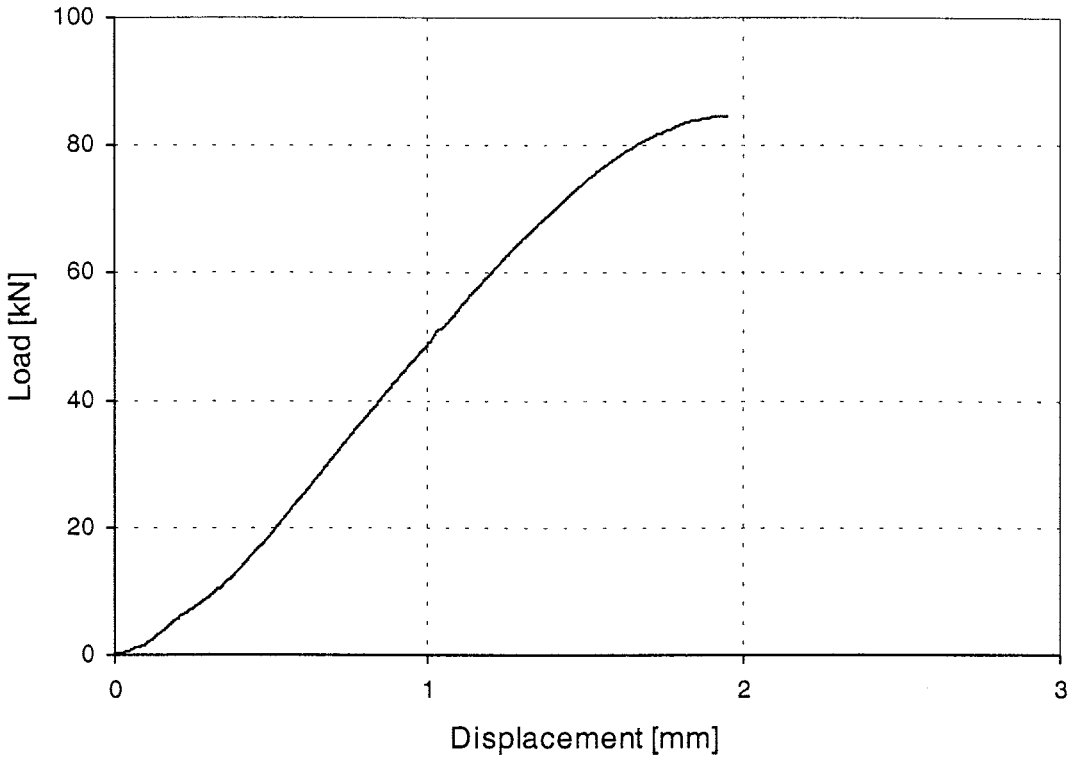

Figure 71: Load-displacement-curve of test Giq2-3

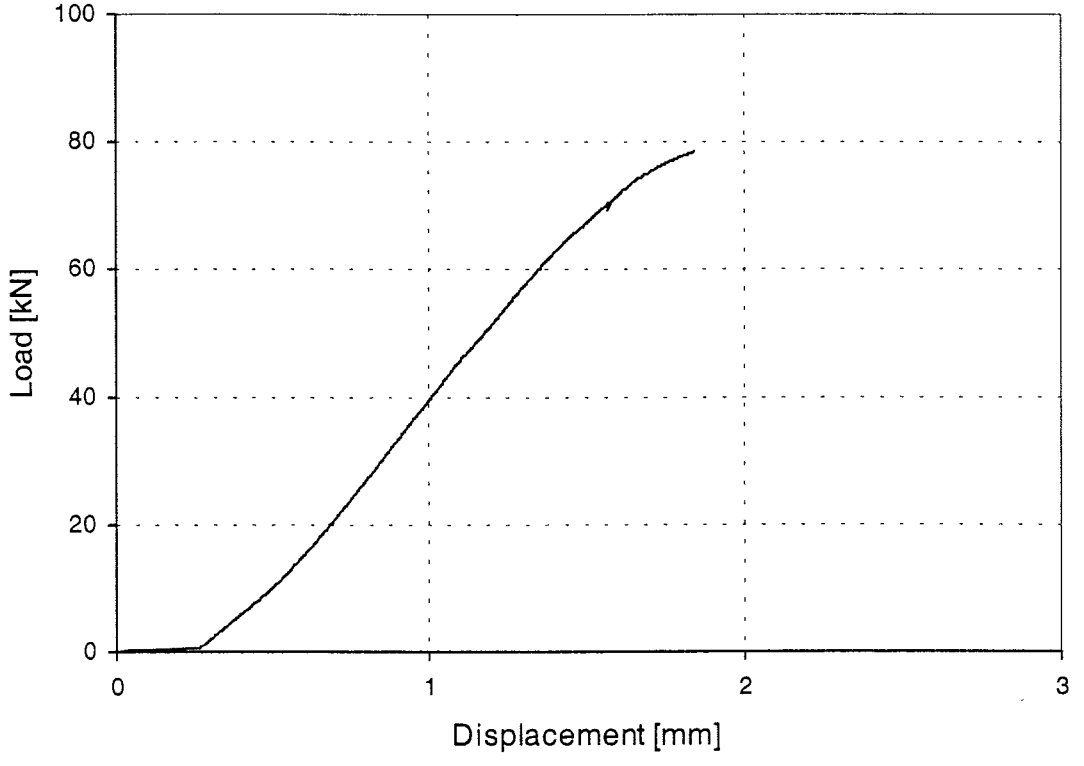

Figure 72: Load-displacement-curve of test Giq2-4

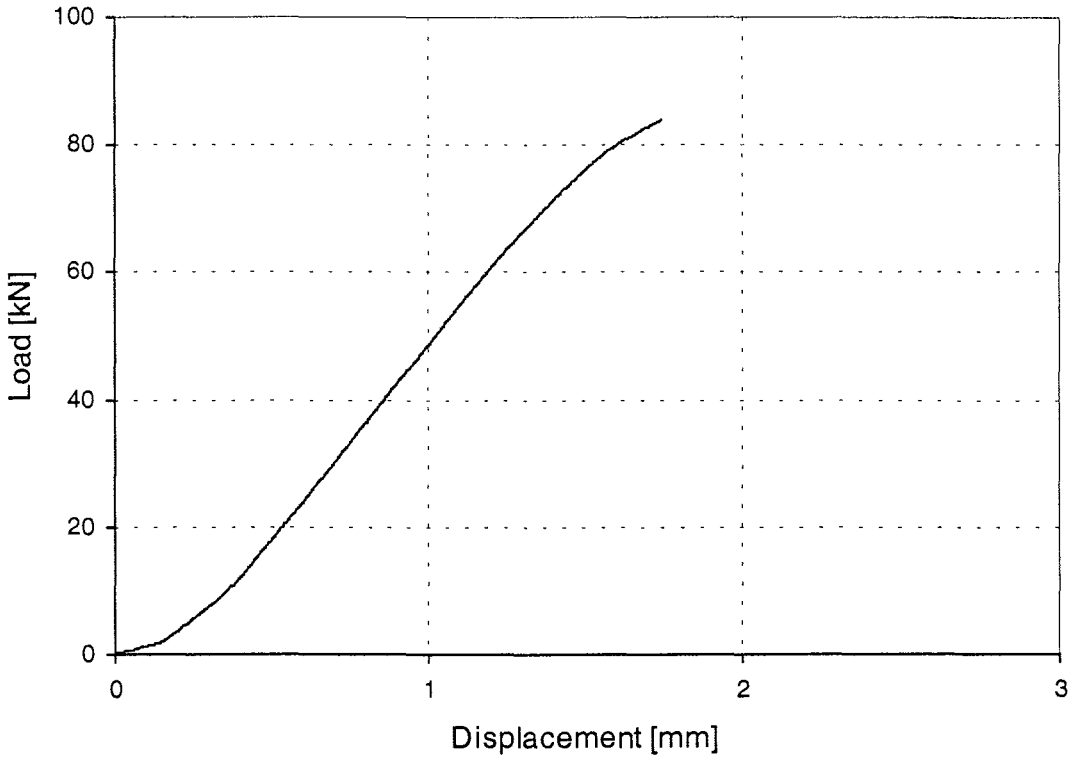

Figure 73: Load-displacement-curve of test Giq2-5

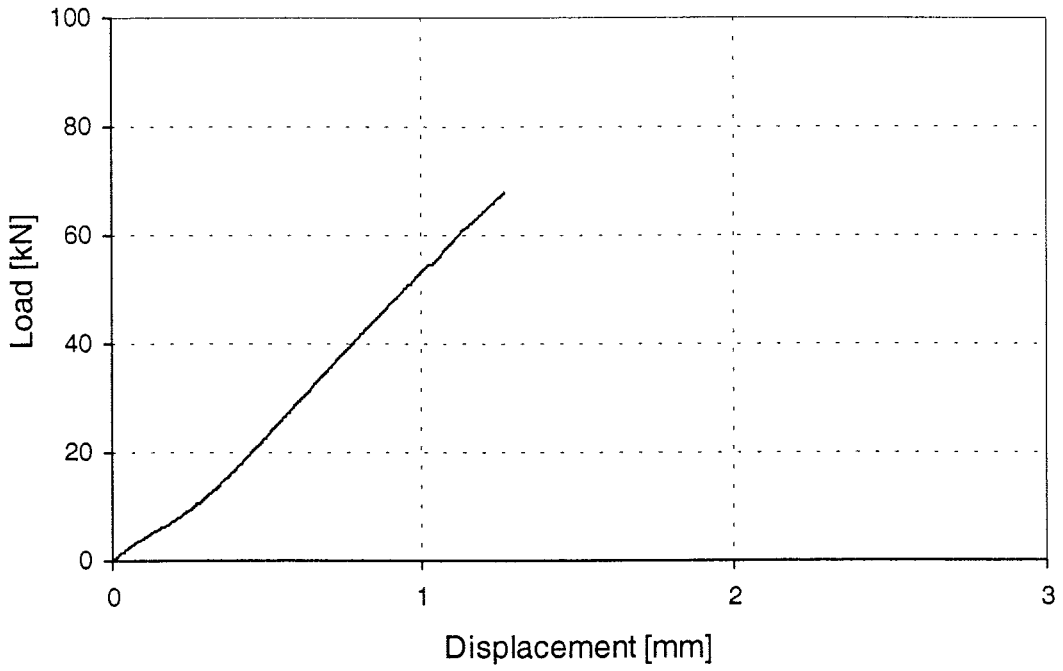

Figure 74: Load-displacement-curve of test Giq3-1

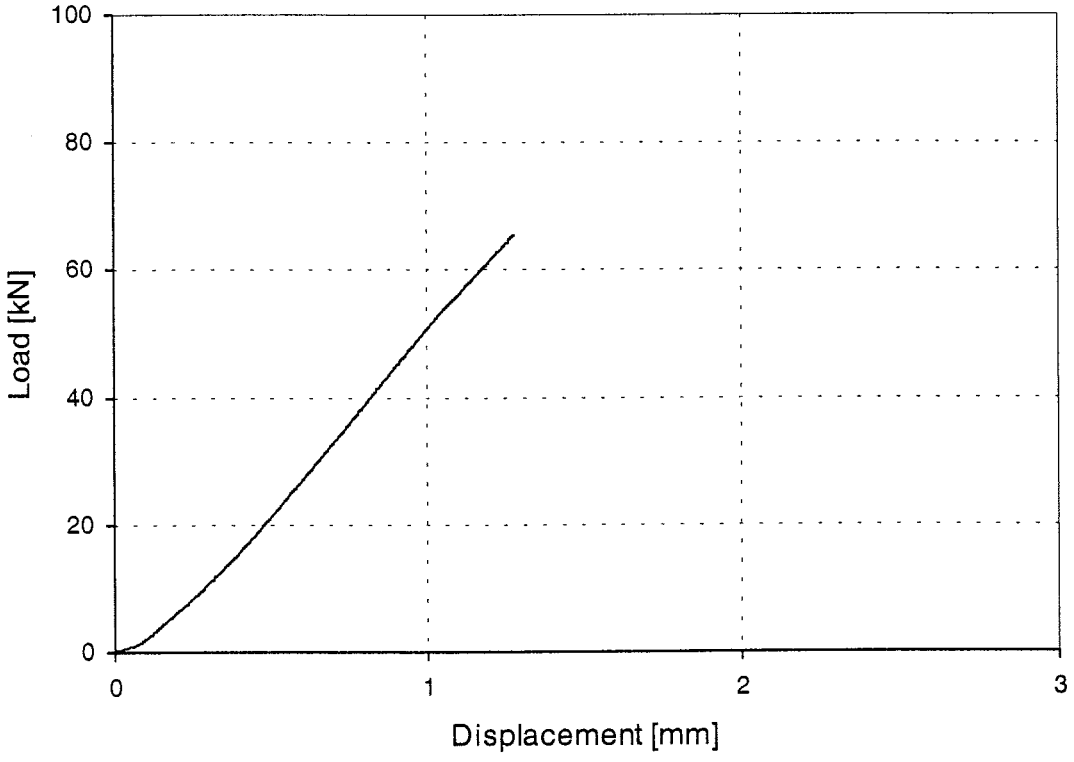

Figure 75: Load-displacement-curve of test Giq3-2

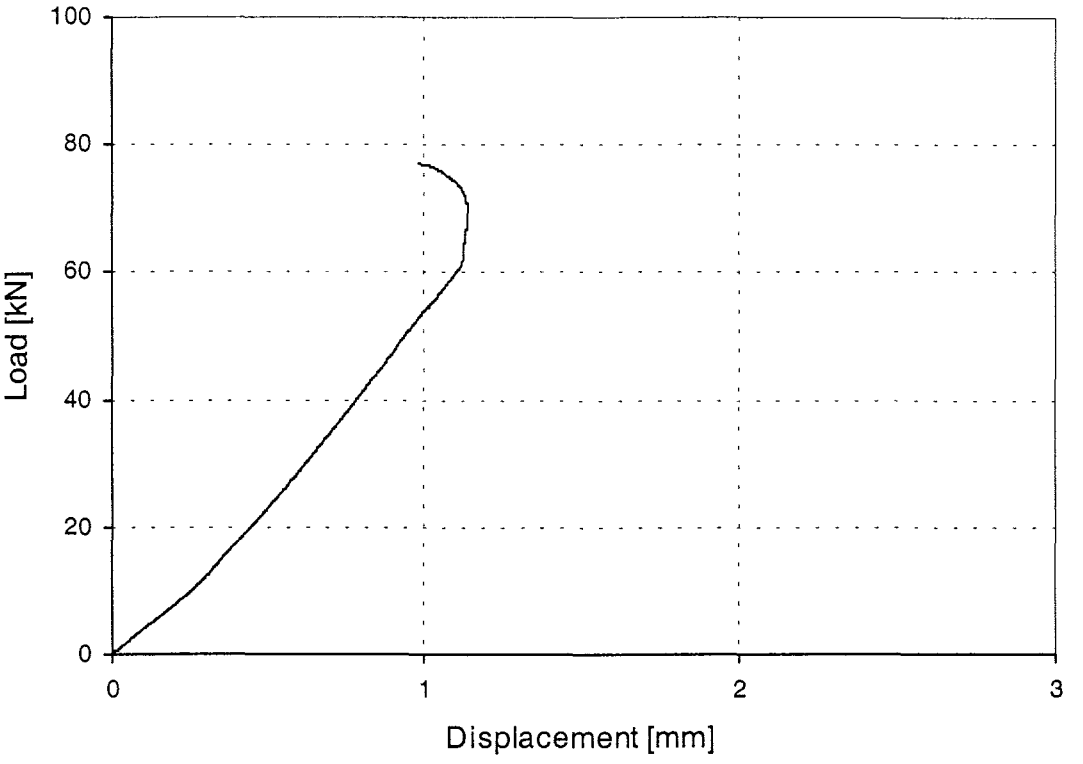

Figure 76: Load-displacement-curve of test Giq3-3

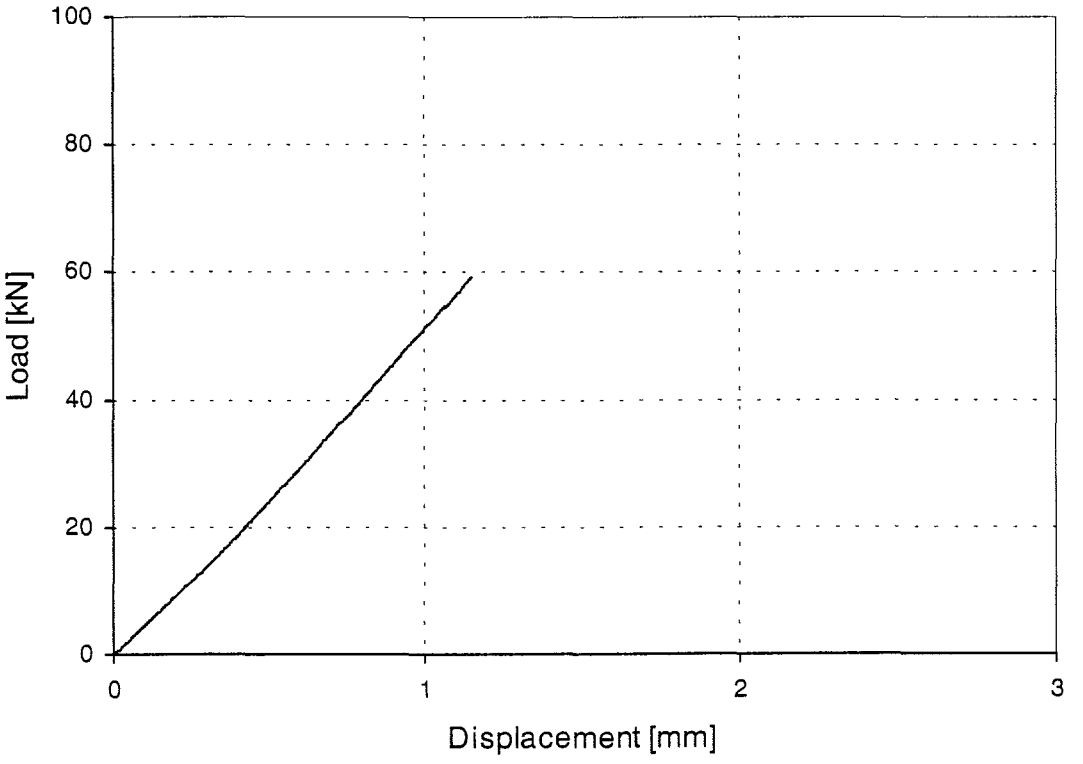

Figure 77: Load-displacement-curve of test Giq3-4

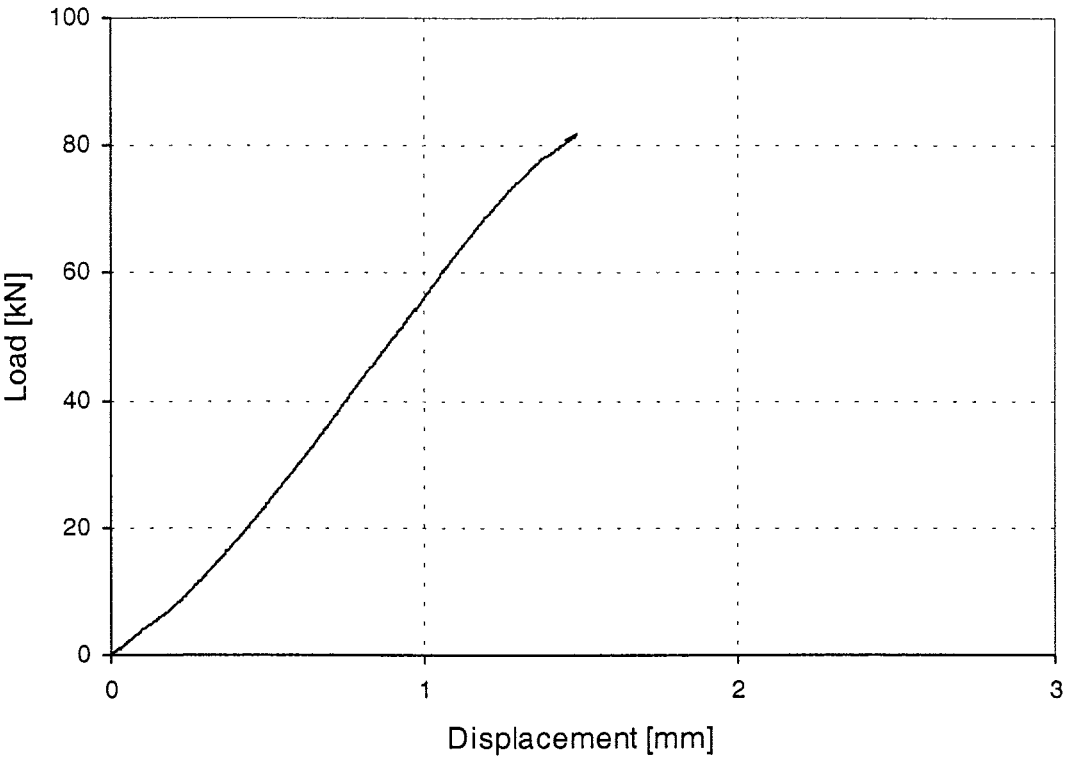

Figure 78: Load-displacement-curve of test Giq3-5

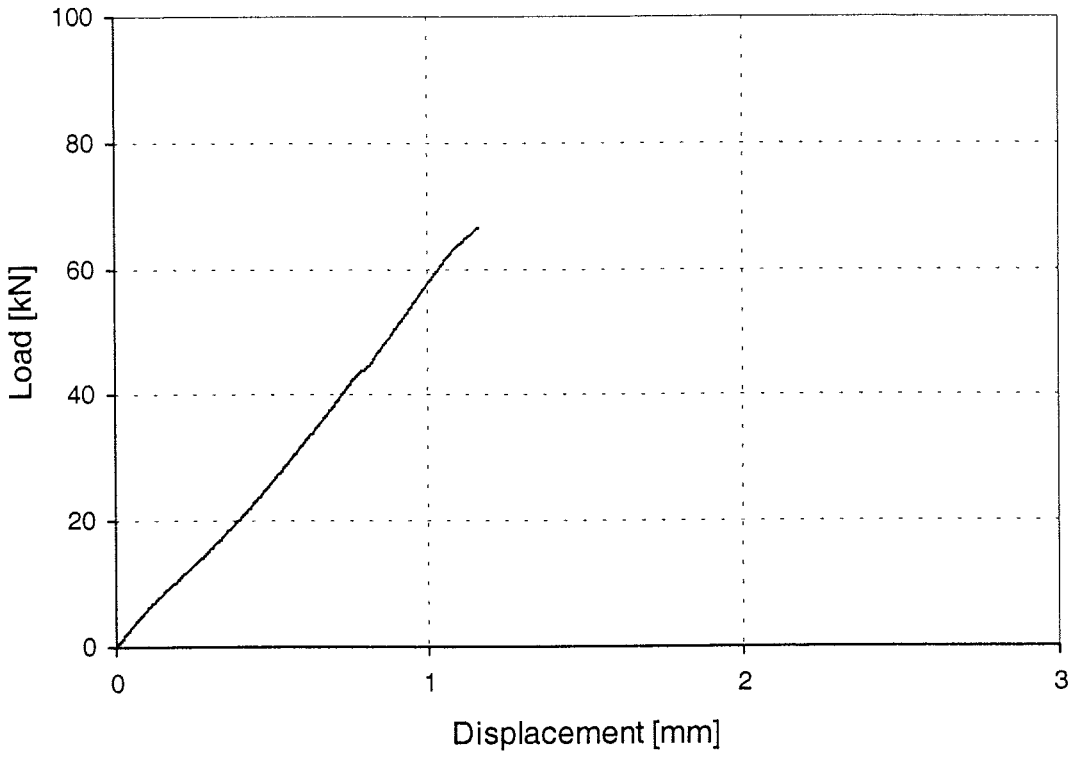

Figure 79: Load-displacement-curve of test Giq4-1

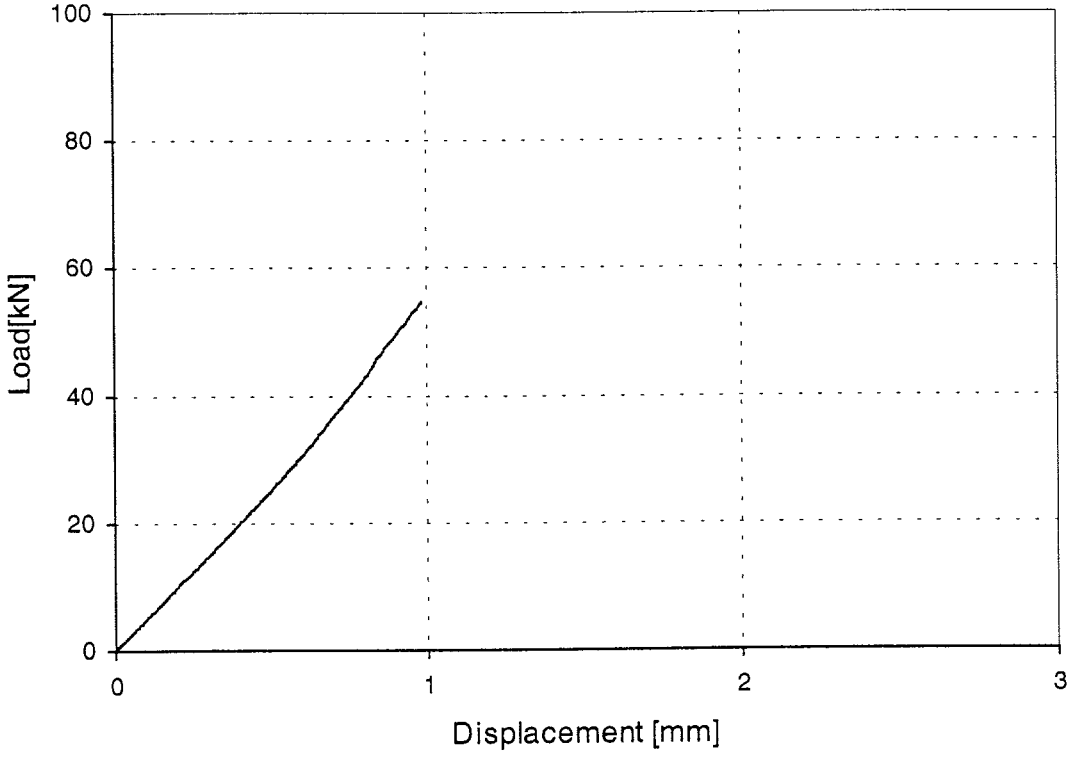

Figure 80: Load-displacement-curve of test Giq4-2

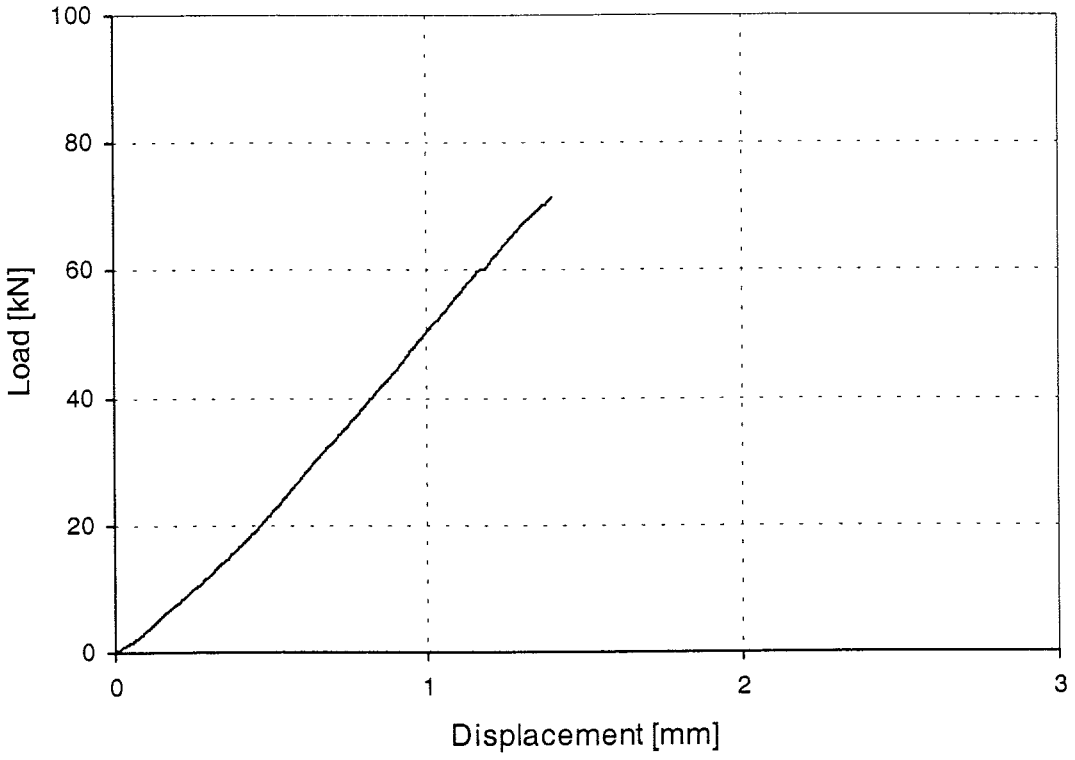

Figure 81: Load-displacement-curve of test Giq4-3

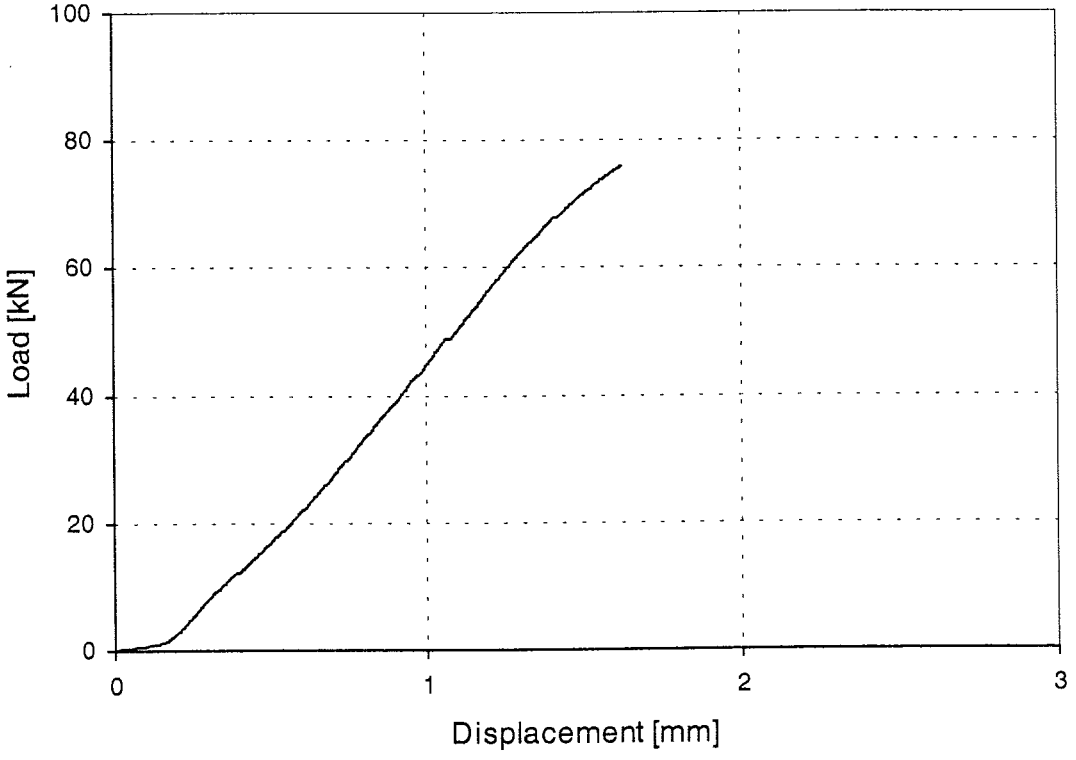

Figure 82: Load-displacement-curve of test Giq4-4

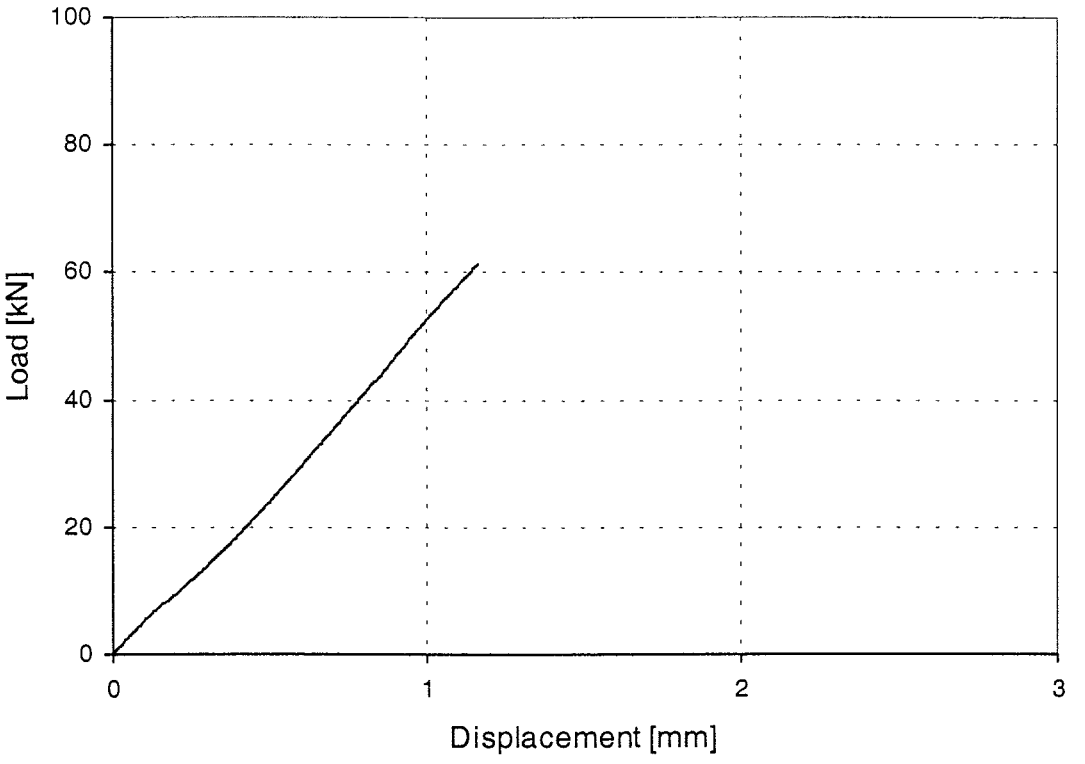

Figure 83: Load-displacement-curve of test Giq4-5

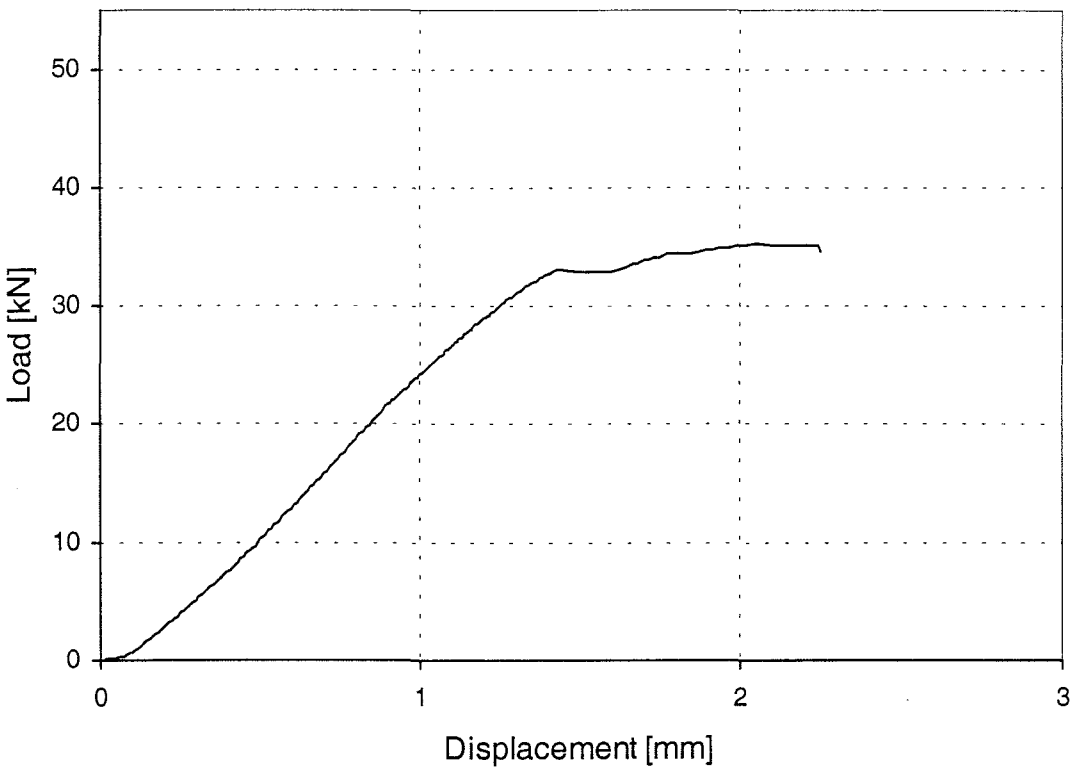

Figure 84: Load-displacement-curve of test Giq5-1

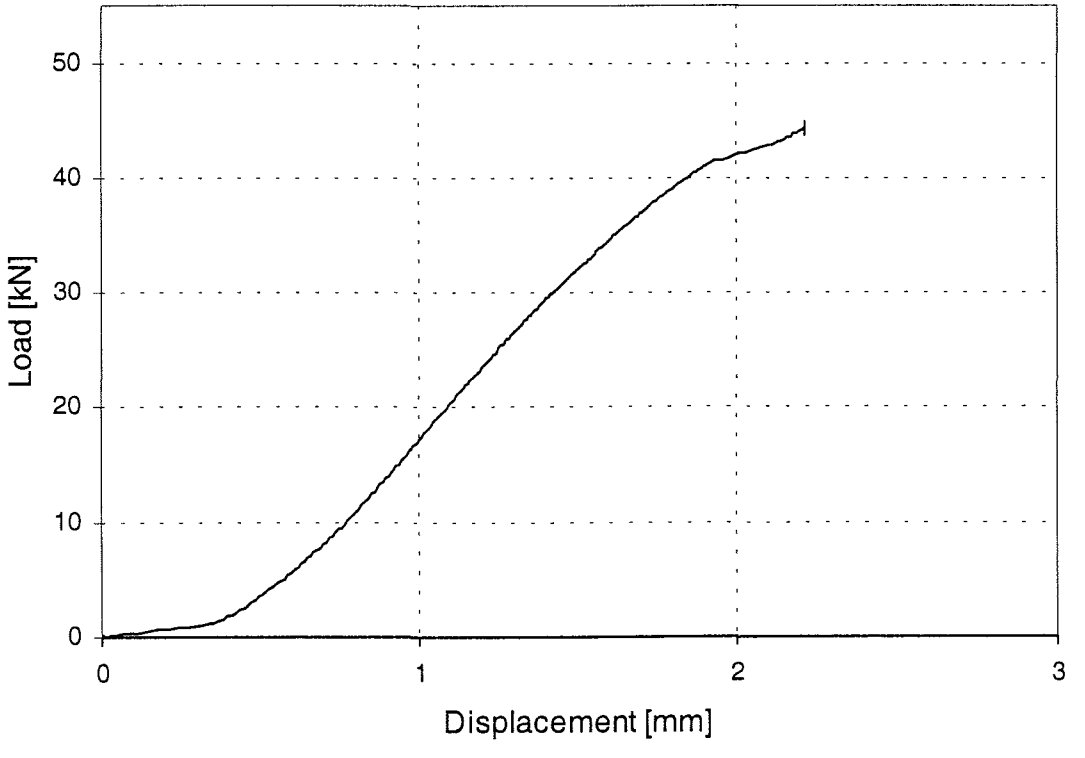

Figure 85: Load-displacement-curve of test Giq5-2

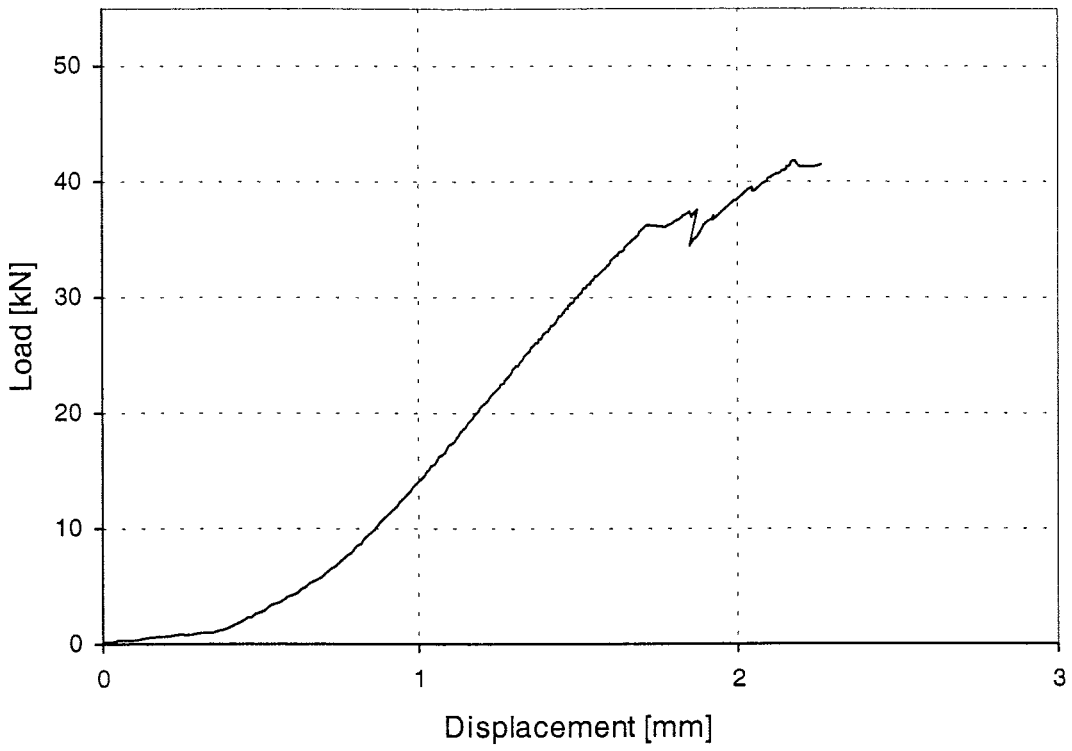

Figure 86: Load-displacement-curve of test Giq5-3

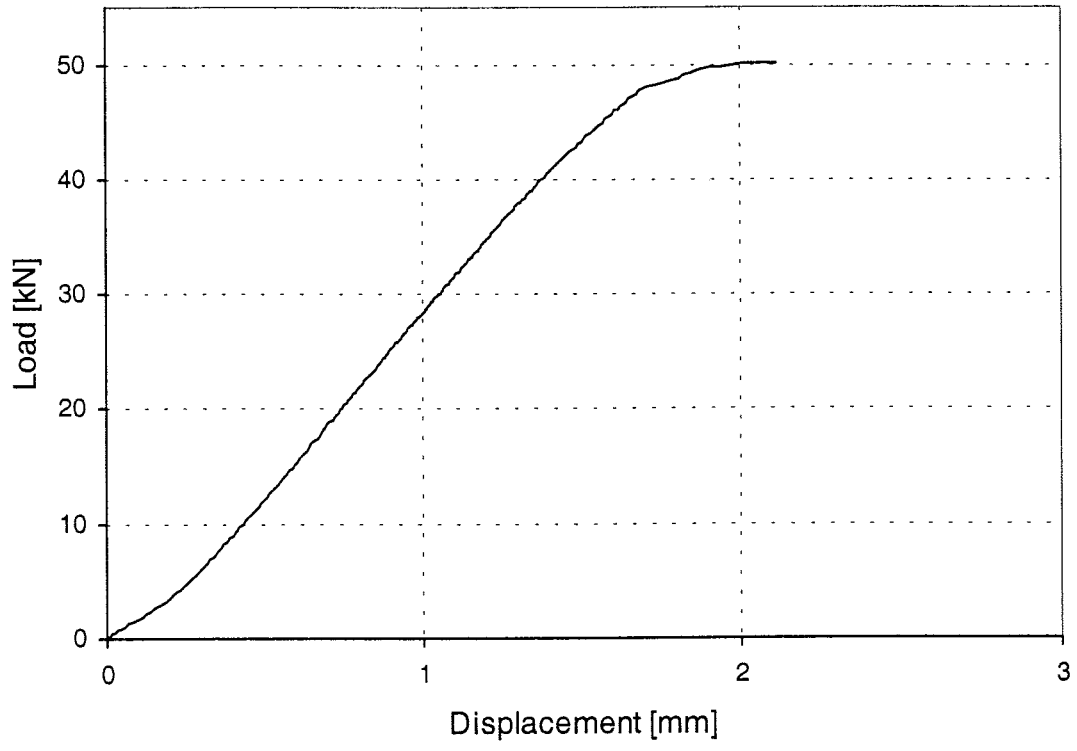

Figure 87: Load-displacement-curve of test Giq5-4

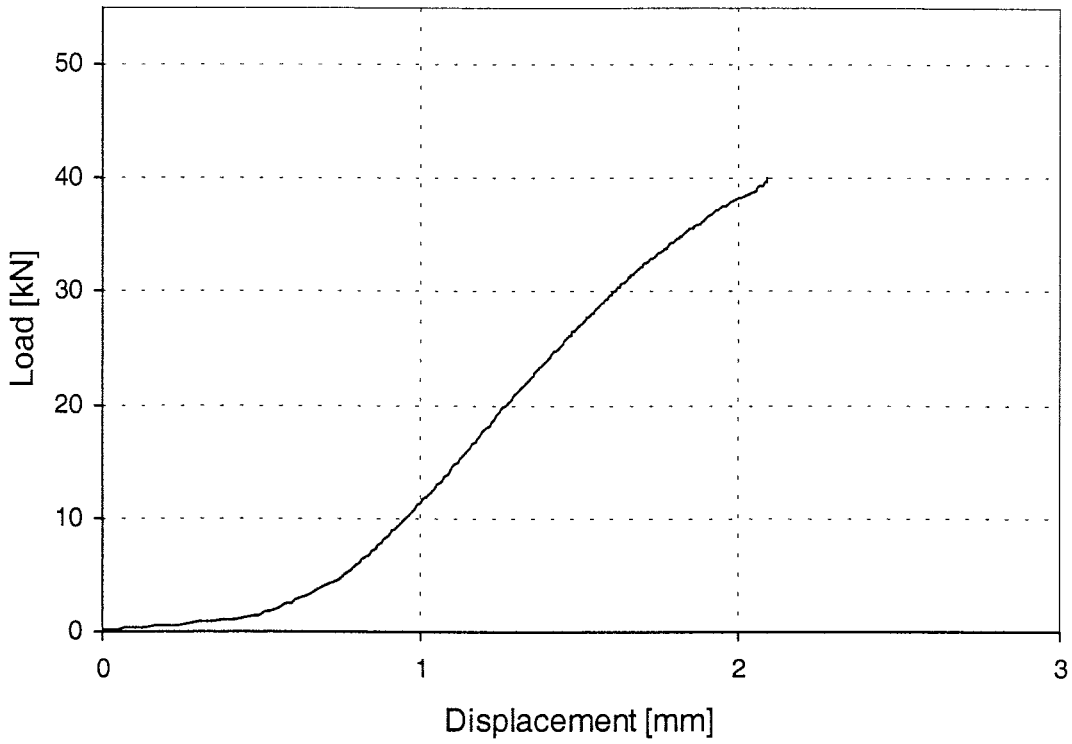

Figure 88: Load-displacement-curve of test Giq5-5

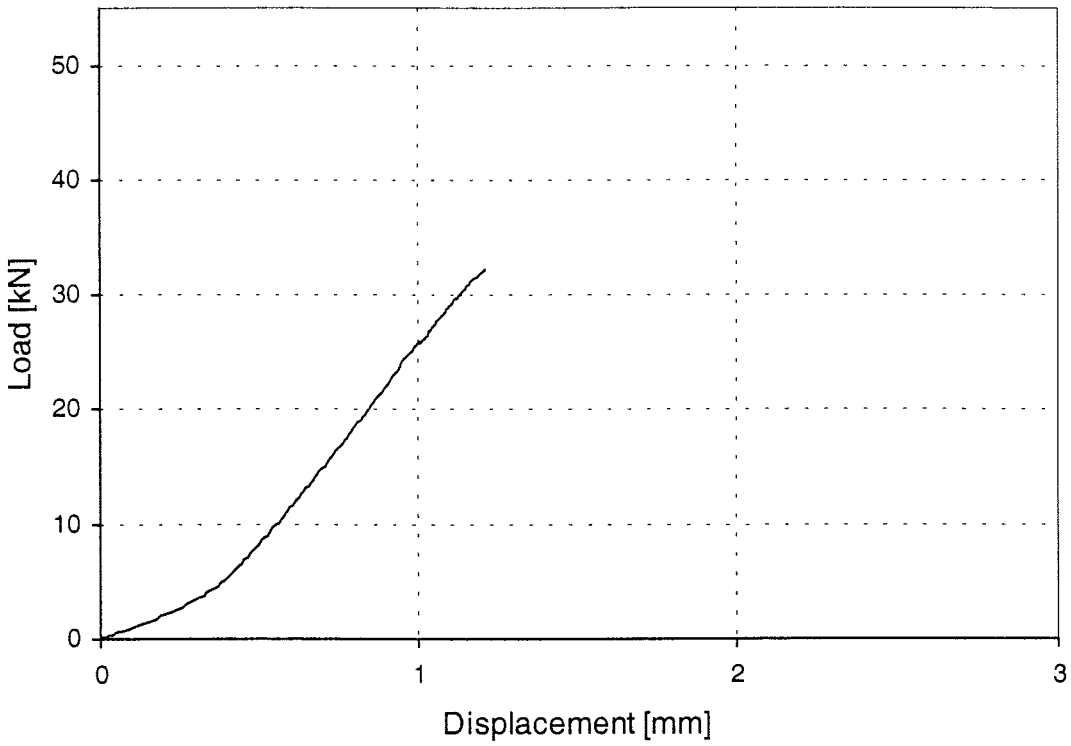

Figure 89: Load-displacement-curve of test Giq6-1

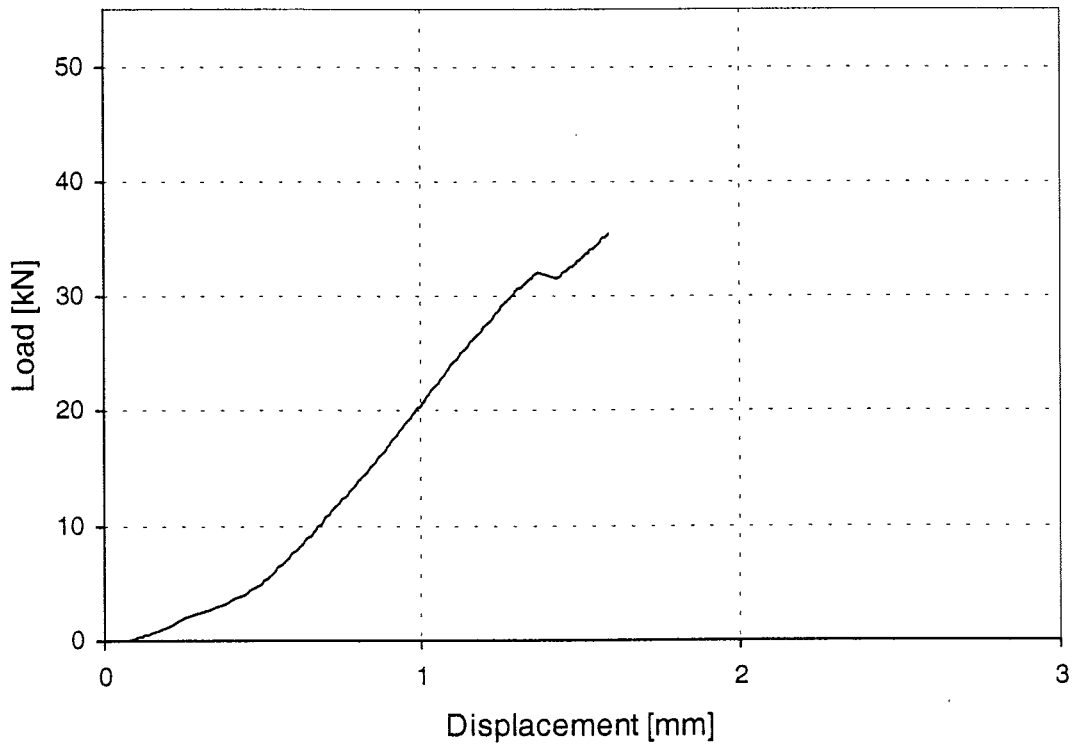

Figure 90: Load-displacement-curve of test Giq6-2

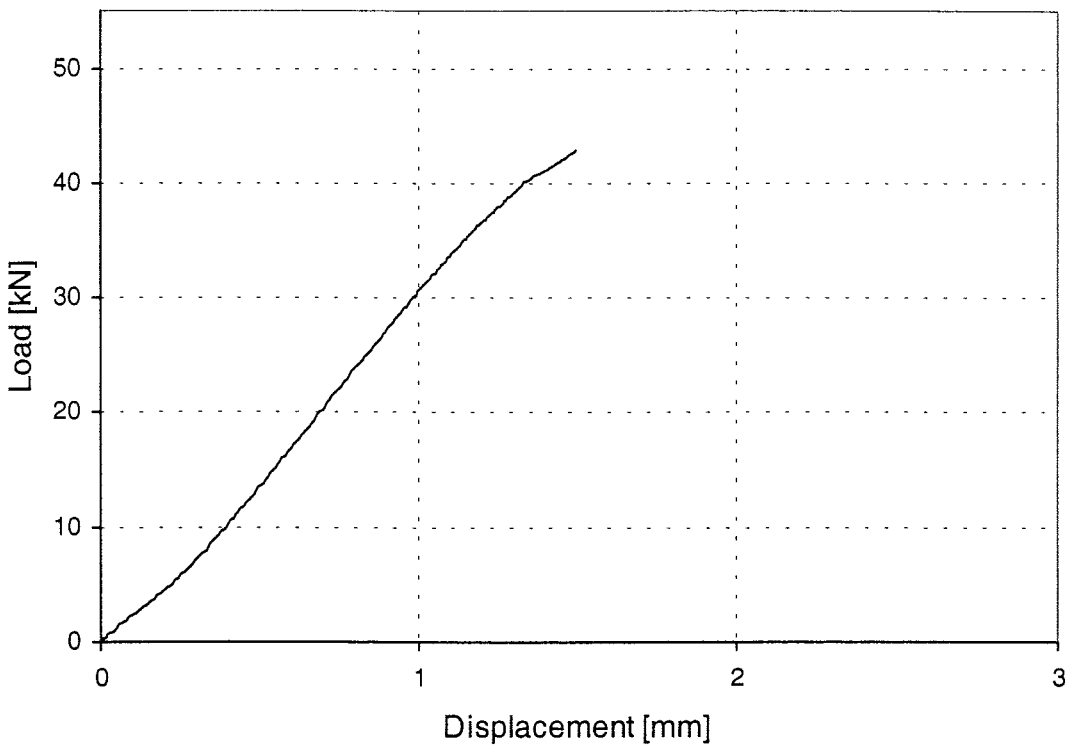

Figure 91: Load-displacement-curve of test Giq6-3

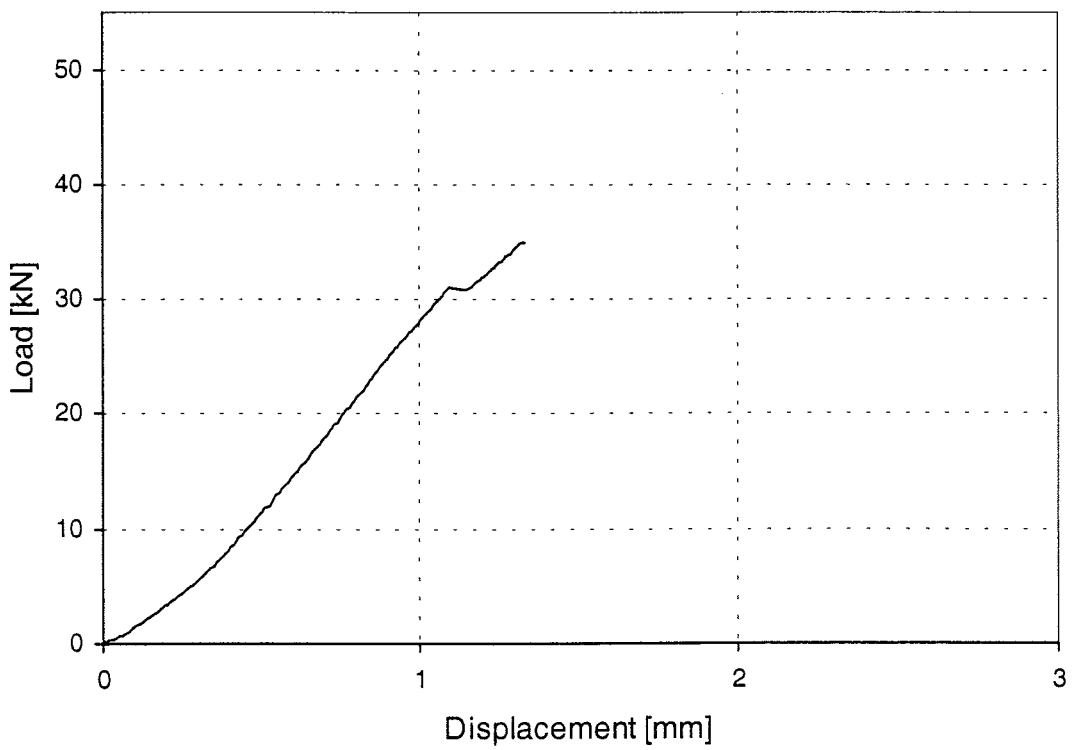

Figure 92: Load-displacement-curve of test Giq6-4

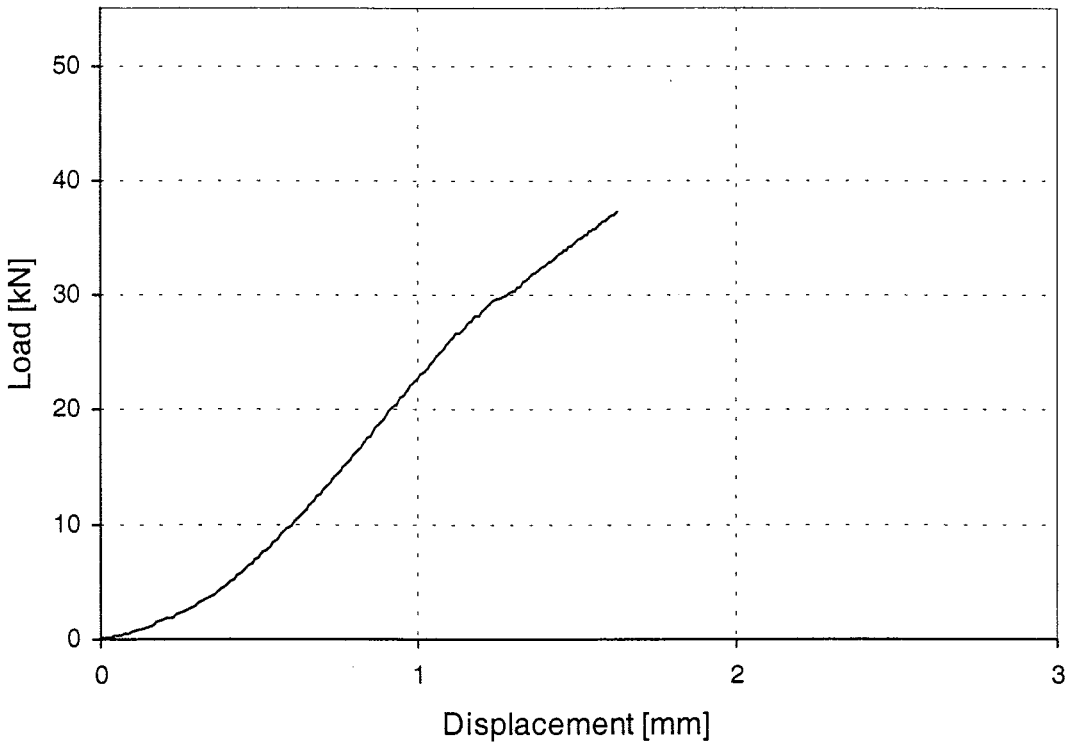

Figure 93: Load-displacement-curve of test Giq6-5

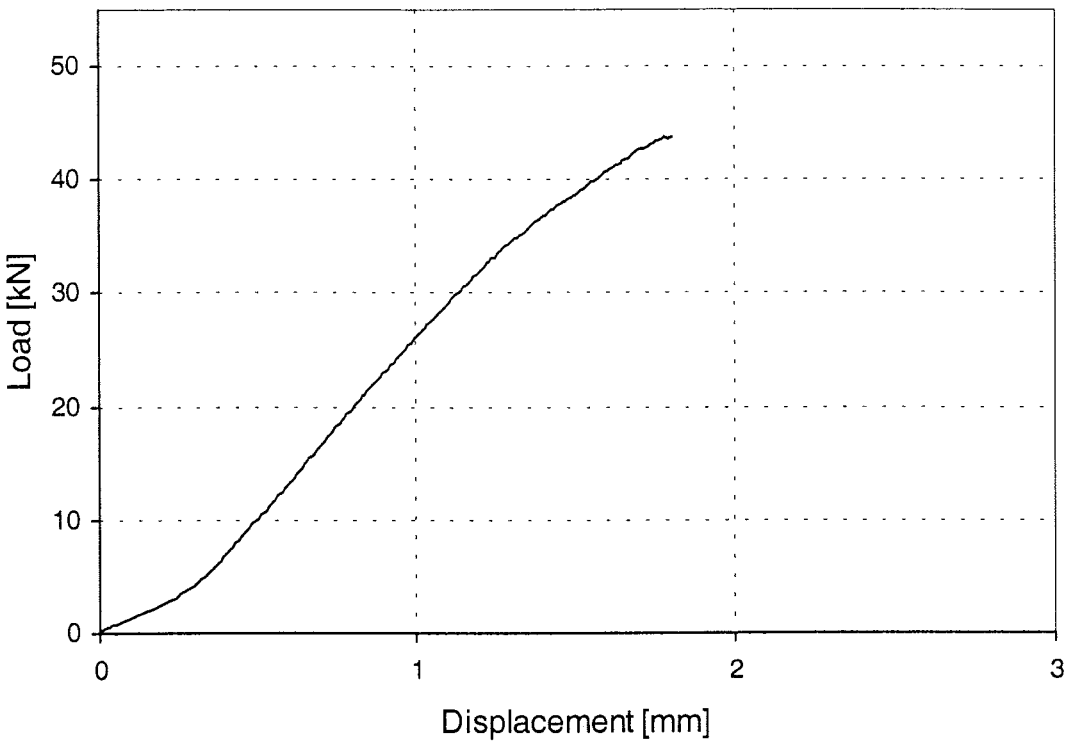

Figure 94: Load-displacement-curve of test Giq7-1

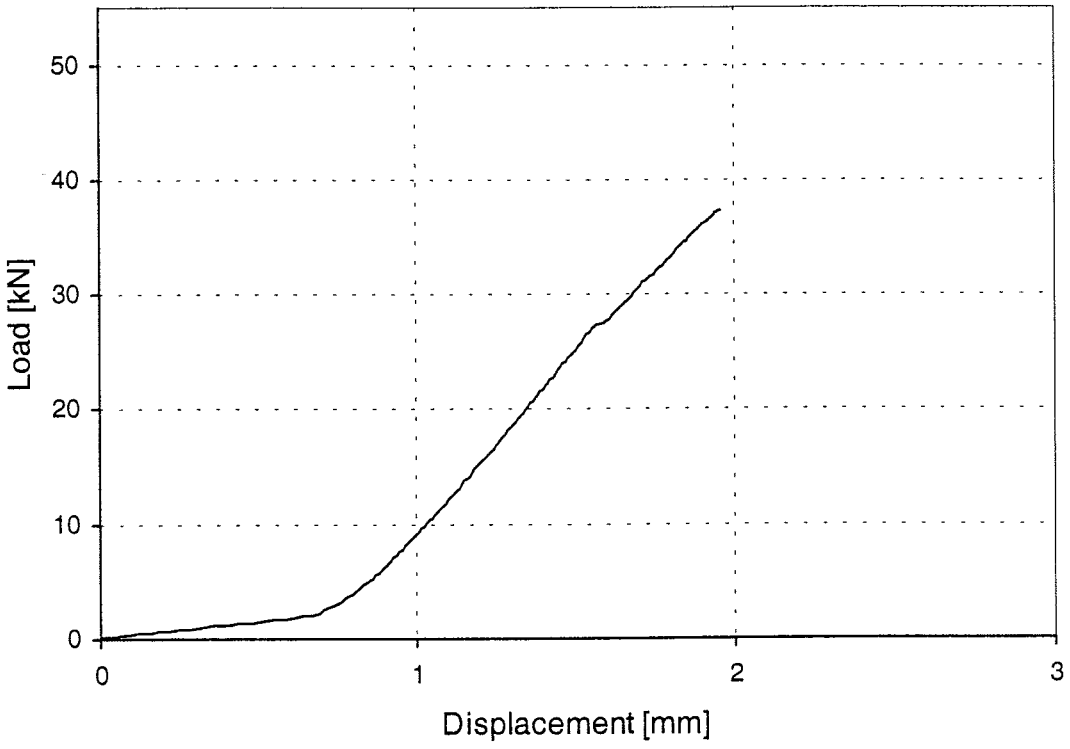

Figure 95: Load-displacement-curve of test Giq7-2

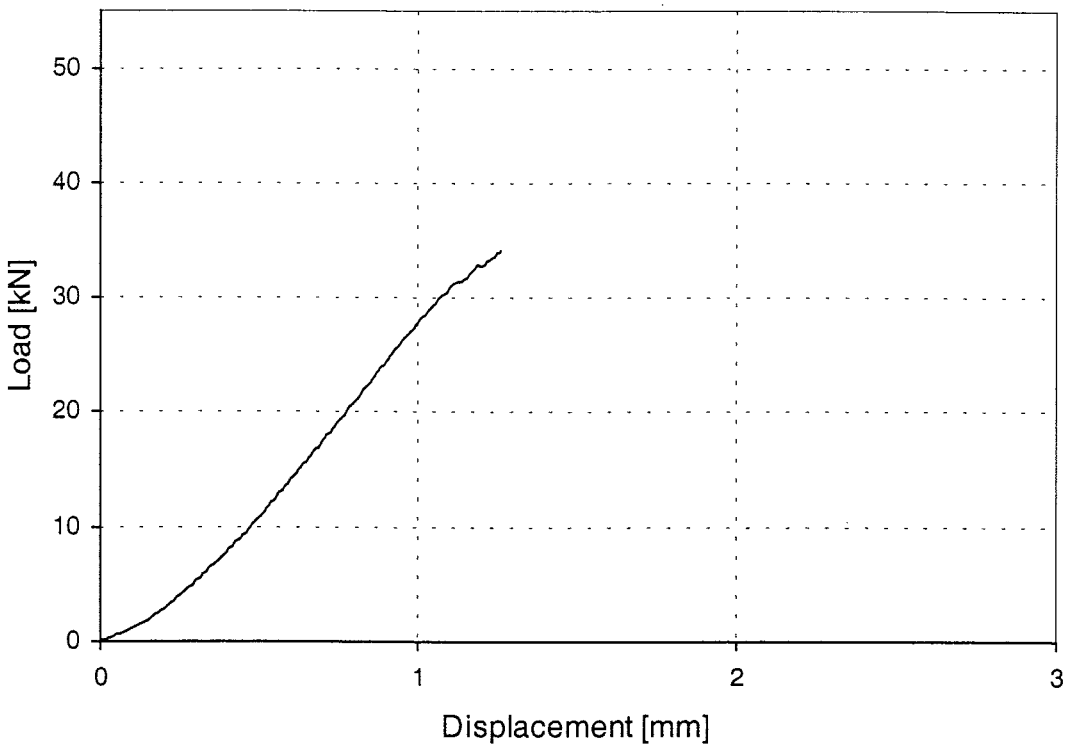

Figure 96: Load-displacement-curve of test Giq7-3

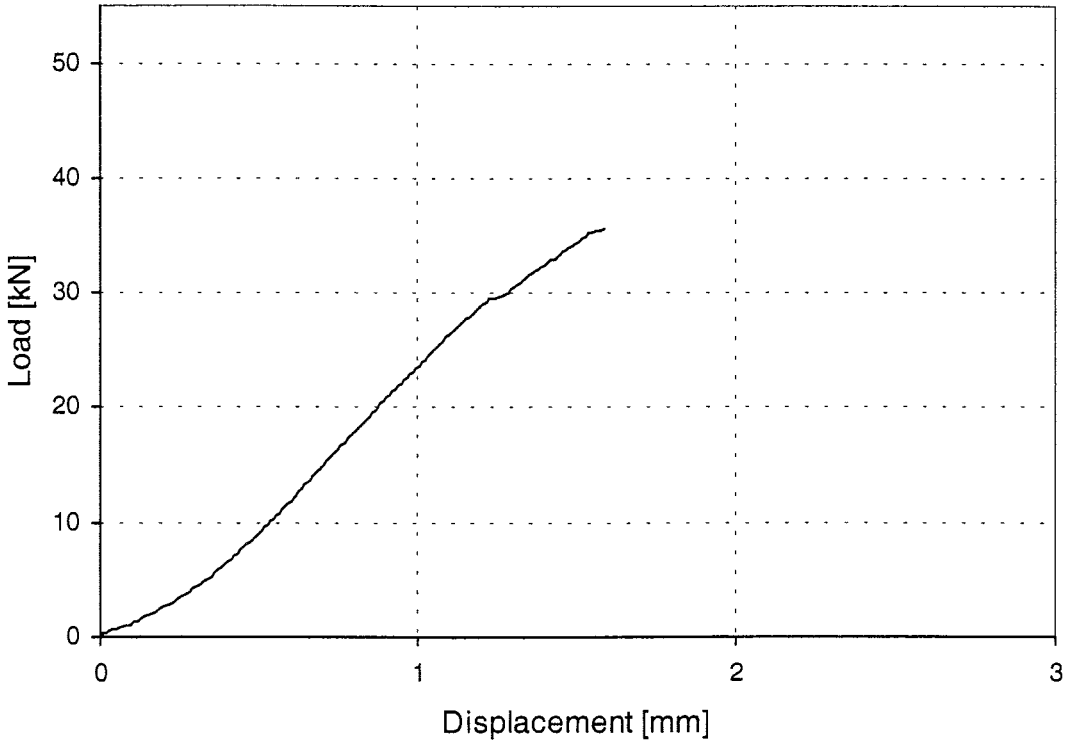

Figure 97: Load-displacement-curve of test Giq7-4

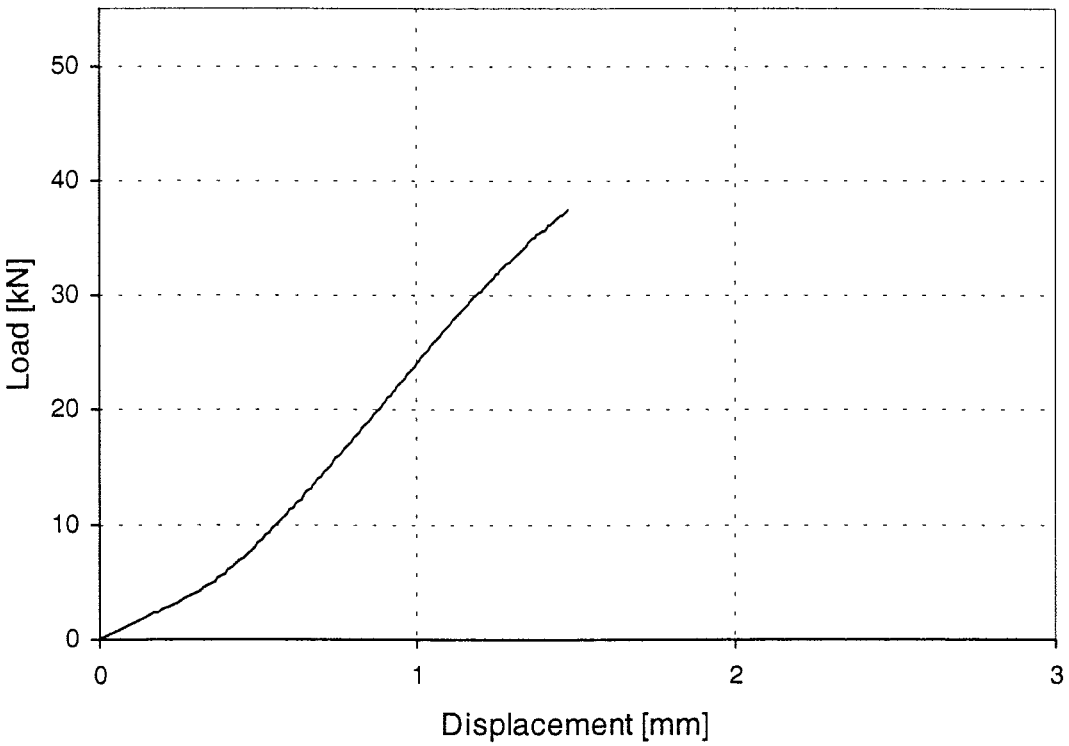

Figure 98: Load-displacement-curve of test Giq7-5

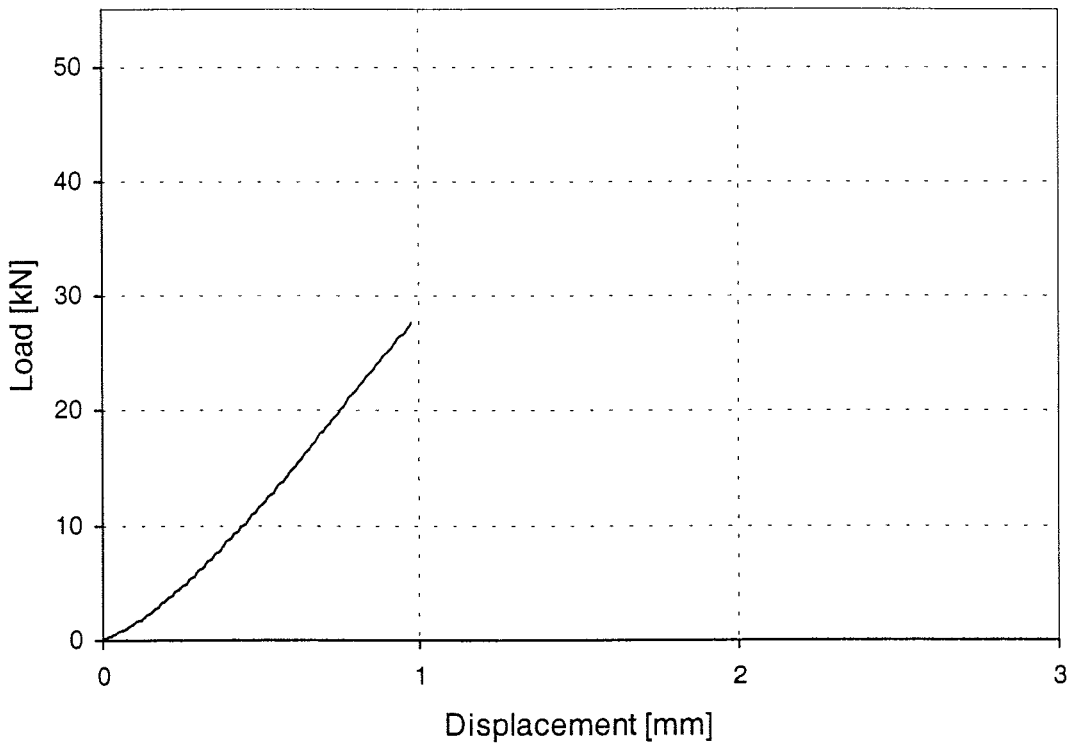

Figure 99: Load-displacement-curve of test Giq8-1

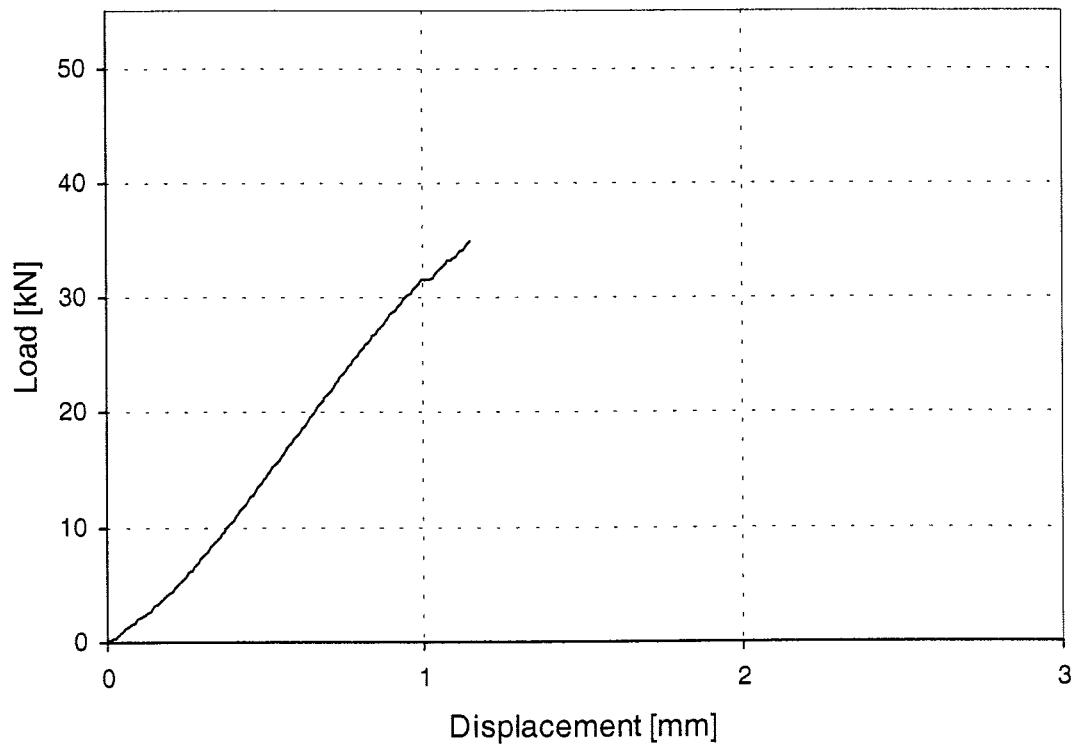

Figure 100: Load-displacement-curve of test Giq8-2

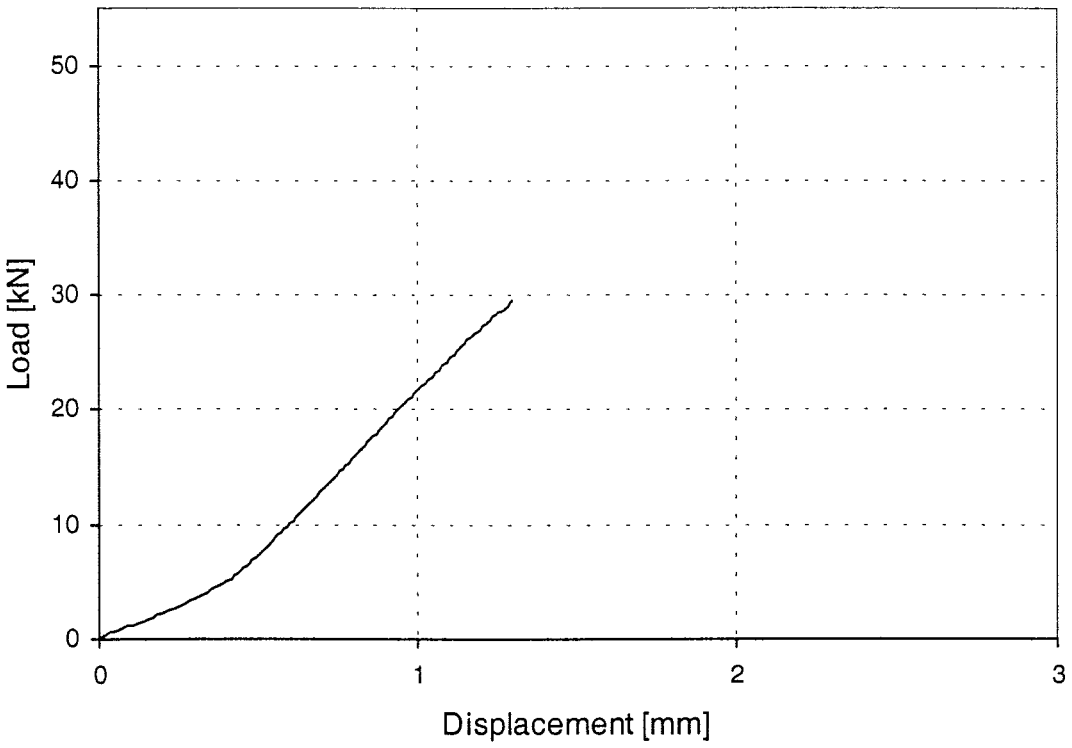

Figure 101: Load-displacement-curve of test Giq8-3

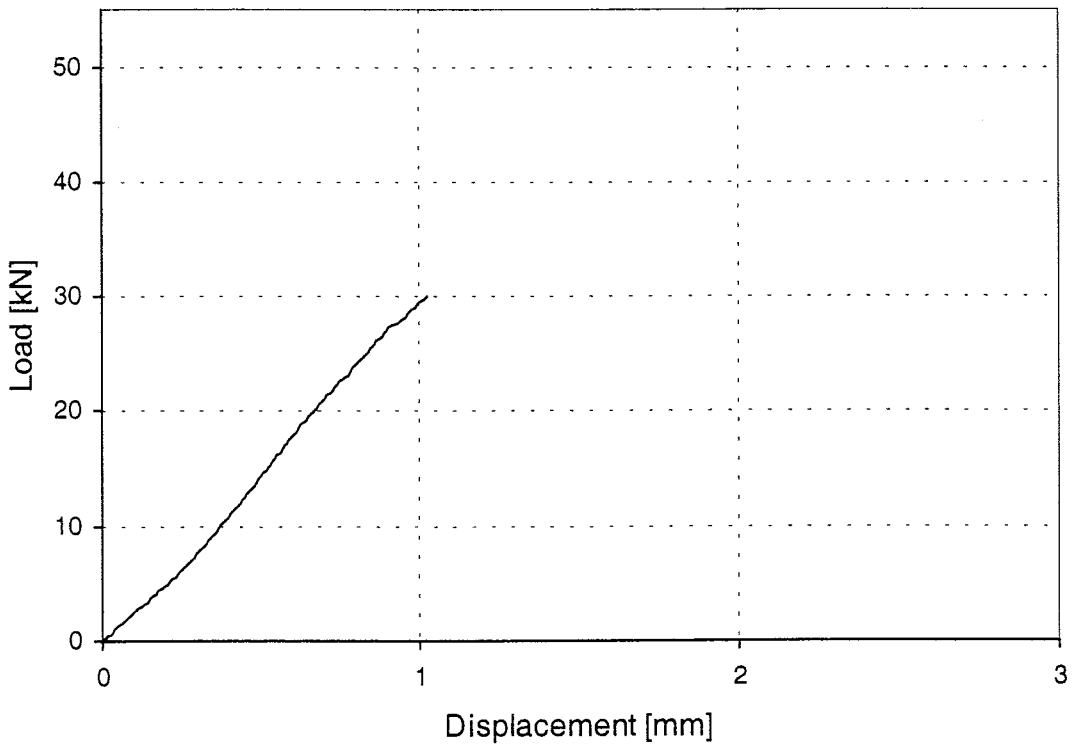

Figure 102: Load-displacement-curve of test Giq8-4

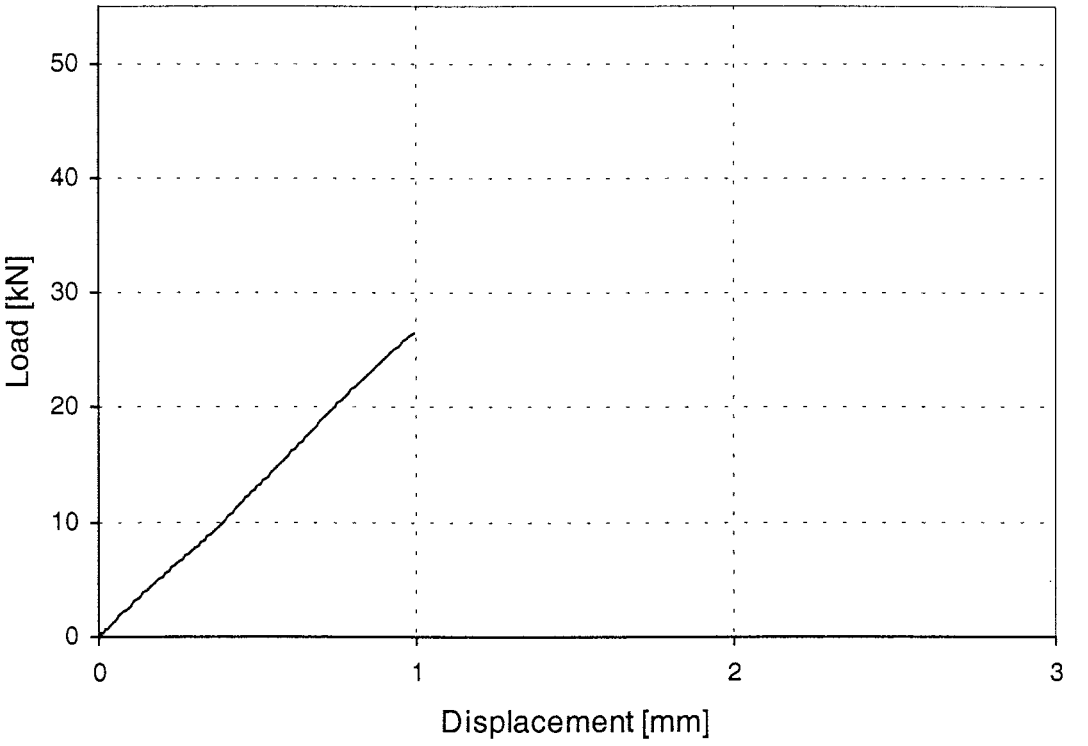

Figure 103: Load-displacement-curve of test Giq8-5

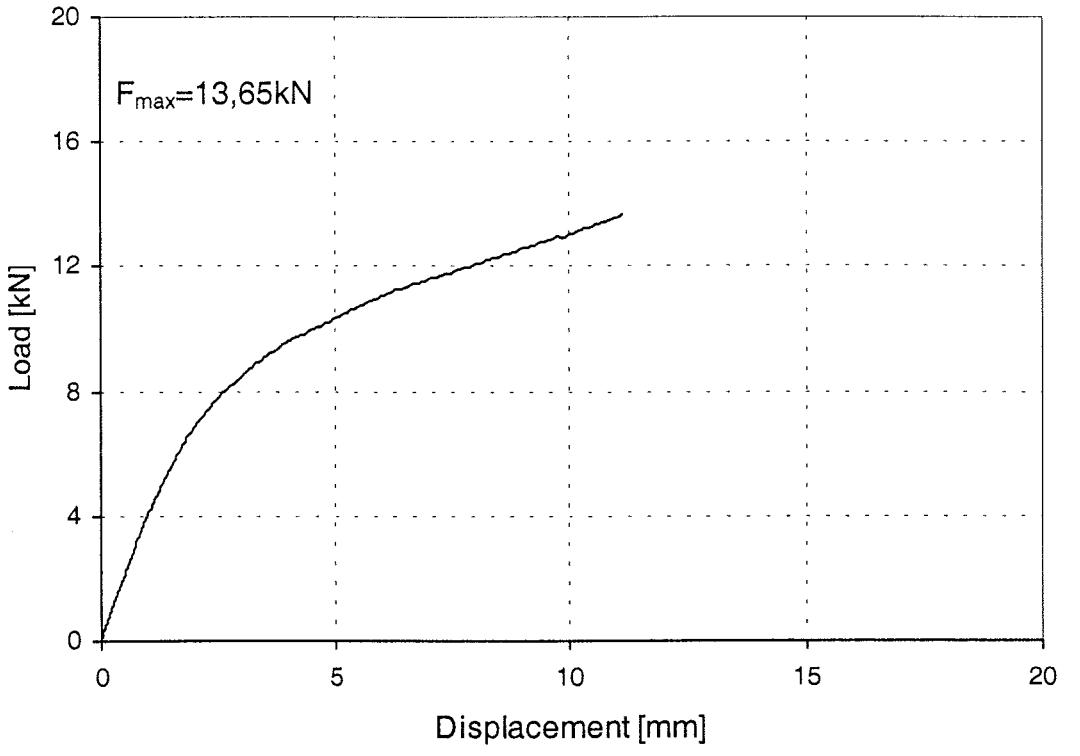

Figure 104: Load-displacement-curve of test Gil4.6-1-1

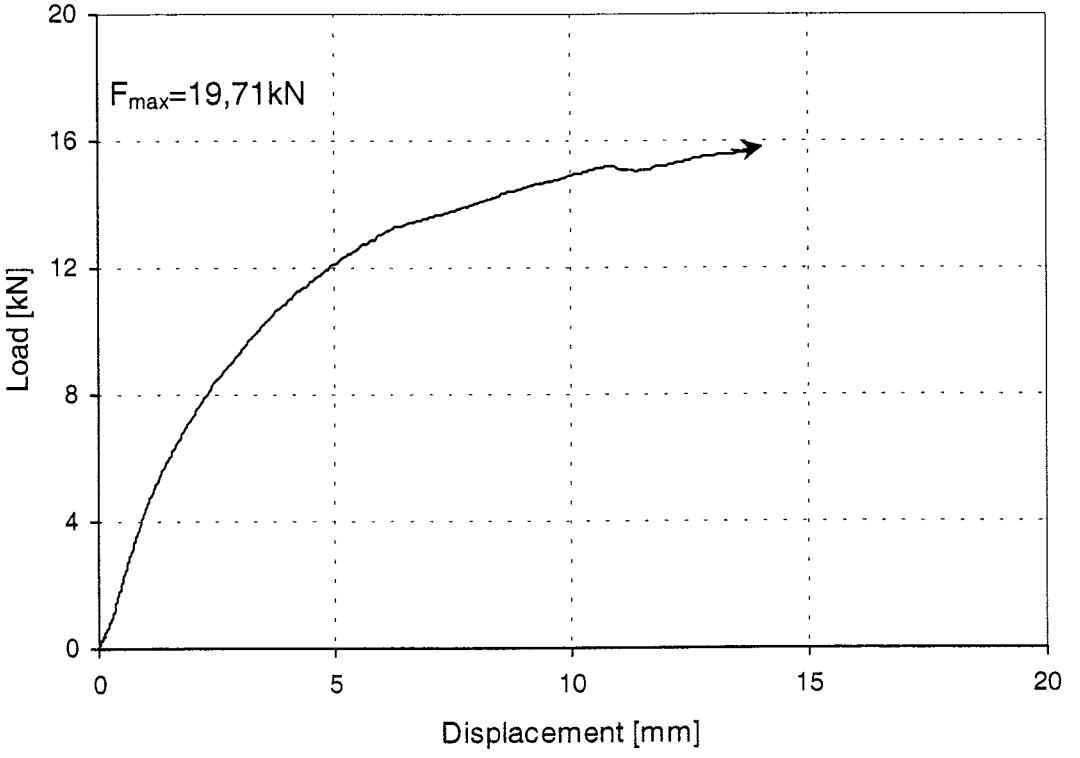

Figure 105: Load-displacement-curve of test Gil4.6-1-2

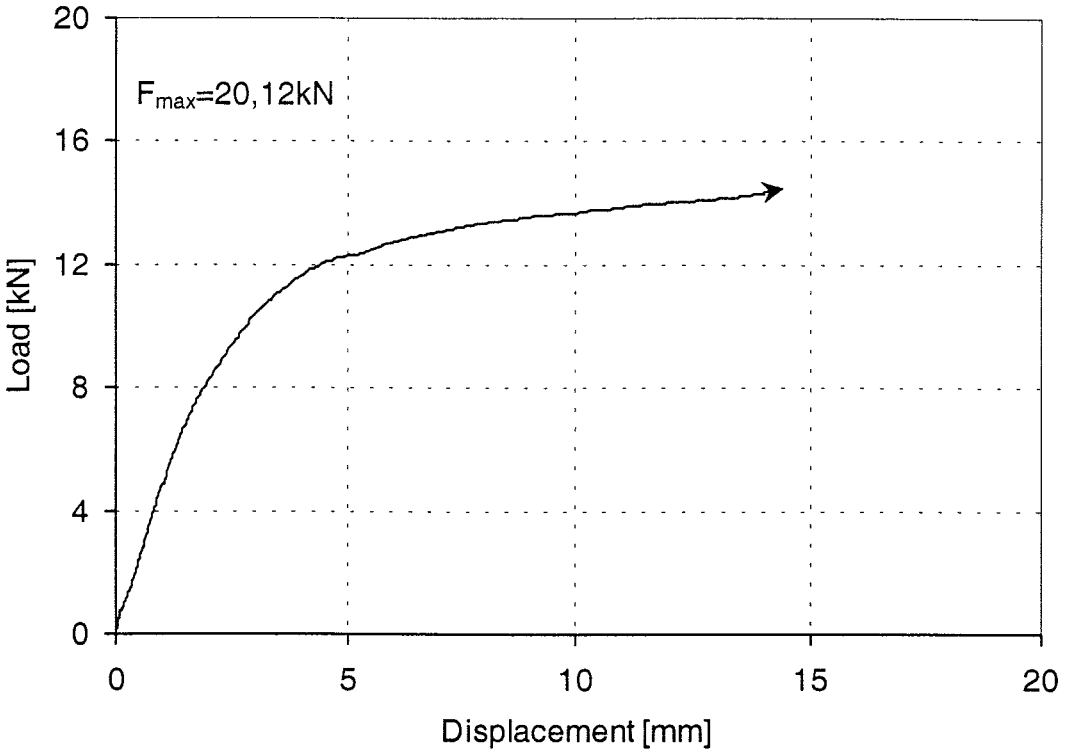

Figure 106: Load-displacement-curve of test Gil4.6-1-3

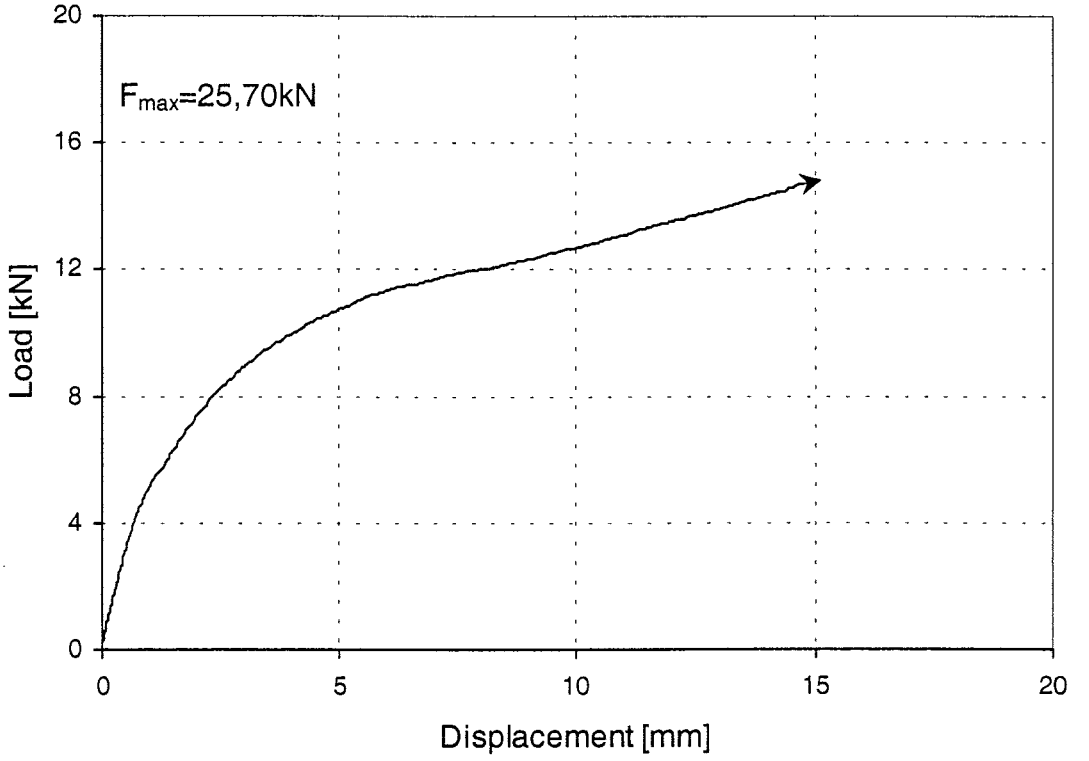

Figure 107: Load-displacement-curve of test Gil4.6-1-4

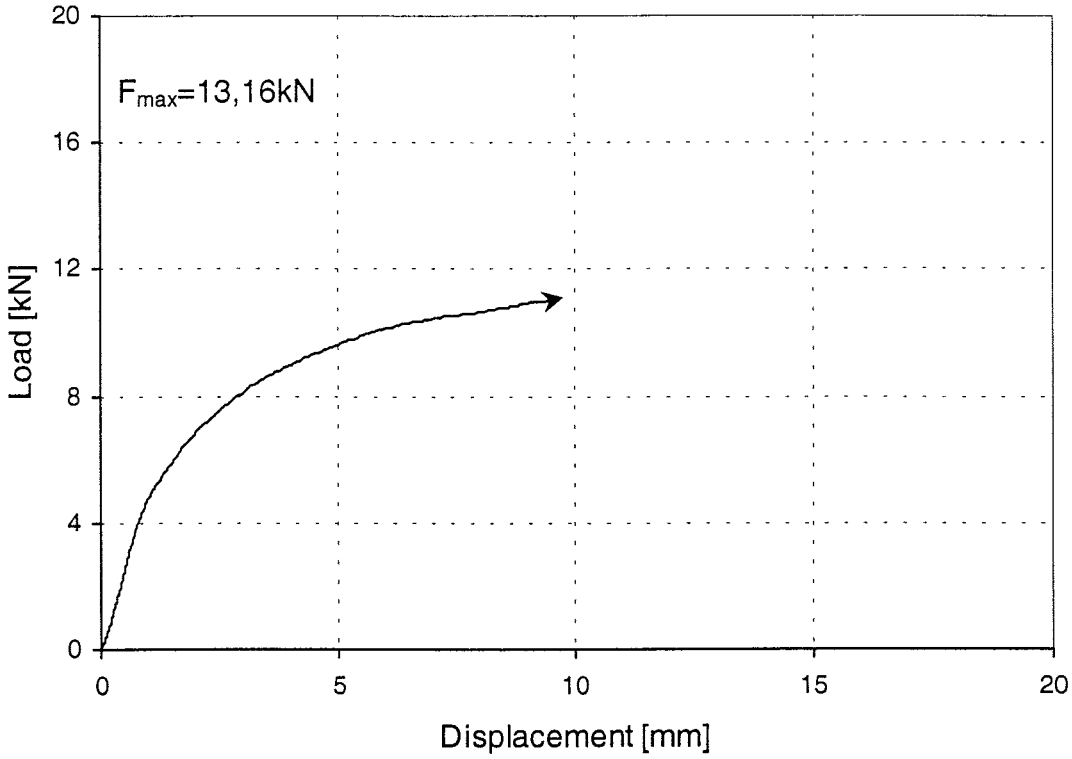

Figure 108: Load-displacement-curve of test Gil4.6-1-5

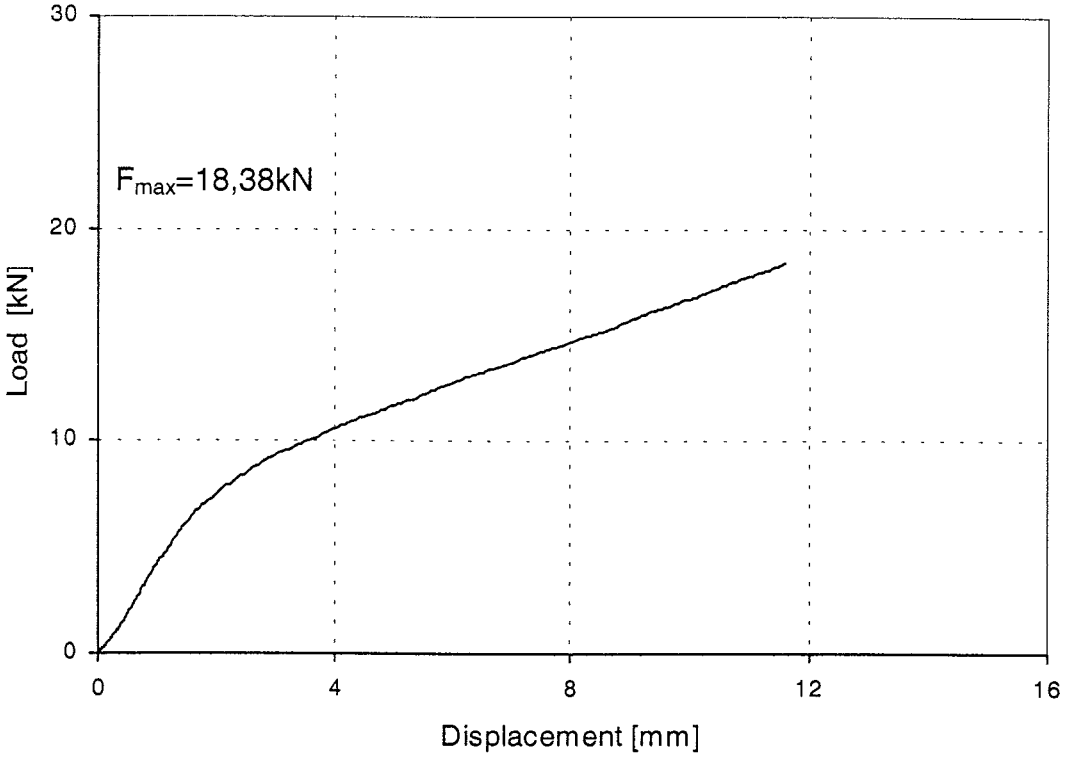

Figure 109: Load-displacement-curve of test Gil8.8-1-1

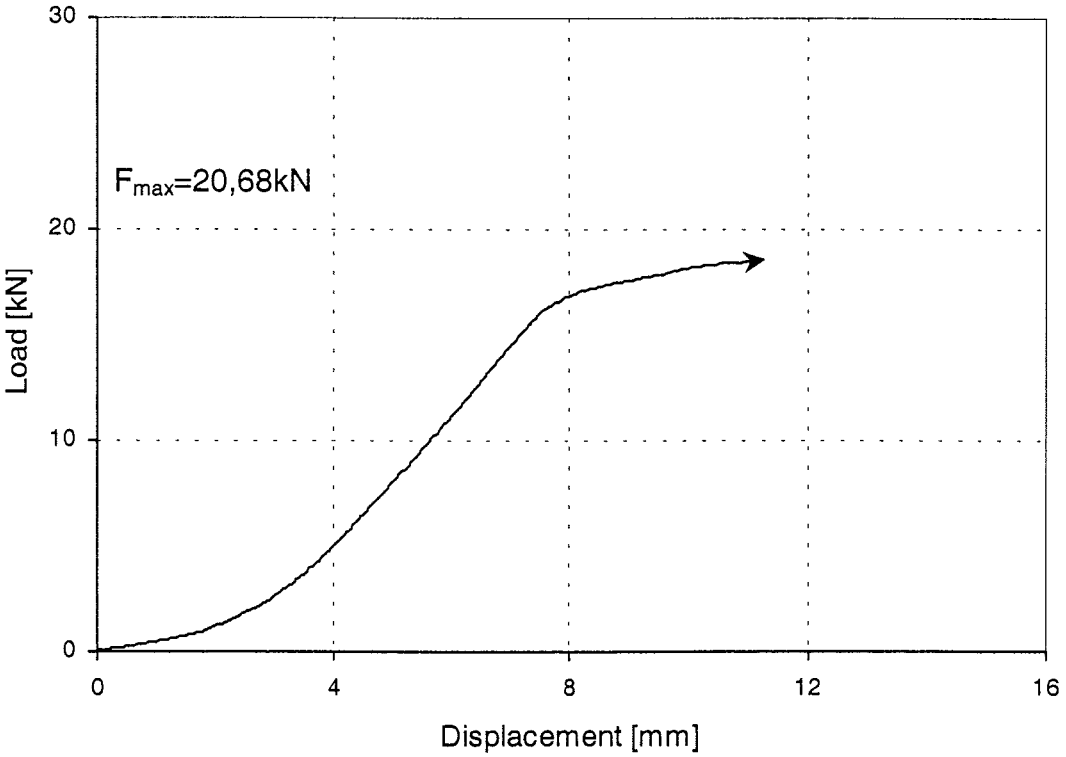

Figure 110: Load-displacement-curve of test Gil8.8-1-2

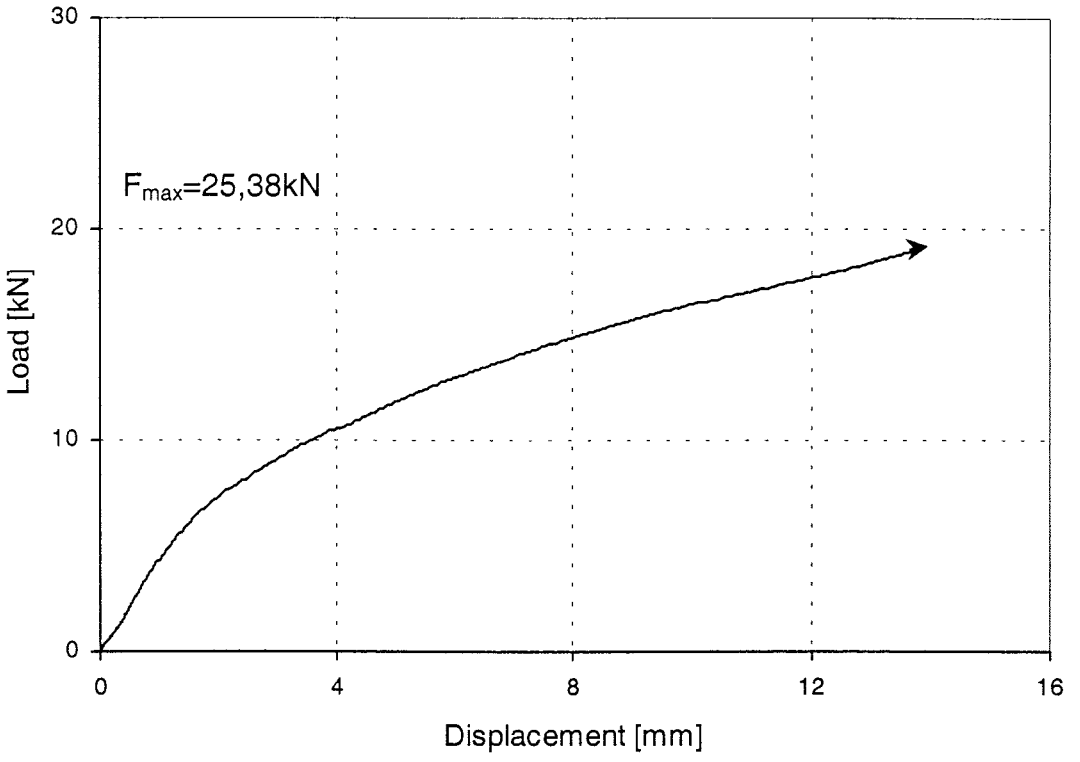

Figure 111: Load-displacement-curve of test Gil8.8-1-3

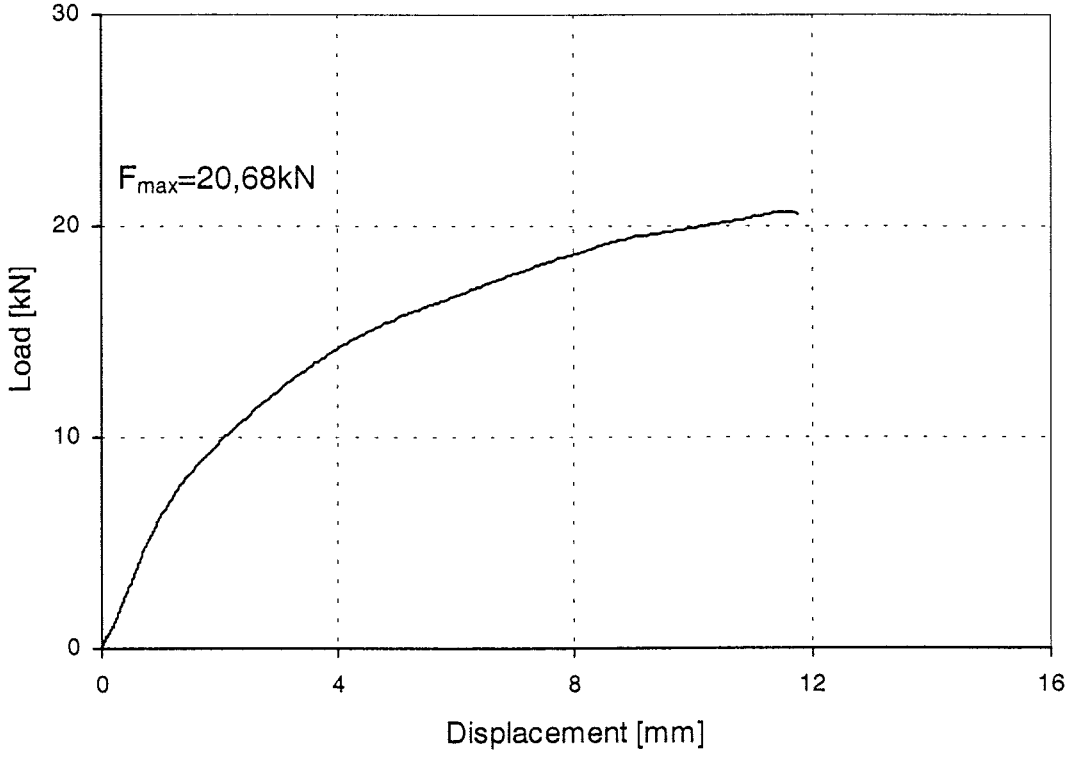

Figure 112: Load-displacement-curve of test Gil8.8-1-4

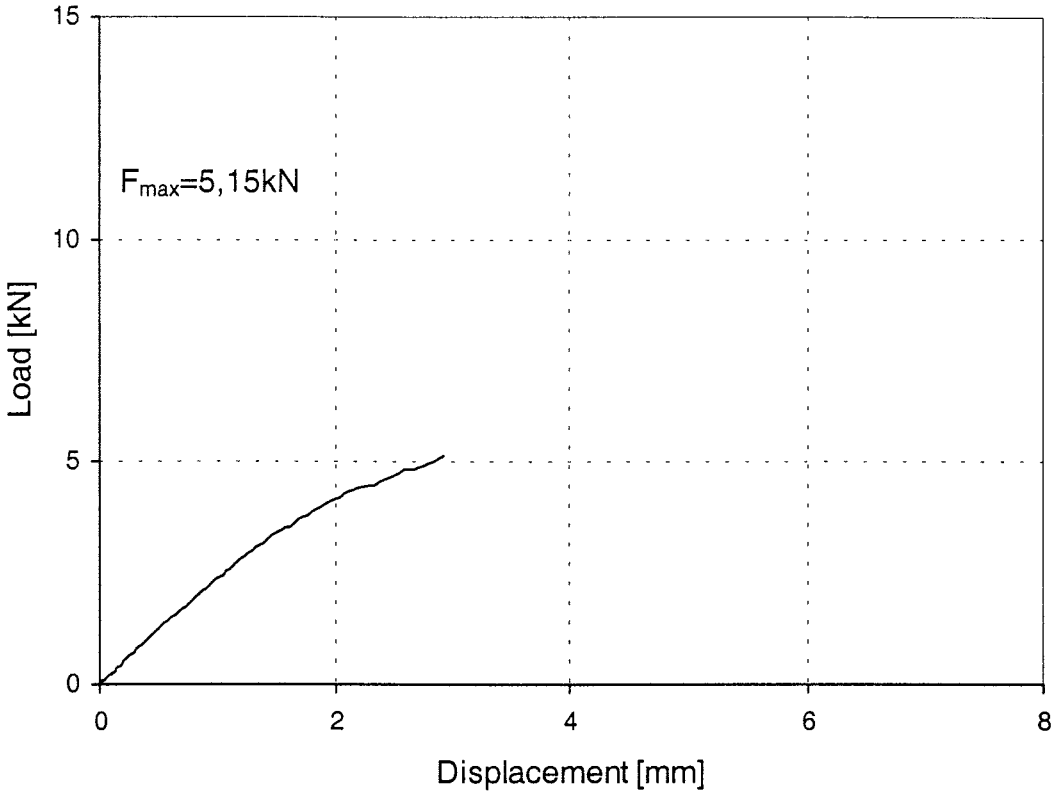

Figure 113: Load-displacement-curve of test Gil8.8-2-1

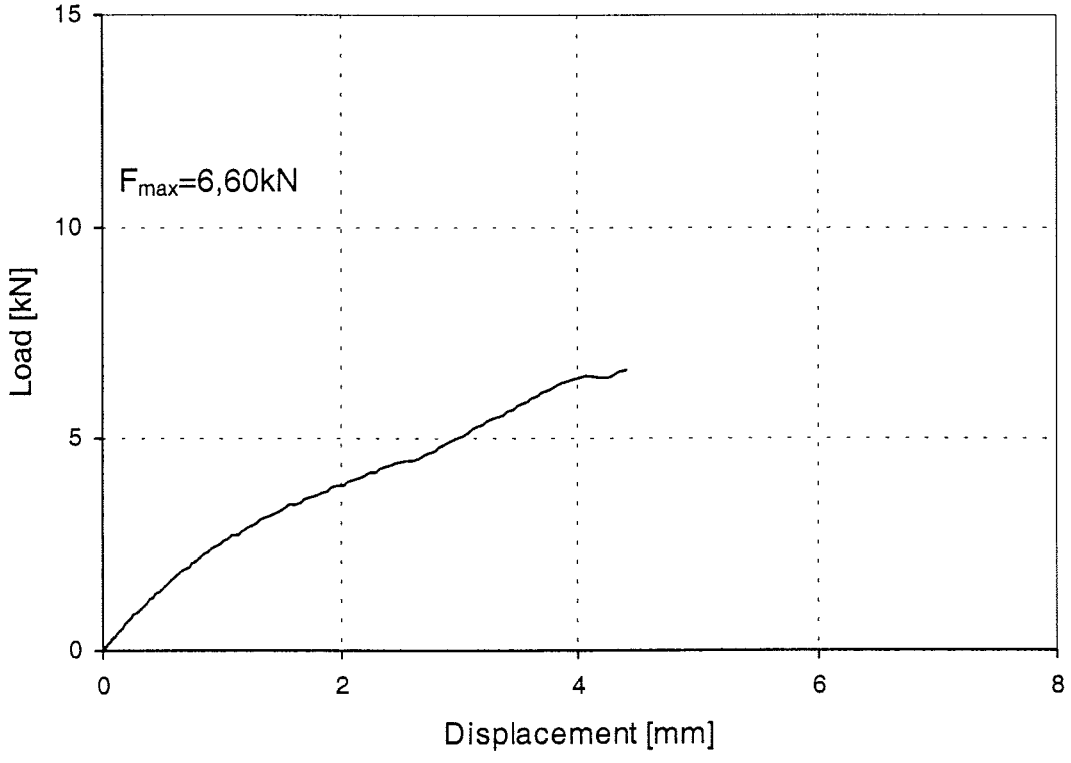

Figure 114: Load-displacement-curve of test Gil8.8-2-2

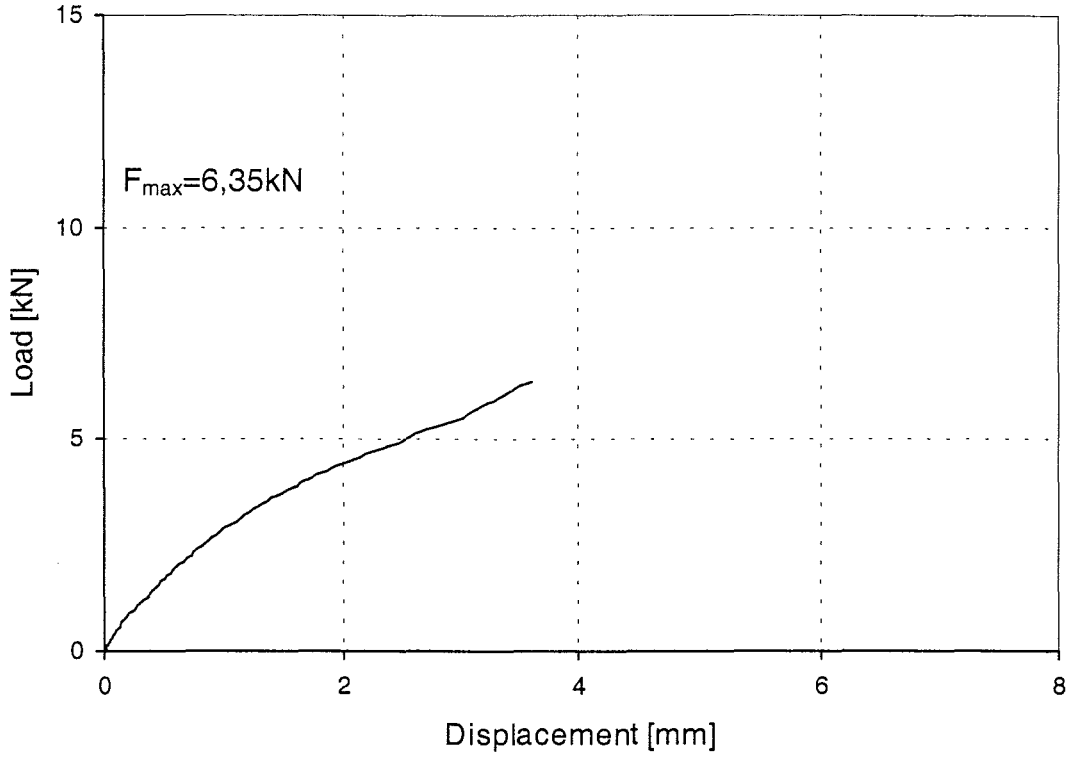

Figure 115: Load-displacement-curve of test Gil8.8-2-3

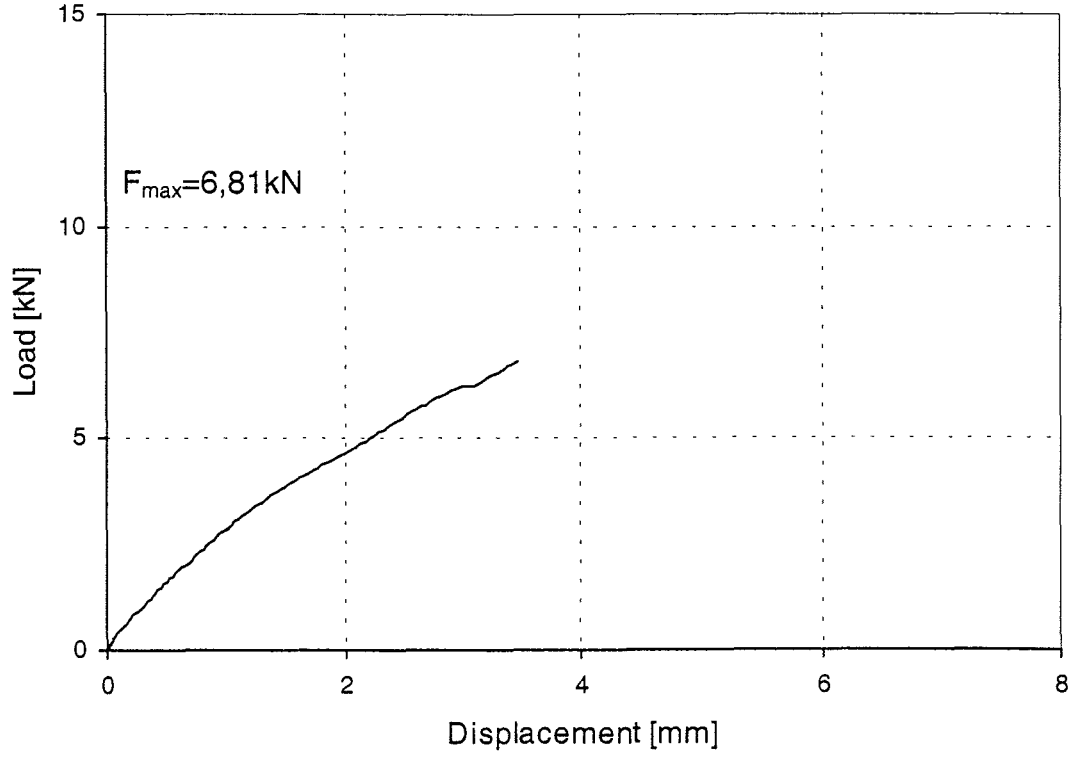

Figure 116: Load-displacement-curve of test Gil8.8-2-4

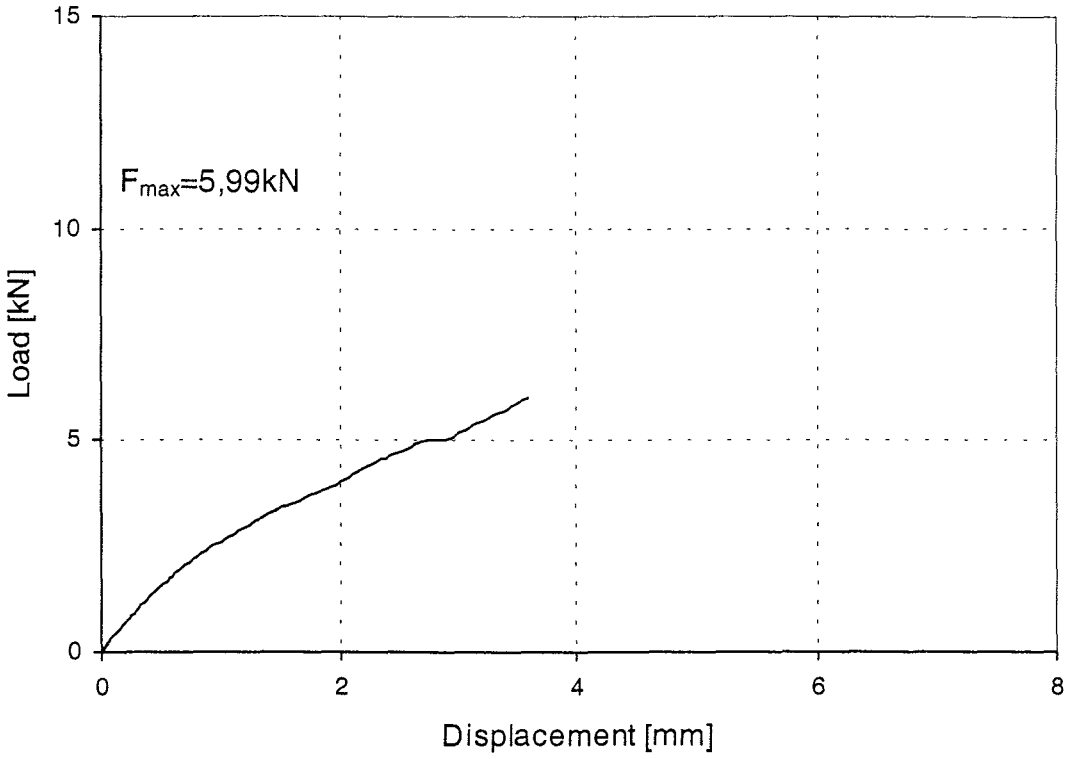

Figure 117: Load-displacement-curve of test Gil8.8-2-5

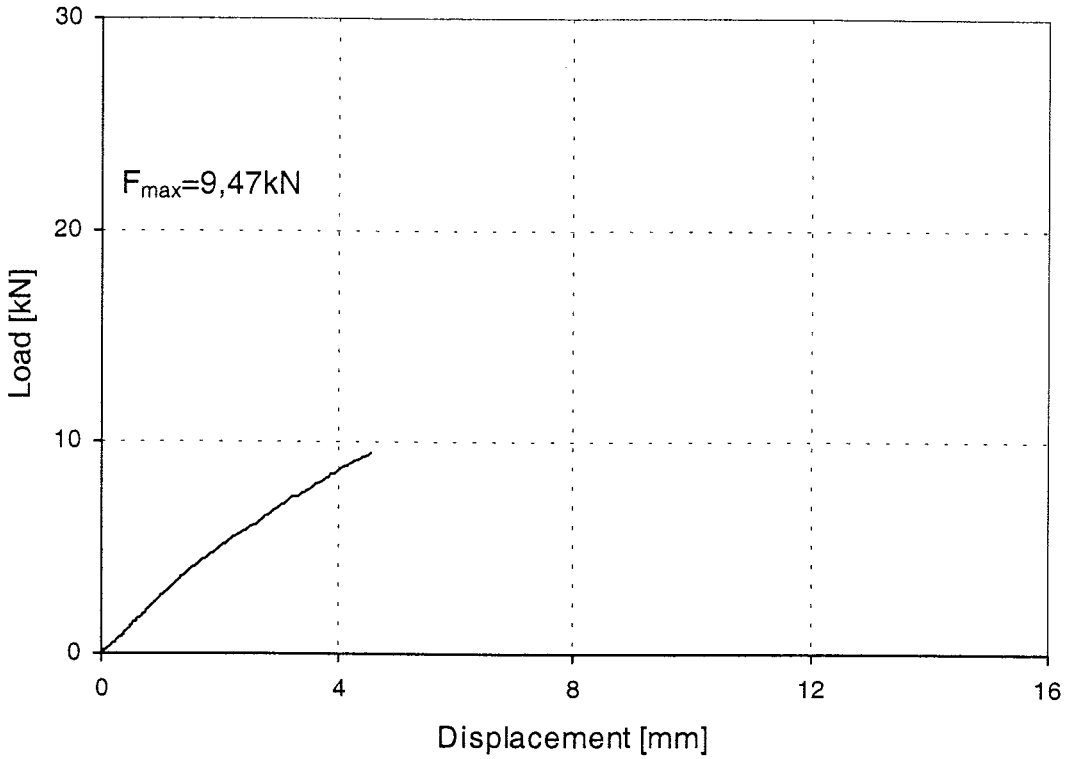

Figure 118: Load-displacement-curve of test Gil8.8-3-1

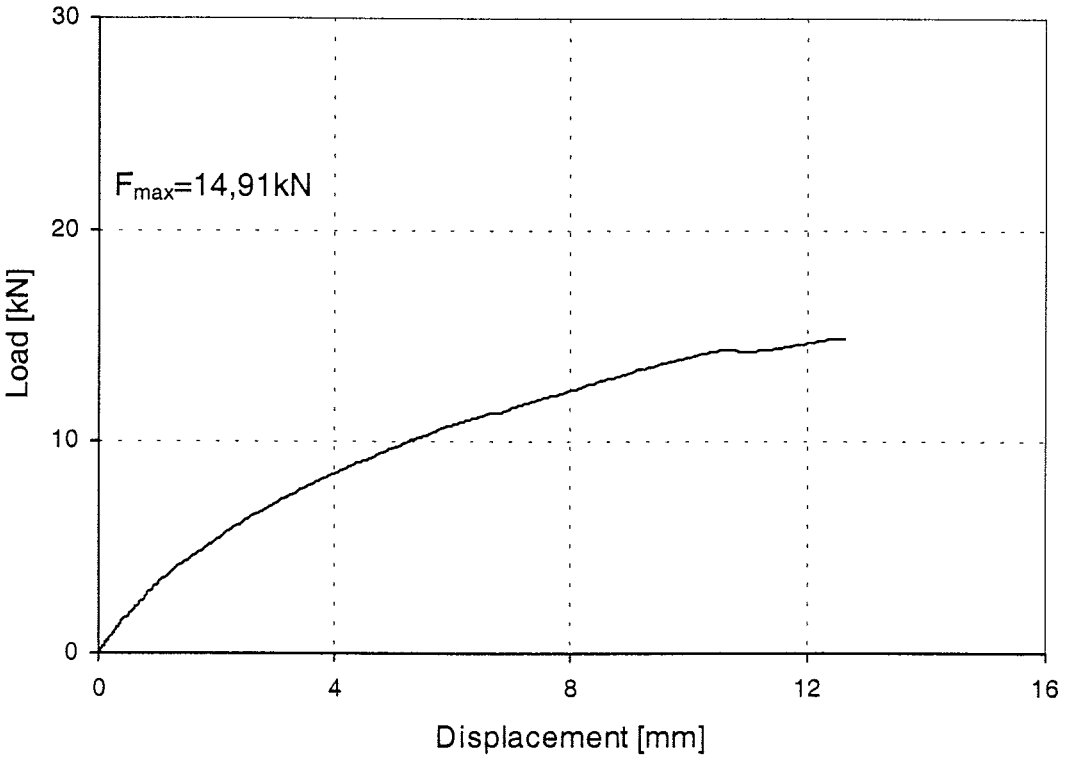

Figure 119: Load-displacement-curve of test Gil8.8-3-2

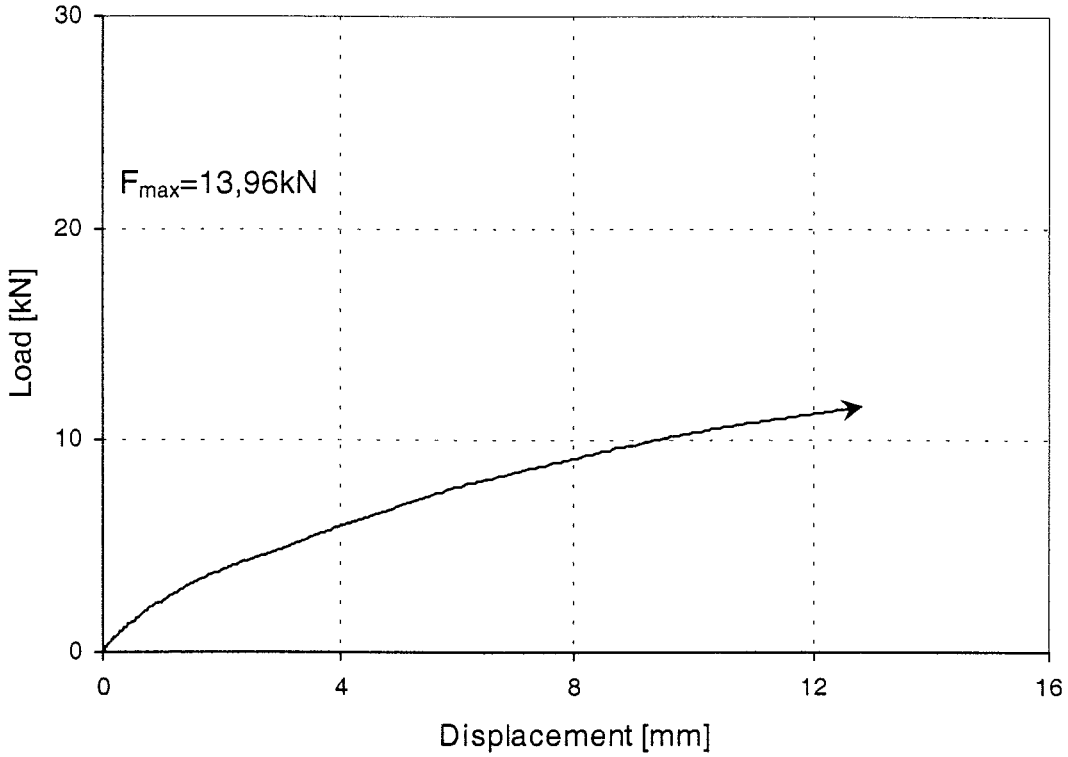

Figure 120: Load-displacement-curve of test Gil8.8-3-3

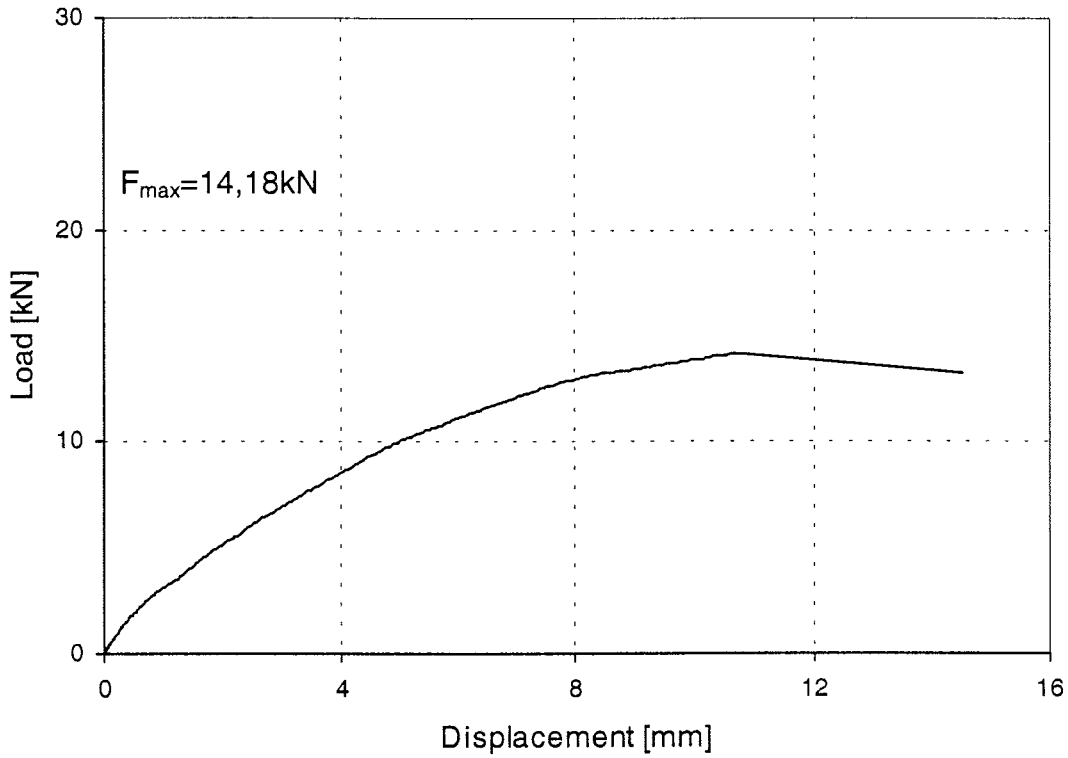

Figure 121: Load-displacement-curve of test Gil8.8-3-4

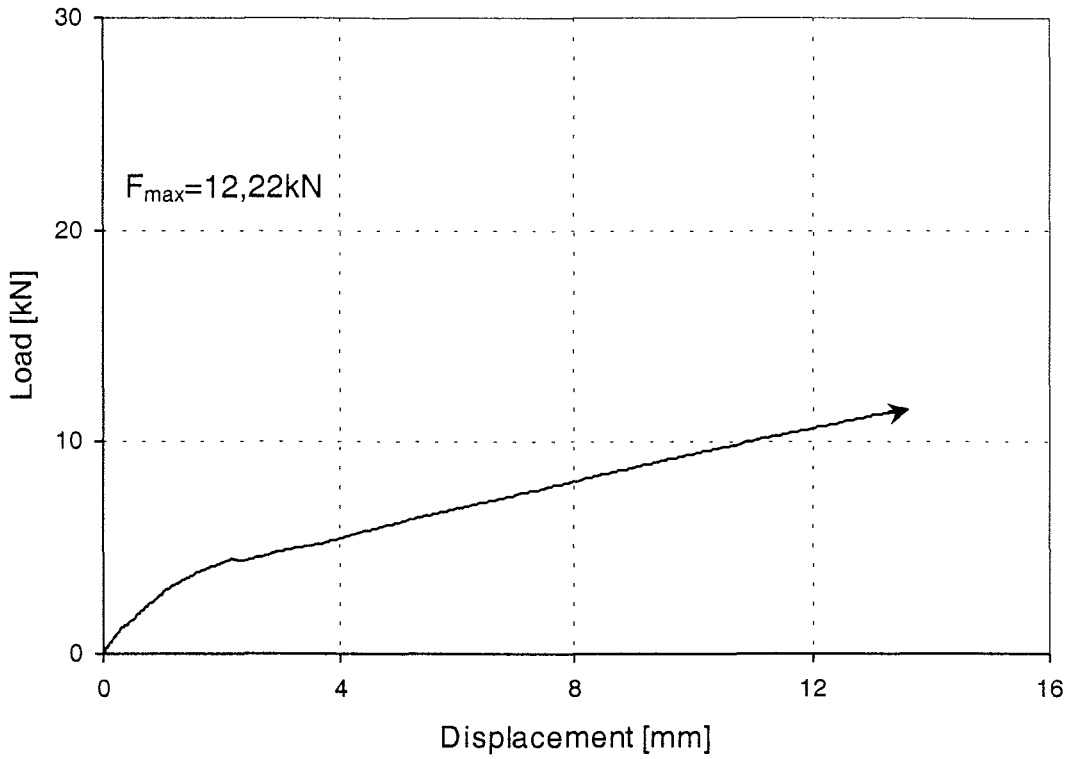

Figure 122: Load-displacement-curve of test Gil8.8-3-5

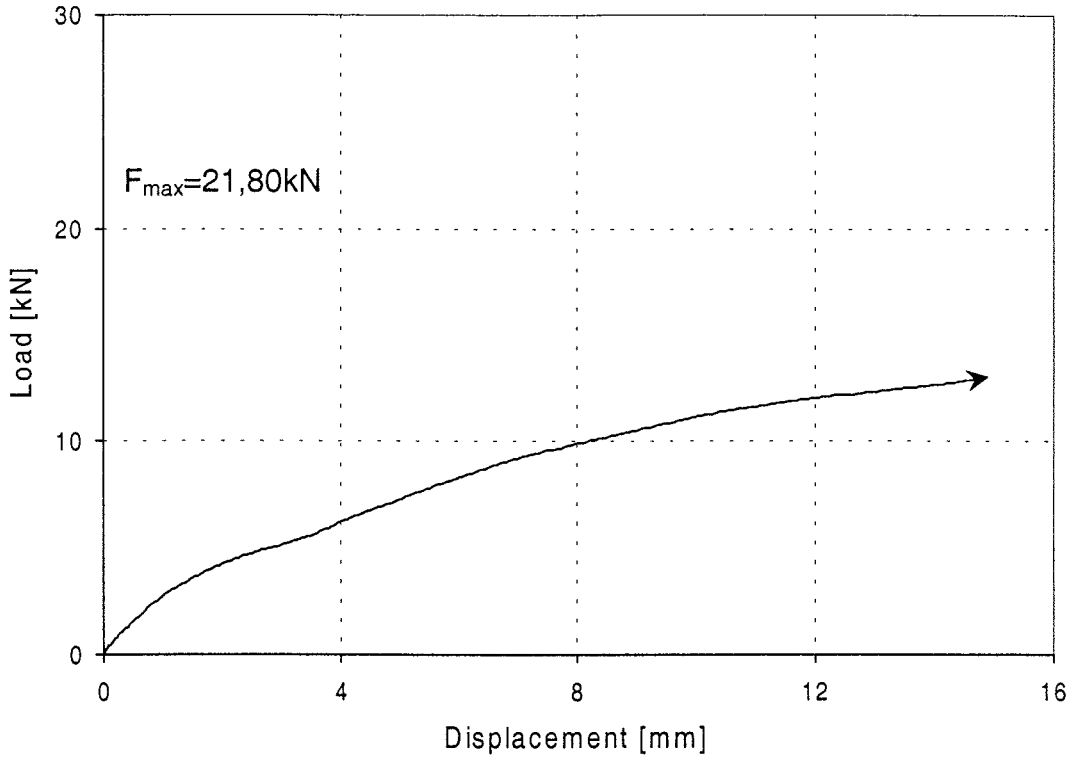

Figure 123: Load-displacement-curve of test Gil8.8-4-1

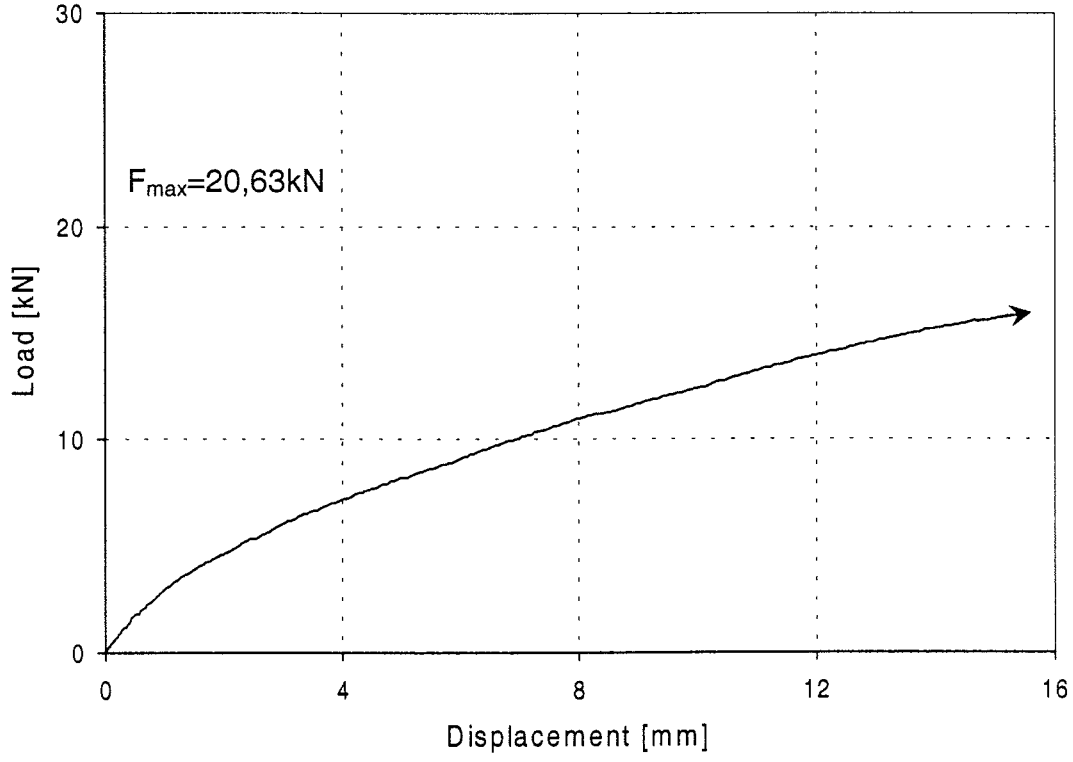

Figure 124: Load-displacement-curve of test Gil8.8-4-2

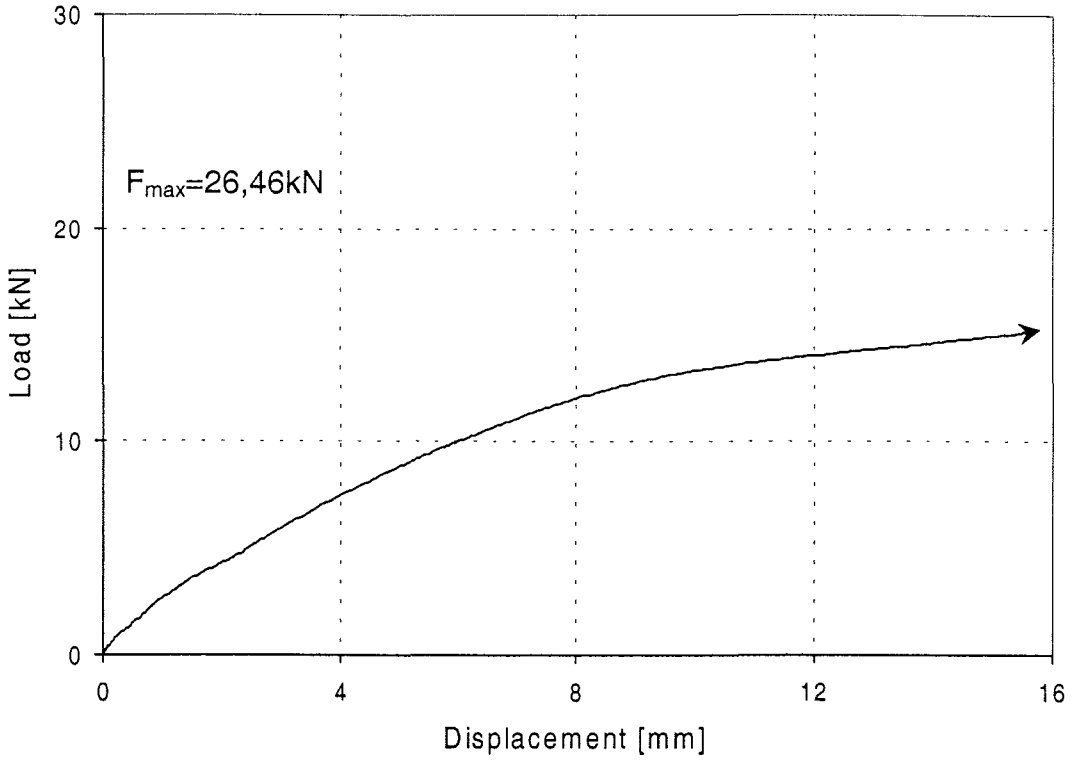

Figure 125: Load-displacement-curve of test Gil8.8-4-3

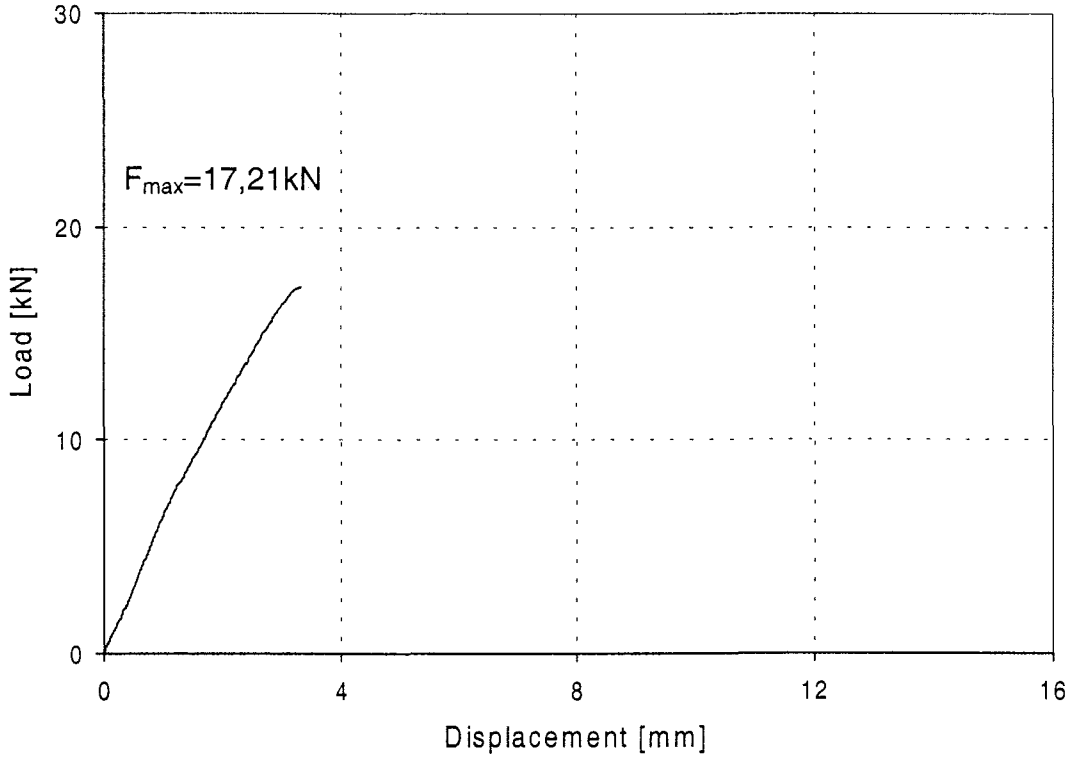

Figure 126: Load-displacement-curve of test Gil8.8-4-4

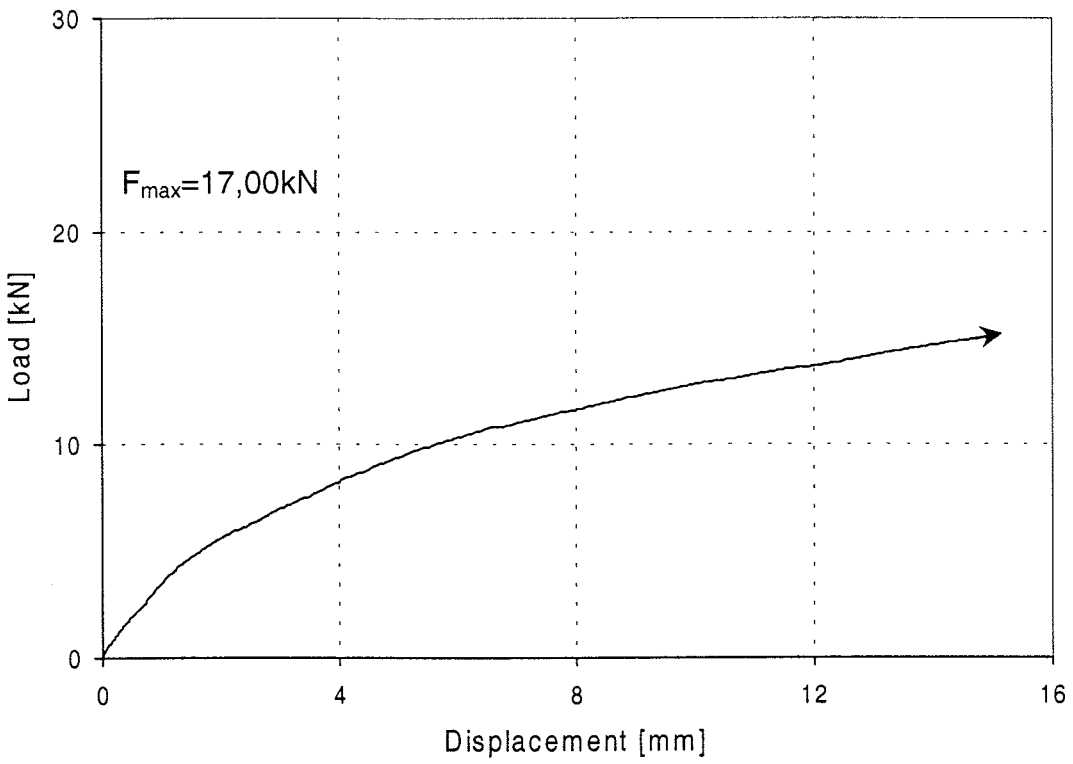

Figure 127: Load-displacement-curve of test Gil8.8-4-5

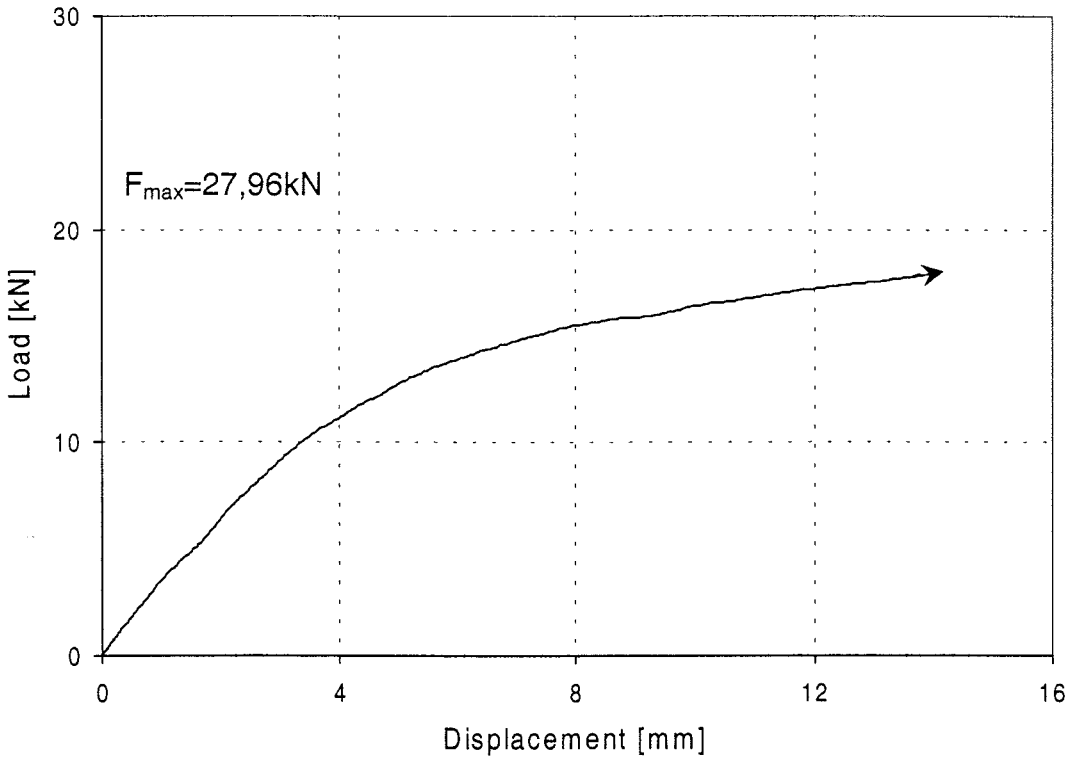

Figure 128: Load-displacement-curve of test Gil8.8-5-1

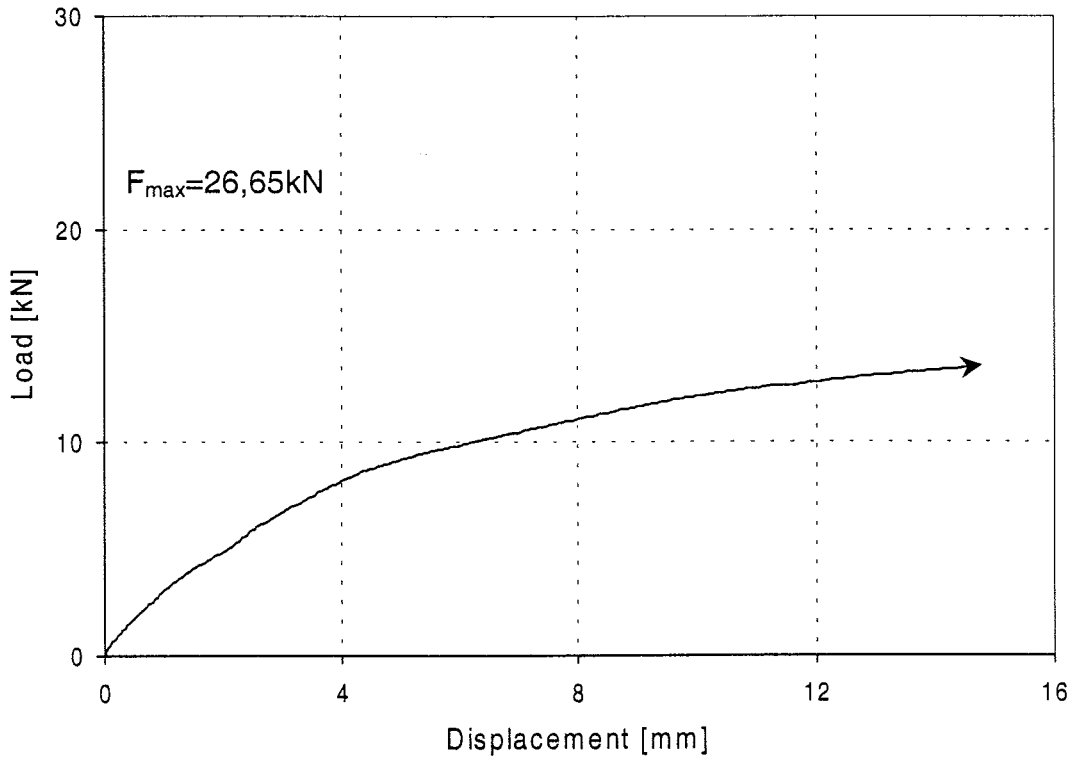

Figure 129: Load-displacement-curve of test Gil8.8-5-2

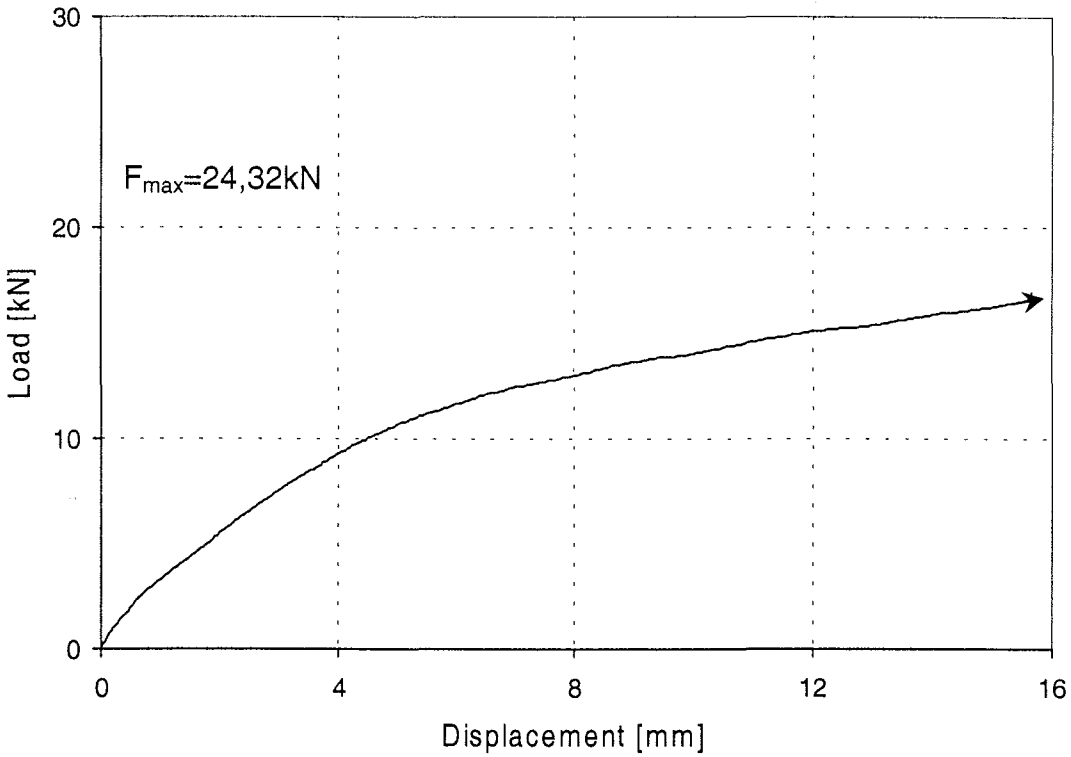

Figure 130: Load-displacement-curve of test Gil8.8-5-3

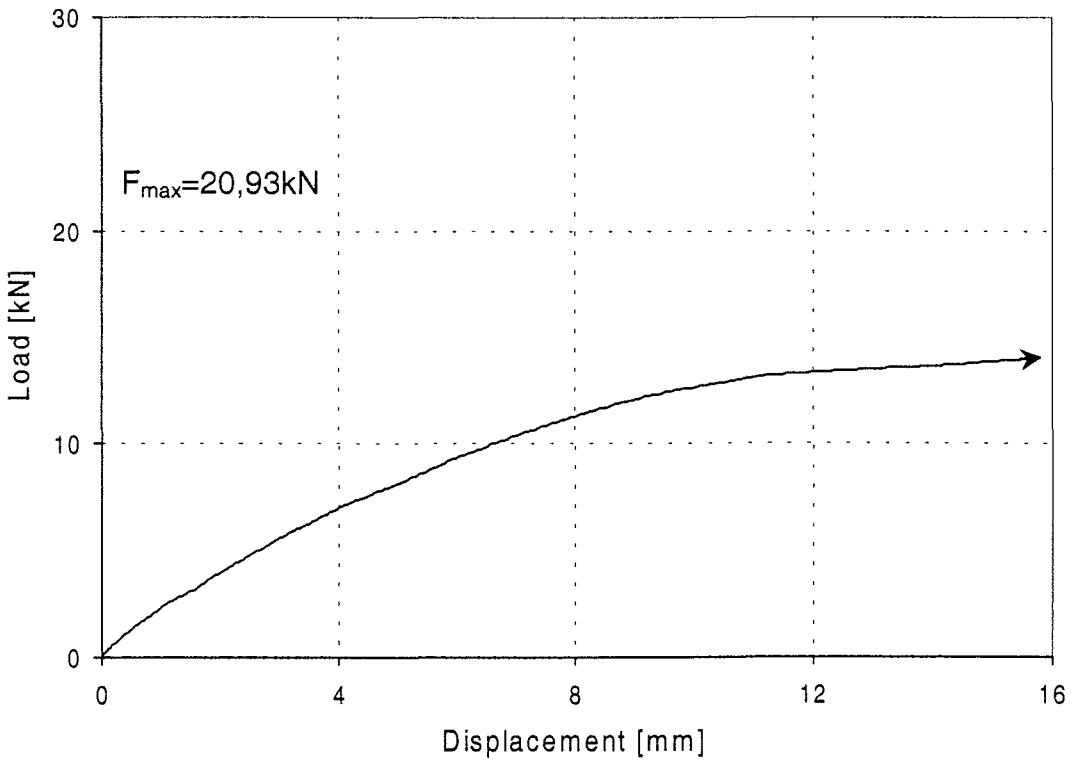

Figure 131: Load-displacement-curve of test Gil8.8-5-4

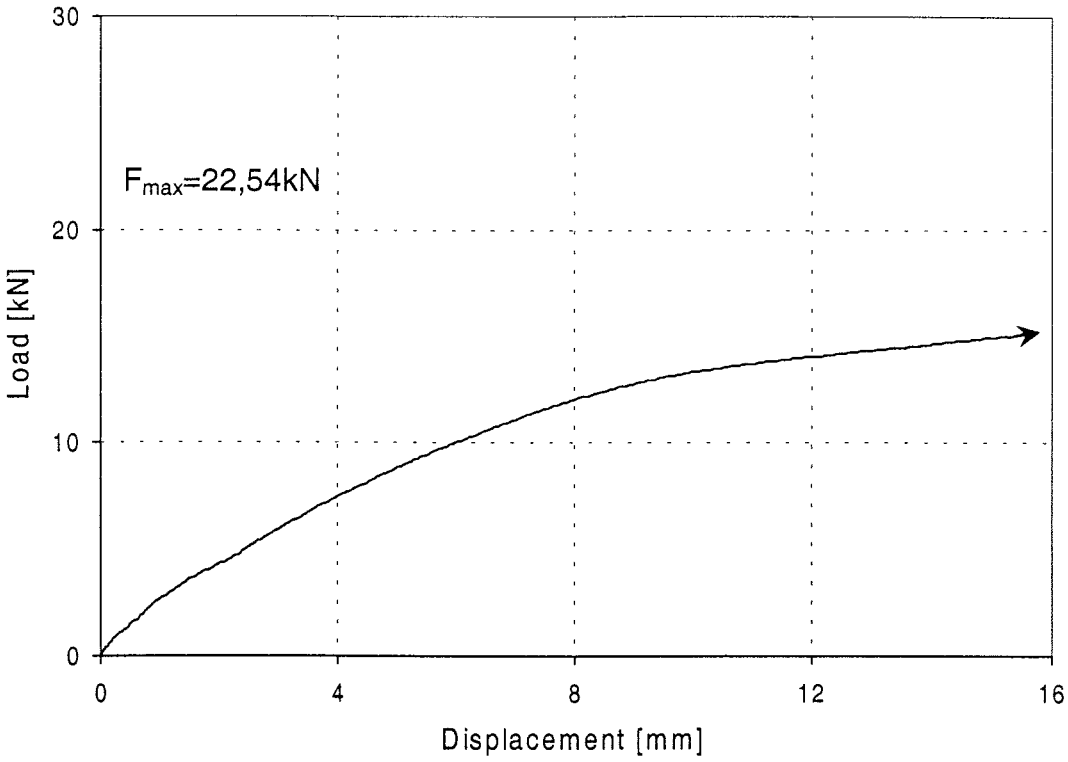

Figure 132: Load-displacement-curve of test Gil8.8-5-5

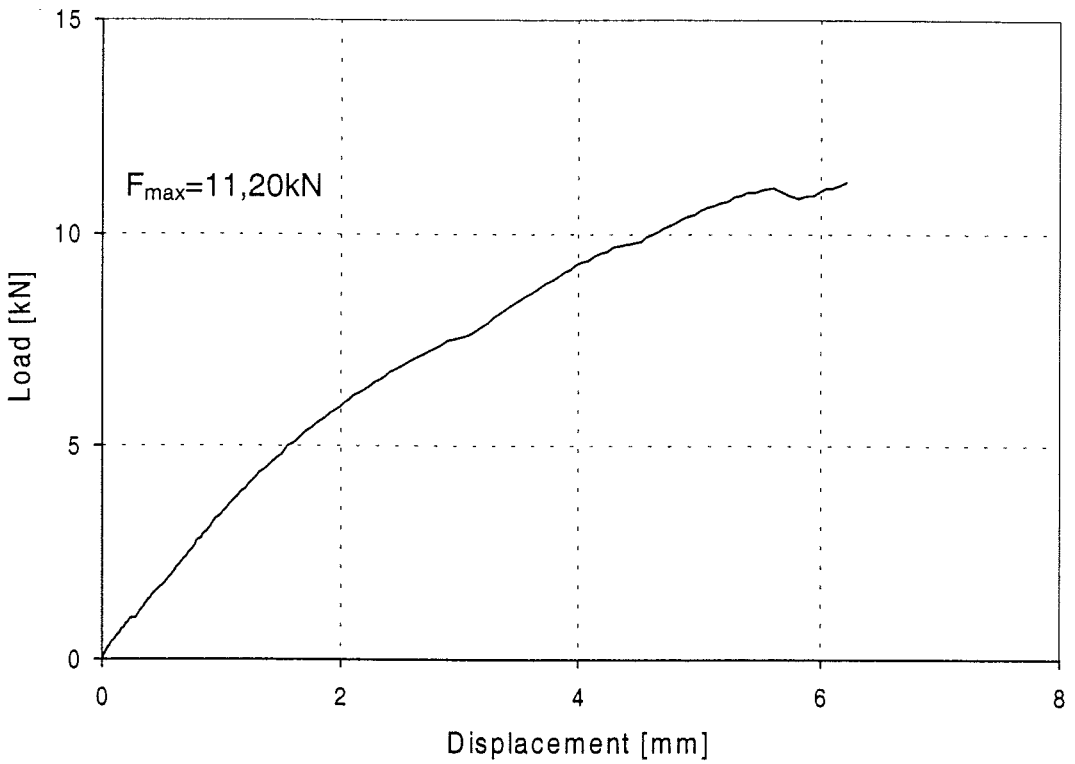

Figure 133: Load-displacement-curve of test Gil8.8-6-1

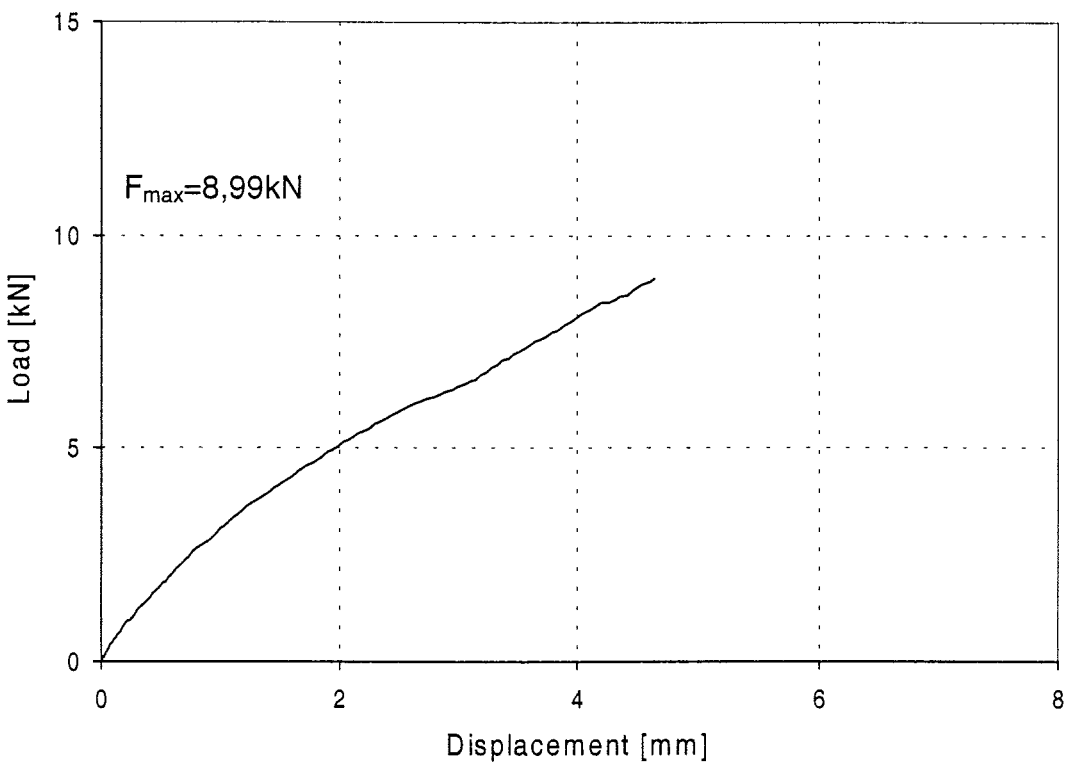

Figure 134: Load-displacement-curve of test Gil8.8-6-2

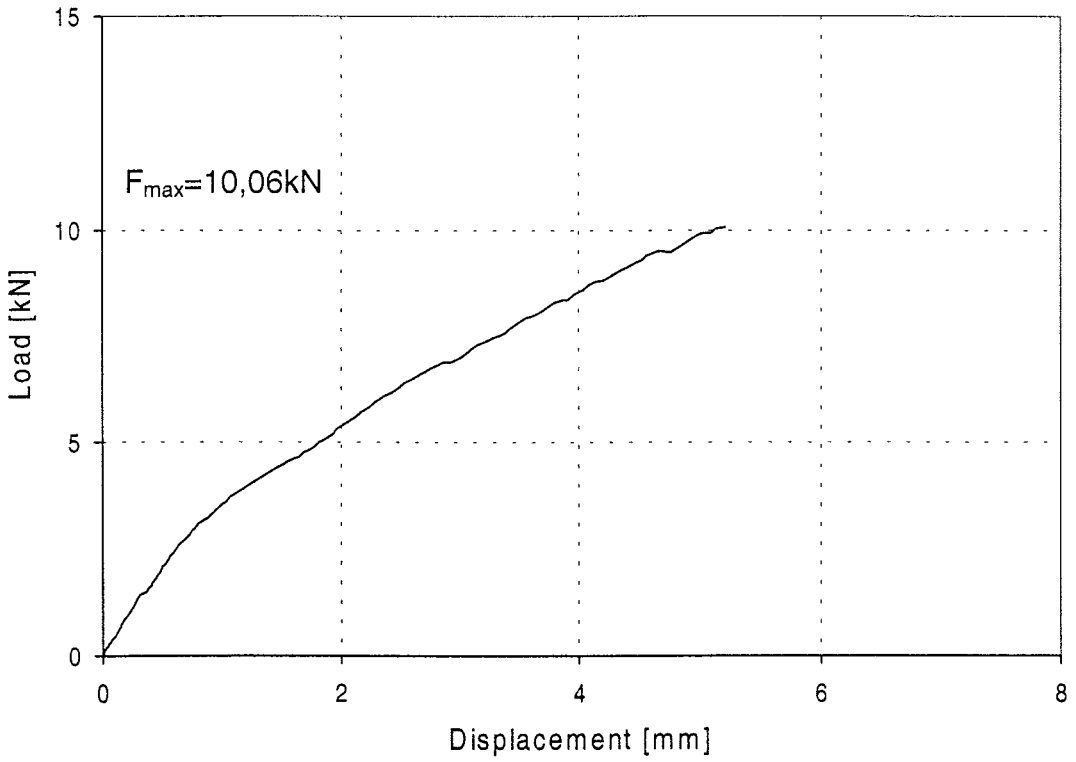

Figure 135: Load-displacement-curve of test Gil8.8-6-3

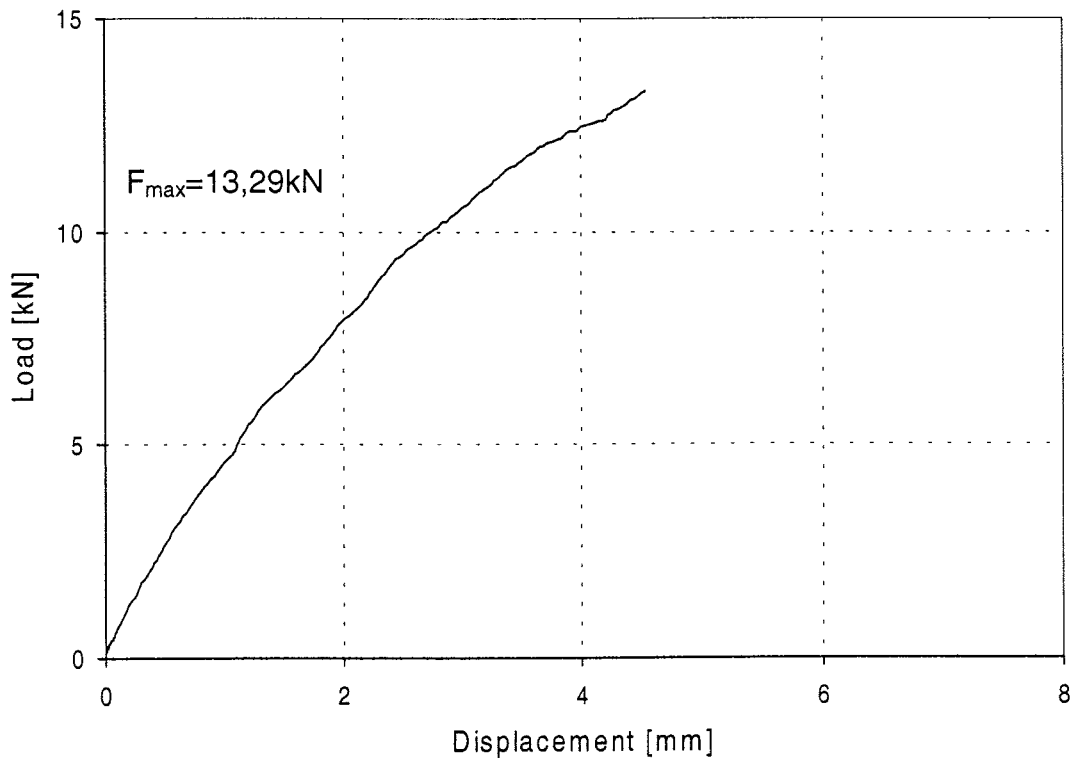

Figure 136: Load-displacement-curve of test Gil8.8-6-4

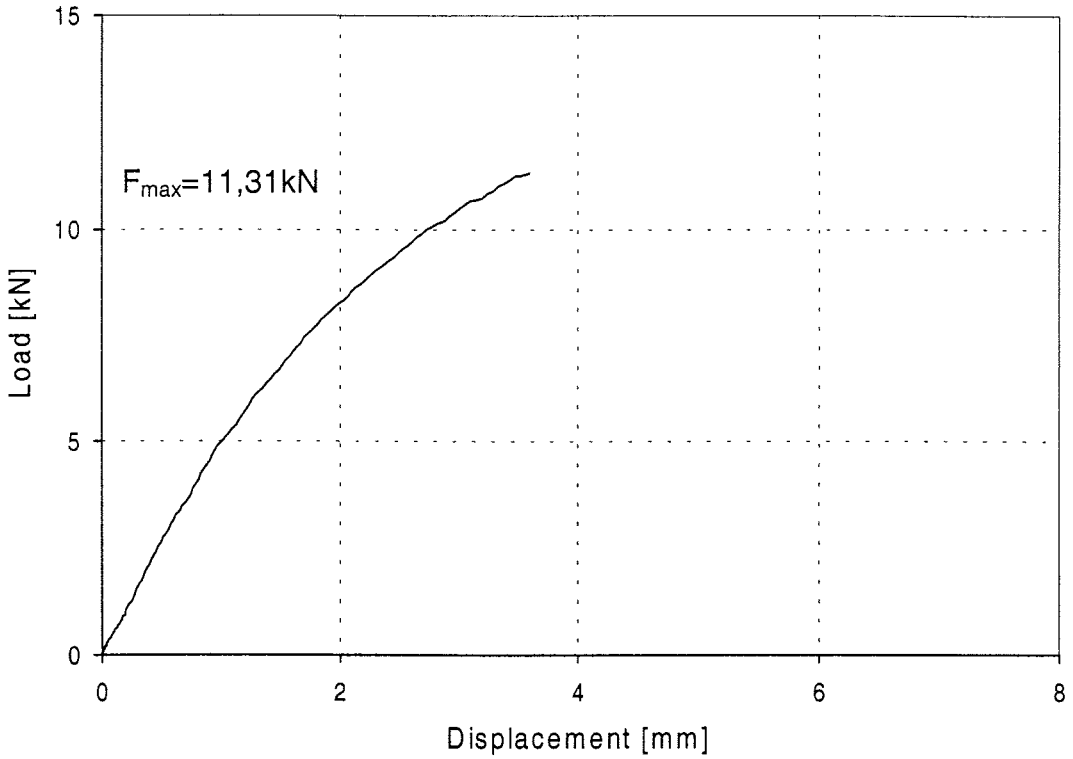

Figure 137: Load-displacement-curve of test Gil8.8-6-5

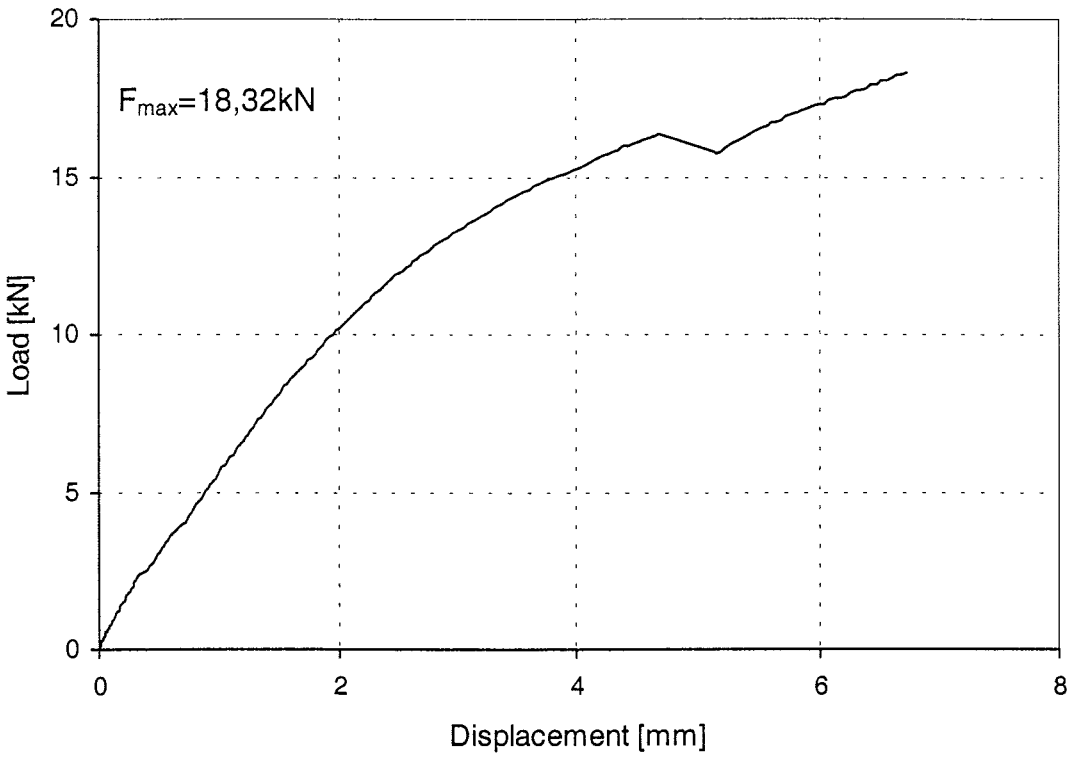

Figure 138: Load-displacement-curve of test GiIII-1-1

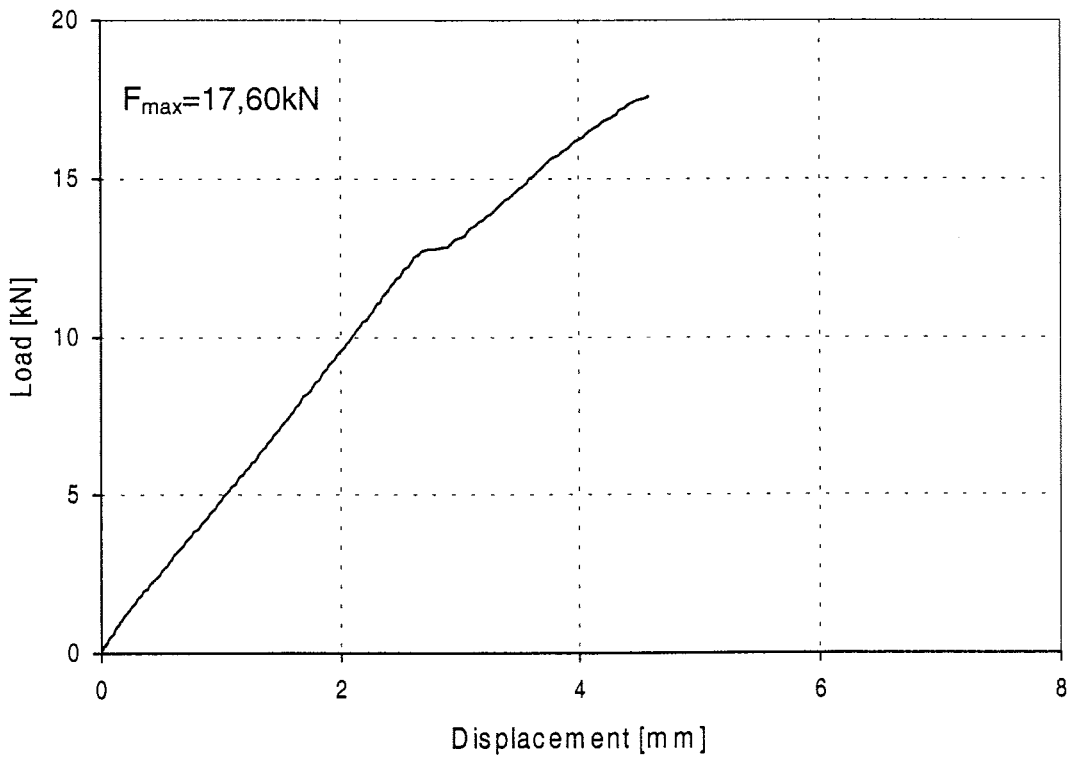

Figure 139: Load-displacement-curve of test GiIII-1-2

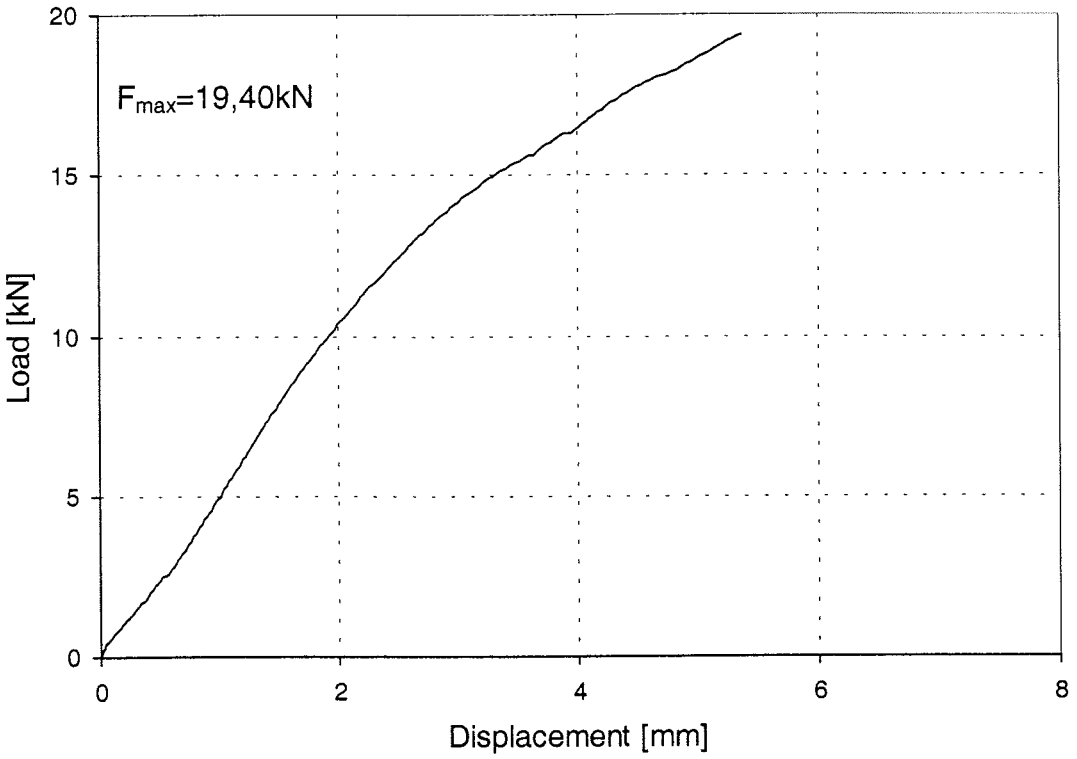

Figure 140: Load-displacement-curve of test GiIII-1-3

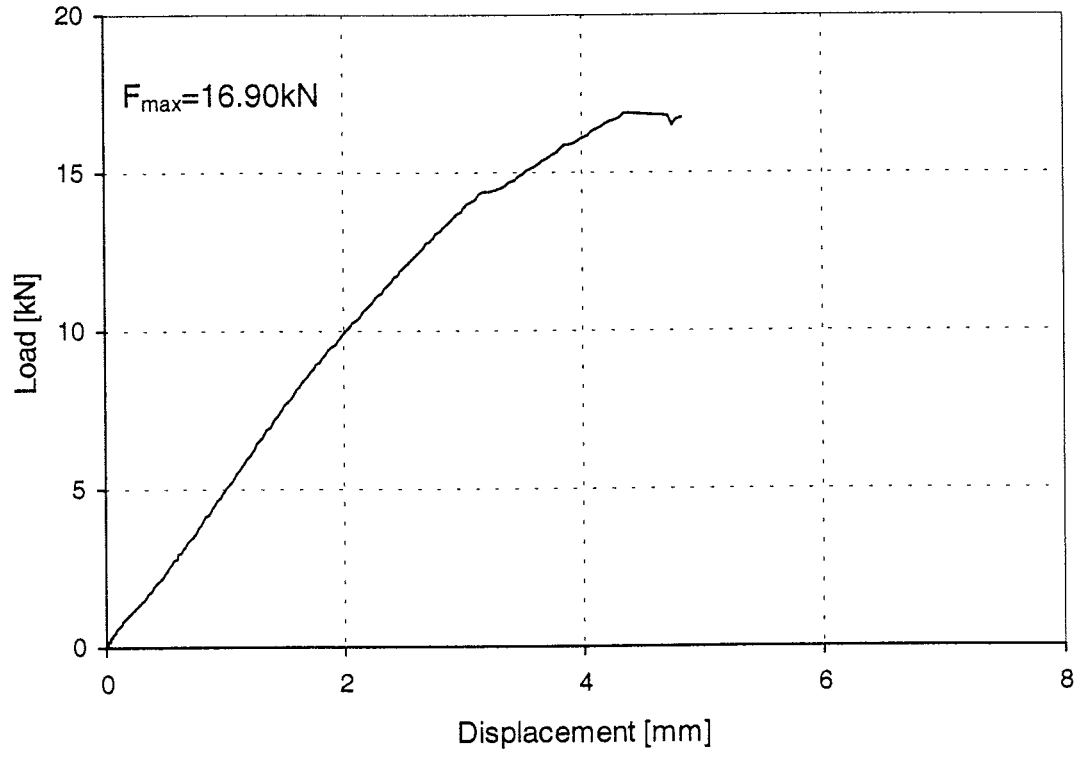

Figure 141: Load-displacement-curve of test GiIII-1-4

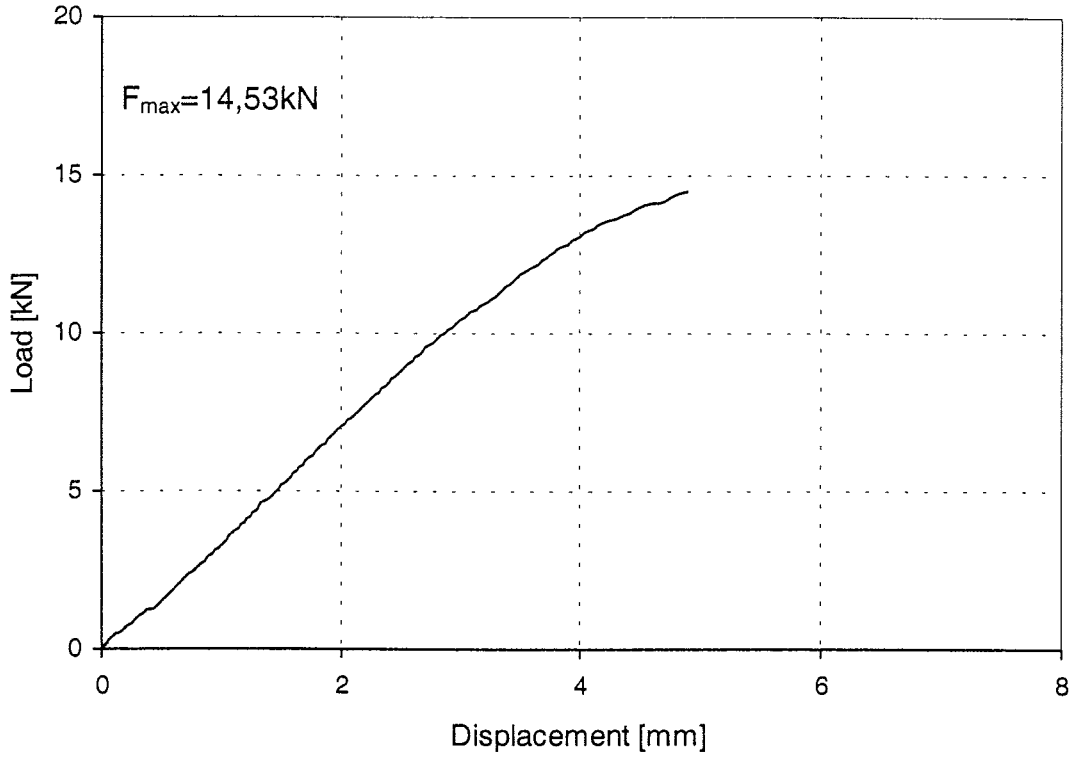

Figure 142: Load-displacement-curve of test GilII-1-5

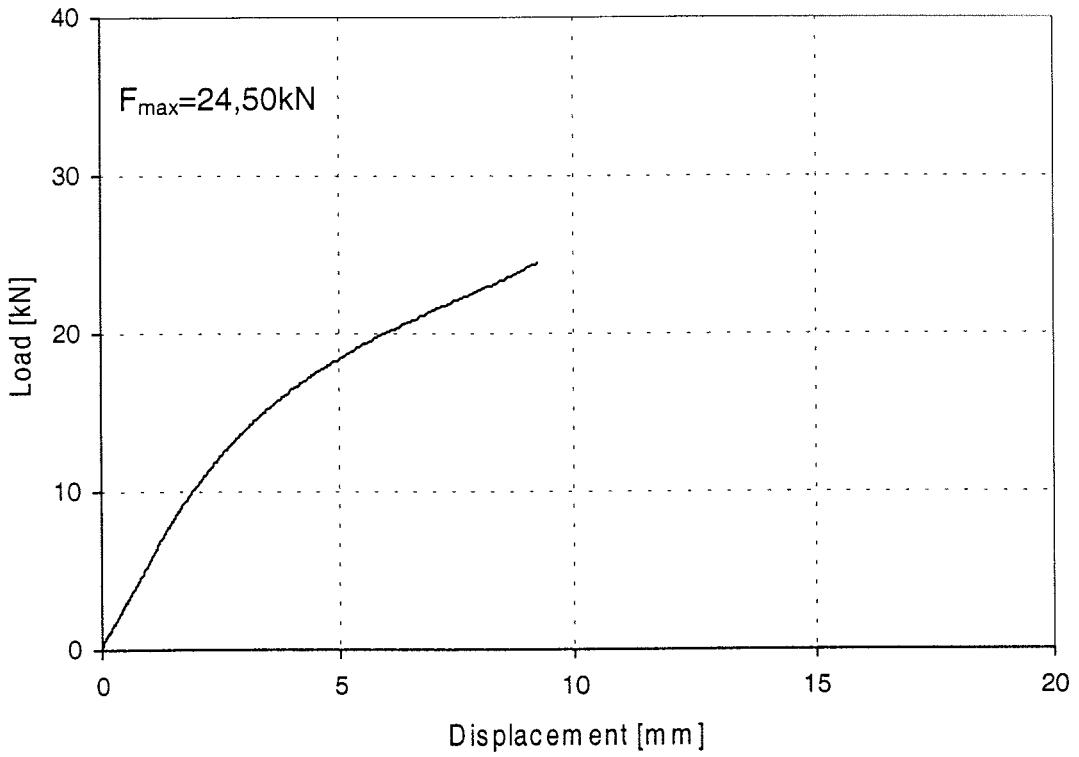

Figure 143: Load-displacement-curve of test GiIII-2-1

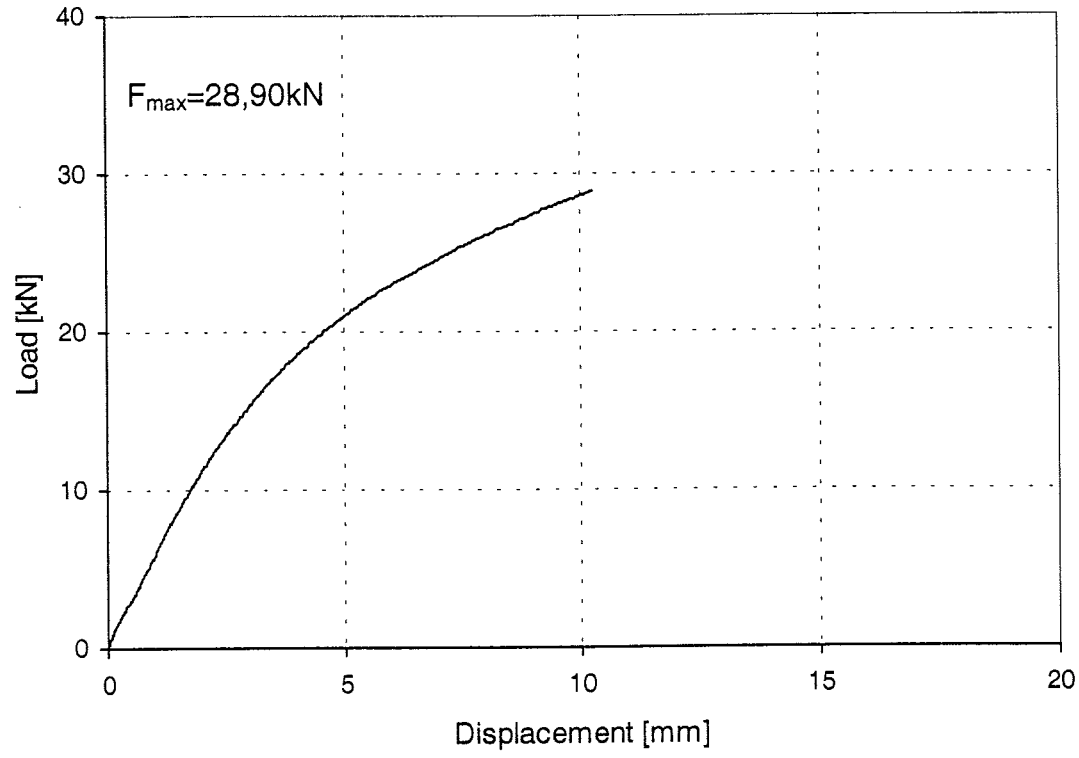

Figure 144: Load-displacement-curve of test GiIII-2-2

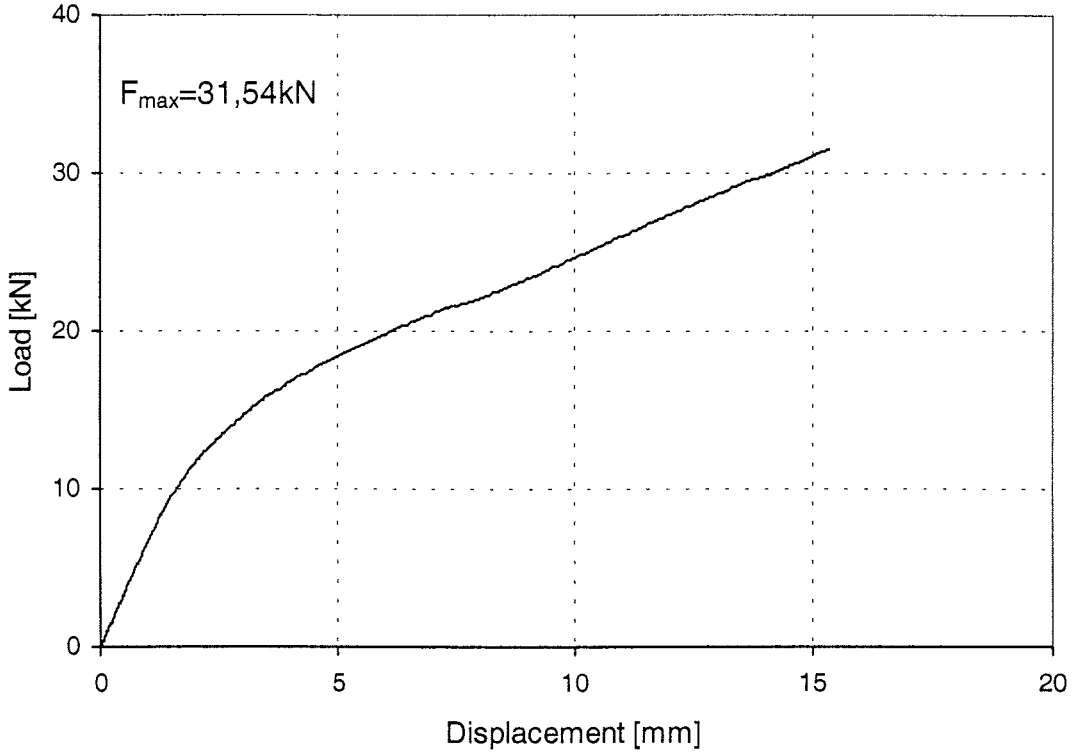

Figure 145: Load-displacement-curve of test GilII-2-3

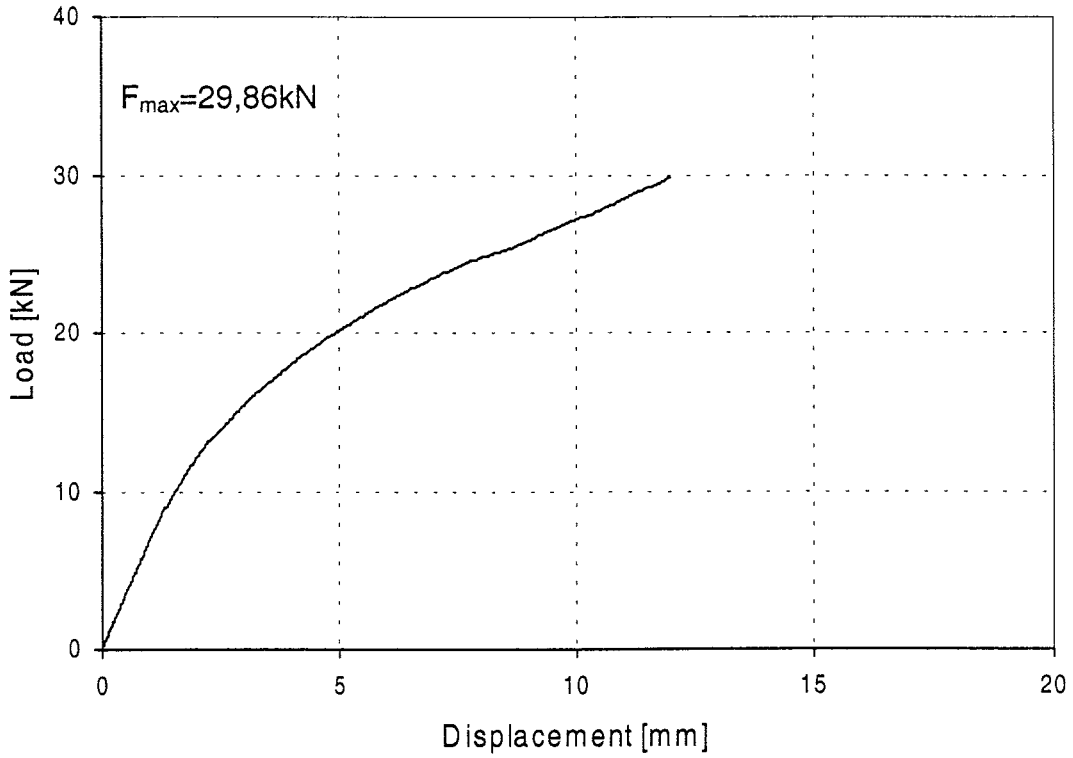

Figure 146: Load-displacement-curve of test GilII-2-4

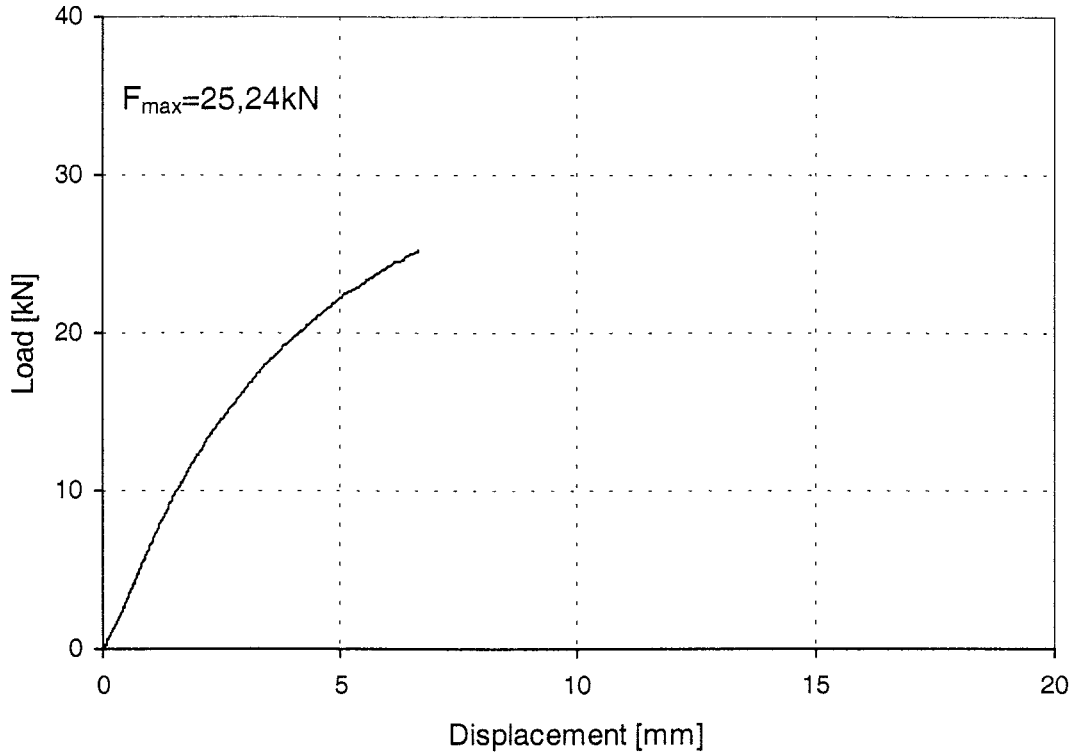

Figure 147: Load-displacement-curve of test GiIII-2-5

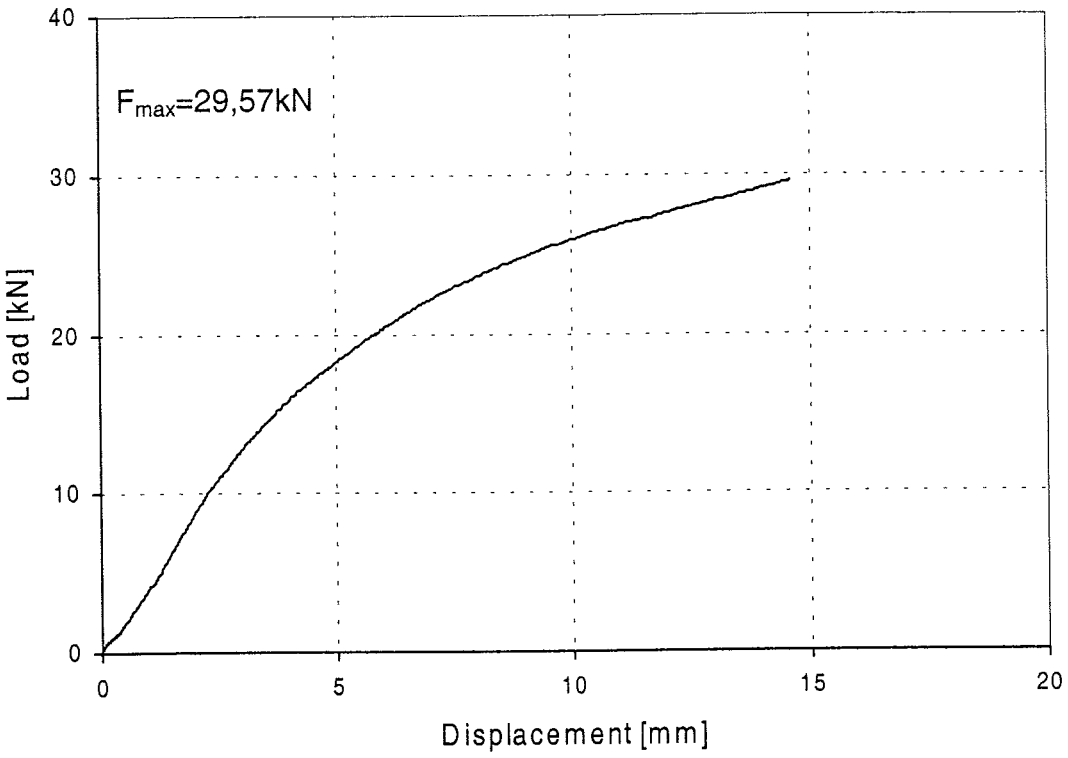

Figure 148: Load-displacement-curve of test GiIII-3-1

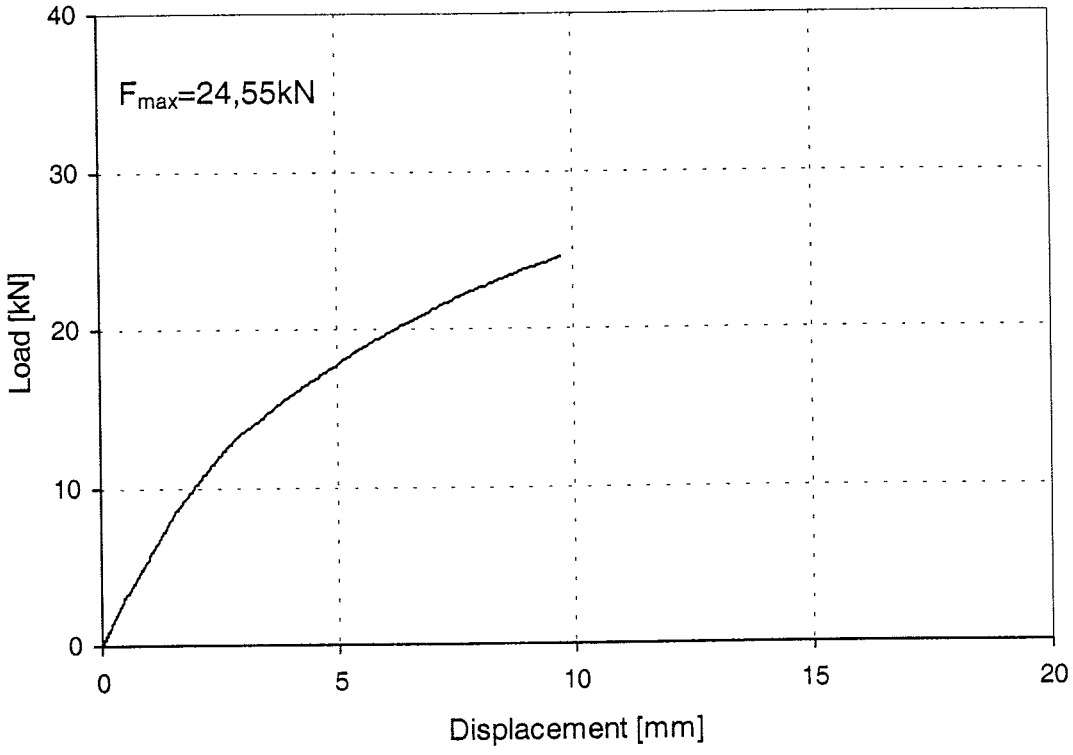

Figure 149: Load-displacement-curve of test GiIII-3-2

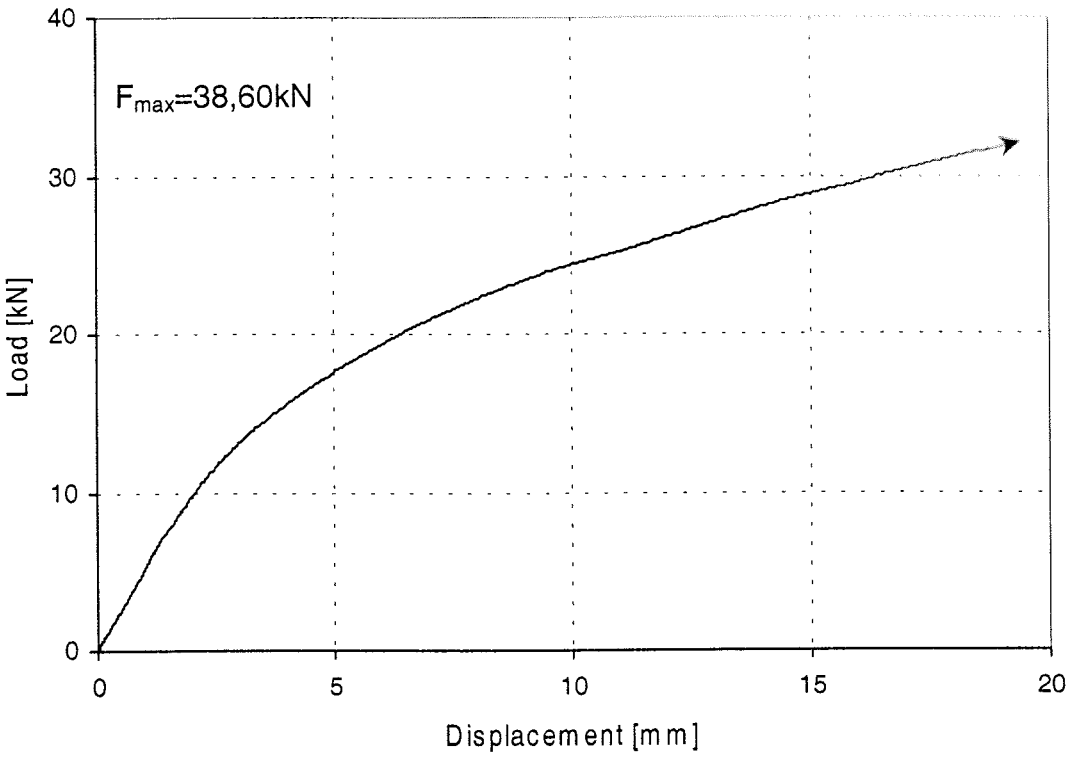

Figure 150: Load-displacement-curve of test GilII-3-3

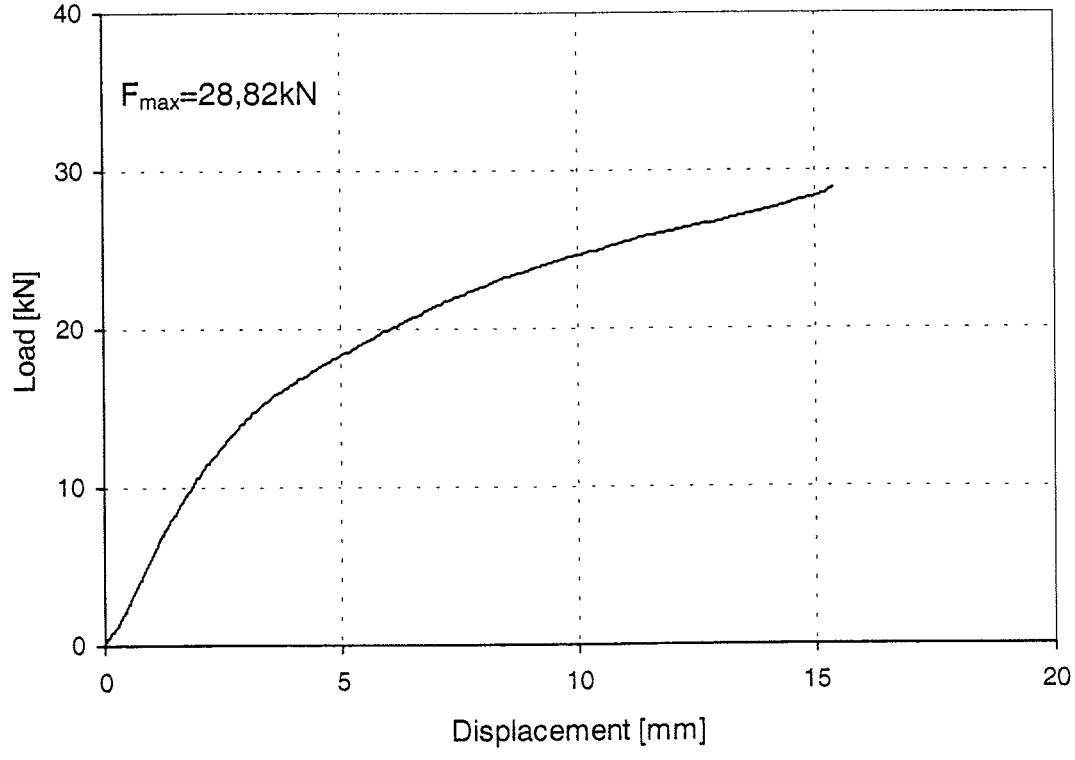

Figure 151: Load-displacement-curve of test GilII-3-4

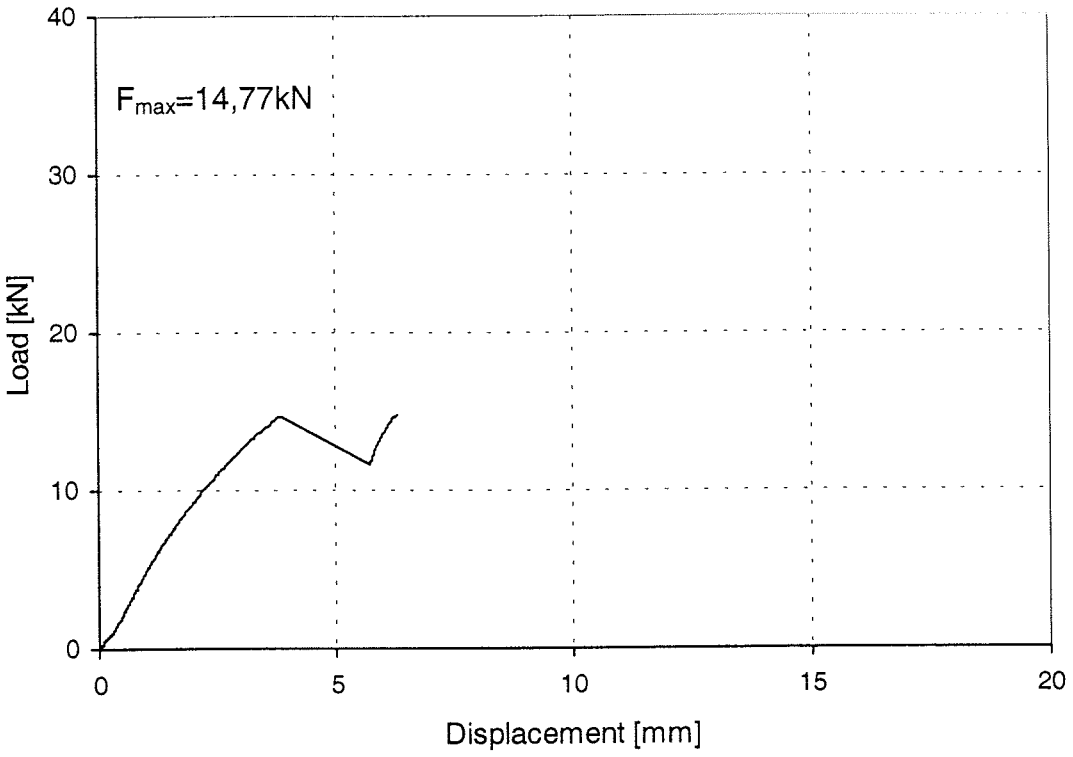

Figure 152: Load-displacement-curve of test GiIII-3-5

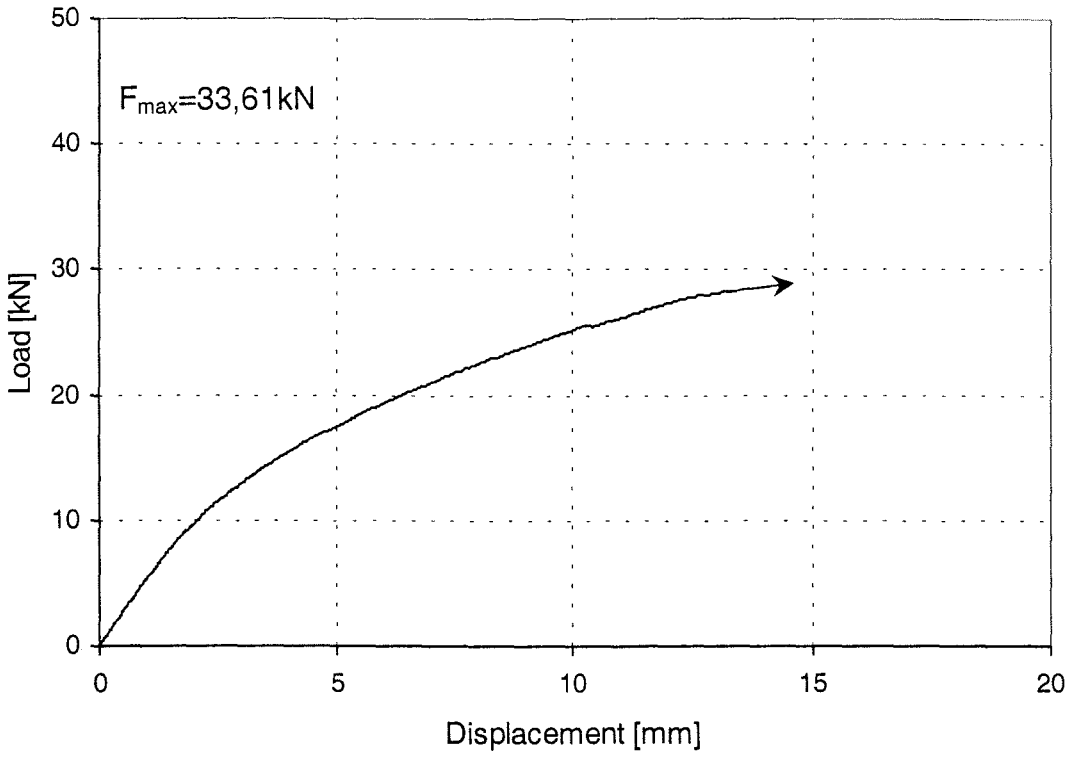

Figure 153: Load-displacement-curve of test GilII-4-1

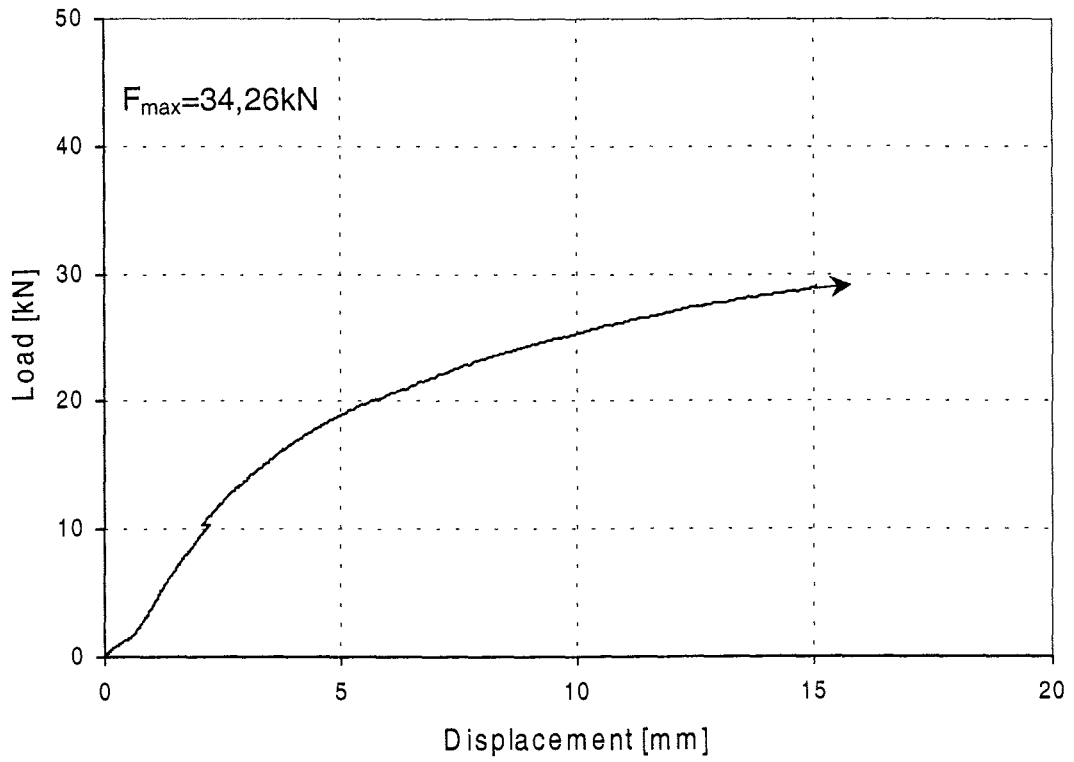

Figure 154: Load-displacement-curve of test GilII-4-2

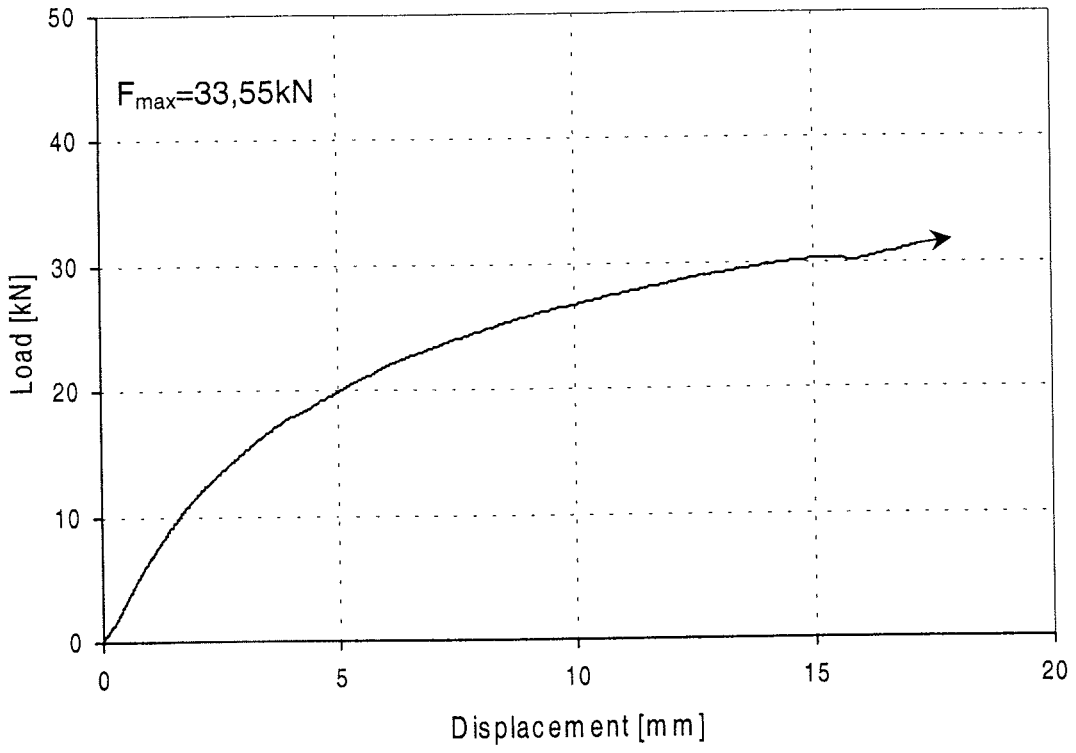

Figure 155: Load-displacement-curve of test GillI-4-3

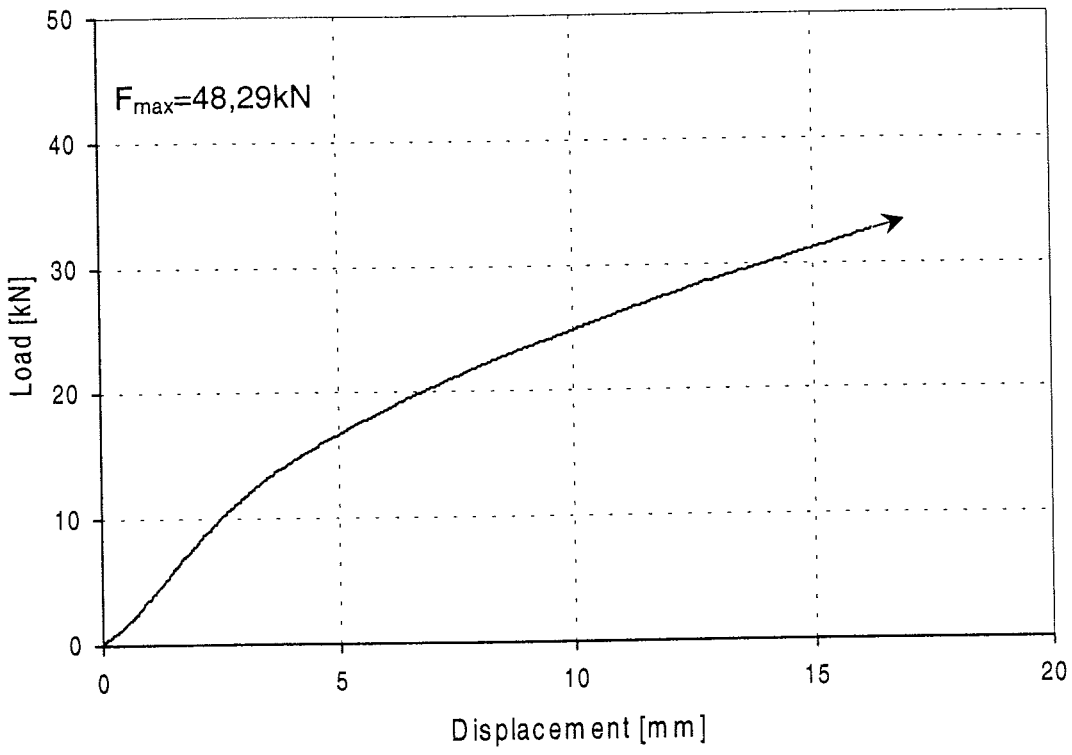

Figure 156: Load-displacement-curve of test GillI-4-4

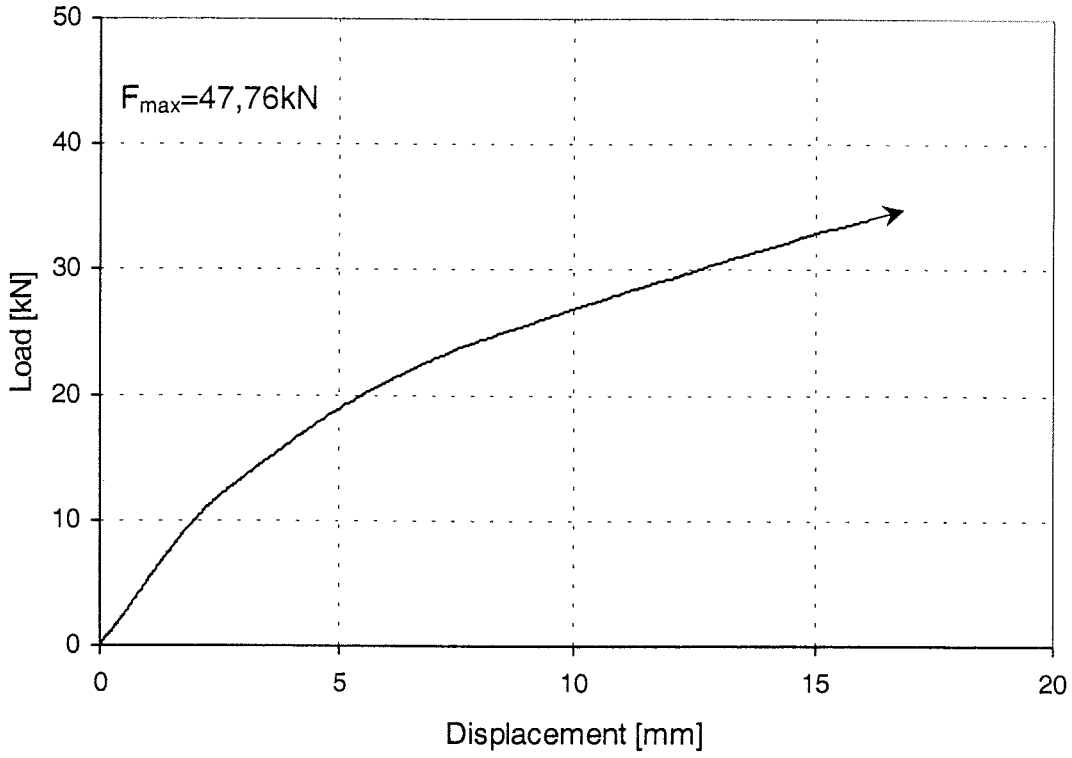

Figure 157: Load-displacement-curve of test GilII-4-5

Table E1a: Plastic moments of the rods

Denotation of Test d=16mm	Fmax [N]	plastic moment [Nm]
Gil 4.61	367	318,17
Gil 4.611	362	314,19
Gil 4.612	337	292,31
Gil 4.613	369	320,15
Gil 4.614	296	256,52
Mean		300,27
COV		8,95

Denotation of Test d=16mm	Fmax [N]	plastic moment [Nm]
Gil 8.8 1-1	530	459,47
Gil 8.8 1-2	535	463,47
Gil 8.8 1-3	535	463,47
Gil 8.8 1-4	532	461,47
Gil 8.8 2-1	548	475,45
Gil 8.8 2-2	498	431,50
Gil 8.8 2-3	530	459,47
Gil 8.8 2-4	530	459,47
Gil 8.8 2-5	541	469,46
Gil 8.8 3-1	537	465,46
Gil 8.8 3-2	528	457,78
Gil 8.8 3-3	537	465,46
Gil 8.8 3-4	493	427,51
Gil 8.8 3-5	551	477,72
Gil 8.8 4-1	532	461,47
Gil 8.8 4-2	541	469,46
Gil 8.8 4-3	530	459,51
Gil 8.8 4-4	532	461,47
Gil 8.8 4-5	532	461,47
Gil 8.8 5-1	535	463,47
Gil 8.8 5-2	530	459,47
Gil 8.8 5-3	537	465,46
Gil 8.8 5-4	541	469,46
Gil 8.8 5-5	530	459,47
Gil 8.8 6-1	544	471,46
Gil 8.8 6-2	528	457,78
Gil 8.8 6-3	558	483,79
Gil 8.8 6-4	537	465,46
Gil 8.8 6-5	537	465,46